THE UNIVERSITY
of EDINBURGH

INVESTIGATING NEW GENETIC SUSCEPTIBILITY LOCI IN OSTEOARTHRITIS

Mr Simon Benedict Roberts MBChB BSc MSc MRCS(Ed)

A thesis submitted for the degree of Doctor of Philosophy

University of Edinburgh

2017

Investigating New Genetic Susceptibility Loci in Osteoarthritis

Simon Benedict Roberts

University of Edinburgh

ABSTRACT

Primary osteoarthritis (OA) is a late-onset, degenerative condition of synovial joints, and is the major cause of pain and disability in older persons. OA represents a significant disease burden and focus of research, especially as no disease-modifying therapies exist to manage the condition. The genetic influence to OA is complex and polygenic. The arcOGEN study, the most powerful genome-wide association study yet to investigate OA in humans, identified the 9q33.1 locus to be significantly associated with hip OA in females. *TRIM32* lies within the 9q33.1 susceptibility locus and may have strong biological relevance to OA; it encodes a protein with E3 ubiquitin ligase activity.

Sanger sequencing of *TRIM32* in the youngest 500 female patients with hip OA from the arcOGEN study was performed to identify rare variants in *TRIM32* that are associated with OA of the hip in females. Polymorphisms were identified in the proximal promoter, and 3'untranslated regions (3'UTR) of *TRIM32* that are disproportionately represented in female patients with hip OA, compared to the control population.

In vitro studies identified expression of TRIM32 in human femoral head cartilage; reduced expression of TRIM32 was also demonstrated in femoral head primary articular chondrocytes from patients with hip OA compared to control patients. *Trim32* knockout resulted in increased aggrecanolysis in murine femoral head explants. Murine chondrocytes deficient in *Trim32* also exhibited increased expression of markers of a mature chondrocyte phenotype in response to anabolic cytokine stimulation, and increased expression of markers of a hypertrophic chondrocyte phenotype upon catabolic cytokine stimulation.

In vivo studies of joint degeneration in *Trim32* knockout mice demonstrated increased cartilage degradation and tibial epiphyseal bone changes after surgically induced knee joint instability, compared to wild-type mice. Increased cartilage degradation and medial knee subchondral bone changes were also identified upon ageing of *Trim32* knockout mice.

These results further implicate *TRIM32* in the genetic predisposition to OA, and indicate a role for TRIM32 in the joint degeneration evident in OA. These results support the further study of TRIM32 in the pathophysiology of OA and development of novel therapeutic strategies to manage OA.

Investigating New Genetic Susceptibility Loci in Osteoarthritis

Simon Benedict Roberts

University of Edinburgh

LAY SUMMARY

Primary osteoarthritis (OA) is a degenerative condition affecting joints and is a leading cause of pain and disability in elderly persons. As the proportion of older persons in the population increases, OA represents an increasing disease burden and its management has significant economic implications. No therapies exist to prevent progression of OA, which is therefore a focus of research. OA has an established hereditary component, though the exact genetic mechanisms predisposing to the disease are incompletely understood. The most powerful population-wide genome study investigating OA in humans identified variation within a region on chromosome 9 as associated with the development of OA. *TRIM32* is a gene at this region that may have strong biological relevance to OA.

In this study, genetic fine mapping of *TRIM32* was performed in female patients with early-onset primary hip OA to identify variants that may predispose to the disease. Variants were identified in the region proximal to the gene and in the non-coding region immediately downstream of *TRIM32* that were present at a disproportionate frequency in patients with OA, thereby further implicating *TRIM32* in the genetic predisposition to OA.

The expression of TRIM32 protein was reduced in chondrocytes, the predominant cell type of joint cartilage, from patients with hip OA compared to samples from patients without OA. Hip joint cartilage from mice deficient in *Trim32* demonstrated increased cartilage degradation. Joint chondrocytes from mice deficient in *Trim32* also expressed increased markers associated with OA upon exposure to pro-inflammatory stimuli.

The role of *Trim32* was also investigated in models of OA in mice lacking *Trim32*. Mice deficient in *Trim32* developed increased cartilage degradation and adjacent bone changes typical of OA following surgically induced knee joint instability and upon ageing, compared to normal wild-type mice.

These results indicate a role for TRIM32 in the joint degeneration evident in OA, and support the further study of TRIM32 in the pathophysiology of OA and the development of novel therapeutic strategies to manage OA.

To my family

DECLARATION

I hereby declare that this thesis has been composed by myself and the work described within, except where specifically acknowledged, is my own and that it has not been accepted in any previous application for a degree. The information obtained from sources other than this study is acknowledged in the text or included in the references.

Simon Roberts

November 2017

CONTENTS

ACKNOWELDGEMENTS

I first wish to thank my supervisors Professors Stuart Ralston and Donald Salter for their guidance, support, and enthusiasm throughout this project.

I would like to thank several members of the Bone and Osteoarticular research groups at the Centre for Genomics and Experimental Medicine, within the Institute for Genetics and Molecular Medicine at the University of Edinburgh. In particular, I would like to thank Omar Albagha, Huilin Jin, Nerea Alonso, and Michaela Rios-Visconti for help with sequencing studies; Asim Azfer, Ying Zhou, Sachin Wani, and Michelle Ricketts for help during cell culture techniques; Antonia Sophocleous, Anna Borjesson and Sue Fleetwood-Walker for help with murine studies; and Helen Caldwell and Elaine McLay for help with histology techniques.

I would also like to acknowledge the help of staff at several other clinical and research centres: staff at the HGU services for performing the sequencing; members of the Centre for Integrated Genomic Medical Research (CIGMR) BioBank at the University of Manchester for providing DNA samples; the steering committee of the arcOGEN study for collaborative access to resources; members of the Biomedical Research Facility (BRF) at the University of Edinburgh for murine breeding and husbandry; Jens Schwamborn of the University of Münster for kindly providing genetically modified mice; Professors John Iredale, Andrew Jackson, and Brian Walker of the University of Edinburgh for support through the Edinburgh Clinical Academic Track scheme; and the Wellcome Trust for their funding.

Finally, I would like extend my sincere gratitude to my brother and my father for their continued support.

PRESENTATIONS

Oral Presentation: ‘Micro-computed tomography demonstrates accelerated subchondral bone changes in *TRIM32* knockout mice after destabilisation of the medial meniscus (DMM) surgery and ageing’; Roberts SB, Borjesson AE, Sophocleous A, Salter DM, Ralston SH. British Orthopaedic Research Society Annual Meeting 2015, Liverpool.

Oral Presentation: ‘*TRIM32* knockout mice develop accelerated knee OA after DMM surgery and upon ageing’; Roberts SB, Borjesson AE, Sophocleous A, Salter DM, Ralston SH. Joint Meeting of the Bone Research Society and Bone Matrix Research Society 2015, Edinburgh.

Oral Presentation: ‘Role of TRIM32 in osteoarthritis: TRIM32-deficient mice develop accelerated knee osteoarthritis after destabilisation of the medial meniscus (DMM) surgery and upon ageing’; Roberts SB, Borjesson AE, Sophocleous A, Salter DM, Ralston SH. Osteoarthritis Research Society International Annual World Congress 2016, Amsterdam.

PRIZES

Best Young Investigator Prize at British Orthopaedic Research Society Annual Meeting 2015, Liverpool.

Best Oral Presentation at Joint Meeting of the Bone Research Society and Bone Matrix Research Society 2015, Edinburgh.

PUBLICATIONS

Roberts SB, Wootton E, De Ferrari L, Albagha O, Salter DM. Epigenetics of osteoarticular diseases: recent developments. Rheumatology International. 2015; 35 (8): 1293-1305. PMID: 25812537.

Roberts SB, Borjesson A, Sophocleous A, Salter DM, Ralston SH. Role of *Trim32* in osteoarthritis: *Trim32*-deficient mice develop accelerated knee osteoarthritis after destabilisation of the medial meniscus (DMM) surgery and upon ageing. Osteoarthritis and Cartilage 2016; 24 (Suppl 1): S18.

LIST OF ABBREVIATIONS

3D	Three-dimensional
3'UTR	Three prime untranslated region
5-caC	5-carboxylcytosine
5-fC	5-formylcytosine
5-hmC	5-hydroxymethylcytosine
5-mC	5-methylcytosine
5'UTR	Five prime untranslated region
A	Adenine
AC	Articular cartilage
ACAN	Aggrecan
ACL	Anterior cruciate ligament
ACLT	Anterior cruciate ligament transection
ADAMTS	A Disintegrin and metalloproteinase with thrombospondin motif
ADAMTS4	A Disintegrin and metalloproteinase with thrombospondin motif 4
ADAMTS5	A Disintegrin and metalloproteinase with thrombospondin motif 5
ADAMTS9	A Disintegrin and metalloproteinase with thrombospondin motif 9
ALDH1A1	Aldehyde dehydrogenase 1 family member A1
ALDH1A2	Aldehyde dehydrogenase 1 family member A2
ALSPAC	Avon Longitudinal Study of Parents and Children
AMP	Adenosine monophosphate
ANOVA	Analysis of variance
arcOGEN	Arthritis Research UK Osteoarthritis Genetics Consortium
AS1	Antisense RNA 1
ASTN1	Astrotactin 1
ASTN2	Astrotactin 2
bp	Base pairs
BA	Butyric acid
BBS	Bardet-Beidl syndrome
BMP	Bone morphogenic protein
BMP7	Bone morphogenic protein 7
BP.Th	Bone plate thickness
BRF	Biomedical Research Facility
BSA	Bovine serum albumin
BTNL2	Butyrophilin-like 2
BV/TV	Trabecular volume
C	Cytosine
C3b	Complement 3b
C57Bl/6	C57 black 6
CCL	Chemokine (C-C motif) ligand
CCL19	Chemokine (C-C motif) ligand 19
CCR	C-C chemokine receptor
CCR7	C-C chemokine receptor 7
CD	Cluster of differentiation
CDC5L	Cell division cycle 5-like
cDNA	Complimentary DNA

CEU CEP (Centre d'Etude du Polymorphisme Humain) Utah Residents with Northern and Western European ancestry
CGI CpG island
χ^2 Chi-squared
ChIP Chromatin immunoprecipitation
CHST11 Carbohydrate (chondroitin-4)-sulfotransferase
CI Confidence interval
CIGMR Centre for Integrated Genomic Medical Research
cm Centimetre
CNP C-type natriuretic peptide
CNV Copy number variant
CO_2 Carbon dioxide
COL1A1 Collagen type I alpha 1
COL2A1 Collagen type II alpha 1
COL9A1 Collagen type IX alpha 1
COL10A1 Collagen type X alpha 1
COL11A1 Collagen type XI alpha 1
COL12A1 Collagen type XII alpha 1
Col I Type I collagen
Col II Type II collagen
Col VI Type VI collagen
Col IX Type IX collagen
Col X Type X collagen
Col XI Type XI collagen
COMP Cartilage oligomeric matrix protein
COX2 Cyclooxygenase 2
COX7A2 Cytochrome C oxidase subunit 7A2
CpG Cytosine-guanine dinucleotides
CREB cAMP response element-binding protein
CT Computed tomography
D2 Deiodinase 2
DAB Diaminobenzedine
DAMP Damage-associated molecular patterns
dbSNP Single Nucleotide Polymorphism database
DDR2 Discoidin domain receptor 2
DEAF-1 Deformed epidermal autoregulatory factor 1 homolog
DEPC Diethylpyrocarbonate
DIO2 Type II iodothyronine deiodinase
DMM Destabilisation of the medial meniscus
DMMB Dimethylmethylene blue
DMEM Dulbecco's Modified Eagle's medium
DMOADs Disease-modifying osteoarthritis drugs
DMR Differentially methylated regions
DNA Deoxyribonucleic acid
DNMT De novo methyltransferase
dNTP Deoxynucleotide

DOT1L	DOT1 like histone H3K79 methyltransferase
DPX	Di-n-butylphthalate in xylene
DVWA	Dual von Willebrand factor A domains
ECM	Extracellular matrix
EDTA	Ethylenediaminetetraacetic acid
eQTL	Expression quantitative trait loci
ERK	Extracellular-regulated kinase
ETOH	Ethanol
EUR	European
FCS	Foetal calf serum
FGF	Fibroblast growth factor
FGF2	Fibroblast growth factor 2
FGF4	Fibroblast growth factor 4
FGF8	Fibroblast growth factor 8
FGFR	Fibroblast growth factor receptor
FGFR1	Fibroblast growth factor receptor 1
FGFR3	Fibroblast growth factor receptor 3
FILIP1	Filamin A interacting protein 1
FTO	Fat mass and obesity associated gene
g	Grams
G	Guanine
GA	General anaesthesia
GAG	Glycosaminoglycan
GAPDH	Glyceraldehyde 3-phosphate dehydrogenase
GDF	Growth differentiation factor
GDF5	Growth differentiation factor 5
GEP	Granulin-epithelin precursor
GLA	Vitamin K-dependent carboxylation/gamma-carboxyglutamic
GLM	Generalised linear model
GLT8D1	Glycosyltransferase 8 domain containing 1
GNL3	Guanine nucleotide binding protein-like 3
GNP	Gross national product
GPCR	G-protein coupled receptor
GRCh	Genome Reference Consortium human genome
GRP22	Glycine-rich_protein_Aa1-291
GTEX	Genotype-Tissue Expression
GTP	Guanosine triphosphate
GWAS	Genome-wide association study
H_2O	Water
H_2O_2	Hydrogen peroxide
H3K4me	Histone H3 lysine 4 methylation
HA	Hyaluronan
HAT	Histone acetyltransferases
HCl	Hydrogen chloride
HDAC	Histone deacetylase
HEPES	4-(2-hydroxyethyl)-1-piperazineethanesulfonic acid

HET	Heterozygous
HGU	Human Genetics Unit
HH	Hedgehog
HIF1α	Hypoxia inducible factor 1 alpha
HIF2α	Hypoxia inducible factor 2 alpha
HLA	Human leukocyte antigen
HMGB	High-mobility group box
HRP	Horseradish peroxidase
HTRA1	High temperature requirement A1
iNOS	Inducible nitric oxide synthase
ID	Identification
IGD	Interglobular domain
IGF	Insulin like growth factor
IGF1	Insulin like growth factor 1
IGF2	Insulin like growth factor 2
IGFBP	Insulin like growth factor binding protein
IGFBP3	Insulin like growth factor binding protein 3
IGFBP4	Insulin like growth factor binding protein 4
IHH	Indian hedgehog homolog
IL	Interleukin
IL1	Interleukin 1
IL4	Interleukin 4
IL6	Interleukin 6
IL8	Interleukin 8
IL17	Interleukin 17
IL18	Interleukin 18
IL1α	Interleukin 1 alpha
IL1β	Interleukin 1 beta
IMDM	Iscove's Modified Dulbecco's medium
IMPG1	Interphotoreceptor matrix proteoglycan 1
JNK	c-Jun N-terminal kinase
kb	Kilobases
kDa	Kilodalton
kV	Kilovolts
KLHDC5	Kelch domain containing 5
KO	Knockout
LD	Linkage disequilibrium
LEP	Leptin
LFC	Lateral femoral condyle
LGMD2H	Limb girdle muscular dystrophy
LMW	Low molecular weight
LREC	Lothian Research Ethics Committee
LTP	Lateral tibial plateau
mA	Milliampere
mBSA	Methylated bovine serum albumin
mg	Milligram

miRNA	MicroRNA
ml	Millilitre
mm	Millimetre
mM	Millimolar
mOsm	Milliosmoles
mPGES1	Microsomal prostaglandin E synthase-1
mRNA	Messenger RNA
μA	Microampere
μCT	MicroCT
μg	Microgram
μm	Micrometre
μM	Micromolar
μl	Microlitre
MAF	Minor allele frequency
MAPK	Mitogen-activated protein kinase
MCF2L	MCF.2 cell-line-derived transforming sequence-like
MFC	Medial femoral condyle
MHHGS	Mankin histological-histochemical grading system
MIA	Monoiodoacetate
MMP	Matrix metalloproteinase
MMP1	Matrix metallopeptidase 1
MMP3	Matrix metallopeptidase 3
MMP9	Matrix metallopeptidase 9
MMP13	Matrix metallopeptidase 13
MMTL	Medial meniscotibial ligament
MOPS	3-(*N*-morpholino)propanesulfonic acid
MPa	Megapascal
MRI	Magnetic resonance imaging
MSC	Mesenchymal stem cell
MSX1	Msh homeobox 1
MTP	Medial tibial plateau
MYO6	Myosin VI
Na_3VO_4	Sodium vanadate
NaCl	Sodium chloride
NCOA3	Nuclear receptor coactivator 3
NFAT	Nuclear factor of activated T-cells
NFκB	Nuclear factor kappa-light-chain-enhancer of activated B cells
NFYA	Nuclear transcription factor Y subunit alpha
NGF	Nerve growth factor
NGS	Next generation sequencing
NHL	NCL-1/HT2A/LIN-41
NHS	National Health Service
ng	Nanogram
nm	Nanometre
NO	Nitric oxide
NOS2	Nitric oxide synthase

OA	Osteoarthritis
OARSI	Osteoarthritis Research Society International
ODF	Osteoclast differentiation factor
OMIM	Online Mendelian Inheritance in Man
OPG	Osteoprotegerin
OPGL	OPG ligand
OR	Odds ratio
ORF	Open reading frame
OSM	Oncostatin-M
PAPPA	Pappalysin 1 (also known as Pregnancy-associated plasma protein A)
PAPPA2	Pappalysin 2
PBS	Phosphate buffered saline
PBS-T	PBS-Tween 20
PCM	Pericellular matrix
PCR	Polymerase chain reaction
PGE2	Prostaglandin E2
Pias3	Protein inhibitor of activated STAT3
Piasy	Protein inhibitors of activated STATs
PolyPhen	Polymorphism Phenotyping
PRG4	Proteoglycan 4
PTHLH	Parathyroid hormone-like hormone
PTHrP	Parathyroid hormone-related protein
PVDF	Polyvinylidenedifluoride
qPCR	Quantitative PCR
RA	Retinoic acid
RANK	Receptor activator of nuclear factor kappa-B
RANKL	RANK ligand
RAR	Retinoic acid receptor
RARα	Retinoic acid receptor alpha
RING	Really Interesting New Gene
RNA	Ribonucleic acid
ROI	Region of interest
ROS	Reactive oxygen species
rpm	Revolutions per minute
rs	Reference SNP
RUNX1	Runt-related transcription factor 1
RUNX2	Runt-related transcription factor 2
RUNX3	Runt-related transcription factor 3
S100A11	S100 calcium-binding protein A11
SAPL	Surface-active phospholipids
SD	Standard deviation
SDS	Sodium dodecyl sulphate
SEM	Standard error of the mean
SENP6	Sentrin specific peptidase 6
SET-1A	SET domain-containing protein 1A
SIFT	Sorting Intolerant From Tolerant

SIRT1	Sirtuin 1
SMAD3	SMAD family member 3
SNAP	SNP Annotation and Proxy Search
SNP	Single nucleotide polymorphism
SOCS2	Suppressor of cytokine signalling 2
SOD2	Superoxide dismutase 2
SOX5	SRY (Sex Determining Region Y)-Box 5
SOX6	SRY (Sex Determining Region Y)-Box 6
SOX9	SRY (Sex Determining Region Y)-Box 9
Sp1	Trans-acting transcription factor 1
Sp3	Trans-acting transcription factor 3
sPLA2	Soluble phospholipase A2
SPSS	Statistics Package for the Social Science
STAT	Signal transducer and activator of transcription
SULF2	Sulfatase 2
SUMF1	Sulfation of proteoglycans by sulphate-modifying factor 1
SUPT3H	Suppressor of Ty3 homolog
T	Thymine
T1DGC	Type 1 Diabetes Genetics Consortium
TBE	Tris/borate/ethylenediaminetetraacetic acid
Tb.N	Trabecular number
TBS	Tris buffered saline
Tb.Sp	Trabecular separation
TBS-T	TBS-Tween
Tb.Th	Trabecular thickness
TFAP2A	Transcription factor AP-2 alpha
TFAP2C	Transcription factor AP-2 gamma
TGFβ	Transforming growth factor beta
TGFβ1	Transforming growth factor beta 1
TGFβ2	Transforming growth factor beta 2
TGFβ3	Transforming growth factor beta 3
THR	Total hip replacement
TJR	Total joint replacement
TKR	Total knee replacement
TLR	Toll-like receptor
TLR4	Toll-like receptor 4
TMEM30A	Transmembrane protein 30A
TNFα	Tumour necrosis factor alpha
TNFSF11	Tumour necrosis factor ligand superfamily member 11
TP63	Tumour protein 63
TRANCE	TNF-related activation-induced cytokine
TRAP	Tartrate-resistant acid phosphatase
TRIM32	Tripartite motif-containing protein 32
TRPV1	Transient receptor potential cation channel subfamily V member 1
TSA	Trichostatin A
UCSC	University of California Santa Cruz

UK	United Kingdom
UPL	Universal probe library
USA	United States of America
V	Volts
VEGF	Vascular endothelial growth factor
VHL	Von Hippel Lindau
VWA	Von Willebrand factor type A
WT	Wild type
WTCCC	Wellcome Trust Case Control Consortium
w/v	Weight/volume
XIAP	X-linked inhibitor of apoptosis

LIST OF FIGURES

LIST OF TABLES

Chapter 1

Introduction

1.1 Osteoarthritis (OA)

1.1.1 Definition

Osteoarthritis (Online Mendelian Inheritance in Man® (OMIM (1)) ♯165720) is defined by the Osteoarthritis Research Society International (OARSI) (2) as:

> '… a progressive disease of synovial joints that represents failed repair of joint damage that results from stresses that may be initiated by an abnormality in any of the synovial joint tissues, including articular cartilage, subchondral bone, ligaments, menisci (when present), periarticular muscles, peripheral nerves, or synovium. This ultimately results in the breakdown of cartilage and bone, leading to symptoms of pain, stiffness, and functional disability.'

1.1.2 Epidemiology: burden of disease

Primary osteoarthritis (OA) is a late-onset, degenerative condition that affects 70% of persons over 60 years of age (3). Secondary OA can develop following infection, trauma, deformity, congenital abnormalities, local or systemic medical conditions, or previous surgery affecting a joint. Primary OA is the most prevalent form of OA globally, and is the major cause of pain and disability in older persons (3). It is reported to affect 8.75 million persons in the United Kingdom (UK), and costs the UK economy 1% of gross national product (GNP) per year. Although OA may affect any synovial joint, this research has investigated OA affecting the hip and knee joint, which are two of the most clinically relevant sites affected by OA. Hip and knee OA affect 8% and 18% of persons in the UK aged over 45 years, respectively (4). With the population aging, the prevalence of OA is increasing in both developed and developing countries (5). This increasing burden has led to OA being adopted as a major research focus, especially as no disease-modifying therapies exist to manage the condition (6). Current medical management comprises analgesic medication until the development of severe disease, characterised by unremitting pain and disability, necessitates joint replacement

surgery. Indeed, 93% of total hip replacements (THR), and 98% of total knee replacements (TKR) in the UK are performed to manage OA (4).

1.1.3 Clinical features

OA may be primary in nature, in which no cause is identified, or develop secondary to a traumatic injury, or an infective, inflammatory, metabolic, congenital, developmental or neurological condition (7-9). OA usually develops and progresses gradually over several years. The diagnosis of OA depends upon both clinical and radiological evidence of disease (10). Radiological features of OA do not directly correlate with clinical symptoms, and approximately 50% of patients with radiological features of disease experience no symptoms. The principal symptoms comprise joint pain, stiffness, deformity, and a consequent reduced functional capacity and quality of life (11, 12). Current treatment modalities to treat OA include analgesic medications, low-impact exercise, weight reduction, acupuncture, chondroitin sulphate, glucosamine, and joint surgery (13-17). Risk factors for developing OA include both environmental and genetic factors, and differ depending on the joint affected (10). Identified risk factors include increasing age, female gender, vitamin-D deficiency, obesity, joint injury, and excessive mechanical loading of joints (18).

1.2 Pathology of OA

1.2.1 Structure of synovial joints

Synovial joints, also known as diarthrodial joints, are comprised of congruent layers of articular cartilage, supported by subchondral bone, encompassed by synovium that produces synovial fluid (Figure 1.1). Joints are stabilised by supporting muscles surrounding the joint, ligaments in the joint capsule, and also by menisci within the knee joint and labrum within the hip joint (19). OA develops as a consequence of dysregulation of the normal balance of synthesis and degradation of joint tissues (7), resulting in the failure of articular cartilage (20).

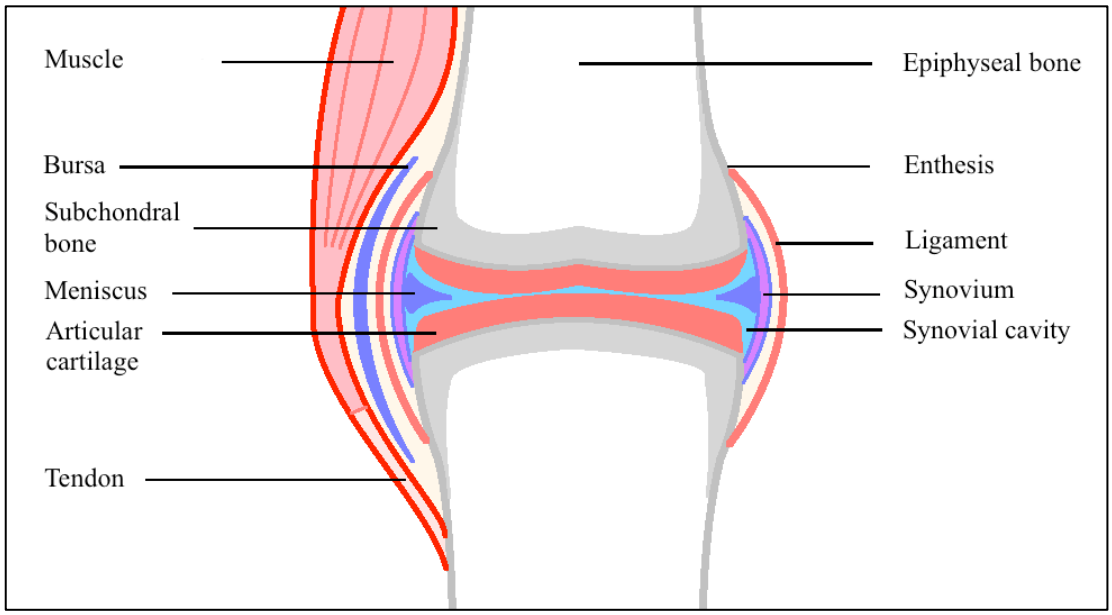

Figure 1.1 - Schematic diagram of the structure of synovial joints

Synovial tissue develops from mesenchymal stem cells (MSCs) and is composed of two distinct layers: an outer layer of dense connective tissue termed the stratum fibrosum, and an inner layer called the synovial membrane (7, 21). This membrane contains in its luminal surface a unique cellular lining. The synovial intimal cells, referred to as synoviocytes, produce synovial fluid, resorb constituents of the synovial cavity, and enact the exchange of components between the blood and synovial fluid (22). Two principal types of synoviocytes have been identified: type A and type B cells (22). A further synovial intimal cell type displaying properties of both type A and B cells has also been reported (23). Type A cells are derived from blood mononuclear cells, protect the joint from bacterial infection, and possess phagocytic and antigen-presenting characteristics. Type B cells are characterised by an abundance of rough endoplasmic reticulum and dendritic processes that form a structured network in the luminal surface of the synovial membrane. Type B cells produce the specialised joint matrix constituents including hyaluronan, lubricin, collagens and fibronectin for the intimal interstitium and synovial fluid (24, 25). The synovial matrix provides both a

permeable membrane through which exchange of molecules may occur, and sufficient resistance to outflow of the constituents of synovial fluid (26).

Synovial fluid is an ultra-filtrate of blood plasma with high viscosity. In diathrodial joints, the role of synovial fluid is as a biological lubricant and a medium through which nutrients and regulatory cytokines may pass to the articular chondrocytes and subchondral bone (27). The low-friction and low-wear properties of synovial joints are imparted largely by the presence of proteoglycan 4 (PRG4), hyaluronan, (HA), and surface-active phospholipids (SAPL) in the synovial fluid (28-30).

1.2.2 Structure of articular cartilage

Articular cartilage comprises chondrocytes within a hydrated extracellular matrix (ECM) composed mainly of type II collagen (Col II) and proteoglycans. Chondrocytes are the only cell type present in articular cartilage and are responsible for the generation and homeostasis of the cartilaginous extracellular environment (31). Articular cartilage is normally aneural and avascular, and the hydrated matrix provides articular cartilage with tensile and compressive strength to maintain the biomechanical function of diarthrodial joints (32, 33).

1.2.2.1 Chondrocytes

In mature articular cartilage, chondrocytes are embedded within lacunae, a glycocalyx-filled fibrillar pericellular capsule surrounded by ECM. The organisation and structure of chondrocytes varies depending on their progression through the zonal architecture of articular cartilage (34). Mature chondrocytes have small nuclei with dispersed chromatin, and granular cytoplasm with a prominent rough endoplasmic reticulum. These features reflect the activity of chondrocytes in the synthesis of the ECM, which is entirely dependent on the viability of the chondrocytes, and both anabolic and catabolic factors required for cartilage homeostasis (35).

1.2.2.2 Chondrogenesis

Chondrogenesis, the process by which cartilage is developed, occurs *in utero.* The generation of cartilage is initiated by the differentiation of stellate-shaped mesenchymal stem cells (MSCs) into rounded precursor cells termed chondroblasts (36). Sequential mitotic divisions produce aggregations of chondroblasts that start to produce ground substance and fibrous ECM, thereby enclosing each chondroblast within cartilage matrix. Individual chondroblasts subsequently undergo further mitotic divisions to form small clusters of mature chondrocytes separated by ECM (37). Proliferating chondrocytes are organised in parallel columns, and characteristically express type II, IX and XI collagen (Col II, Col IX, and Col XI) and proteoglycans, especially aggrecan (ACAN). Chondrocytes become hypertrophic as they differentiate and express high levels of alkaline phosphatase and type X collagen (Col X).

SRY (Sex Determining Region Y)-Box 9 (SOX9) is a critical transcription factor involved in chondrogenesis. It is expressed at the mesenchymal osteoprogenitor stage and transactivates genes specific for chondrocyte proliferation, including *COL2A1* that encodes Col II (38, 39). SOX5 and SOX6 interact with SOX9 to activate enhancers specific to chondrocytes. Hypertrophic maturation of chondrocytes also requires the transcription factors runt-related transcription factor 2 (RUNX2) and RUNX3 that transactivate *IHH (Indian hedgehog homolog), COL10A1* (encoding Col X), and *MMP13* (*Matrix metallopeptidase 13)* genes (40-42).

Fibroblast growth factors (FGFs) are also fundamental to chondrogenesis by activating signalling through FGF receptors (FGFRs). In particular, *FGFR3* is expressed early during chondrogenesis by mesenchymal cells and also by proliferating chondrocytes (43). Mature hypertrophic chondrocytes preferentially express *FGFR1* (44). The onset of hypertrophic proliferation of chondrocytes is regulated by both a local negative feedback mechanism between IHH and parathyroid hormone-related protein (PTHrP), and by IHH-independent activation of Wnt and bone morphogenic protein (BMP) signalling (45, 46). Other important regulators of chondrogenesis include transforming growth factor beta (TGFβ), insulin-like growth factors (IGFs), C-type natriuretic peptide (CNP), and thyroid hormone (47).

As chondrocytes mature, cell-matrix interactions have an increasingly significant influence upon chondrogenesis. Association with the ECM is mediated by integrins and cell surface transmembrane receptors. Chondrocytes express many integrin subunits, though β1 integrin is particularly important for integrin-mediated signalling via the ECM (48). Sulfation of proteoglycans by sulphate-modifying factor 1 (SUMF1) also modulates chondrocyte proliferation and differentiation by regulating FGF signalling (49). Vinculin is also important for signalling between chondrocytes and the ECM through integrins by regulating IGF1-induced upregulation of *COL2A1* and *ACAN* (50).

1.2.2.3 Extracellular matrix

The ECM constitutes approximately 98% of the volume of articular cartilage in adults; the remaining 2% is occupied by chondrocytes. The ECM consists of a hydrated collagen fibre network enmeshed with proteoglycans and other non-collagenous proteins.

1.2.2.4 Collagen network

Collagen fibrils form an extensive network throughout the ECM, varying in size from 20 nm in the superficial zone of articular cartilage to 120 nm in the deep zone, and 90% of which comprise Col II (51). Type VI collagen (Col VI) is concentrated in pericellular regions, and forms a highly branched network that binds both decorin and hyaluronan (52). Col IX is contained within the fibrils, is also present at pericellular locations, and represents 2% of total collagen (53). Col X is expressed predominantly by hypertrophic chondrocytes, and Col XI is present within collagen fibrils and at their surface.

1.2.2.5 Proteoglycans

The other main structural component of articular cartilage is the proteoglycan ACAN. Proteoglycans confer compressive stiffness upon the articular cartilage through hydration of chondroitin sulphate and keratan sulphate chains. ACAN binds to HA that is associated with collagen fibrils; the interaction between ACAN and HA is stabilised by link protein. HA also binds to chondrocytes through the CD44 (CD; cluster of differentiation) cell surface receptor (54). In addition to ACAN, other less abundant proteoglycans that contribute to the structural integrity of ECM include biglycan, chondroadherin, fibromodulin, lumican, and versican (55).

1.2.2.6 Other matrix molecules

Cartilage oligomeric matrix protein (COMP) is a non-collagenous glycoprotein and a member of the thrombospondin family that binds collagen molecules, particularly Col IX. It may have a significant role in collagen fibril assembly in which five collagen molecules interact to form a microfibril (56). Fibrillin-1 is a protein present in pericellular regions where it is arranged into banded fibrils. Perlecan is a heparan sulphate-containing proteoglycan cell surface molecule that binds Col VI and is essential for ECM integrity (57). Vitamin K-dependent carboxylation/gamma-carboxyglutamic (GLA) protein prevents calcification of the ECM; in its absence calcification of cartilage develops (58). Matrilin-1 is a developmental cartilage matrix protein that is absent from healthy mature cartilage in adults; its presence in articular cartilage reflects immaturity, degeneration or regeneration of the cartilage (59).

1.2.2.7 Architecture of articular cartilage

The structure of articular cartilage is directly related to its function (Figure 1.2). At the superficial layer, adjacent to the synovial fluid of the joint, the chondrocytes and collagen fibrils are elongated and arranged parallel to the articular surface. In this superficial zone, chondrocytes produce superficial zone protein, also known as lubricin. Lubricin is fundamental to the low-friction articulation with diarthrodial joints. The collagen fibrils in the superficial zone are closely organised in parallel to the overlying joint surface. The ECM at this level predominantly comprises the cartilage fibrillar network (60). The proportional presence of ACAN is at its lowest in this level, whereas the proteoglycans decorin and biglycan are most abundant here. The tensile strength of cartilage is also greatest in the superficial zone, which is exposed most to tensile, shear and compressive forces during articulation (61).

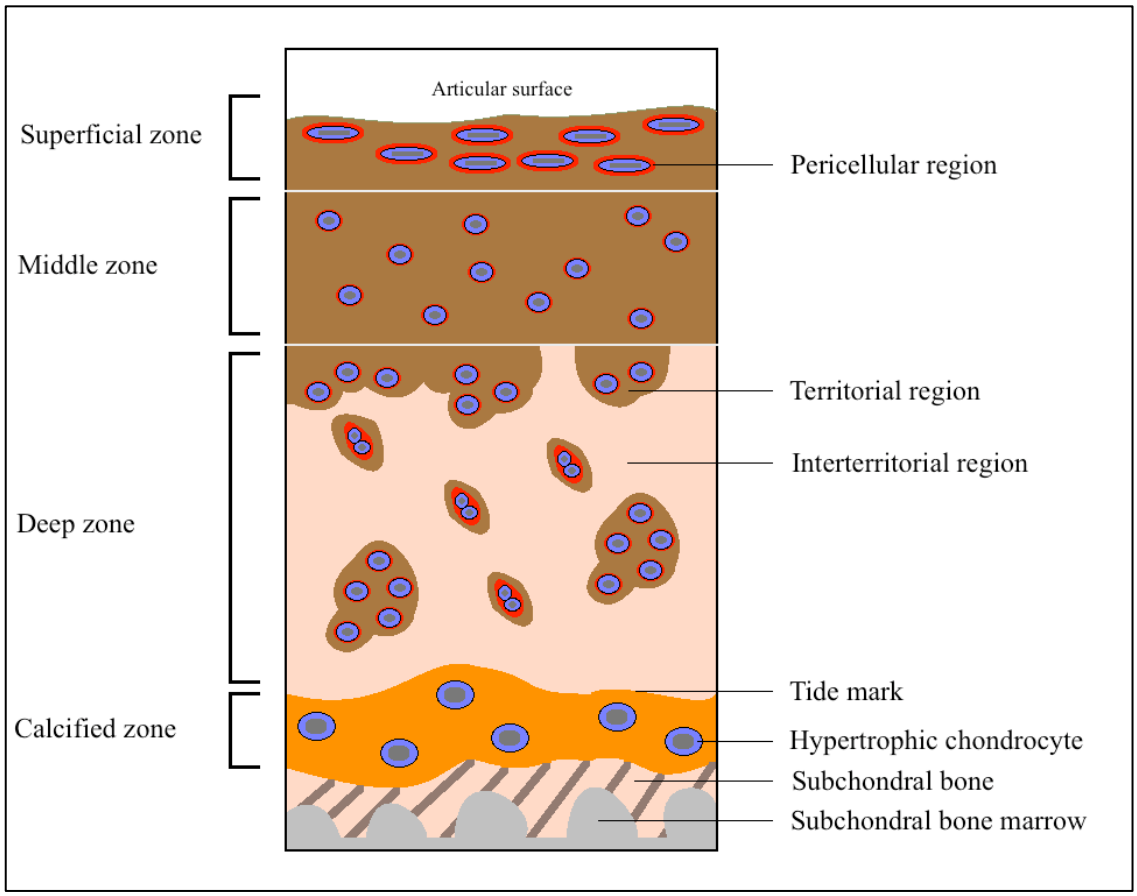

Figure 1.2 – Structure of human articular cartilage; the zones, regions, and relationship to the subchondral bone are shown. Adapted from Poole et al (59).

Beneath the superficial zone is the mid zone of articular cartilage. The midzone displays typical characteristics of articular cartilage, with spherical chondrocytes of low density, an ECM abundant with ACAN, and enmeshed collagen fibrils of large diameter. The midzone is situated immediately above the deep zone of articular cartilage, in which ACAN is present at its highest concentration, but chondrocyte density and collagen content are at their lowest (60). The deepest layer of articular cartilage is the calcified cartilage, an intermediate zone between the more superficial uncalcified cartilage and the supportive subchondral bone. Hypertrophic chondrocytes predominate in the calcified cartilage, producing Col X and calcifying the ECM to provide a structural interface with subchondral bone that resists vascular invasion in healthy mature articular cartilage.

The features of the ECM surrounding, and between, chondrocytes also varies across and within the zones of articular cartilage. Chondrocytes are immediately surrounded by a 2 μm diameter pericellular region, which contains predominantly Col II fibrils at a low density, and relatively high concentrations of Col VI, decorin, and ACAN (62, 63). The region surrounding the pericellular region is termed the territorial region, and is present in all zones of articular cartilage. In the deep zones only, an interterritorial region is also evident; this is the region of the ECM most distant from chondrocytes. Breakdown products of ACAN and other proteoglycans following incomplete proteolysis are concentrated in the interterritorial region (64).

1.2.2.8 Cartilage homeostasis

Chondrocytes are responsible for the balanced synthesis and degradation of the ECM of articular cartilage. In healthy articular cartilage, this is a strictly regulated process influenced by anabolic and catabolic cytokines, growth factors, and physiological mechanical stimulation.

The catabolic cytokines interleukin-1 (IL1), tumour necrosis factor alpha (TNFα), IL17, and IL18 result in increased synthesis of matrix metalloproteinases (MMPs), a decrease in MMP enzyme inhibitors, and reduced ECM production. Anabolic cytokines, including insulin growth factor 1 (IGF1), TGFβ1, -2, and -3, FGF2, -4, and -8, and BMPs stimulate ECM synthesis (65). Articular chondrocytes synthesise and store BMPs in both their active and inactive forms; BMP7 is particularly important for both ECM synthesis and chondrogenesis in healthy cartilage (66). The balanced production of anabolic and catabolic cytokines regulates the activity of chondrocytes and maintenance of the ECM, with no single cytokine able to stimulate all required metabolic activities in healthy cartilage. Homeostasis of ECM metabolism balances the degradation of macromolecules of the ECM with their replacement by newly synthesised macromolecules. Proteoglycan turnover can take up to 25 years, while the half-life of collagen is estimated as being beyond several decades (67, 68).

Col II accounts for 90% of the total collagen content of articular cartilage. Fibrils of Col II are stabilised by Col IX and Col XI. The individual Col II molecules comprise a triple helix of three α-chains covalently linked at each end (69). The native collagen fibrils are very resistant to proteases. The initial cleavage of Col II is mediated by the collagenases MMP1, MMP8, and MMP13 at a single site close to the C-terminus. The resulting fragments of Col II are further degraded by gelatinases (MMP2 and MMP9) and stromelysin (MMP3) (70). Degradation of Col II can be stimulated by IL1 and plasminogen, and also involves induction of IL6 and IL8 (71, 72).

In healthy cartilage, the extracellular proteolytic enzymes are present in latent forms. The presence of specific tissue inhibitors of metalloproteinases (TIMPs) regulates the activity of the proteolytic enzymes. TIMP3 can inhibit both MMPs and ADAMTSs (A Disintegrin And Metalloproteinase with Thrombospondin Motif), it is a central regulator of normal turnover of cartilage macromolecules. In healthy cartilage, approximately 10-15% of the ACAN molecules are present in a non-aggregated state, and lack their N-terminal region (73). The presence of fragmented ACAN reflects the normal turnover of ACAN within the ECM. Other proteinases, such as m-calpain, may also contribute to extracellular cleavage of ACAN (74). ACAN fragments are internalised within chondrocytes and degraded within lysosomes by cathepsins, which are activated by interacting with glycosaminoglycans (GAGs) (75). The degradation of endocytosed GAGs within lysosomes is highly ordered and involves endoglycosidases, exoglycosidases, sulfatases, and non-catalytic proteins.

Physiological mechanical stimulation is necessary for homeostasis of normal cartilage. Mechanical load causes movement of synovial fluid, and facilitates the diffusion of molecules between the cartilage and synovial fluid that is important for the nutrition of cartilage (76). Mechanical stimulation increases ACAN production and reduces MMP3 expression by human chondrocytes, and inhibits IL1α and TNFα-induced catabolic processes (77, 78). Sensors of mechanical stimulation in chondrocytes include integrins, cell surface receptors such as syndecans, and the primary cilium.

The primary cilium is a non-motile organelle that projects from the cell to function as a mechanical sensor and contributes to cartilage homeostasis through

regulation of intracellular signalling (79, 80). Detection of mechanical stimulation by the primary cilium in chondrocytes is exerted through integrins and calcium channels (81). Primary cilia are critical for chondrocyte organisation and normal deposition of matrix constituents (82, 83). The primary cilium regulates hedgehog (HH) signalling pathways in chondrocytes, important for the maintenance of normal articular cartilage structure (82). Furthermore, induction of inflammatory pathways involving prostaglandin E2 (PGE2) and nitric oxide (NO) in chondrocytes are also regulated by the primary cilium (84).

Due to the avascular nature of articular cartilage and a long diffusion distance from nourishing arteries, chondrocytes are particularly well adapted to survival in a hypoxic tissue microenvironment. Oxygen and nutrients are delivered to the articular cartilage from the vascular supply to the joint capsule, synovium, and subchondral bone. Hypoxia promotes a protective environment for chondrocyte metabolism in which production of Col II is relatively high, and the release of IL1α, TNFα, MMP1 and MMP13 are relatively low, compared to normoxic conditions (85, 86). Hypoxia inducible factor 1α (HIF1α) protein levels are responsive to tissue oxygen levels; it is present in cartilage and is crucial in promoting chondrocyte activity and viability (87).

1.2.2.9 Mechanobiology of articular cartilage

Mechanical loading results in compression of articular cartilage, deformation of the ECM, and stimulates chondrocyte metabolism. Unloading of articular cartilage leads to an influx of nutrients into the cartilage from the adjacent synovial fluid. Different joints are exposed to different compressive forces, with pressures of between 0.1 to 4 megapascal (MPa) occurring in human hip joints during walking (88). During monolayer chondrocyte cell culture, cyclical mechanical stimulation and intermittent hydrostatic pressure at physiological levels leads to increase ACAN and Col II gene expression (89). In three-dimensional (3D) chondrocyte cultures, intermittent dynamic compression, or strain, at physiological levels also increases proteoglycan synthesis and proliferation of chondrocytes (90, 91). Cyclical compression of cartilage explants also

stimulates the expression of fibronectin and COMP (92). In contrast to mechanical loading within a physiological range, static and pathological mechanical forces induce catabolic responses in articular cartilage with increased expression of MMP3, MMP9, MMP13, IL1β and TNFα, and reduced expression of ACAN and Col II (93, 94). Compression of articular cartilage also leads to changes in the ECM, chondrocyte metabolism, hydrostatic pressure gradients, water content of the ECM, the osmotic pressure gradient, and concentration of ions (95). Chondrocyte mechanoreceptors, including mechanosensitive ion channels, integrins, the primary cilium, and non-selective cell surface channels, mediate mechanotransduction in cartilage (96).

The pericellular matrix (PCM) is a 1-5 μm region that surrounds the chondrocyte. In the PCM, Col VI and perlecan are highly expressed, whereas the expression of Col II is relatively low compared to the surrounding matrix (97). The PCM has fundamental mechanosensing properties and may amplify mechanical signals transmitted through the ECM (98). Transmission of mechanical signals from the ECM may be mediated by interaction of the chondrocyte with molecules within the PCM, such as integrins and discoidin domain receptors (99). Biglycan and decorin are small leucine rich repeat molecules that may connect type II and type VI collagen between the PCM and territorial matrix (100).

Mechanical stimulation of cartilage results in the activation of ion channels in chondrocytes, permitting the influx of ions such as calcium, and leads to the activation of intracellular signalling pathways. This is associated with alterations of the actin cytoskeleton and activation of intracellular signalling molecules including phospholipase C, calmodulin, tyrosine protein kinase, and protein kinase C (88). Loading of chondrocytes also leads to hyperpolarisation of the cell membrane due to activation of slow conductance Ca^{2+} sensitive K^{+} channels (101). Mechanical stimulation of chondrocytes also activates stretch activated calcium channels, L-type calcium channels, which are involved in the regulation of protein synthesis in response to mechanical loading (102).

Integrins are heteromeric transmembrane glycoproteins that consist of α and β subunits, the combination of which contributes to the ligand specificity of the receptor. Integrins

are located between the ECM and the chondrocyte cytoskeleton and act as mechanoreceptors. Chondrocytes express several integrins in healthy adult cartilage *in situ* (103). The α5β1 integrin is an important mechanoreceptor in articular chondrocytes, which can control the flow of K^+ ions across the cell membrane, activation of cell signalling molecules, expression of COMP, and regulation of proteoglycan synthesis in response to dynamic mechanical stimulation (104, 105). Integrin mechanoreceptor expression and interaction between integrins and the ECM are also modulated by growth factors. Both IGF1 and TGFβ increase chondrocyte cell surface expression of integrins and stimulate adhesion of chondrocytes to fibronectin and Col II (106). Basic fibroblast growth factor (bFGF) also mediates the release and activation of chondrocyte growth factors from within the ECM (107). In response to mechanical stimulation, both bFGF and integrin-mediated signalling induce ERK activation. Substance P can also regulate integrin activity (108). IL4 is another important mediator of electrophysiological responses by chondrocytes to mechanical stimulation. IL4 is another important mediator of chondrocyte responses to loading, and can stimulate increased expression of ACAN by influencing integrin signalling pathways (78, 108). G-protein coupled receptors (GPCRs) are also involved in hyperosmotic stress induced volume changes and calcium flux in chondrocytes, and may be associated with integrins in mechanotransduction (109). Cyclic adenosine monophosphate (cAMP) activates protein kinase A and is also an important mediator of chondrocyte responses to mechanical stimulation (110).

Chondrocyte volume is directly influenced by osmolarity, and this has a significant effect on cellular responses by chondrocytes, including ECM metabolism (111). Alterations of the osmotic environment regulate the expression of the chondrogenic transcription factor Sox9, which may regulate expression of genes encoding ECM proteins, including *Col2a1* and *ACAN* (112). Increasing osmolarity results in reduced chondrocyte necrosis following pathological loading and iatrogenic injury to cartilage (113-115). Osmotic changes also initiate signalling cascades that involve regulation of intracellular Ca^{2+} concentration, which play a role in chondrocyte cell death (116-118). The mean osmolarity of human synovial fluid is approximately 400 milliosmoles (mOsm). Cartilage contains a high concentration of free cations, predominantly Na^+, and a low concentration of free anions, mainly Cl^-, compared to the

surrounding synovial fluid (119). Proteoglycans carry fixed negative charges and attract a high concentration of cations. The local proteoglycan concentrations in cartilage therefore determine the ionic composition and extracellular osmolarity of cartilage. The extracellular osmolarity within cartilage is higher than that in the surrounding tissues, and the resultant swelling pressure is resisted by an intact collagen network (114). Consequently, the net result of ECM degradation, such as occurs in OA, is cartilage swelling and a decrease in extracellular osmolarity (114).

1.2.2.10 Aggrecanolysis and degradation of ECM macromolecules in OA

Degradation of collagen and ACAN in the ECM of cartilage is key to the pathogenesis of OA. ACAN is a large proteoglycan containing the hydrophilic GAGs chondroitin sulphate and keratan sulphate, which confer resistance to compressive forces upon articular cartilage. Proteolysis of ACAN occurs at several sites along the protein. In the development of OA, the most important site of cleavage of ACAN is in the interglobular domain (IGD) between the N-terminal G1 and G2 globular domains. Cleavage of ACAN at this site releases the GAG-binding region of ACAN, leading to loss of both GAGs and the function of ACAN. Studies demonstrating cartilage degradation following treatment with papain or vitamin A provided initial evidence that cartilage proteoglycans, of which ACAN is the most abundant, are vulnerable to proteolytic degradation (120, 121). Metalloproteinases present in both bone and cartilage were identified as able to degrade proteoglycans at a physiological neutral pH (122, 123). MMP3 present in human articular cartilage was subsequently demonstrated as capable of cleaving the Asn^{341}-Phe^{342} bond in the IGD of ACAN (124). This site has also been found to be cleaved by other MMPs including MMP1, MMP2, MMP7, MMP8, MMP9, and MMP13, which may also act at additional cleavage sites at the C-terminus of ACAN (125-127).

However, the majority of ACAN fragments present in synovial fluid of patients with OA are generated from cleavage at the Glu^{373}-Ala^{374} bond, rather than at the Asn^{341}-Phe^{342} site of the IGD (128). *In vitro* studies in bovine and murine cartilage

subsequently identified several ADAMTS metalloproteinases as capable of cleavage of ACAN at the Glu^{373}-Ala^{374} bond site in the IGD (129). *In vitro* and *in vivo* studies in KO mice demonstrated that ADAMTS-5, followed by ADAMTS-4, is the most active aggrecanase in articular cartilage and of most pathological significance to the development of OA (124, 130). ADAMTS4 mRNA is induced by cytokines such as IL1β and TNFα in human cartilage and chondrocytes, but ADAMTS5 mRNA is not regulated by cytokines and it expressed more constitutively in human cartilage (131). The relative contribution of ADAMTS-4 and ADAMTS-5 in pathological degradation of human cartilage is incompletely understood, as their activity is influenced by multiple processes including promoter activity, epigenetic modifications, alternative splicing, and non-coding RNA activity (132). However, proteolysis of ACAN at the Glu^{373}-Ala^{374} site is the most important mechanism of pathological aggrecanolysis in osteoarthritic cartilage. Aggrecanolysis at the Asn^{341}-Phe^{342} site may also occur to a lesser extent during advanced stages of OA. Cleavage of ACAN at the Asn^{341}-Phe^{342} C-terminal site by MMPs has less pathological significance as it does not result in the release of the GAG-binding region of ACAN (133).

The order in which the principal components of the ECM of cartilage are degraded in the development of OA is incompletely understood, though *ex vivo* studies indicate that collagen degradation is initiated only after depletion of ACAN from cartilage has occurred (134). Loss of collagen, but not ACAN, is an irreversible process in the progression of OA (135). MMP13 is the most significant collagenase in the development of OA, possibly due to its very deep S_1' subsite (136). MMP3 is the most abundant MMP in osteoarthritic cartilage, though its expression may be reduced in end-stage OA (137). MMP3 may activate other MMPs, including MMP1 and MMP13, contributing to the development of OA by activating other latent collagenases (138).

1.2.2.11 COMP

The degradation of COMP may also have a significant role in the pathogenesis of OA. COMP fragments have been demonstrated in cartilage and synovial fluid of patients with primary OA (139). Several MMPs and ADAMTS4 have been identified as capable

of cleaving COMP (140). IL1β and TNFα also induce expression of ADAMTS7 and ADAMTS12, which can degrade COMP (141). COMP also interacts with granulin-epithelin precursor (GEP). GEP is a growth factor expressed by chondrocytes. GEP inhibits ADAMTS7 by inhibiting the effect of TNFα and by directly interrupting the association of ADAMTS7 and ADAMTS12 with COMP. As such, ADAMTS7, ADAMTS12, COMP, GEP, and inflammatory cytokines interact to also regulate the degradation of the ECM.

1.2.2.12 Retinoic acid

Retinoic acid (RA) is also a potent inducer of aggrecanolysis. ACAN fragments generated by ADAMTS4 and ADAMTS5-mediated cleavage have been identified in response to retinoic acid (142). RA is preferentially bound by the α, β, and γ retinoic acid receptors (RARs). In chondroprogenitor cells, activation of retinoid receptors decreases Sox9 activity at the *Col2a1* enhancer and reduces the content of GAGs in the ECM (143). Increasing RA levels accelerates hypertrophy of chondrocytes, and contributes to the progression of degenerative joint diseases (144). RARs have a prominent role in growth plate and skeletal development, and regulate both ACAN expression and content (145). RA also regulates MafB, a transcription factor that mediates chondrocyte gene expression and ECM formation through regulation of ACAN, MMP3, and MMP13 expression (146).

1.2.3 Subchondral bone

The subchondral bone is porous and calcified, provides structural support for overlying articular cartilage, is separated from the articular cartilage by calcified cartilage, and may be divided into cortical and trabecular regions (147). The thin layer of cortical subchondral bone is hypovascular, non-porous, and calcified. The cortical subchondral bone is supported by trabecular subchondral bone, which is cancellous and less dense, and contains the haematopoietic bone marrow (148).

Osteoid, also known as unmineralised bone matrix, comprises a fibrillar network of type I collagen (Col I) and mucopolysaccharide. Homeostasis of the bone matrix is maintained by the coordinated activity of osteoblasts, osteoclasts, and osteocytes (149). Osteoblasts derive from MSCs and are responsible for the synthesis of the substance of bone matrix. Soon after osteoid is synthesised, inorganic salts are deposited in the osteoid to form mineralised bone. Osteoblast differentiation is initiated by BMPs that induce the expression of the transcription factors *Runx*2 and *osterix* (150). As osteoblasts mature, they may become encompassed by mineralised osteoid and develop into osteocytes, or survive at the bone surface as inactive osteoblasts (148). Osteoclasts differentiate from macrophages and function primarily to resorb mineralised bone matrix through the secretion of hydrogen ions and proteolytic enzymes that degrade the hydroxyapatite nanocrystals and Col I network, respectively. The differentiation of promyeloid precursors into osteoclasts is stimulated by receptor activator of nuclear factor (NF)-κB ligand (RANKL), osteoprotegerin ligand (OPGL), and osteoclast differentiation factor (ODF) (151).

The remodelling of bone involves the action of several cytokines including RANKL (also known as tumour necrosis factor ligand superfamily member 11 (TNFSF11), TNF-related activation-induced cytokine (TRANCE), OPGL, and ODF. RANKL binds the receptor activator of nuclear factor NFκB (RANK) receptor, activating a signalling pathway that culminates in osteoclastogenesis and bone resorption (148). The activity of RANKL is antagonised by osteoprotegerin (OPG), which can effect osteoclast apoptosis (151). Endocrine factors, including parathyroid hormone, calcitriol, and vitamin D3 also affect bone matrix homeostasis by regulating calcium levels. The metabolic activity of bone can also be regulated by thyroid hormones, systemic glucocorticoids, and oestrogen. The principal growth factors affecting bone remodelling include IGF, FGF, TGFβ, BMPs, and vascular endothelial growth factor (VEGF), and the cytokines IL1β and TNFα promote osteoclast differentiation, whereas IL6 is involved in the coupling between both bone formation and resorption (152, 153).

1.2.4 Joint pathology and progression of OA in articular cartilage

OA develops due to failure of the repair mechanisms of cartilage in response to biochemical and biomechanical changes in the joint. During the early phases of OA, clusters of chondrocytes develop in areas of degenerate cartilage with an associated increase in concentration of growth factors in order to effect cartilage regeneration (154). As cartilage repair fails, the production of the degradative proteinases such as MMPs and aggrecanases increases, chondrocyte apoptosis increases, and ECM synthesis becomes insufficient, resulting in an ECM that cannot tolerate physiological mechanical stress (155). Thus, articular cartilage gradually degenerates due to an imbalanced synthesis and turnover of ECM. Clinical symptoms and signs often develop relatively late in the disease process, at which point the innervated and more vascular components of synovial joints may also be affected.

Although cartilage is particularly affected by the pathophysiology of OA, an integrated process involving subchondral bone and synovial tissue to varying degrees of severity exists (156). Inflammation and hypertrophy of the synovium correlates closely with clinical signs and symptoms in patients with OA, such as joint effusion and pain; synovitis develops in response to increasing fragmentation of cartilage and catabolic cytokines present in the synovial fluid. In response, synovial macrophages secrete inflammatory mediators, further disrupting the normal homeostasis of articular cartilage (157). Characteristic changes that develop in subchondral bone include osteophyte formation, remodelling, sclerosis, and cystic changes. Synovitis and subchondral bone changes develop gradually throughout the progression of OA from mild to severe joint disease (158).

1.2.4.1 Effects on chondrocytes, cartilage homeostasis, and ECM

During the development of OA, articular chondrocytes undergo a phenotypic shift from a normal quiescent state to an activated state, typified by chondrocyte proliferation, formation of clusters, abnormal hypertrophy, and an increased synthesis of matrix proteins and MMPs (159). This is associated with increased calcification of cartilage by

chondrocyte-derived apoptotic bodies, advancement of the cartilage tidemark, and vascular invasion from the underlying subchondral bone (160).

Hypertrophic chondrocytes in osteoarthritic cartilage express genes encoding RUNX2, MMP13, and Col X. The normal pattern of primary cilia on the chondrocyte also becomes dysregulated in OA, which may be a direct cause of, or result from the loss of, cartilage homeostasis (82, 161). Vascular invasion of the osteochondral junction exposes cartilage to soluble mediators secreted by osteoblasts and osteoclasts; TGFβ1 is produced by osteoclasts of the subchondral bone upon initiation of OA, and 14-3-3ε protein secreted by osteoblasts directly stimulates chondrocytes to secrete catabolic cytokines (162, 163). As neovascularisation of the calcified cartilage progresses, sensory nerve terminations also develop, which may sensitise the subchondral junction, and correlate with exacerbation of clinical symptoms (164). Exacerbation of pain in OA also correlates with the development of lesions in the adjacent bone marrow.

1.2.4.2 Molecular mechanisms related to OA pathogenesis

The primary enzymes responsible for the degradation of cartilage are zinc-dependent metalloproteinases, including MMPs and ADAMTSs enzymes. The main collagenases are MMP1 and MMP13, the latter being particularly effective in the degradation of Col II, and also MMP3, which is highly efficient in activating both aggrecanase and additional MMPs. ADAMTS4 and ADAMTS5 also act predominantly as aggrecanases in articular cartilage. In OA, the normal balance between TIMP3 and ADAMTS4 synthesis is disturbed in favour of catabolism. This disturbance could be attributed to *de novo* synthesis of ADAMTS4 and may also involve post-translational activation of ADAMTS4 and ADAMTS5 (165, 166). Cathepsin-K, in addition to other serine and cysteine proteases, is another matrix-degrading enzyme acting within cartilage (167).

The arrangement of chondrocyte integrin receptors responds to detected alterations in mechanical stress or inflammatory stimuli. The association of Col II with proteoglycans in the interterritorial region of cartilage usually protects against degradation of Col II. Depletion of ACAN and activation of MMPs both contribute to the initiation of cartilage erosion; disruption of the collagen fibrillar network heralds subsequent irreversible cartilage degradation (168, 169).

The expression of MMPs by chondrocytes may be induced by biomechanical stress and in response to matrix degradation. A mechanism by which mechanical stimulation can initiate MMP expression may involve the breakdown of the chondrocyte pericellular matrix by the protease High Temperature Requirement A1 (HTRA1) that then permits discoidin domain receptor 2 (DDR2) to interact with Col II, thus increasing expression of MMP13 (170, 171). As proteins of the ECM are degraded in osteoarthritic cartilage, chondrocyte integrin receptors detect fragments of matrix proteins, such as fibronectin, small leucine-rich proteoglycans, and collagen and initiate the production of pro-inflammatory cytokines, chemokines, and MMPs (172, 173). The innate immune system may also be activated in response to the presence of matrix degradation products in osteoarthritic cartilage. Fibromodulin and decorin, which are members of the small leucine-rich proteoglycan family, may activate the classic complement pathway, whereas COMP is an efficient activator of the alternative complement pathway, and

synovial fluid from osteoarthritic joints contain complexes of COMP and complement 3b (C3b) (174).

In addition to activation of MMPs, mechanical stimulation induces the production and release of cyclooxygenase-2 (COX2), microsomal prostaglandin E synthase-1 (mPGES1), soluble phospholipase A2 (sPLA2), and inducible nitric oxide synthase (NOS2) in osteoarthritic cartilage. These pro-inflammatory mediators are detected by chondrocytes, particularly those in clonal clusters, and respond by upregulating the expression of MMPs and pro-inflammatory cytokines (175). Subsequent cartilage degradation may be mediated by chondrocytes through both IL1β-dependent and IL1β-independent signalling pathways (176).

Abnormal biomechanical stress also stimulates the activation and translocation of NFκB, and mitogen-activated protein kinase (MAPK) signalling pathways, thereby influencing the expression of downstream target genes including *MMP13*, *NOS2*, *COX2*, *ADAMTS*, and *IL1β* (177, 178). Whether or not these are primary or secondary processes in cartilage degradation is not certain, but does indicate mechanisms by which feedback amplification and further matrix destruction may occur. Additional signalling pathways activated in osteoarthritic cartilage and which regulate the catabolic activity of chondrocytes include the extracellular-regulated kinase (ERK), c-Jun N-terminal kinase (JNK), and p38 MAPK cascades (175). Increased release of reactive oxygen species (ROS) through mechanical stress and generation of fragments of matrix proteins may also contribute to chondrocyte necrosis (179). With increasing severity of OA, the ability of chondrocytes to undergo autophagy, normally a protective mechanism for cells under physiological stress, also reduces (180).

Osteoarthritic articular tissue also demonstrates a specific chemokine profile, with an increased expression of chemokine (C-C motif) ligand 19 (CCL19) and its ligand C-C chemokine receptor 7 (CCR7), correlating with exacerbation of joint symptoms in patients with OA (181). The recruitment of an inflammatory cell infiltrate into osteoarthritic joint tissue may in part be modulated by damage-associated molecular patterns (DAMPs), also known as alarmins, that interact with Toll-like receptors (TLRs)

expressed by chondrocytes with an increased abundance in OA (182, 183). DAMPs such as S100 calcium-binding protein A11 (S100A11) can enact chondrocyte hypertrophy and catabolic activity (184). A 32-mer ACAN cleavage fragment can also act as a DAMP, increasing MMP13 and ADAMTS5 expression and decreasing Col II and ACAN expression, effects that are NFκB dependent and mediated through TLR2 (185). High-mobility group box protein (HMGB) can potentiate the response of chondrocytes to DAMPs and contribute to a hypertrophic phenotypic shift of chondrocytes during the development of OA (186).

A low-grade systemic inflammatory state associated with obesity may significantly contribute to the established association of an increased risk of OA in overweight patients. Mediators of joint inflammation may include adipokines produced by white adipose tissue acting as an endocrine tissue, or locally by chondrocytes. The expression of adipokines by chondrocytes can be stimulated by inflammatory cytokines, and adipokines such as leptin, adiponectin, and visfatin can increase the expression of MMPs and NOS2 by chondrocytes (187-189). Although an association with dysregulated cartilage homeostasis is recognised, the exact mechanisms by which individual adipokines contribute to the development of OA have not yet been determined.

1.2.5 Grading of OA

The diagnosis and monitoring of joint tissue damage currently utilises surrogate markers of actual joint degeneration. Biomarkers of OA are not yet validated for use in clinical practice. Cartilage can be visualised directly by arthroscopy, but this requires an invasive procedure and may not be sufficiently sensitive to detect different stages of joint degeneration and regeneration (190). Plain radiography is the gold standard for imaging of osteoarthritic joints. The severity of OA can be graded radiographically using the Kellgren and Lawrence classification (191). This classification system examines osteophyte formation, joint-space narrowing, and bone sclerosis in affected joints and it has been adapted to analyse radiographic features of hand, hip, and knee

joints (192). The most important variable in reproducibility of radiographic grading of OA is standardisation of the radiographs. Ultrasound may be used to examine osteoarthritic joints and is beneficial in evaluating the soft tissue changes associated with OA, but ultrasound is limited as a grading tool as it is very dependent on the experience and skill of the operator (193). Computed tomography (CT) can provide three-dimensional joint analysis, but, in addition to the disadvantages of plain radiography, requires a high radiation exposure (194). Magnetic resonance imaging (MRI) can provide detailed quantitative evaluation of the morphology and integrity of articular cartilage but is relatively expensive, time-consuming, and complex to analyse (195).

The first histological grading system to evaluate cartilage degeneration was described by Collins and McElligott, in which sulphate uptake by chondrocytes correlates with cartilage structural changes; hypertrophic chondrocytes present in osteoarthritic cartilage exhibit increased sulphate uptake (196). The Mankin system grades cartilage degradation by determining glycosaminoglycan content by Safranin-O staining, assessing cellularity and scoring structural changes involving the tidemark. The most validated histological system for grading cartilage degeneration due to OA is the OARSI score. The OARSI score incorporates the histological staining described by Mankin with staging criteria depending on the depth of the cartilage erosion (197). The OARSI grading system is shown in Figure 1.3.

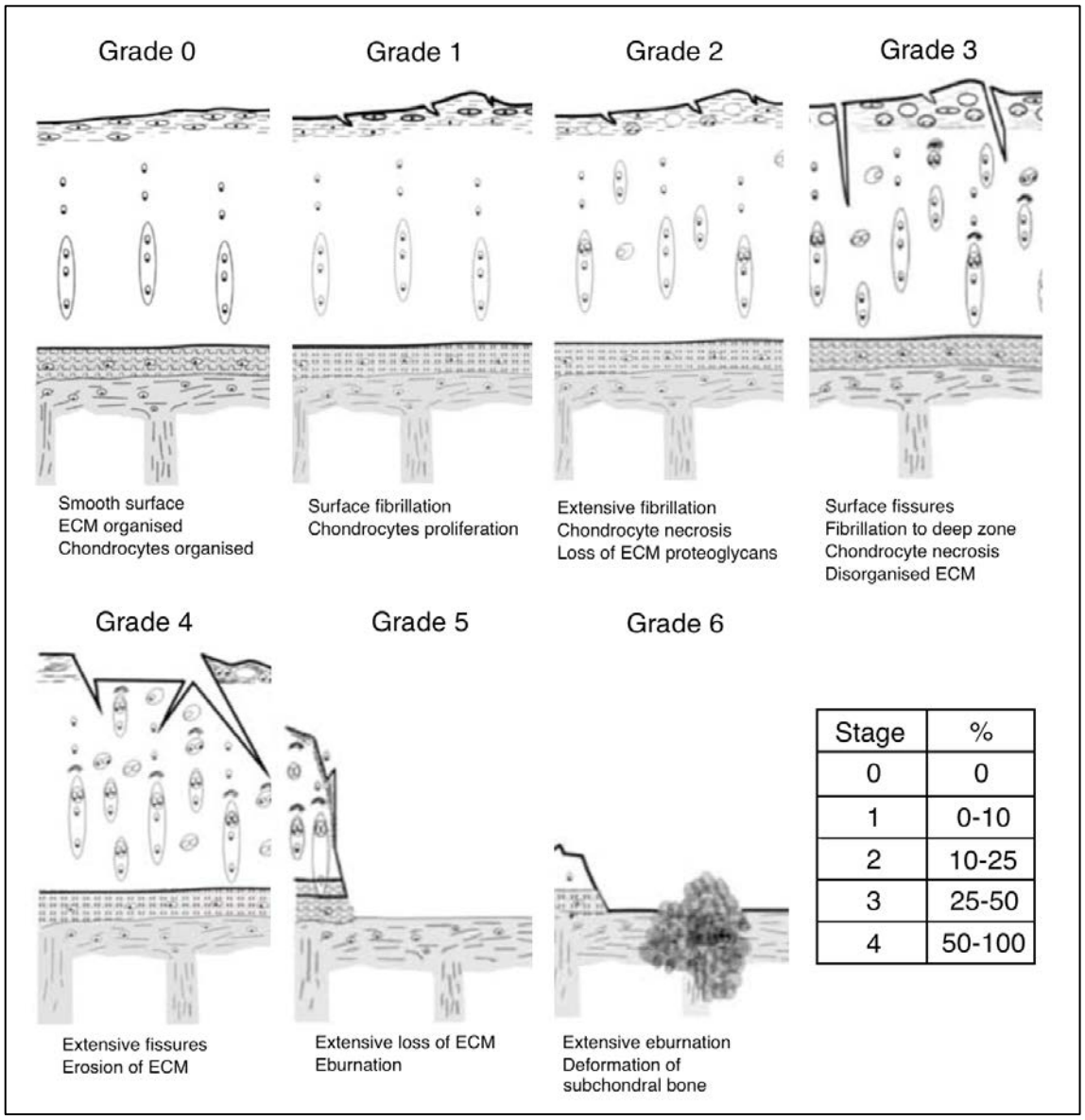

Figure 1.3 – OARSI histological grading system for OA in human articular cartilage; the histopathological features of each grade are shown. Staging describes the percentage area of affected cartilage. Adapted from Pritzker et al (197).

1.3 Evidence for a genetic predisposition to OA

OA is considered to be a complex disease, the development of which is influenced by environmental, genetic, mechanical and systemic factors. The genetic influence on susceptibility to OA is polygenic. As for other diseases caused by complex trait genetics, susceptibility to OA is likely to be conferred by several common genetic variants each exerting a moderate effect on disease susceptibility (198). In addition to multiple genetic risk loci with modest individual effects, interrogation of the genetic susceptibility to OA is made challenging by the phenotypic variability associated with joint degeneration, with multiple phenotypes such as pain, joint morphology, and joint-space narrowing each representing separate endophenotypes that may have different genetic aetiologies (199, 200). Distinct genetic predisposition may also exist for the association of OA with different ethnic groups, gender, and joints (198). Identification of genetic risk loci in affected populations therefore requires adequate sample size, carefully defined subjects, and robust phenotypic characterisation.

In most ethnic groups OA is relatively common, with varying estimates of prevalence and incidence depending on the individual joints assessed, methods of detection, and diagnostic criteria. Prior to the advent of large-scale molecular genetic analyses, several epidemiological studies demonstrated a compelling genetic contribution to the susceptibility of OA, and characterising OA as a disease with a complex, polygenic predisposition. Familial inheritance of Heberden's nodes, a cardinal feature of OA of the hand, was first described in 1941, with an increased incidence in females (201). An early epidemiological study in the UK also implied a polygenic predisposition to the development of both Heberden's nodes and more generalised OA (202). The Framingham Offspring Study and the Baltimore Longitudinal Study of Aging demonstrated an increased risk of developing hand and knee OA among persons with affected relatives and that inheritance of susceptibility to OA exhibited a recessive Mendelian pattern (203, 204). Several European sibling studies also demonstrated that individuals with a sibling who had undergone joint replacement surgery for OA, were at an increased risk of developing OA themselves when compared to control subjects (205-209). As both shared environmental and genetic factors may influence disease

susceptibility amongst related individuals, the genetic contribution to OA was further examined in twin studies, which can better scrutinise the genetic contribution to the development of disease independent of environmental risk factors. In a classic twin study of mono- and di-zygotic female twins, it was estimated that the heritability of hand and knee OA was between 39-65%, and subsequently, in an extension of this study heritability for hip OA was estimated at 60% (210, 211). Interestingly, similar estimates of heritability for hip OA have been reproduced in studies of hip OA amongst mono- and di-zygotic male twins in the United States of America (USA).

Epidemiological studies of OA susceptibility thus indicated that the disease exhibited a non-Mendelian, and likely complex polygenic pattern of inheritance. The genetic susceptibility to OA was subsequently investigated further in genetic linkage studies of small- to medium-sized cohorts, identifying broad genetic regions associated with the development of OA. More significant progress in identifying OA risk alleles has been achieved recently using genome-wide association (GWAS) in large case-control studies and detailed sampling of polymorphic markers. GWAS studies have further been complemented by expression and functional studies in joint tissues that have begun to elucidate the molecular mechanisms that are responsible for the genetic predisposition to OA.

1.3.1 Linkage studies and candidate genes

Linkage studies, or genetic association analyses, utilise genetic markers such as single nucleotide polymorphisms (SNPs) and short tandem repeats (microsatellites) to identify regions of genetic linkage that co-segregate with OA phenotypes. Using this methodology, several candidate genes have been identified as containing risk alleles for OA and supported on the basis that the encoded proteins modulate joint development, maintenance or morphology (212). These studies have highlighted that OA risk alleles are often specific to ethnic groups or individual joints; this is a reflection of the differing frequencies of risk alleles and genetic background in populations of different ethnicity,

that non-genetic factors also influence the effect of the risk alleles, and that OA may be a more joint-specific disease rather than a systemic skeletal condition.

The *GDF5* (growth differentiation factor 5) gene located on 20q11.2 is the most established candidate association signal for OA, which was initially interrogated due to its role in skeletogenesis (213). *GDF5* encodes growth differentiation factor 5, which is a growth factor belonging to the TGFβ superfamily (214); the associated single nucleotide polymorphism (SNP) rs143383 (rs; reference SNP) has been associated with knee OA in both European and Asian populations at highly significant levels of $p < 5.0 \times 10^{-8}$ (215, 216). A meta-analysis study including both European and Asian cohorts later also identified an association with hip OA (217). A further meta-analysis of the rs143383 in association with knee OA in only European cohorts achieved genome-wide significance ($p = 4.1 \times 10^{-11}$; odds ratio (OR) 1.18, 95% confidence interval (CI) 1.12 - 1.23) (218). This variant exerts its effect by regulating *GDF*5 transcription, whereby the susceptibility allele results in reduced expression levels (213). The differential allelic expression is itself regulated by four trans-acting factors Sp1 (trans-acting transcription factor 1), Sp3, P15, and DEAF-1 (deformed epidermal autoregulatory factor 1 homolog) that bind differentially to the alleles of rs143383 (219). DEAF-1, Sp1, and Sp3 form a repressive complex that binds and differentially modulates the expression of the C (cytosine) and T (thymine) alleles, whereas P15 may interact with this complex and other transcription factors (219).

Linkage analysis also identified the *DIO2* (type II iodothyronine deiodinase) gene, which is located at 14q24.2 - q24.3 and encodes the D2 (deiodinase 2) enzyme determining the availability of locally active thyroid hormone, as a susceptibility gene for OA (220). Differential allelic expression of *DIO2* messenger ribonucleic acid (mRNA) has been demonstrated in musculoskeletal tissue, with the effect allele over-expressed relative to the wild-type allele in heterozygous (HET) individuals, implicating a functional role for genetic variation at *DIO2* in susceptibility to OA (221). Upregulation of *DIO2* may mediate upregulation of cartilage degrading enzymes including MMP13 and ADAMTS5 (222).

SMAD3 (SMAD family member 3) is another highly compelling candidate association signal for OA; this association relates to the common SNP rs12901499 within intron 1 of the gene region. *SMAD3* encodes an intracellular signal transducer that is also involved in the TGFβ pathway, and the rs12901499 risk allele was associated with both knee OA ($p = 7.5 \times 10^{-6}$; OR 1.22, 95% CI 1.12 - 1.34) and hip OA ($p = 4.0 \times 10^{-4}$; OR 1.22, 95% CI 1.09 - 1.36). Furthermore, rare and penetrant haploinsufficient mutations within *SMAD3* are also associated with the development of the aneurysms-OA syndrome, which is characterised by early-onset OA and vascular malformations (223). That both SNPs, which likely exert modest effects on gene function, (such as rs12901499) and detrimental mutations in *SMAD3* both result in similar OA phenotypes strongly implicate *SMAD3* as a candidate gene for susceptibility to OA.

1.3.2 Genetic association analysis and GWAS

In contrast to candidate gene studies, GWAS utilise a hypothesis-free approach to discover genetic susceptibility loci for complex diseases such as OA. Using high throughput microarrays, millions of SNPs may be genotyped in tens of thousands of affected individuals and disease-free control subjects. The strength of association of implicated variants is enhanced by initially genotyping a discovery cohort of both cases and control subjects, and subsequently prioritising any SNPs significantly associated with disease status for replication in a second larger cohort (224).

GWAS utilise the co-segregation of alleles within the same genetic region, termed linkage disequilibrium (LD), to refine the number of SNPs required to be genotyped; several hundred thousand SNPs can be used to sufficiently cover over 85% of the Caucasian genome (225). As SNPs identified in GWAS studies as associated with disease status may not be the causal variant, but only in LD with the true causal variant, more detailed interrogation of the genetic loci surrounding implicated risk alleles is required (225). Additional genotyping of susceptibility can be performed by imputing information from data sets such as HapMap (http://hapmap.ncbi.nlm.nih.gov/) and 1000 Genomes Project (http://www.1000genomes.org/) to determine the extent of regions

with LD at susceptibility loci (226). Fine-mapping of focused regions represented by the disease-associated allele can subsequently be performed, to discover true causal variant(s) and subsequently to perform functional studies in the relevant biological tissues, to further validate potential susceptibility genes in the pathogenesis of OA (227). By adopting a hypothesis-free study design and sampling the whole genome, GWAS enables the identification of novel pathways associated with complex diseases.

1.3.2.1 arcOGEN and GWAS in OA

The Arthritis Research UK OA Genetics Consortium (termed arcOGEN) study is the most powerful published GWAS investigating patients with OA (228, 229). It was the first GWAS investigating OA to identify multiple novel independent susceptibility loci with significance beyond the genome-wide significance threshold ($p < 5 \times 10^{-8}$) required after adjusting for the multiple tests performed during GWAS. The multicentre arcOGEN study investigated patients of European ancestry with primary OA of the hip or knee, defined as radiographic evidence of advanced disease (Kellgren-Lawrence grade ≥ 2), of which 80% of patients had undergone total joint replacement (TJR). All cases were genotyped using the Illumina® 610-BeadChip, and genotypes for disease-free control subjects were retrieved from public databases including the Wellcome Trust Case Control Consortium (WTCCC), Type 1 Diabetes Genetics Consortium (T1DGC), Avon Longitudinal Study of Parents and Children (ALSPAC).

In the initial stage 1 of arcOGEN, genotyping was performed in 3177 OA cases and 4894 control subjects for 514898 SNPs. In this interim analysis of 43.8% of the full GWAS sample size, SNPs associated with disease status were then replicated *in silico* in 4124 OA cases and 37581 control subjects. Meta-analysis of 36 SNPs were selected for *de novo* replication in a further 6188 OA cases and 8280 control subjects and *in silico* replication in 213 OA cases and 2531 control subjects. None of the identified association signals in stage 1 of arcOGEN reached genome-wide statistical significance (228). This lack of success indicated that the genetic architecture of OA is likely to

consist of several signals of modest effect necessitating large sample sizes for their detection at genome-wide significance levels.

The results of the full-scale GWAS were reported in stage II of arcOGEN, which performed genotyping of 485491 SNPs for 7410 unrelated OA cases and 11009 unrelated control subjects from the UK (229). The most promising SNPs were then replicated *in silico* in 7473 OA cases and 42938 control subjects of either UK or European descent. Meta-analysis of discovery and replication cohorts identified five genome-wide significant loci ($p < 5.0 \times 10^{-8}$; Table 1.1) for association with OA and three loci just below this threshold. Three of the five genome-wide significant signals were specific for OA of the hip joint only, and did not show association with OA of the knee joint. This further indicated that the molecular genetic susceptibility to OA is not uniform across joint sites by demonstrating that a polymorphism (SNP) can be associated with OA at the hip without exhibiting association also at the knee, corroborating similar findings from epidemiological studies (230).

Locus	SNP	Effect Allele	Nearest Gene	Protein Function	Gene Region	p-value (discovery & replication)	Odds Ratio (95% CI) (discovery & replication)
3p21.1	rs6976	T	*GLT8D1*	Glycosyltransferase	3' UTR	7.24×10^{-11}	1.12 [1.08-1.16]
	rs11177	A	*GNL3*	Nucleotide-binding protein	Exon 3	1.25×10^{-10}	1.12 [1.08-1.16]
9q33.1	rs4836732	C	*ASTN2*	Cell membrane protein	Intron 18	6.11×10^{-10}	1.20 [1.13-1.27]
6q13-q14.1	rs9350591	T	*FILIP1*	Neocortical cell migration	38kb upstream	2.42×10^{-9}	1.18 [1.12-1.25]
			SENP6	Sumoylation/post-translation protein modification	70kb upstream		
12p11.22	rs10492367	T	*KLHDC5*	Unknown	59kb downstream	1.48×10^{-8}	1.14 [1.09-1.20]
			PTHLH	Endochondral bone development	96kb downstream		
12q23.3	rs835487	G	*CHST11*	Chondroitin sulfotransferase	Intron 2	1.64×10^{-8}	1.13 [1.09-1.18]

Table 1.1 – New genome-wide significant susceptibility loci for OA identified by stage II of arcOGEN study (229).

Of the five identified loci with genome-wide significant association for OA, the locus associated with the greatest effect size was at 9q33.1, tagged by the rs4836732

SNP (OR 1.2, 95% CI 1.13 - 1.27). This polymorphism was specifically associated with females requiring THR for primary OA (representing a severe OA phenotype), and is located within intron 18 of the gene *ASTN2* (astrotactin 2) (231). Two further protein-encoding genes are present at this locus, tripartite motif-containing protein 32 (*TRIM32*), and pappalysin 1 (*PAPPA*) (212). This OA susceptibility locus is discussed in detail in section 1.3.2.2.

The locus with the greatest statistical significance, but not effect size, for association with TJR for hip or knee OA was at 3p21.1 and was tagged by two SNPs in perfect LD with each other (see Table 1.1; $r^2 = 1$); rs11177, a missense polymorphism within exon three of the nucleostemin encoding gene guanine nucleotide binding protein-like 3 (*GNL3*) and rs6976, located in the 3' untranslated (3'UTR) region of the glycosyltransferase 8 domain containing 1 (*GLT8D1*) gene. Although the exact role of *GLT8D1* remains to be determined, the protein product belongs to the glycosyltransferase family of proteins (232); an altered pattern of glycosylation of articular glycoproteins or proteoglycans might alter their stability and subsequently the integrity of articular cartilage. *GNL3* encodes the protein nucleostemin, a member of the Y1qF/YawG GTPases family of proteins (GTP; guanine triphosphate), which migrates between the nucleolus and nucleoplasm in response to intracellular and extracellular signalling (233, 234).

The three further loci identified in the arcOGEN stage II study as having genome-wide significance were specific for OA of the hip joint (Table 1.1). The polymorphism rs9350591 is located on 6q13 - q14.1 and two genes, sentrin specific peptidase 6 (*SENP6*) and filamin A interacting protein 1 (*FILIP1*) lie in close proximity, and type XII collagen (α1 chain) (*COL12A1*) is positioned 326 kilobases (kb) downstream on chromosome 6: *COL12A1* is a fibril-associated collagen that regulates osteogenesis (235). Other genes within this susceptibility locus include transmembrane protein 30A (*TMEM30A*), cytochrome C oxidase subunit 7A2 (*COX7A2*), interphotoreceptor matrix proteoglycan 1 (*IMPG1*), and myosin VI (*MYO6*). Located within the locus tagged by rs10492367 is parathyroid hormone-like hormone (*PTHLH*), a strong candidate gene for OA due to its role in chondrocyte maturation, endochondral

ossification, and in human articular chondrocytes it up-regulates *COL2A1* through *SOX9* (236). Also contained within this locus and in close proximity to rs10492367 is kelch domain containing 5 (*KLHDC5*). The final SNP associated with OA at genome-wide significance was rs835487, which is contained within intron 2 of carbohydrate (chondroitin-4)-sulfotransferase (*CHST11*) that regulates glycosaminoglycan synthesis and growth factor signalling, chondrogenesis, and osteogenesis; RNA expression levels are dysregulated in degenerate cartilage, indicating a role for *CHST11* in the loss of normal cartilage homeostasis that occurs in OA (237, 238).

In addition to the five loci described, the arcOGEN study also identified three loci close to genome-wide significance. Firstly, rs12107036 located within intron 12 of tumour protein 63 (*TP63*) was associated with severe knee OA requiring TKR in female patients only. *TP63* has a fundamental role in limb, epithelial, and craniofacial development (239, 240). OA in females was also associated with the rs8044769 polymorphism, which resides within intron 1 of the fat mass and obesity associated gene (*FTO*). The *FTO* gene is also associated with susceptibility to obesity, which itself an established risk factor for OA (241). The only locus associated with OA specifically in male individuals was represented by the rs10948172 polymorphism. The genes in closest proximity to rs10948172 are suppressor of Ty3 homolog (*SUPT3H*), cell division cycle 5-like (*CDC5L*), and *RUNX2*, the latter of which is an important transcription factor in skeletogenesis (242).

Prior to arcOGEN, several susceptibility loci had been identified by GWAS in smaller cohorts and non-European populations. The rs7639618 SNP in *DVWA* (dual von Willebrand factor A domains), discovered in a GWAS of Japanese and Han Chinese patients, has been associated with knee OA ($p = 7.3 \times 10^{-8}$; OR = 1.54, 95% CI 1.32 - 1.81) (243). *DVWA* is expressed specifically in cartilage and encodes a protein related to the von Willebrand factor type A domain (VWA domain); the DVWA protein itself interacts with β-tubulin. The association of this polymorphism with knee OA may be specific to Asian populations, as it was not replicated in a meta-analysis that also included European patients (244). Another GWAS in the Japanese population identified the rs10947262 SNP in the *BTNL2* (butyrophilin-like 2) gene, in proximity to the *HLAII*

and *HLAIII* (human leucocyte antigen) genes as demonstrating genome-wide significance for association with knee OA ($p = 6.73 \times 10^{-8}$; OR 1.32, 95% CI 1.19 - 1.46) (245). The *BTNL2* gene is a member of the immunoglobulin gene superfamily. Importantly, this signal was maintained in a meta-analysis including European subjects ($p = 5.1 \times 10^{-9}$; OR 1.31, 95% CI 1.20 - 1.44) (245). A Dutch GWAS identified the common variant C-allele of rs3815148, in proximity to the *GRP22* gene (glycine-rich_protein_Aa1-291) as associated with the risk of developing knee and/or hand OA ($p = 8.0 \times 10^{-8}$; OR 1.14, 95% CI 1.09 - 1.19) (246). In subsequent functional studies, GRP22 expression was identified in murine articular chondrocytes upon the development of knee OA (246). In a GWAS of 3177 OA patients and 4894 control subjects, the rs11842874 SNP in *MCF2L* (MCF.2 cell-line-derived transforming sequence-like) was identified as a major novel risk variant ($p = 2.1 \times 10^{-8}$; OR 1.17, 95% CI 1.11 - 1.23) (247). Although the association did not surpass the accepted genome-wide significance threshold, this remains an important susceptibility locus, as MCF2L modulates nerve growth factor, NGF, against which treatment with monoclonal antibodies in patients with knee OA is associated with reduced pain and improved joint function (248).

Following arcOGEN, several other genome-wide genetic association studies investigating OA in large cohorts have been reported. A meta-analysis of over 11277 patients with hip OA and 67473 control subjects, all of European descent, identified a novel genome-wide significant polymorphism, SNP rs6094710 on chromosome 20q13, associated with hip OA ($p = 7.9 \times 10^{-9}$; OR 1.28, 95% CI 1.18 - 1.39) (249). Two candidate genes with strong biological plausibility for OA are located downstream of this polymorphism: *NCOA3*, which encodes the protein nuclear receptor coactivator 3, and *SULF2* (sulfatase 2), which encodes the protein heparan sulphate 6-O endosulfatase 2. RNA expression levels of *NCOA3* have been demonstrated as reduced in degenerate articular cartilage compared to preserved cartilage from the same individuals (249). In contrast, RNA expression levels of *SULF2* are increased in osteoarthritic cartilage compared to unaffected cartilage (250). The rs6094710 SNP is in perfect LD with several other SNPs at this locus, though none result in functionally significant alteration to the structure of either *NCOA3* or *SULF2*, and it is more likely that polymorphisms at

this susceptibility locus may modulate expression of *NCOA3* or *SULF2* to exert their effect in the development of OA.

Another well-powered GWAS that examined specifically for association with OA of the hand identified a signal at 15q22, marked by the SNP rs3204689 ($p = 1.1 \times 10^{-11}$; OR 1.46, 95% CI 1.31 - 1.63) (251). This SNP resides in the 3'UTR of *ALDH1A2* (aldehyde dehydrogenase 1 family member A2). This gene encodes an enzyme involved in the synthesis pathway for RA, which is a signalling molecule involved in several developmental pathways, including in skeletogenesis. The risk-conferring C-allele of rs3204689 correlated with reduced expression of the gene in both knee and hip cartilage from patients with OA, though expression in relevant tissue of affected joints of the hand was not assessed (251). However, in wider analysis, the SNP was specific for association with OA of the hand, but not at other skeletal sites. This may indicate that a functional effect may not directly correlate with a genetic risk.

A further recent GWAS investigating hip OA, defined by severe disease necessitating total hip joint replacement, and which included 654 patients with OA and 4697 control subjects, discovered a signal at 7p12.3, tagged by the SNP rs788748 ($p = 2.0 \times 10^{-8}$; OR 0.71, 95% CI 0.63 - 0.80) (252). Further combined analysis of the SNP for association with OA of the hip on five further cohorts and the discovery cohort identified that the SNP did not have genome-wide significance for association with hip OA ($p = 0.02$; OR 0.92, 95% CI 0.86 - 0.99). The lack of genome-wide significance upon replication in the larger combined cohorts may indicate a false-positive signal generated in the in the smaller discovery cohort. Further functional studies were performed to investigate *IGFBP3* (insulin like growth factor binding protein 3), the gene closest to the disease-associated rs788748 SNP. It was reported that genotype of rs788748 correlated with serum levels of IGFBP3; suggesting that the risk A (adenine) allele of rs788748 might alter expression of *IGFBP3* to effect the association with hip OA. This gene encodes insulin-growth factor binding protein 3; loss of expression and overexpression of the IGFBP3 protein resulted in significant effects associated with development of OA in articular cartilage, compared to control treatments in several chondrogenesis models. Knockdown of *IGFBP3* in chondrocytes decreased chondrocyte

hypertrophy, whereas overexpression of *IGFBP3* in chondrocytes resulted in cartilage catabolism and osteogenic differentiation. Although these functional results implicate *IGFBP3* as having a role in cartilage homeostasis, direct effect of the risk allele of rs788748 on *IGFBP3* expression in articular tissue has not yet been demonstrated and additional assessment of the association of rs788748 in additional large OA cohorts is needed to confirm or refute the association, and help determine whether or not the susceptibility locus containing *IGFBP3* is a repository of genetic risk for OA.

A meta-analysis of recent GWAS in European populations comprising 9789 patients with hip OA and 31873 control subjects has also identified a risk C-allele of *DOT1L* (DOT1 like histone H3K79 methyltransferase) rs12982744 to correlate with hip OA ($p = 8.1 \times 10^{-8}$; OR = 1.10, 95% CI 1.06 - 1.14) (253). The effect size was significantly greater in males compared to females, although genome-wide significance was demonstrated for both genders. The *DOT1L* gene encodes DOT1-like histone H3 methyl-transferase, which has been implicated in endochondral bone formation (254). The associated polymorphism in *DOT1L* has previously been shown to be associated with minimum joint space width at the hip joint, which is itself greater in males than females, and may help to explain the gender dimorphism at this particular OA susceptibility locus (254).

The candidate gene analysis approach has also been subject to re-evaluation in a recent meta-analysis (255). In total, SNPs marking 199 candidate genes for association with OA were assessed by meta-analysis of nine GWAS including 9985 patients with hip or knee OA, and 34808 control subjects, all of European ancestry. After Bonferroni multiplicity correction for number of independent tests, no SNPs surpassed the significance threshold. Two genes contained SNPs that approached, but did not reach, statistical significance: one SNP within *COL11A1* demonstrated association with hip OA (rs4907986 $p = 1.29 \times 10^{-5}$; OR 1.12, 95% CI 1.06 - 1.17), and one SNP at the *VEGF* gene showed association with hip OA specifically in male patients (rs833058 $p = 1.35 \times 10^{-5}$: OR 0.85, 95% CI 0.79 - 0.91). The *COL11A1* (collagen type XI alpha 1) gene encodes a component, the pro-alpha1 (XI) chain, of Col XI, and has an important role in both chondrogenesis and skeletogenesis as demonstrated by mutations in

COL11A1 that are associated with Stickler syndrome, lumbar disc degeneration and fibrochondrogenesis (256-258). *VEGF* encodes a protein fundamental in angiogenesis, which is also involved in endochondral ossification, physeal development, cartilage formation, and development of OA phenotype in animal models (259, 260). Although identification of variants within these two strong candidate genes as approaching significance for association with OA is encouraging, the results should be reviewed with caution as a relatively tolerant threshold was used for significance due to the focused analysis. Some limitations of this approach include the exclusion of relevant genetic variants that were not adequately covered, especially those with low frequency or multiple allelic polymorphisms. Nevertheless, the results of this meta-analysis indicate that the genetic association for OA is unlikely to be discovered through traditional candidate gene studies. The genetic risk for OA is more successfully investigated through the GWAS approach, with candidate gene studies more appropriate in the subsequent validation and refinement of genetic susceptibility loci identified from hypothesis-free genome-wide studies. The OA susceptibility loci with genome-wide significance identified by studies other than arcOGEN are shown in Table 1.2.

Comparison of the OA susceptibility loci with genome-wide significance identified by arcOGEN (Table 1.1) and other GWAS of OA (Table 1.2) reveals the identification of distinct susceptibility loci from separate studies. However, bioinformatics analysis of the association signals identified by arcOGEN and other GWAS studies has revealed a number of common biological pathways through which the genetic variants predisposing to OA may exert their effect. These include biological pathways involving skeletogenesis, differentiation of osteoblasts and chondrocytes, transcriptional regulation, and cell signalling (261). The differences in susceptibility loci identified between different GWAS studies may also be due to heterogeneity of the populations studied, as the same genetic variations may have unequal effects in the susceptibility to OA in different populations, as reflected by the genome-wide association of *HLA class II/III* and *DVWA* in Japanese populations, but not European populations (243, 245). Furthermore, genetic variants may also exert joint-specific and gender-specific effects on the susceptibility to OA, as highlighted by the results of the arcOGEN study (229). It is also notable that the arcOGEN study did not identify a

genome-wide association between OA susceptibility and *GDF5* or the 7q22 locus, despite genome-wide associations being identified in previous studies (216, 246). This may be due to the limited statistical power of the first phase of the arcOGEN study, the allelic frequencies of the SNPs, and for *GDF5*, that the rs143383 SNP was not included in the genotyping (262).

Locus (ref)	**SNP / Nearest gene(s)**	**Putative or known function**	**OA phenotype**	**Population**	**p-value (discovery & replication)**	**Odds ratio [95% CI] (discovery & replication)**
20q11.2 (218)	rs143383 *GDF5*	Inhibition of chondrogenesis	Knee OA	Asian & European	4.1×10^{-11}	1.18 [1.12 - 1.23]
3p24.3 (243)	rs7639618 *DVWA*	Cartilage-specific tubulin binding	Knee OA	Japanese & Han Chinese	7.3×10^{-8}	1.54 [1.32 - 1.81]
6p21.3 (245)	rs10947262 *BTNL2*	T cell responses	Knee OA	Japanese & European	5.1×10^{-9}	1.31 [1.20 - 1.44]
7q22.3 (246)	rs3815148 *GPR22*	G-protein coupled receptor	Knee and/or hand OA	Dutch	8.0×10^{-8}	1.14 [1.09 - 1.19]
20q13.12 (249)	rs6094710 *NCOA3* / *SULF2*	Nuclear receptor / heparan sulfate sulfatase	Hip OA	European	7.9×10^{-9}	1.28 [1.18 - 1.39]
15q21.3 (251)	rs3204689 *ALDH1A2*	Aldehyde dehydrogenase	Hand OA	European	1.1×10^{-11}	1.46 [1.31 - 1.63]
19p13.3 (253)	rs12982744 *DOT1L*	Wnt signalling	Hip OA	European	8.1×10^{-8}	1.10 [1.06 - 1.14]

Table 1.2 – Genetic susceptibility loci for OA with genome-wide significance identified by studies other than arcOGEN (229).

Despite the recent significant advances in identifying OA susceptibility loci using the GWAS approach, the heritability of OA risk is not yet fully explained. There are several possible aspects to the genetic architecture of susceptibility to common complex diseases, such as OA, that may contribute to this unexplained heritability. Many risk alleles are likely to be to present at a low frequency (minor allele frequency (MAF) < 1%) and therefore may not be captured by many of the genotyping platforms previously used (263). Genetic variants contributing to OA susceptibility may also have low effect sizes and, therefore, to have sufficient power to detect these small individual effects conferred by rare risk alleles, even larger multinational cohort studies will be required. In this regard, the advent of next generation sequencing (NGS), enabling multiplexed detailed fine-mapping of casual and rare variants in larger cohorts may be particularly informative (227). Furthermore, more detailed phenotypic characterisation of the OA patients and control subjects may permit detection of variants associated with finer endophenotypes that may not only enable identification of additional risk variants, but also inform the potential pathological nature of variants. In relation to OA, this was demonstrated with particular success in the association of the risk C-allele of *DOT1L* rs12982744 with reduced minimal hip joint space width and development of OA. More detailed clinical, demographic and radiological phenotypic characterisation of participants enrolled in genetic association studies may help address the missing heritability (254).

Finally, it is evident that a proportion of the genetic susceptibility to OA is conferred by variation other than SNPs. This may include copy number variants (CNVs), which are represented in relatively low number on current genotyping arrays (264). Epigenetic changes have been proposed as another form of genetic variation that may explain the small cumulative effect sizes of the existing susceptibility loci identified by GWAS investigating OA. This has been supported by initial functional studies that have demonstrated that risk alleles of certain SNPs can create CpG (cytosine-guanine dinucleotides) sites that may be regulated by deoxyribonucleic acid (DNA) methylation. Furthermore, OA is a phenotypically heterogeneous condition and epigenetic variation is also likely to be specific to patient subgroups or certain skeletal

sites. Joint site specificity may also exist in relation to epigenetic changes, and this may be elucidated as the pathological mechanisms are revealed.

1.3.2.2 9q33.1 susceptibility locus for hip OA in females

The susceptibility locus with the greatest effect size was that on chromosome 9q33.1 (OR 1.20 [1.13-1.27]; p-value of 6.11×10^{-10}), and which was associated with the specific phenotype of hip OA in females (Figure 1.4). This was the only locus that maintained its effect size estimate in both discovery and replication analyses. This locus is also delimited by two recombination hot-spots, and it contains only three protein-coding genes, *ASTN2*, *PAPPA*, and *TRIM32*, in addition to five recently identified non-coding genes *PAPPA-AS1* (antisense RNA 1), *ASTN2-AS1*, *LOC105376238*, *LOC105376239*, and *LOC105376240*.

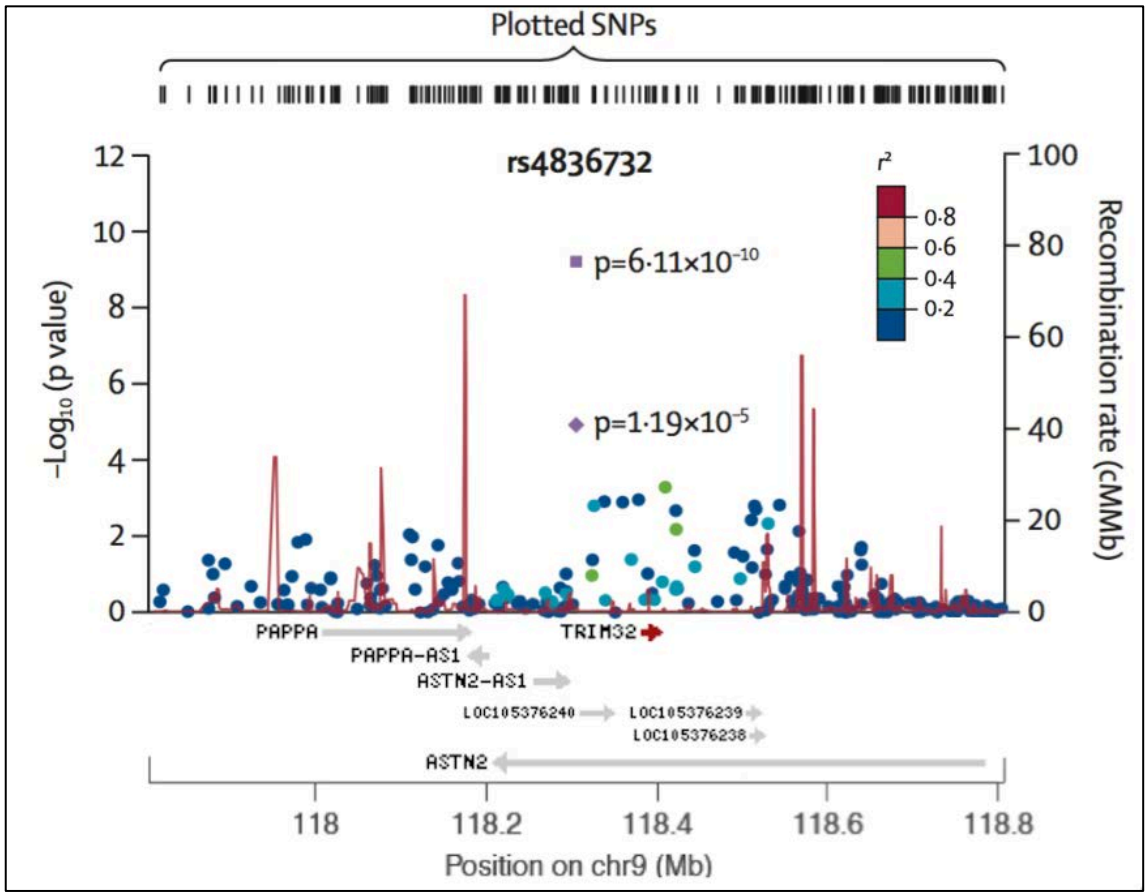

Figure 1.4 – Regional plot of the susceptibility locus at chromosome 9q33.1 for female hip OA centred on rs4836732; the data shown are from the arcOGEN study (229). Case-control results ($-\log_{10}$[p-value]) for genotyped SNPs in the discovery set are plotted against genomic position for total hip replacement in female patients. The index genotyped SNP (rs4836732) is denoted by the purple diamond in the discovery set and by the purple square in the meta-analysis including discovery and replication sets. The circles indicate association results of genotyped SNPs in the region from the discovery analysis only; the colour reflects the correlation coefficient (r^2) of each genotyped SNP with the index SNP estimated with the CEU HapMap II panel. The regional plot is annotated with the location and direction of transcription of the identified genes at this locus.

The *ASTN2* gene at the 9q33.1 locus encodes a protein that is highly expressed in developing neurons, and GWAS studies have associated *ASTN2* with the development of bipolar disorder, cognitive decline, migraine, adult attention-deficit/hyperactivity disorder, addiction vulnerability, autism, and schizophrenia (231, 265-269). The function of ASTN2 is most characterised in the neurocortex and hippocampus where it regulates the cell surface expression of ASTN1 (astrotactin 1), which is a critical cell adhesion molecule in neuron-glia binding during developmental periods of glial-guided neuron migration in the brain (231, 268). CNVs disrupting all transcripts of *ASTN2* are significantly associated with neurodevelopmental disorders in humans (270). A significant association of genetic variants within *ASTN2* with the age of onset of Alzheimer's disease has also been demonstrated (271). *ASTN2* therefore seems to be particularly important in the risk of neurodevelopmental, neurodegenerative, and neuropsychiatric disorders in humans. The expression of *ASTN2* in musculoskeletal tissue has not previously been investigated.

Results from previous research indicate that two other genes at this locus, *PAPPA* and *TRIM32*, may have stronger biological relevance to the development of OA. The *PAPPA* gene encodes the pregnancy-associated plasma protein A (PAPPA) that is a zinc-binding metalloproteinase with IGFBP4 as its substrate. The IGFBP proteases regulate the structure, function and bioactivity of IGF1 and IGF2, which themselves are important determinants of fetal growth and postnatal development (272). PAPPA-mediated IGF1 signalling is particularly important for postnatal skeletal development (273). Cleavage of IGFBP4 by PAPPA results in increased bioavailability and mitogenic effectiveness of IGFs in vitro. Overexpression of PAPPA has been shown to result in increased bone formation in transgenic mice, and this effect is primarily mediated by increasing the bioavailability of IGF (274). PAPPA proteolytic activity has been identified in cultured human fibroblasts and osteoblasts (275), human vascular smooth muscle cells (276), and ovarian granulosa cells (277). Mice with targeted inactivation of *PAPPA* exhibit delayed endochondral ossification, implicating a role for PAPPA in chondrocyte function, and growth retardation (274, 278). Loss of PAPPA activity in mice results in reduced cortical and trabecular bone thickness and bone mineral density compared to wild-type littermates (272). Loss of function of *PAPPA2* (pappalysin 2), a

homologue of *PAPPA*, in mice leads to dysmorphic proximal femoral and pelvic girdle development, though the phenotype in articular cartilage and subchondral bone has not yet been investigated (279). Despite some potential role for *PAPPA* in skeletal development, this gene is located peripheral to the region marked by the rs4836732 SNP and recombination hotspots.

The *TRIM32* gene at the 9q33.1 locus is ubiquitously expressed and encodes a protein with E3 ubiquitin ligase activity (280), and which is a member of the TRIM-NHL protein family (NHL refers to NCL-1/HT2A/LIN-41, the proteins in which the domain was first identified), whose common features include Really Interesting New Gene (RING) finger, B-box, coiled-coil, and NHL repeat domains (281) (Figure 1.5). In TRIM-NHL proteins, the RING domain is characterised by a conserved sequence of cysteine and histidine residues in the core of the domain. This sequence controls the binding of two zinc ions that is fundamental to maintaining the domain structure. The RING domain can function as an E3 ubiquitin ligase (282). In TRIM32, the RING domain acts as an independent dimerisation unit and promotes formation of a TRIM32 tetramer (283). The role of oligomerisation of TRIM32 on catalytic activity and substrate recognition is not yet known. The B-box domain also coordinates binding of two zinc ions in an interleaved fashion. The B-box domain may function together with the coiled-coil domain as a binding site for ubiquitination of substrates by the RING domain (284). B-box domains are divided into two types, termed B-box1 and B-box2, which regulate the binding of the two zinc proteins by slightly different mechanisms (285, 286). TRIM32 contains a single B-box2 domain. The B-box domain of TRIM32 does not affect oligomerisation of the protein, and has only a small effect on catalytic activity (283). The coiled-coil domain usually comprises a non-conserved sequence of hundreds of amino acids. It is a structural motif in which usually two or three α-helices are coiled together, stabilised by hydrophobic interactions. This domain enables the formation of protein complexes, and may be involved in mRNA regulation by TRIM-NHL proteins (287). The NHL domain comprises five or six repeats, each of approximately forty residues, which form a β-propeller structure. NHL domains often function in protein binding, but in TRIM-NHL proteins NHL domains may also directly interact with the RNA phosphate backbone, providing RNA regulatory activity (288).

TRIM32 is a member of the RING finger E3 ligases (289), and the diverse pathological processes in which *TRIM32* is implicated may be due to the variety of substrates that each E3 ligase can ubiquitinate (281). A recessive loss of function mutation in the B-box domain in one family was associated with the Bardet-Biedl syndrome (BBS) (290). Several BBS proteins have been shown to have nuclear export signals and to localise to the nucleus to interact with RING finger transcriptional repressors (291). Mutations in most of the 14 genes that cause BBS affect ciliogenesis (292). Mice with mutations in BBS 1, -2 and -6 genes have articular abnormalities including joint space narrowing and reduced proteoglycan content compared to wild type (WT) littermates, and a reduced proportion of ciliated cells in chondrocyte cultures (293). The expression pattern of *TRIM32* shows significant positive correlation with other known BBS genes, loss of *trim32* expression in zebrafish results in phenotypes identical to those of other known BBS genes, and functional studies of other TRIM-NHL proteins indicates involvement with cytoskeletal elements (290). *Kif3A* mutant mice lack cilia and similarly have reduced proliferation and defective organisation of chondrocytes, and loss of cilia is associated with early signs of OA (290, 294).

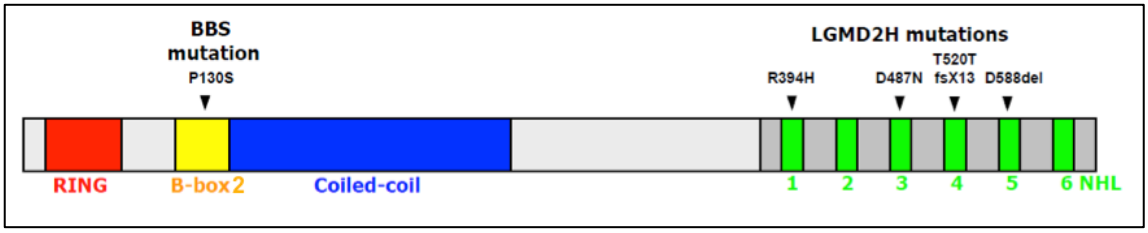

Figure 1.5 – Schematic of TRIM32 domain structure with known pathogenic mutations; adapted from Kudryashova et al (295). The schematic illustrates the domains of the TRIM32 protein including the RING domain that can function as an E3 ubiquitin ligase, B-box2 domain that may function with the coiled-coil domain as a binding site for ubiquitination of substrates by the RING domain, the coiled-coil domain that is also involved in forming protein complexes, and the NHL domain involved in protein binding and RNA regulation (282, 284, 287, 288). The pathogenic mutations displayed include the P130S allele in the B-box domain associated with development of the autosomal recessive ciliopathy BBS, and the R394H, D487N, T520TfsX13, and D588del alleles in the NHL domain associated with the development of the autosomal recessive limb-girdle muscular dystrophy LGMD2H (290, 296).

TRIM32 also binds myosin heavy chain via the coiled-coil domain and ubiquitinates actin for degradation during muscle regeneration (281). Missense mutations in the NHL domain result in limb girdle muscular dystrophy (LGMD2H) (297). Loss of TRIM32 function causes myopathy by inhibiting skeletal muscle regeneration (298). The mutation associated with LGMD2H restricts TRIM32 interacting with Piasy (protein inhibitors of activated STATs). By regulating Piasy stability, TRIM32 may control induction of apoptosis through induction of NFκB (299). TRIM32 has also been demonstrated to sensitise cells to TNFα-induced apoptosis by ubiquitinating X-linked inhibitor of apoptosis (XIAP) for proteasome-mediated degradation (300). In both neural and skeletal muscle stem cells, TRIM32 regulates proliferation and differentiation by ubiquitination of c-myc for degradation (298, 301). TRIM32 can suppress proliferation, functions as an activator of the microRNA (miRNA) pathway, and distributes asymmetrically to direct progenitor cell differentiation (301). It also concentrates in the retracting basal process (with which other BBS proteins associate), which is a structural feature of mammalian cells that is involved in directing asymmetric cell division, and which may also acts as a template for microtubule and cilia formation (281, 302). Lin-41, another TRIM-NHL family protein, interacts with integrin and actin cytoskeletal elements via the B-box and coiled-coil domains (281).

The TRIM-NHL proteins have emerging roles in cell differentiation and proliferation, and potentially primary cilia development, homeostasis and signalling. These processes may be linked, as has been shown for the von Hippel-Lindau (VHL) protein, another E3 ubiquitin ligase, mutations in which cause microtubule disorientation, cilial dysfunction, and cell-cycle dysregulation, leading to the VHL syndrome (303). Potential mechanisms by which TRIM32 may influence the development of musculoskeletal disorders could include the role of TRIM32 in both cell differentiation and proliferation, and ciliogenesis in tissues expressing TRIM32. It will therefore be important to establish the expression, and also the function, of TRIM32 in joint tissues.

Five further genes have been recently identified at the 9q33.1 locus. These include *PAPPA-AS1*, *ASTN2-AS1*, *LOC105376238*, *LOC105376239*, and *LOC105376240*. These five genes are non-coding RNA genes. Although these genes are untranslated, transcript variants (which have been demonstrated for *LOC105376240*) could influence the regulation of the other genes at this susceptibility locus. MicroRNAs specifically expressed in cartilage have previously been identified, and many miRNAs likely act as a network to control cartilage homeostasis and repair (304).

1.3.3 Epigenetic modifications and OA

Epigenetic variation includes several types of modifications that may be broadly categorised into DNA methylation, histone modification, nucleosome positioning, and miRNA expression. Epigenetic modifications are suggested as a mechanism that mediates the interaction between the environment and genetic influences on disease susceptibility. Traditional disease pathogenesis models of environmental factors acting upon a genetic predisposition to disease are thus becoming increasingly complex. Several environmental factors are known to affect the epigenome, including pollutants (such as tobacco smoke), chemicals (including silica), temperature, ultraviolet light exposure, and an individual's diet (305). These factors may exert their effect on an individual's epigenome from the earliest stages of foetal development and throughout an individual's life (306). Indeed, the summation of environmentally mediated epigenetic modifications, termed 'epigenetic drift', may help explain differences in phenotype and disease risk between monozygotic twins.

Epigenetic modifications may also occur during normal ageing, irrespective of environmental factors. Such changes seem to occur in a locus-specific pattern. Indeed, hypermethylation tends to develop primarily at bivalent chromatin domains and CpG-rich regions, whereas CpG-deficient regions tend to become hypomethylated over time (307). In addition to variations in DNA methylation, histone modifications and miRNA expression occur during normal ageing, though the processes governing these are largely unknown at present.

1.3.3.1 DNA methylation and OA

DNA methylation is the most extensively studied epigenetic mechanism. It is usually used to describe the addition of a methyl group to the fifth carbon of a cysteine nucleotide (5-mC; 5-methylcytosine), though other forms of methylation have been described, including 5-hydroxymethylcytosine (5-hmC), 5-formylcytosine (5-fC), and 5-carboxylcytosine (5-caC). Two types of enzymes mediate traditional 5-mC methylation: de novo methyltransferases (DNMT3A and DNMT3B) and maintenance methyltransferases (DNMT1). DNA methylation has been identified as fulfilling several purposes in humans, including gene expression regulation, genomic imprinting, inactivation of the X-chromosome, and genome defence. Methylation primarily occurs at CpG sites commonly found in DNA regions called CpG islands (CGIs), which are often concentrated in the promoter regions of genes. CpGs are also present at the periphery of CGIs, where they cluster to form CGI shores, in addition to being present within introns and exons. Methylation is a very stable modification, preserved through mitotic cell division and readily detectable in easily obtainable tissue such as saliva, plasma, serum and urine. Nevertheless, epigenetic modifications are believed to be specific to particular tissues or cell types within individuals and to also be regulated in a temporal manner. Analysis of DNA methylation patterns associated with disease is therefore facilitated by purification of biological samples into single-cell populations and application of bioinformatic approaches that utilise available reference epigenomes for specific cell types (308).

One of the first studies of DNA methylation in OA, using chromatography, demonstrated no difference between osteoarthritic cartilage compared to controls, nor in measured levels of DNMT1 and DNMT3A (309). More thorough analyses of DNA methylation have since been performed. Using Illumina® methylation arrays examining over 27,000 CpG sites, focused on CpGIs of promoter regions of genes, DNA methylation was compared in trabecular bone from female patients with either OA or osteoporosis (310). Methylation status differed by more than 10% at 45 sites concentrated in genes associated with bone traits: 43 were hypermethylated in

osteoarthritic bone, especially within homeobox genes that are transcription factors involved in embryonic skeletal development. In subsequent functional studies, the expression levels of two of these genes correlated with disease status.

A further study examined full-thickness cartilage retrieved from the tibial plateau of OA patients and control subjects, using the same Illumina® array. This study identified 91 sites differentially methylated between OA patients and normal controls. Significant hypomethylation, usually associated with increased transcription, was found in genes enriched in inflammatory pathways and positive control of transcription, including *RUNX1*, a transcription factor regulating chondrogenesis. Hypermethylation, which generally correlates with reduced transcription, was demonstrated at genes implicated in regulation of phosphorylation and mitogen-activated protein kinase activity; for example, in *MSX1* (msh homeobox 1), a repressor of transcription. This study isolated a distinct group of OA patients with a specific methylation pattern from the rest of the study participants (311). As for genetic polymorphism association studies, correlating specific methylation patterns to detailed clinical phenotypic parameters in OA patients may improve discovery of causal variants and interpretation of their implications.

A recent study of DNA methylation in association with OA examined hip and knee chondrocytes obtained from a larger sample of OA patients using the more comprehensive Illumina® methylation array covering 480,000 CpG sites (312). In this study, 5322 differentially methylated regions (DMRs) were identified between samples from OA patients and healthy control subjects. These DMRs were located at genes associated mainly with either inflammation or immunity. DMRs between osteoarthritic cartilage from hip and knee joints have been reproducibly demonstrated, which mark altered expression in homeobox genes (313). Articular cartilage is relatively unique in that it may be considered a unicellular tissue; thus, comparison of methylation profiles of DNA isolated from chondrocytes from the same joints of OA patients and unaffected individuals may identify epigenetic changes associated with development of disease.

Early analyses of chick embryos in 1985 implicated mechanisms by which methylation of *COL1A1* (type I collagen) and *COL2A1* affected chondrogenesis (314).

Methylation profiling of individual candidate genes for OA susceptibility have since been performed. Differential methylation within the promoter regions of *IL1β*, *MMP3*, *MMP9*, *MMP13*, *ADAMTS4*, *NOS2*, *SOX9*, and *LEP* (leptin) have been demonstrated to relate to altered gene expression in osteoarthritic cartilage (315-318).

The pathological mechanisms by which the altered methylation statuses of candidate genes exert their effect on the development of OA are starting to be clarified. The hypomethylated -110 site in *MMP13* functions as a methylation-binding site for the catabolic cartilage transcription factor HIF2α (315). Two hypomethylated sites within the enhancer of *NOS2*, the inducible NO synthetase gene, were shown to mediate expression in OA cartilage by modulating an NFκB binding site (316). Hypermethylation at the promoter region of *SOX9*, an anabolic transcription factor, inhibited binding of the transcription factors NFYA (nuclear transcription factor Y subunit alpha) and CREB (cAMP response element-binding protein), and was associated with reduced expression of *SOX9* in hip joint cartilage from OA patients (317). Genetic association studies have identified *GDF5* as a robust candidate gene for OA risk via a C/T SNP that resides within its 5'untranslated region (5'UTR) (215). The risk C-allele alters *GDF5* expression by forming a CpG dinucleotide that subsequently becomes methylated (319). Demethylation of the 5'UTR of *GDF5* in osteoarthritic knee cartilage regulated the allelic imbalance of the rs1443383 polymorphism and may be responsible for the specific effect of this SNP on susceptibility to OA of the knee joint (320). Similar processes may account for the dysregulated deposition of ECM by chondrocytes that overexpress *DIO2*, polymorphisms of which predispose to OA (222). In addition to 5-mC methylation, globally-increased 5-hmC methylation has been shown in chondrocytes from patients with knee OA compared to healthy control subjects (321). A summary of genes believed to have a role in the development of OA by epigenetic modification is shown in Table 1.3.

Gene (ref)	Function	Study samples	Methylation analysis	Methylation status in OA	Expression level in OA
COL10A1 & *COL2A1* (322)	ECM component	OA and control knee AC	Combined bisulphite restriction	No difference to controls	No difference to controls
ACAN (323)	ECM component	OA and control knee AC	Bisulphite restriction and sequencing	No difference to controls	Decreased
MMP3, *MMP9*, *MMP13*, & *ADAMTS4* (315, 324)	ECM-degrading enzymes	OA and control femoral head AC	Methylation-sensitive restriction enzymes	Hypomethylated	Increased
IL1β (315, 325)	Signalling	OA and control femoral head AC	Bisulphite modification; methylation-sensitive restriction enzymes	Hypomethylated	Increased
SOCS2 (326)	Signalling	OA and control femoral head AC	Pyrosequencing	No difference to controls	Decreased
GDF5 (319)	Development	OA and control femoral head and knee AC	Quantitative bisulphite pyrosequencing	Hypermethylated	Decreased
SOX9 (317)	Anabolic factor	OA and control femoral head AC	Methylation-specific PCR and bisulphite sequencing	Hypermethylated	Decreased

Gene (ref)	Function	Study samples	Methylation analysis	Methylation status in OA	Expression level in OA
SOD2 (327)	Other	OA and control femoral head AC	Bisulphite sequencing	Hypermethylated	Decreased
LEP (318)	Endocrine	OA and control femoral head and knee AC	Bisulphite sequencing	Hypomethylated	Increased
P21$^{WAF1/C1P1}$ (309)	Cell cycle regulation	OA and control knee AC	Bisulphite sequencing	No difference to controls	Decreased
DIO2 (221, 222)	Activates thyroid hormone	OA and control femoral and knee AC	Bisulphite sequencing with mass spectrometry	Two sites hypomethylated; one site hypermethylated	Increased
NOS2 (316)	Signalling	OA and control femoral head AC	Bisulphite modification with pyrosequencing	Two sites hypomethylated	Increased

Table 1.3 – Genes implicated in the development of OA by epigenetic modifications in joint tissue; (AC, articular cartilage; ECM, extracellular matrix).

1.3.3.2 miRNA and OA

miRNA are another component of epigenetic regulation. miRNA are short non-coding RNA molecules, comprising 20-30 single-stranded nucleotide chains. They are transcribed from intergenic regions in association with their own promoter, or from within an intron associated with a gene. The identified functions of miRNA molecules in metazoan genomes are the cleavage of mRNA, suppression of translation of mRNA, and regulation of DNA methylation to modulate gene expression (328). An essential enzyme for miRNA processing is Dicer, and depletion of this enzyme in growth plates in mice has confirmed its fundamental role for miRNAs in chondrogenesis and skeletogenesis (329).

The results of studies investigating the role of miRNAs in the development of OA are exciting though full interpretation is challenging due to the diverse roles of miRNAs, their numerous targets, and limited replication of findings across studies to date. Conflicting findings have been described in two studies profiling miRNA patterns in osteoarthritic tissue (330, 331). More recent studies have provided greater insight into the role of miRNAs in OA: investigating RNA retrieved from cultured chondrocytes has demonstrated upregulation of miR-483 and downregulation of miR-149 (332). A particularly interesting miRNA is miR-140, which is specifically expressed in cartilage, critical to chondrogenesis, and depletion of which is associated with an accelerated development of OA in murine disease models (333). Although reduced levels of miR-140 reported in osteoarthritic knee joint tissue were not reproduced in osteoarthritic hip joint tissue, this may not be directly conflicting evidence, but may instead indicate joint site specificity (334). The important miR-140 may regulate *ADAMTS4* and may also function in consort with another miRNA, miR-455 whose expression is also increased in osteoarthritic cartilage, to suppress the *SMAD3* gene expression and thus contribute to the generation of a catabolic chondrocyte phenotype (334). The expression of other miRNAs associated with OA and for which relevant molecular pathways are being investigated include miR-146a which may regulate IL1β signalling, miR-125b which may regulate ADAMTS4, miR-127-5p that may control MMP13 production, miR-148a, and miR-21 that may target GDF5 (335).

1.3.3.3 Histone modifications and OA

In eukaryotes, DNA envelops histone proteins to form nucleosomes. Histone proteins can be modified after transcription by acetylation, phosphorylation, sumoylation, ubiquitination, or methylation. These post-transcription histone modifications can regulate DNA transcription by two primary mechanisms. Firstly, histone modification results in reconfiguration of chromatin and therefore the exposure of gene promoters for transcription factors. Secondly, histone modification may alter the binding of chromatin-associated factors. Fundamental to the access of regulatory factors to transcription factors, and subsequent gene expression, is histone acetylation that is mediated by histone acetyltransferases (HATs). In contrast to HATs, the main role of histone deacytlase enzymes (HDACs) is histone deactylation, which is associated with suppression or termination of gene expression. Chromatin immunoprecipitation (ChIP), hybridisation to arrays, or a combination of these processes, termed ChIP-seq, are techniques that have been used to examine histone modifications in association with biological and pathological processes.

The principal types of histone modifications that have been studied in relation to OA include acetylation and methylation. The phenotype of chondrocytes is particularly sensitive to acetylation and deacetylation. Several classical HDACs (HDAC1, HDAC2, and HDAC7) have been identified as upregulated in osteoarthritic chondrocytes, thereby stimulating their catabolic activity (336). The overexpression of HDAC1 and HDAC2 results in the suppressed transcription of genes involved in the integrity of the ECM, including *ACAN* and *COL2A1*, whereas HDAC7 promotes transcription of *MMP13* (336). In an attempt to use histone modification as a therapeutic target, HDAC inhibitors have subsequently been developed, such as Trichostatin A (TSA) and butyric acid (BA) that inhibit proteoglycan release and degradation of cartilage in cartilage explants, in addition to suppressing the production of cytokine-induced iNOS (inducible nitric oxide synthase) and COX2 proteins and the transcription of *MMP1*, *MMP13*, *ADAMTS4*, and *ADAMTS9 in vitro* (337, 338).

The sirtuin SIRT1, a subtype of HDAC, has also been implicated in the pathogenesis of OA. SIRT1 is a lysine deacytelase that prevents apoptosis in

chondrocytes. In osteoarthritic cartilage, reduced levels of SIRT1 may therefore potentiate the loss of chondrocytes evident in OA (339, 340). SIRT1 also facilitates the transcription of several genes associated with ECM production, including *ACAN*, *COL2A1*, *COL9A1*, and *COMP* by recruiting HATs and SOX9 and through inhibition of *ADAMTS5* (340). Furthermore, SIRT1 may also act as a mediator of inflammation by modulating both IL1β and TNFα (341, 342).

Finally, the impact of histone modification on the development of OA has not yet been as extensively studied as other epigenetic modifications. There is evidence indicating that levels of the histone methyltransferase SET-1A (SET domain-containing protein 1A) are increased in osteoarthritic cartilage and have been demonstrated *in vitro* to upregulate the expression of both *COX2* and *iNOS* (343). These two genes are overexpressed in osteoarthritic cartilage, causing chondrocyte apoptosis, upregulated transcription of MMPs, and inhibition of collagen production (343). Dysregulated histone modification of the promoters of *SOX9* and *Nfat1* (nuclear factor of activated T-cells) may also contribute to the pathogenesis of osteoarthritic cartilage (317, 344).

1.3.3.4 Implications of epigenetic modifications in OA

As epigenetic modifications associated with the development of OA are gradually characterised, these stable variations have emerged as potential novel therapeutic targets. A particularly attractive therapeutic strategy is hypomethylation of metalloproteinases to ameliorate the degradation of the ECM associated with their overexpression in articular cartilage (345). Metalloproteinase inhibitors have been developed but have not shown efficacy in OA, possibly due to their non-specific nature. Another clinical application of epigenetic modifications could be the use of miRNAs that are overexpressed in serum as disease biomarkers (346). Significant therapeutic potential may also derive from the inhibition of HDACs and SET-1 mediated expression of *iNOS* and *COX2* (338).

Further work is required to better determine the pathological implications of epigenetic modifications in OA. The majority of studies in OA have concentrated on

epigenetic changes identified in DNA retrieved from cartilage specifically. As several articular tissues are also involved in the aetiopathogenesis of OA, it may also be insightful to perform detailed characterisation of epigenetic profiles of synovium, subchondral bone, and adipose tissue from osteoarthritic and healthy joints. Indeed, tissue-specific genome-wide DNA methylation patterns have recently been reported for 17 somatic tissues from autopsied humans (347). Further assessment of the direct, functional relationship between epigenetic and genetic variations at particular alleles is also required, as has been initiated for the rs143383 SNP related to *GDF5* and the rs225014 SNP related to *DIO2* and OA risk. Evaluation of direct functional interactions between epigenetic and genetic variation at individual alleles associated with OA risk is also required. This has only been reported for two candidate genes at present, namely for the rs143383 SNP related to *GDF5*, and the rs225014 SNP related to *DIO2* and OA risk (348). Whether or not methylation status of the susceptibility locus can attenuate or amplify the risk effect associated with a risk polymorphism, by regulating gene expression, is a particularly interesting potential interaction.

1.4 Experimental murine models of OA

Thorough evaluation of potential pathogenic mechanisms and therapeutic targets in OA is difficult due to the limitations of *in vitro* tissue or organ culture techniques in comparison to the complex environment of articular joints in living organisms. Validation of pathogenic pathways is therefore conducted best using *in vivo* models of OA. Exacerbation or amelioration of OA in a genetically-modified animal, such as one in which the gene-of-interest has been deleted (such as a knockout (KO) mouse), using an *in vivo* OA model can provide compelling evidence for a critical role of that gene in the pathogenesis of OA (349). Detailed characterisation of the pathogenic molecular mechanisms in which that gene is involved can then be commenced to identify appropriate targets against which disease-modifying OA drugs (DMOADs) can be developed. Due to the heterogenic pathophysiology and phenotypic manifestations of OA in humans, no single animal model of OA can represent the spectrum of OA in humans. Evaluation of genetically modified mice using several models of OA can more

convincingly implicate a gene of interest in OA pathogenesis or indicate relevance to a particular subgroup of patients with OA.

The molecular genetics of OA in humans has been most extensively studied in murine models of the disease. Over 90% of mouse genes have a homolog in humans and the majority of human diseases have a spontaneous or inducible equivalent in mice in which the associated pathology mirrors the human condition (350). The similarity of musculoskeletal physiology and disease between mice and humans, and the relative ease of breeding, husbandry, and genetic manipulation make genetic studies of OA particularly effective in mice (351-353). Murine models of OA include naturally occurring OA through ageing, transgenic models, and chemically or surgically induced OA. The application of the most appropriate model(s) of OA depends on the specific mechanism under investigation. Spontaneous OA models permit the monitoring of the development of OA from mild to severe disease, but are time-consuming, relatively expensive and may result in phenotypic variability. In contrast, in chemically or surgically induced OA models the disease process is accelerated and the phenotypic manifestations are more reproducible, though they often predominantly represent an inflammatory or post-traumatic form of OA, rather than spontaneous primary OA (354).

1.4.1 Spontaneous and non-invasive OA models

Spontaneous OA develops in some laboratory mice more rapidly than others, and can be influenced by genetic manipulation. Early degenerative changes representing OA develop in the knee joint of C57Bl/6 mice as early as 10 months of age, and severe changes develop by 17 months of age (355, 356). The STR/ort mice strain develop knee OA even earlier, by 5 months of age, which may be exacerbated by their 50% greater body weight than other strains (357). The histopathological joint changes that develop in these strains closely resemble OA in humans (358). Several genetically modified mouse strains have exhibited exacerbation or amelioration of OA. Mice deficient in genes related to the integrity of the ECM often develop OA more rapidly, including mice

carrying mutations in the genes for type II collagen, type IX collagen, and MMP13 (359-361).

Obesity is also a risk factor for OA in humans, and findings in the STR/ort mice indicated that increased body mass may also contribute to the development of OA in mice (362). Due to the multifactorial nature of obesity, it is challenging to discern the causal mechanisms of OA in obesity. Modelling obesity by administering a high-fat diet to mice results in increased severity of OA (363). Moderate exercise in mice, in the form of voluntary wheel running, protects against OA, possibly by increasing musculoskeletal strength or by inducing weight loss (363). Further insights regarding the relationship between obesity and OA have been gained from studies of mice deficient in leptin or the leptin receptor. These mice lack satiety and subsequently develop significantly increased adiposity and weight. Despite both increased adiposity and weight, mice deficient in leptin or the leptin receptor do not have an increased incidence of knee OA (364). This suggests that adiposity and increased weight may not directly predispose to OA, and metabolic dysregulation may be a more profound risk factor for OA. Other non-invasive models used to recapitulate human OA in mice include cyclical tibial compression overloading (365), cyclical knee joint overloading (366), and closed intra-articular fracture of the tibial plateau (367).

1.4.2 Chemically induced OA models

The injection of several chemicals into joints has each been reliably shown to result in accelerated progression to severe OA. Monoiodoacetate (MIA) is an antagonist of the glycolytic pathway, the intra-articular injection of which causes widespread chondrocyte necrosis, neovascularisation, subchondral bone collapse, and extensive inflammation (368). Severe inflammatory OA is also caused by the injection of methylated bovine serum albumin (mBSA) (124). Other intra-articular injections that have previously been relatively frequently used include the injection of collagenase and papain; these enzymes cause direct enzymatic degradation of the cartilage ECM and damage to the knee ligaments and menisci creating secondary damage from joint instability (369). As

the chemically induced murine models of OA essentially generate a non-specific inflammatory form of OA, these models are now less frequently utilised, especially as more refined techniques for tissue-specific genetic manipulation, surgical models of OA, and assessment of disease have become available.

1.4.3 Surgically induced OA models

Surgically induced models of OA in mice cause direct joint instability and altered joint biomechanics, leading to secondary OA, and therefore most accurately model post-traumatic, but also degenerative, OA in humans. The advantages of surgical models of OA are that they induce a rapid progression of disease, the temporality of the initiating event and onset of disease is clear and reliable, and the severity of cartilage degeneration required experimentally can be induced by surgically resecting different intra-articular structures. These models were developed as translational models, as injuries to the menisci and ligaments of the knee joint predispose to OA in humans.

The anterior cruciate ligament transection (ACLT) model causes cartilage destruction and formation of osteophytes 8-12 weeks following surgery (370). As access to the central region of the joint is required to transect the anterior cruciate ligament (ACL), and damage invariably occurs to other structures of the knee joint, this procedure causes a relatively severe phenotype that may not be entirely clinically relevant.

Several variations of menisectomy are described in murine OA studies, including partial, total, medial, or lateral excision. Partial medial menisectomy causes mild degeneration of articular cartilage by 8-12 weeks following surgery (371). Technical challenges of the menisectomy procedures include consistency in the quantity of meniscus removed, as this directly correlates with the extent of abnormal mechanical loading of the joint and the development of further joint lesions, and minimisation of iatrogenic damage to other joint structures, particularly to the articular cartilage itself.

The destabilisation of the medial meniscus (DMM) procedure is the most commonly performed and validated surgical model of OA in mice. DMM is achieved by

incising the anteromedial insertion of the medial meniscotibial ligament, causing instability of the medial meniscus and medial compartment of the knee joint (372). This is a particularly favourable model for the evaluation of potential pathogenic and therapeutic mechanisms in OA because it is reliable, reproducible, results in structural joint changes that closely resemble OA in humans, and several histopathological, radiological, and pain-related end points have been established (373). The DMM procedure was initially utilised to demonstrate that *ADAMTS5* KO mice, but not *ADAMTS4* KO mice, developed less severe joint degeneration after surgical trauma, suggesting that ADAMTS5 is the critical aggrecanase in mice (168). The progression of OA after DMM has since been characterised in several transgenic mice strains. Following the DMM procedure, early osteophytes may be detected as early as seven days, and these osteophytes subsequently increase in size and number (374). Increased sclerosis of the subchondral bone plate and mild cartilage lesions may be detected at two weeks after DMM surgery (374, 375). Corticated osteophytes with expansion of the subchondral bone plate may be demonstrated at four weeks after the DMM procedure (374). Fibrillation of cartilage with loss of proteoglycan content is exhibited at 8 weeks following DMM, and these continue to progress thereafter (376). The subchondral bone gradually becomes sclerotic in the medial tibial plateau, then progresses to the lateral tibial plateau, though the greatest effect occurs at the medial tibial plateau of the operated knee joint (377). Other surgically induced models of OA that are utilised less frequently include ovariectomy and articular groove formation, in which an induced oestrogen deficiency and single-site cartilage defect, respectively, initiate degenerative changes within the joints (378, 379).

1.4.4 Assessment of OA in murine models

Histopathological assessment of OA in animal studies initially utilised the grading system performed by Collins (380), and then subsequently the classic Mankin Histological–Histochemical Grading System (MHHGS) (381), which was developed in humans and utilised Safranin O staining, was applied to animals (382). Due to limitations of these scoring systems in categorising early OA changes, important for research applications, the OARSI histopathology initiative developed a universal scoring system for OA of the knee joint in mice (383). This scoring system focuses on the depth and extent of cartilage lesions, and also provides additional criteria by which to assess changes in synovium, subchondral bone, menisci, tendons, and ligaments. As these scoring systems are only semi-quantitative, they may be complemented by quantitative evidence from histomorphometric analyses of joints.

The assessment of subchondral bone changes associated with OA in murine models of OA can be effectively performed using micro-computed tomography (μCT) scanning of murine joints *ex vivo* or *in vivo* (384). The trabecular separation, trabecular thickness, trabecular volume, cortical thickness, and subchondral bone plate can be measured using high-resolution scanners. Combining results of histological assessment of the cartilage with changes on imaging of subchondral bone may provide insights into specific focal changes associated with specific genetic modifications in mice and also the effects of treatments on bone and cartilage. The use of *in vivo* imaging can also provide longitudinal studies on the evolution of osteoarthritic changes and effects of treatments. High-resolution micro-MRI has also been recently utilised in the assessment of cartilage lesions in surgically induced models of rat OA, but standardisation and optimisation of this technique are still required (385).

Investigating biomarkers in murine models of OA and human OA is a non-invasive method to examine cartilage, bone or synovial turnover associated with disease. Biomarkers such as aggrecan and collagen neoepitopes, which may be sampled as breakdown products of the ECM of cartilage, have been analysed as predictors of the efficacy of novel therapeutic agents tested in murine models of OA (386). However, these particular biomarkers have significant variation between individuals and are very

dilute in the serum and urine. Further investigation of potential biomarkers will help identify those that can better monitor disease severity and the efficacy of treatments.

Finally, several manifestations of pain secondary to OA pathology can be measured in murine models. There is a relative lack of standardised and validated methods for pain measurement, in addition to gait and functional evaluation, of OA in animal models, despite its significant potential for developing OA therapies. A biphasic pain response occurs following the DMM procedure: there is an initial early postoperative pain response that subsides, and then by 8 weeks post-operatively, reduced activity levels and specific pain responses due to joint degeneration may be reliably detected (373). Following the DMM procedure, a temporal expression of micro-opioid receptors in the peripheral nerves supplying the knee joint occurs in the early stages of OA and delays the onset of pain (387). A particularly sensitive method to assess pain associated with the development of OA in mice is the measurement of tactile allodynia. Tactile allodynia describes pain behaviour in response to a stimulus that does not normally cause pain. This can be assessed using von Frey filaments, whereby microfilaments are applied in ascending size order at right angles to the plantar surface of the hind paw of mice until either the filament bends or the limb is withdrawn. A decrease in withdrawal thresholds of the operated limb compared to those of the unoperated control limb can indicate the development of tactile allodynia and is directly related to OA pathology induced by the DMM procedure (384). Other methods to assess pain include gait analysis, motor activity levels, dynamic weight bearing, thermal sensitivity, and measuring vocalisations on applications of pressure to the affected limb (388).

1.5 Aims and objectives

The purpose of this research was to investigate the candidate gene with the greatest biological implication from the 9q33.1 OA susceptibility locus associated with OA in females in the arcOGEN GWAS. The role of *TRIM32* in the development of OA was selected for further investigation. This project focused on *TRIM32* because previous studies have demonstrated its expression in musculoskeletal tissue, and its role in cellular proliferation and regulating apoptosis. Furthermore, mutations in genes similar to *TRIM32* result in articular pathology resembling OA in murine studies, and TRIM-NHL proteins interact with cytoskeletal elements, especially the primary cilia, which are critical to normal chondrocyte homeostasis.

The hypothesis for this research was that *TRIM32* might have a role in the development of OA in humans by influencing susceptibility to OA through genetic variation, or by affecting chondrocyte and cartilage homeostasis.

The specific objectives of this thesis were to:

1. Investigate the genetic variation of *TRIM32* to identify novel or rare variants in *TRIM32* that are associated with OA of the hip in females.
2. Examine the expression of *TRIM32* in articular tissues, and to determine whether *TRIM32* expression is altered in female patients with OA of the hip.
3. Investigate whether *Trim32* affects the response of chondrocytes to anabolic and catabolic stimuli, and whether or not *Trim32* affects the integrity of articular cartilage, *in vitro*.
4. Analyse the effect of *Trim32* knockout on the development of OA *in vivo* in response to ageing or surgically induced joint instability (DMM surgery) in mice.

Chapter 2

Materials and methods

All reagents were obtained from Sigma Aldrich (Dorset, UK) unless otherwise stated.

2.1 Variant screening of *TRIM32*

2.1.1 Samples

2.1.1.1 Patients' DNA samples

DNA sequencing of *TRIM32* was performed in the 500 youngest available female patients with primary hip OA from the arcOGEN cohort; these patients had symptomatic hip OA and at least Kellgren Lawrence grade II OA on radiographic evaluation of the symptomatic hip, or had undergone total hip replacement for primary hip OA. Available samples from the youngest female patients were selected as genetic variants predisposing to primary OA may be enriched in these patients. The mean age of included patients was 60.1 years (range 41 – 67 years).

DNA samples for included patients were retrieved from the Bone Research Group (Centre for Genomics and Molecular Medicine, Institute for Genetics and Molecular Medicine, University of Edinburgh), or from the Centre for Integrated Genomic Medical Research (Institute for Population Health, Institute for Population Health, University of Manchester) at which samples from the arcOGEN study are stored centrally in the UK.

2.1.1.2 DNA extraction

DNA was previously extracted from blood samples from included patients with OA using the QIAmp® DNA blood kit (Qiagen®) by members of the Bone Research Group (Centre for Genomics and Molecular Medicine, Institute for Genetics and Molecular Medicine, University of Edinburgh) or by staff at other UK centres participating in the arcOGEN study. DNA samples were stored at -80ºC until used for DNA sequencing studies.

2.1.1.3 DNA quantification and quality assurance

DNA concentration was measured using a NanoDrop1000 v3.7.0 (Thermoscientific) and sample purity was assessed using the A260/A280 ratio. All samples used for DNA sequencing had A260/A280 ratios of ~2.0 to ensure high purity from potential contaminants such as proteins or phenol.

2.1.2 Polymerase chain reaction (PCR)

2.1.2.1 Primer design

Primers for DNA sequencing of *TRIM32* were designed using the *H. sapiens* (GRCh38) reference genome sequence NC_000009.12 (214) and the online primer design tool Primer3 v.0.4.0 ((389). Overlapping primers were designed to avoid annealing at known polymorphic sites, to cover all known *TRIM32* transcript variants, and primer specificity was validated *in silico* using University of California Santa Cruz (UCSC) polymerase chain reaction (PCR) and UCSC Blat (390).

Primers for the amplification of the proximal promoter (-200 base pairs (bp) upstream of the transcription start site), 5'UTR, both exons, and 3'UTR of *TRIM32* are listed in Appendix 7.1.1 and were obtained from Invitrogen™.

2.1.2.2 Amplification

All PCR reactions for amplifying the *TRIM32* DNA sequence were prepared on ice, using Qiagen®*Taq* DNA polymerase with a final reaction volume of 25 microlitres (μl) and run on the MJ Research® thermocycler, using the reagent concentrations and PCR thermocycling conditions listed in Appendices 7.1.2 and 7.1.3. All samples were subject to the same PCR thermocycling conditions except for the use of different annealing temperatures appropriate for each primer pair (Appendices 7.1.1, 7.1.2, and 7.1.3). DEPC (0.1% diethylpyrocarbonate)-treated water (H_2O) was used as a negative control for all PCR reactions.

2.1.2.3 Visualisation

PCR amplification for each gene region reactions were performed in 0.2 millilitres (ml) 96-well PCR plates (Thermoscientific). To confirm successful amplification, a single column of samples from each PCR plate was visualised. PCR products were diluted 1:1 in 1X Orange-G loading dye (Appendix 7.4.1.2) and run parallel to a low molecular weight marker (New England BioLabs®) on a 1% agarose (Bioline)-tris/borate/ethylenediaminetetraacetic acid (EDTA) (TBE) (1X) gel containing 1:10000 SYBR® Safe (Invitrogen™). Visualisation took place under ultraviolet light using GENEGenius (Syngene) and GeneSnap v6.05.01 (Syngene) software.

2.1.3 DNA sequencing

PCR reaction products were sequenced in both directions by the Human Genetics Unit (HGU) services (Medical Research Council HGU, Institute for Genetics and Molecular Medicine, University of Edinburgh). The sequences of the proximal promoter, 5'UTR, both exons, and 3'UTR of *TRIM32* were then analysed for variants using Mutation Surveyor® software (version 3.97; Softgenetics). Only variants identified by sequencing in both directions were selected for further analysis.

2.1.4 Statistical analysis

All statistical analyses were performed using Statistics Package for the Social Sciences (SPSS) Statistics Version 19.0.0 (IBM; Armonk, New York, U.S.A.). The frequency of confirmed variants identified by screening of *TRIM32* DNA sequences of patients with hip OA from the arcOGEN cohort were compared with the population frequencies of known variants. Chi-squared (χ^2) tests were performed to determine whether the minor allele frequencies observed among the youngest patients with hip OA from the arcOGEN cohort were significantly different from those expected in the control population (1000GENOMES:phase_3:EUR (391)), and odds ratios were calculated to estimate effect size for risk alleles. For the χ^2 tests, one-degree of freedom was used in all tests, and statistical significance was accepted at $p < 0.05$.

2.1.5 Bioinformatic analysis

Several bioinformatic resources were utilised to further investigate the biological consequences and implications of polymorphisms identified by variant screening of *TRIM32*. Haploview 4.2 ((392) and SNAP (SNP Annotation and Proxy Search) were used to examine LD between polymorphisms and indicate whether variants were likely to co-segregate during recombination (393). Non-synonymous variants were assessed *in silico* using SIFT (Sorting Intolerant From Tolerant; version 4.0.3, J. Craig Venter Institute (394, 395)) and PolyPhen-2 software (Polymorphism Phenotyping; v.2.1.0 (396, 397). The GTEX Portal and eqtl.uchicago.edu! online browsers were searched to investigate if any of the identified variants had previously been reported as expression quantitative trait loci (eQTLs); that is the variant is associated with altered gene expression or regulation (398, 399). Finally, the SwissRegulon Portal was reviewed to investigate whether or not any variants of interest were located within a transcription factor binding site or regulatory motifs that may be involved in expression of *TRIM32* (400). The Hardy-Weinberg equation ($p^2 + 2pq + q^2 = 1$) was used to determine whether or not observed genotype frequencies in female patients with OA deviated from Hardy-Weinberg equilibrium.

2.2 The role of *TRIM32* in human and murine articular tissue *ex vivo*

2.2.1 Ethical approval and informed consent for human tissue samples

Human hip cartilage samples from femoral heads were obtained from female patients undergoing hip arthroplasty surgery for either an acute fractured neck of femur or primary osteoarthritis. Control samples were obtained from female patients undergoing hip arthroplasty for fractured neck of femur and patients were excluded if they had any previous hip pain, rheumatological conditions, malignancy, or chronic steroid or antimetabolite medication use. Osteoarthritic samples were obtained from female patients undergoing hip arthroplasty for primary hip OA and patients were excluded if they had any previous hip joint deformity, infection, trauma, or avascular necrosis of the hip, further rheumatological conditions, malignancy, or chronic steroid or antimetabolite medication use. All patients completed full informed consent. Ethical approval for retrieval and analysis of human tissue samples was provided by the Lothian Research Ethics Committees (LREC reference number: 04/S1102/41). All samples were obtained from patients undergoing hip arthroplasty surgery at the Royal Infirmary of Edinburgh (NHS (National Health Service) Lothian) or the Victoria Hospital Kirkcaldy (NHS Fife). Immediately after retrieval of the femoral head during surgery, the femoral head was submerged in Dulbecco's Modified Eagle's medium (DMEM), and cartilage samples processed within 24 hours of tissue retrieval.

2.2.2 Immunostaining of TRIM32 and ASTN2 in human articular cartilage

Hip cartilage samples from femoral heads from female OA and control patients were snap-frozen in liquid nitrogen prior to embedding in paraffin for sectioning. Frozen hip cartilage samples were sectioned at 4 micrometre (μm) thickness by Helen Caldwell (Division of Pathology, University of Edinburgh) using a Leica CM1850 Cryostat. All sections were placed on glass slides (VWR International™ Superfrost® Plus) and fixed with acetone. Archival sections of knee joint cartilage from human patients were kindly donated by Professor Donald Salter. Slides were stored at -20ºC and brought to room temperature before use. Immunostaining signals for TRIM32 protein in hip and knee cartilage sections were visualised using Dako Envision®+ System-horseradish peroxidase (HRP) diaminobenzedine (DAB). Slides were washed with 0.05% phosphate buffered saline (PBS) (1X) (Invitrogen™)-Tween 20 (PBS-T), treated with 0.9% hydrogen peroxide (H_2O_2) and peroxidase-blocked for 10 minutes. Samples were incubated for 1 hour at room temperature with primary monoclonal mouse anti-TRIM32 antibody (Abnova®, H00022954) used at 1:750 dilution, or primary monoclonal mouse anti-ASTN2 (Sigma®, SAB1407191) used at 1:400 dilution. Tumour tissue microarrays (provided by Division of Pathology, University of Edinburgh) were used for controls. Murine serum was used as negative controls in place of the primary anti-TRIM32 or anti-ASTN2 antibodies to demonstrate lack of non-specific staining. Slides were then washed with 0.05% PBS-T and incubated for 30 minutes at room temperature with HRP-linked secondary antibodies, polyclonal rabbit anti-mouse at 1:200 dilution (P0260, Dako). Excess antibodies were then removed with 0.05% PBS-T. Liquid DAB$^+$ substrate-chromogen was used to visualise the antibody binding.

Samples were counterstained with haematoxylin blue (ThermoFisher Scientific) for 5-20 seconds, rinsed in Scott's tap water solution, dehydrated through increasing industrial methylated spirits (Genta Medical) concentrations and xylene (Genta Medical). A glass coverslip was then mounted using di-n-butylphthalate in xylene (DPX) mounting medium (Fisher Scientific) and then the slides were left to dry in air. Haematoxylin stained slides were visualised on a Zeiss Axio Imager A1 microscope.

2.2.3 Isolation and culture of human articular chondrocytes

Isolation and culture of chondrocytes from human tissue samples was performed according to standard protocols (401). Cartilage was dissected from the joint surface of the femoral head, and cut into 1-2 millimetre $(mm)^3$ pieces, then stored in antimicrobial solution (5% Fungizone (Gibco®), 5% L-glutamine (Sigma®), 5% penicillin-streptomycin (Gibco®) in PBS (1X)) for 1 hour. Cartilage pieces were washed with PBS (1X) and incubated in 0.25% trypsin-EDTA (Sigma®) and incubated for 30 minutes at 37ºC and 5% carbon dioxide (CO_2). The trypsin-EDTA solution was then removed, the cartilage washed with PBS (1X) and then immersed in collagenase II (*Clostridium histolyticum*¸ Gibco®) for 24 hours. Digested cartilage was strained through a sterile sieve into a 50 ml polypropylene tube (BD Falcon™) and washed three times by suspension in PBS (1X) and centrifugation (Sigma® 4K15, 2000 revolutions per minute (rpm), 5 minutes). The cell pellet was then re-suspended in 1 ml of complete Iscove's modified Dulbecco's medium (IMDM, Sigma®) with 10% FCS (First Link (UK) Ltd), 1% Fungizone, 1% L-glutamine, and 1% penicillin-streptomycin and strained through a 70 μm cell strainer (BD Falcon™). Cell counting was performed using Trypan Blue dye to ensure $\geq$ 95% cell viability, and chondrocytes were seeded in 75 centimetre $(cm)^2$ culture flasks (Greiner Cellstar®) at a density of 5×10^4 cells/ml in 20 ml of complete IMDM. Primary chondrocytes were not passaged and were grown as a monolayer culture for up to 10 days, exchanging complete IMDM medium every 3-4 days. At 75% confluence (no more than 10 days' culture), cultures were processed for total protein extraction.

2.2.4 Total protein extraction and quantification

At 75% cell confluence or 10 days' of culture, all culture media was removed from human primary chondrocyte cultures. Cells were then washed twice with PBS (1X) containing 0.1 millimolar (mM) sodium vanadate (Na_3VO_4). Total protein extraction was then performed on ice. The cells were covered with lysis buffer (Protease inhibitor cocktail tablet (Roche Diagnostics), 1.0 mM sodium vanadate (Na_3VO_4), 1% Igepal in 10 ml PBS (1X) for 30 minutes. Cells were then scraped from the flask, placed in a 1.5 ml tube (Eppendorf®) and centrifuged (Eppendorf® 5415R) at 13000 rpm for 15 minutes at 4^oC. The protein-containing supernatant was then transferred to a clean tube and frozen at -80^oC until further use.

A Pierce protein assay was used to determine the protein concentration of the samples. In a 96 well plate, 10 µl of each sample, diluted 1:4 and 1:1 in H_2O (Gibco®), was aliquoted in duplicate; pre-diluted bovine serum albumin (BSA) standards (Thermoscientific) were used. Copper (II) sulphate was then diluted 1:50 in bicinchoninic acid and 200 µl was added to each well. Plates were then sealed and incubated at 37^oC for 15 minutes. The absorbance of each well at 562 nanometres (nm) was measured using a BIO-TEK™ SynergyHT plate reader. Protein concentration was then calculated, using Gen5™ software, by colorimetric comparison of each sample against the standard curve.

2.2.5 Western blot detection of TRIM32 in human articular chondrocytes

Before loading protein samples for gel electrophoresis, 25 micrograms (µg) of protein was denatured through incubation at 95^oC for 5 min in 5X loading buffer (Appendix 7.4.2); two molecular weight standards were also incubated, Magic Mark™ XP (Life Technologies™) and Kaleidoscope (Bio-Rad). Samples and standards were then loaded into a Criterion™ XT precast (12% bis-tris) polyacrylamide gel immersed in XT MOPS (3-(*N*-morpholino)propanesulfonic acid) (1X) running buffer (Bio-Rad) in an electrophoresis tank (Bio-Rad). Gels were then run at 200 volts (V) for 45 minutes.

A polyvinylidene difluoride (PVDF) membrane (GE Healthcare Amersham Hybond™-P) was activated in 100% methanol for 5 minutes and then equilibrated for 10 minutes in transfer buffer (Appendix 7.4.3). The gel containing the sample proteins and standards was removed from the electrophoresis tank and cassette, and then placed into transfer buffer for 5 minutes. Extra thick blot paper pre-soaked in transfer buffer was then placed on the negative electrode of the transfer apparatus (Hoeffer TE77XP). A blotting sandwich was then created within the transfer apparatus comprising the sequential layering of the PVDF membrane, the polyacrylamide gel, and a further layer of extra thick blot paper against the positive electrode. The electrophoretic transfer of proteins from the gel to the PVDF membrane was then performed at 90 milliamperes (mA) for 120 minutes.

The PVDF membrane containing the transferred proteins was then incubated for 30 minutes at room temperature in 5% w/v (weight/volume) skimmed milk (Marvel) – tris buffered saline (TBS) (1X)-Tween 20 (TBS-T) (Appendix 7.4.5) as a blocking solution against non-specific binding sites. The PVDF membrane was then washed with TBS (1X)-T and incubated overnight at 4ºC in primary monoclonal mouse anti-TRIM32 (Abnova, H00022954) antibody solution at 1:1000 dilution in 5% (w/v) milk-TBS (1X)-T solution. The next day, the PVDF membrane was washed in TBS (1X)-T for one hour for three times, and then incubated for one hour at room temperature in the secondary HRP-linked donkey anti-mouse (Jackson-ImmunoResearch Laboratories Inc, 715-035-151) antibody solution at 1:10000 dilution in 5% (w/v) milk-TBS (1X)-T solution. The PVDF membrane was again washed in TBS (1X)-T for one hour for three times. All washes and incubations were performed in a rocker (Biometra®) to ensure even distribution over the PVDF membrane.

Prior to performing chemiluminescent protein detection, the PVDF membrane was washed in TBS (1X) (Appendix 7.4.4.2) for 10 minutes at room temperature to ensure optimal efficiency of the chemiluminescence by removal of any Tween 20. Protein expression was then detected using 1 ml of Immun-Star™ WesternC™ chemiluminescence HRP-detection reagents (Bio-Rad), prepared in accordance with the manufacturer's instructions. Images were captured using a Syngene GeneGnome Bio

Imaging System using GeneSnap v.7.05.02 (Syngene) image software. Protein expression was quantified using GeneTool v.3.06.04 (Syngene) software. Automatic correction was performed for background fluorescence. Care was taken not to overexpose captured images. Protein expression levels were normalised against expression levels of β-Actin that were detected using 1:1000 primary rabbit antibody (Sigma®, A5060) and 1:10 000 secondary HRP-linked donkey anti-rabbit secondary antibody (Jackson-ImmunoResearch Laboratories Inc, 711-035-152).

2.2.6 Isolation and culture of murine femoral head cartilage explants

Isolation and culture of murine femoral head cartilage explants was performed according to established protocols (402). Femoral heads were retrieved from wild type and *Trim32* knockout (KO) (*Trim32*$^{-/-}$) mice aged 3 weeks. Mice were culled by inhalation of escalating concentration of CO_2. The skin was sterilised with 70% ethanol (ETOH). The skin overlying the hip joint was incised and the hip joint identified by dissecting the proximal femur free of muscle. The hip joint was disarticulated by placing opposing forces on the acetabulum and proximal femur, thereby exposing the femoral head. Fine-pointed forceps were used to create a fracture through the capital femoral epiphysis, thereby releasing the entire cartilaginous femoral head. The extraction process was then performed for the contralateral femoral head. Pairs of femoral heads from each mouse were immediately incubated in culture wells of a 48-well flat bottom microtiter plate (Greiner Bio-One, 677180) containing 400 µl of DMEM (supplemented with 10% foetal calf serum (FCS), 1% penicillin-streptomycin, 1% L-glutamine, and 20 mM (4-(2-hydroxyethyl)-1-piperazineethanesulfonic acid (HEPES))) for 48 hours. Femoral head explants were then washed with serum-free media (DMEM supplemented with 1% penicillin-streptomycin, 1% L-glutamine, and 20 mM HEPES) and transferred into wells of fresh 48-well flat bottom microtiter plates containing 400 µl of serum-free media containing either 10 micromolar (µM) RA (Sigma®, R2625) or 10 nanograms/ml (ng/ml) human recombinant IL1α (Sigma®, I2778) and cultured for 72 hours; control samples were incubated in 400 µl of serum-free media with no additional stimulation.

Conditioned media was then aspirated from each well, and stored in 1.5 ml tubes (Eppendorf®) at -20ºC until used for the glycosaminoglycan (GAG) dye-binding assay.

2.2.7 Papain digestion of murine femoral head explants

Pairs of femoral heads were retrieved from each well of 48-well microtiter plates following treatments described in section 2.2.6, placed in a 1.5 ml tube (Eppendorf®), and subjected to papain digestion to liberate GAGs that were not extracted during previous incubations. Pairs of femoral heads were submerged in 125 μg/ml papain solution (Sigma®, P3125) in 200 μl of papain buffer (Appendix 7.4.7), and incubated overnight at 60ºC on a rocker (Biometra®). Upon completion of papain digestion the next day, samples were stored at -20ºC until used for the GAG dye-binding assay.

2.2.8 Glycosaminoglycan dye-binding assay

Dimethylmethylene blue (DMMB) dye-binding assay was performed to measure GAG content of conditioned media following stimulation of murine femoral head cartilage explants (section 2.2.6), and murine femoral head cartilage explants following papain digestion (section 2.2.7). Flat bottom 96-well microtiter plates (Greiner Bio-One, 655101) were prepared with 40 μl of chondroitin sulphate (Sigma®, C4384) standards in duplicate from 0 to 60 μg/ml. Serum-free culture media was used for blank samples. Samples were added in duplicate to the microtiter plate; conditioned media was assayed at 1:4 dilution, and papain-digested samples were assayed at 1:16 dilution. 150 μl of DMMB solution (Appendix 7.4.6) was added to the standards, blanks, and samples. The absorbance of the wells was then measured immediately using a FLUOstar Omega microplate reader (BMG Labtech) set at a wavelength of 595 nm, with a reference wavelength of 655 nm. The absorbance of the standards was plotted as a function of the concentration of the chondroitin sulphate in the standards. The standard curve was then used to determine the quantity of GAG present in each sample. Total GAG for each

sample was calculated as the sum of GAG released in the media and papain digests. The cumulative release of GAG into the media was calculated as a percentage of total GAG.

2.2.9 Isolation and culture of immature murine chondrocytes

Immature murine articular chondrocytes for primary culture were isolated according to standard techniques (403). Mice used for isolation of murine chondrocytes were generated from mating breeding pairs of either WT mice or homozygous *Trim32* KO (*Trim32*$^{-/-}$) mice (for details regarding construct and generation of *Trim32* KO mice, see section 2.3.1). Femoral heads were harvested from newborn (5-10 days' of age) wild type and *Trim32* KO mice. Mice were culled by inhalation of escalating concentration of CO_2. The skin was sterilised with 70% ETOH. The skin overlying the hip joint was incised and the hip joint identified by dissecting the proximal femur free of muscle. Gentle opposing forces on the femur and pelvis enabled disarticulation of the hip joint to expose the femoral head. Fine-pointed forceps were used to carefully retrieve the entirely cartilaginous femoral head, which was then placed in a universal tube containing complete culture media (DMEM (supplemented with 10% FCS, 1% penicillin-streptomycin, 1% L-glutamine, and 20 mM HEPES)). The extraction process was then performed for the contralateral femoral head. Pooled femoral heads from WT or *Trim32*$^{-/-}$ mice were then transferred to a sterile 100 mm (58 cm^2) culture dish (Greiner, CELLSTAR®) and incubated in 20 ml of 3 mg/ml collagenase II (*Clostridium histolyticum*¸ Gibco®) prepared in culture media (DMEM supplemented with 1% penicillin-streptomycin, 1% L-glutamine, and 20 mM HEPES) for 45 minutes at 37ºC with 5% CO_2. The femoral heads were then agitated using a sterile pastette for 30 seconds, then transferred to a fresh sterile 100 mm culture dish and submerged in 20 ml of fresh 3 mg/ml collagenase II for a second incubation period of 45 minutes at 37ºC. The femoral heads were agitated again, then transferred to a fresh sterile 100 mm culture dish and submerged in 20 ml of 0.5 mg/ml collagenase II and incubated at 37ºC overnight. The next day, the femoral heads were agitated again, and the cell suspension mixed thoroughly before the cell suspension was aspirated and passed through a 48 μm nylon mesh into a sterile 50 ml universal tube (BD Falcon™) to remove any soft tissue

debris. The filtered cell suspension was centrifuged for 10 minutes at 1500 rpm, following which the supernatant was discarded. The cell pellet was washed in PBS (1X; Invitrogen™) by further centrifugation for 10 minutes at 1500 rpm; the resultant supernatant was discarded. The cell pellet was resuspended in 3 ml of complete culture media (DMEM supplemented with 10% FCS, 1% penicillin-streptomycin, 1% L-glutamine, and 20 mM HEPES) and cell counting was performed using Trypan Blue dye to ensure $\geq$ 95% cell viability.

Chondrocytes were then seeded at a density of 1 x 10^5 cells/cm^2 in complete culture media in 24-well culture plates (Corning®, Costar®) and incubated overnight (37°C, 5% CO_2). The next day, the media was removed and seeded chondrocytes were washed with serum-free media. The seeded chondrocytes were then incubated for 48 hours in serum-free media containing no treatment (unstimulated), murine recombinant TNFα (100 ng/ml; R&D®, 410MT010), human recombinant IL1α (10 ng/ml; Sigma®, I2778), recombinant murine Oncostatin-M (OSM, 100 ng/ml; R&D®, 495MO025), or human recombinant IGF1 (100 ng/ml; R&D®, 291G1200), after which cultures were processed for total RNA extraction of treated chondrocytes.

2.2.10 RNA extraction and quantification

RNA was extracted from immature murine chondrocytes using the GenElute™ Mammalian Total RNA kit (Sigma®). RNA was extracted from murine chondrocytes in culture plates according to the manufacturer's instructions. Lysis solution was prepared comprising 10 μl of β-mercaptoethanol for each 1 ml of lysis solution required. Lysis solution contained guanidine thiocyanate to lyse adherent cells; β-mercaptoethanol acts to inactivate any RNAses. Media was aspirated from the culture wells, and adherent cells were submerged in 500 μl of lysis solution for 2 minutes. The lysed cell suspension was then collected and centrifuged at 14000 rpm for 2 minutes. The filtered lysate was then thoroughly mixed with 500 μl of 70% ETOH (Sigma®) using a P1000 pipette (Eppendorf®). The lysate/ethanol mixture was then centrifuged in 500 μl aliquots at 14000 rpm for 15 seconds in a RNA-binding column, to remove DNA and cellular debris. The lysate was centrifuged in a silica column with wash solutions containing ethanol (Sigma®) twice (14000 rpm for 15 seconds). The RNA was then eluted from the column by a final centrifugation with elution solution (14000 rpm for 1 minute). RNA concentration was measured using a NanoDrop1000 v3.7.0 (Thermoscientific) and sample purity was assessed using the A260/A280 ratio. All samples used for subsequent complementary DNA (cDNA) synthesis had A260/A280 ratios of ~2.0 to ensure high purity from potential contaminants such as proteins or phenol. The RNA was then stored at -80^{o}C until used for cDNA synthesis.

2.2.11 Reverse transcription cDNA synthesis

The RNA samples were reverse transcribed to produce cDNA using qScript™ cDNA Supermix (Quanta Biosciences™) reagents. All reactions were performed on ice in a laminar flow hood (Envair Ltd) using RNAse-free equipment. All incubation steps were performed using a MJ Research® thermocycler. An equal quantity of RNA (1000 ng) was combined in a microcentrifuge tube with 4 µl of qScript™ cDNA Supermix (5X) and the requisite volume of DEPC-treated H_2O for a total reaction volume of 20 µl. Microcentrifuge tubes were then incubated at 25°C for 5 minutes, 42°C for 30 minutes, and 85°C for 5 minutes. After completion of cDNA synthesis, cDNA was stored at 4°C for a maximum of 2 weeks until utilised for quantitative PCR.

2.2.12 qPCR amplification and analysis

Quantitative PCR (qPCR) reactions were performed to assess the expression of chondrocyte markers following treatment of murine immature chondrocytes with anabolic and catabolic cytokines. All reactions were prepared on ice and protected from direct light. Reactions were performed using cDNA produced by reverse transcription using primers and TaqMan probes specific to the genes being studied (Appendix 7.2). Primers were designed using the Roche Universal Probe Library (UPL) Assay Design Center (available at www.universalprobelibrary.com). The TaqMan probes have two labels, one that fluoresces, and another that quenches that fluorescence. During the extension phase of the PCR reaction, the Taq polymerase cleaves the probe from its target sequence causing the fluorescent reporter label to be separated from the quencher, thereby permitting it to fluoresce. Fluorescence resulting from qPCR reactions was detected and quantified using a MJ Research® Chromo 4 Real Time PCR thermocycler and MJ OpticonMonitor 3.1 analysis software. The cDNA and reagents were combined in the proportions shown in Table 2.1, and reactions performed using the thermocycling conditions shown in Table 2.2.

Reagent	Volume (μl)	Final Concentration
2X SensiFAST probe No-ROX	10	1X
10 μM Forward primer	0.8	400 nM
10 μM Reverse primer	0.8	400 nM
10 μM Probe	0.2	100 nM
cDNA template	2	-
RNAse-free H_2O	6.2	-
Total volume	**20**	-

Table 2.1 – Reagent concentrations for qPCR reactions; (nM, nanomolar)

Step	Temperature (ºC)	Time
1. Denature template	95	5 minutes
2. Denature template	95	10 seconds (40 cycles of steps 2-5)
3. Anneal primers	60	30 seconds
4. Extend primers	72	15 seconds
5. Read fluorescence	-	-
6. Completion	4	Incubate

Table 2.2 – qPCR thermocycling conditions

All cDNA samples used in qPCR reactions were generated using equal quantities of RNA template (1000 ng). All qPCR reactions to evaluate gene expression of chondrocyte markers were run simultaneously alongside reactions to evaluate the expression of the housekeeping gene *GAPDH* (glyceraldehyde 3-phosphate dehydrogenase) from the same sample. Chondrocyte marker target gene expression was determined relative to *GAPDH* gene expression using the 'delta-delta C_t' method, without efficiency correction: the relative target gene expression (R) quantification is established using the equation $R = 2^{-\Delta\Delta Ct}$ (404). All experiments were performed in triplicate with three replicates from independent samples.

2.2.13 Statistical analysis

All statistical analyses were performed using SPSS Statistics Version 19.0.0 (IBM; Armonk, New York, U.S.). All continuous dependent variables measured for independent groups were assessed for conformity with a normal distribution using the Shapiro-Wilk Test of Normality, with $p < 0.05$ indicating deviation from a normal distribution. Student's t-Test was performed to compare normally distributed continuous dependent variables for two independent groups. For comparison of continuous dependent variables for two independent groups in which the dependent variable did not conform to a normal distribution in either group, a Mann-Whitney *U* test was performed.

TRIM32 protein expression by human femoral head primary articular chondrocytes between control patients and patients with hip OA, and the age of control patients and patients with hip OA, were compared using Student's t-Test, with statistical significance accepted at $p < 0.05$.

Total ACAN content, ACAN content of femoral head explants, ACAN release by femoral head explants, and percentage ACAN release by femoral head explants from WT and *Trim32*$^{-/-}$ mice following treatment with no stimulation, IL1α, or RA were compared using Student's t-Test, with statistical significance accepted at $p < 0.05$. Comparisons of groups of data that did not conform to a normal distribution, and which

were analysed using the Mann-Whitney *U* test, are indicated within the results section (see section 4.4.3; statistical significance accepted at $p < 0.05$). For analysis of the percentage aggrecan release by femoral heads (section 4.4.3.3, Figure 4.7), a two-way analysis of variance (ANOVA) with post-hoc Tukey tests was performed as comparisons were made between both genotype and treatment groups, with statistical significance accepted at $p < 0.05$.

Trim32 mRNA expression by primary chondrocytes from WT and *Trim32*$^{-/-}$ mice following cytokine treatments was analysed using Student's t-Test, with statistical significance accepted at $p < 0.05$. The expression of differentiation markers by primary chondrocytes from WT and *Trim32*$^{-/-}$ mice following treatment with no stimulation, IL1α, TNFα, OSM, or IGF1 was compared using Student's t-Test, with statistical significance accepted at $p < 0.05$. Comparisons of groups of data that did not conform to a normal distribution, and which were analysed using the Mann-Whitney U test, are indicated within the results section (see sections 4.4.4 and 4.4.5). A Bonferroni correction was performed to correct for multiple testing in all comparisons of the expression of differentiation markers by primary chondrocytes following cytokine treatments, with statistical significance accepted at $p < 0.0025$. All results are mean +/- standard deviation (SD).

2.3 The role of *Trim32* in the development of OA *in vivo*: surgically induced and ageing induced OA in *Trim32* knockout mice

2.3.1 *Trim32* knockout mice

Breeding pairs of C57Bl/6 mice with *Trim32* haploinsufficiency were obtained by collaboration with Dr Jens Schwamborn of the University of Münster**.** These mice carry a gene trap insertion in the *Trim32* gene within exon 2, which includes the entire open reading frame (ORF) (Fig 2.1). *Trim32* is located on mouse chromosome 4 and resides within an intron flanked by exons 16 and 15 of the *Astn2* gene, which is transcribed in the opposite direction on chromosome 4. The tissue expression of *Astn2* is fully preserved and *Trim32* expression is disrupted in mice homozygous for the *Trim32* gene trap insertion (*Trim32*$^{-/-}$ mice) (295). These mice have normal size, reproduce normally, have normal survival, but have been reported to develop a mild skeletal myopathy after 5 months of age, and also to exhibit increased weight after 8 weeks of age (295). The WT and *Trim32*$^{-/-}$ (KO) mice used in the ageing and DMM experimental OA models were generated by mating heterozygote breeding pairs. The mice were housed in pathogen-free rooms of a designated animal facility, at constant temperature, under a 12-hour dark-to-light cycle with water and pelleted standard commercial diet made available *ad libitum*. The Animal Welfare and Ethical Review Body of the University of Edinburgh approved all animal experiments, which were performed in accordance with the UK Animals (Scientific Procedures) Act 1986. All animal experiments were performed under the Home Office project licence number 70/7964, and under the University of Edinburgh establishment licence number 6002605.

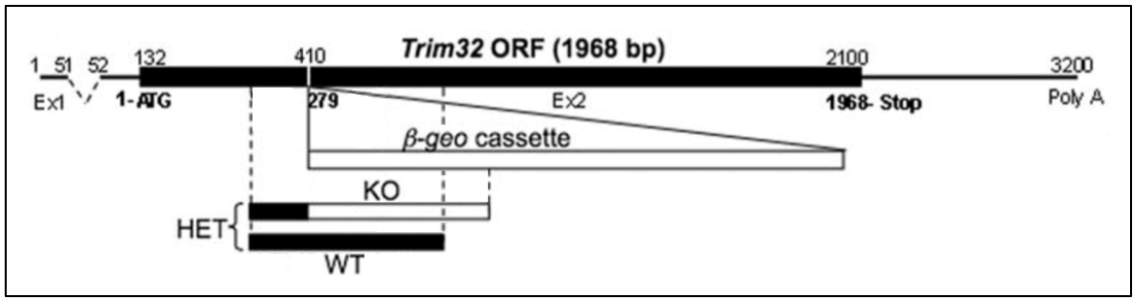

Figure 2.1 – Gene trap insertion generating *Trim32* deficient mice; schematic of the *Trim32* gene with integrated *β-geo* cassette disrupting the entire open reading frame. Adapted from Kudryashova et al (295).

2.3.2 Genotyping of *Trim32* transgenic mice

DNA was extracted from murine ear notches using the Invisorb® Spin Tissue Mini Kit (STRATEC Molecular). Genotyping of extracted DNA was performed by PCR using the oligonucleotide primer pairs listed in Table 2.3 for the WT *Trim32* allele and the *β-geo* fusion vector element. PCR amplification was performed using the Qiagen® *Taq* DNA polymerase reagents prepared on ice and as shown in Table 2.4, PCR cycling conditions as shown in Table 2.5, and processed using the MJ Research® thermocycler. Water was used as a negative control in all PCR reactions. All amplified products were diluted 1:1 in 1X Orange-G loading dye and run parallel to a low molecular weight marker (LMW) (New England BioLabs®) on a 1% agarose (Bioline)-EDTA-TBE (1X) gel containing 1:10000 SYBR® Safe (Invitrogen™). Visualisation took place under ultraviolet light using GENEGenius (Syngene) and GeneSnap v6.05.01 (Syngene) software. A representative image from reactions for genotyping *Trim32* transgenic mice is shown in Figure 2.2.

Target	Forward primer (5'-3')	Reverse primer (5'-3')	PCR product size (bp)
B-Geo fusion vector	caaatggcgattaccgttga	tgcccagtcatagccgaata	625
Trim32	agcttctcacctgaacctggatgc	agccttataccttgcctgaagatccc	535

Table 2.3 – Oligonucleotide primer sequences for PCR genotyping of *Trim32* transgenic mice

Reagent	Volume (µl)
Taq Reaction Buffer	2.5
dNTPs	2
Forward Primer	1.25
Reverse Primer	1.25
Distilled H_2O	7.875
Q solution	5
DNA	5
Q-*Taq* Polymerase	0.125
Total	**25**

Table 2.4 – Reagents for PCR genotyping of *Trim32* transgenic mice; (dNTP, deoxynucleotide)

Step	Temperature (ºC)	Time
1. Denature template	94	3 minutes
2. Denature template	94	45 seconds (30 cycles of steps 2-4)
3. Anneal primers	55	30 seconds
4. Extend primers	72	90 seconds
5. Extend primers	72	10 minutes
6. Completion	4	Incubate

Table 2.5 – PCR cycling conditions for genotyping *Trim32* transgenic mice

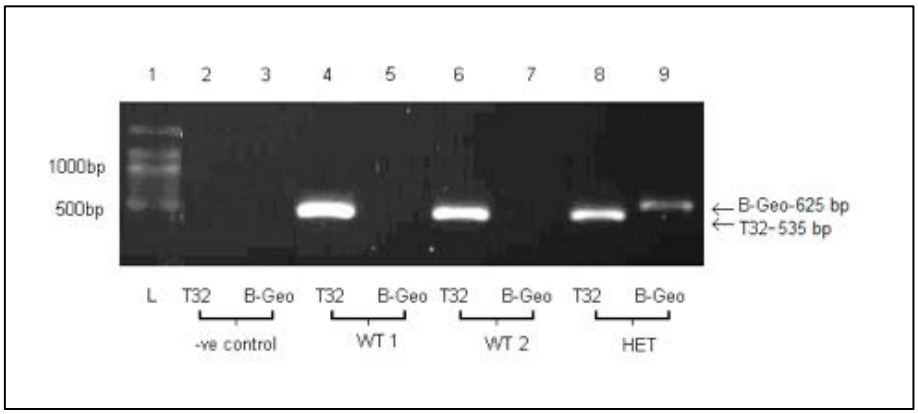

Figure 2.2 - PCR genotyping of *Trim32* heterozygous mice and wild-type mice; a 1% agarose gel showing products from PCR genotyping for *Trim32*-disrupting gene trap insertion *B-Geo* (B-Geo, 625 base pairs (bp)) and *Trim32* (T32, 535 bp) using DNA from wild-type C57BL/6 mice (WT) and mice heterozygous for the gene trap disruption (HET). Lanes: 1) LMW bp ladder (L); 2) -ve control for *Trim32* (no DNA); 3) -ve control for *B-Geo* (no DNA); 4) *Trim32* for WT mouse 1 (WT1); 5) *B-Geo* for WT1; 6) *Trim32* for WT mouse 2 (WT2); 7) *B-Geo* for WT2; 8) *Trim32* for HET mouse (HET); and 9) *B-Geo* for HET. Both *B-Geo* and *Trim32* is detected in heterozygote mice; only *Trim32* is detected in wild-type mice; neither *B-Geo* nor *Trim32* is detected in mice homozygous for the *Trim32*-disrupting gene trap insertion.

2.3.3 Destabilisation of the medial meniscus (DMM) surgically induced OA model

Osteoarthritis was surgically induced in female mice by performing DMM surgery at eight weeks of age, in a manner similar to the initial reports of the procedure (405). General anaesthesia (GA) was induced by administering inhaled isoflurane (IsoFlo®, Abbott Laboratories, UK) at a concentration of 3-5% mixed in oxygen through an anaesthetic circuit and delivered using a nose cone. Maintenance of anaesthesia was achieved by administering isoflurane at 1-2%. Prior to the start of the procedure, mice were also administered 0.3 milligrams (mg)/ml buprenorphine (Vetergesic®, Champion Alstoe, UK; diluted in sterile water) by subcutaneous injection. The right lower limb was shaved to remove hair, and prepared with povidone-iodine (Videne®, EcoLab Ltd, UK). The mice were placed on a sterile heated stage under a surgical microscope (Leica S6D, Leica Microsystems, UK). All surgical instruments were obtained from Wetlab (Kenilworth, UK), except for microsurgical knives (3 mm blade size, WPI, UK); all instruments were sterilised pre-operatively. Using sterile technique, a 1 cm anterior paramedian skin incision was performed centred over the medial joint line. A 0.5 cm vertical incision in the capsule of the medial aspect of the knee joint was then performed. The medial meniscotibial ligament (MMTL) was identified and transected at its mid-portion to enact full release of the anterior portion of the medial meniscus, which was confirmed intra-operatively during each procedure (Figure 2.3). Direct care was taken not to cause iatrogenic injury to the cruciate ligaments, medial collateral ligament, or articular surfaces throughout the procedure. After thorough irrigation of the wound with sterile saline, the wound was closed with two or three 5-0 absorbable sutures (Vicryl, Ethicon, UK). The mice were recovered from GA in an incubation chamber at 25ºC. Mice were returned to fresh cages and housed as previously described, but provided with standard commercial mashed diet for first 24 hours post-operatively. There were no wound problems and no post-operative morbidity in any mice following the procedure.

Following DMM surgery, mice were followed-up for eight weeks and culled at 16 weeks of age by inhalation of escalating concentration of CO_2. The lower limbs were

carefully dissected free, the skin was removed and the limbs were fixed for 24 hours in 4% formaldehyde, and then transferred into 70% ETOH until further analysis.

Sham surgery (skin and joint capsule incision, but no transection of MMTL) was not performed on the contralateral knee as a control in these experimental mice. No sham surgery was selected to protect animal welfare, because previous studies have demonstrated no significant difference in histological OA scores between sham-operated and non-operated knee joints following DMM surgery on the contralateral knee joint, and because the primary objective in this research was to investigate the response to DMM surgery in *Trim32*$^{-/-}$ mice, *Trim32*$^{+/-}$ mice, and WT mice (387, 405). In the analysis of the operated right knee for the development of OA by histological and histomorphometric measurements, the non-operated left knee of each mouse was used as an internal control. DMM surgery was performed on the right knee, and the contralateral left knee was used as the control knee. As the contralateral left knee was used as an internal control, and sham surgery was not performed in separate control group of mice, randomisation was not performed for the DMM procedures. At the time of performing DMM surgery, the operator was blinded to the genotype of the mice, and only aware of the study ID number of the mice.

As the 9q33.1 locus in which *Trim32* resides was associated with hip OA in females, the DMM procedure was performed in female WT, *Trim32*$^{+/-}$ (HET), and *Trim32*$^{-/-}$ (KO) mice (229). Previous studies have demonstrated the response (change in histological cartilage degradation scores at 8 weeks) of female mice to the DMM procedure (376). Using data, from this study, it was determined that to detect a one SD difference in the histological total knee cartilage degradation scores at 8 weeks following the DMM procedure, with a significance threshold of 0.05, and 80% power, a total of 14 female mice would be required in the WT, HET, and KO groups. During the course of the experiments, it was possible to include a total of 14 WT, 14 *Trim32*$^{+/-}$, and 13 *Trim32*$^{-/-}$ mice in the DMM surgically induced OA experiments, providing an approximate 80% power to detect a one SD difference in the histological cartilage degradation scores, with a significance threshold of 0.05.

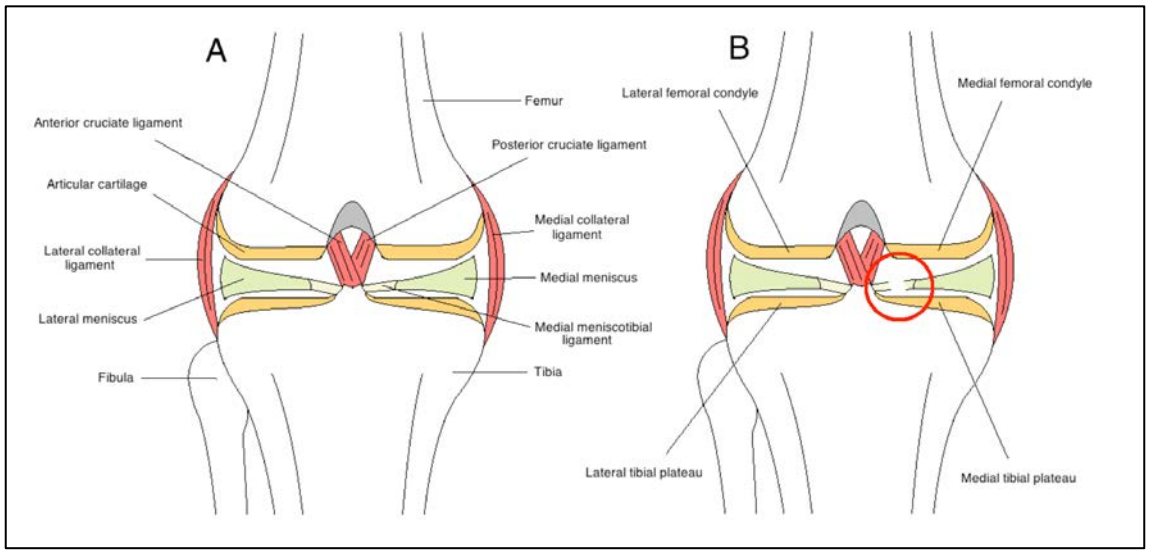

Figure 2.3 – Schematic diagram illustrating the medial meniscotibial ligament before and after transection by destabilisation of the medial meniscus (DMM) surgery; the normal bony and ligamentous architecture of the knee joint in mice is shown in panel A; panel B shows the transected medial meniscotibial ligament (highlighted by a red circle) and subsequent instability of the medial compartment of the knee joint after DMM surgery.

2.3.4 Ageing induced OA

A second OA model was utilised, in which the severity of spontaneous OA induced by ageing was compared in female WT, *Trim32*$^{+/-}$, and *Trim32*$^{-/-}$ mice that had not undergone any specific experimental procedures. At 10 months of age mice were culled by inhalation of escalating concentration of CO_2. The right lower limb was carefully dissected free, the skin was removed, and the limb fixed for 24 hours in 4% formaldehyde, and then transferred into 70% ETOH until later assessed for the development of hip and knee OA by both joint histology and histomorphometry.

As the 9q33.1 locus in which *Trim32* resides was associated with hip OA in females, the experiments evaluating the development of spontaneous OA in aged WT, *Trim32*$^{+/-}$, and *Trim32*$^{-/-}$ mice included female mice only. Previous studies have demonstrated the response (change in histological knee cartilage degradation scores) in aged C57Bl/6 mice (406). Using data, from this study, it was determined that to detect a one SD difference in the histological total knee cartilage degradation scores in aged

mice, with a significance threshold of 0.05, and 80% power, a total of 16 female mice would be required in the WT, HET, and KO groups. During the course of the experiments, it was possible to include a total of 12 WT, 12 *Trim32*$^{+/-}$, and 13 *Trim32*$^{-/-}$ mice in the ageing induced OA experiments. This provided a 70% power to detect a one SD difference in the histological cartilage degradation scores, with a significance threshold of 0.05.

2.3.5 Micro-computed tomography (µCT) of murine joint tissue

Analysis of periarticular bone of hip and knee joints from murine lower limbs was performed by µCT using a Skyscan 1172 instrument (Bruker, Belgium) set at 60 kilovolts (kV) and 167 microamperes (µA), at a resolution of 5 µm. Following acquisition of images for each sample, the images were reconstructed using the Skyscan NRecon programme and analysed using Skyscan CTAn software. The regions of interest (ROI) analysed were the subchondral trabecular bone situated within the distal femoral and proximal tibial epiphyses and the subchondral bone plates of the distal femur and proximal tibia; these regions were analysed separately in both the medial and lateral compartments of the knee joint (Appendix 7.3.1A). For analysis of hip joints, the subchondral trabecular bone and the subchondral bone plate were analysed in the proximal femoral epiphyses of the femoral head (Appendix 7.3.1B). A constant number of consecutive image sections were included across all samples for the analysis of subchondral and trabecular bone of the hip and knee joints. Image contrast thresholds for the detection of subchondral and trabecular bone were constant across all samples for the analysis of hip and knee joints. The µCT analyses were performed in the coronal plane. Representative 3D reconstructions of the µCT images of subchondral and trabecular bone of the hip and knee joints from mice studied in the experimental OA models are shown in Appendix 7.3.2. During capture and analysis of µCT data, blinding of the mice genotype from which samples were retrieved was performed, with only the study ID number of the mice known.

2.3.6 Histological analysis of murine joint tissue

Hip and knee joints were dissected from lower limbs previously fixed in 4% formaldehyde and 70% ETOH. Individual joints, with the majority of muscle removed were then decalcified in 10% formic acid for 48 hours at 4^{o}C with agitation, with two exchanges of the formic acid. Samples were washed in distilled H_2O, and stored in 70% ETOH for 24 hours prior to paraffin embedding. Paraffin embedding was performed for individual joints by immersing sequentially for one hour each in 80% ETOH, 95% ETOH, three exchanges of 100% ETOH, three exchanges of xylene, and then wax embedding for three hours for three cycles, the third cycle performed under vacuum.

Orientation of knee joints for mounting in blocks was standardised with the medial aspect down and proximal (femoral) extent positioned superior for subsequent sectioning using a Leica RM2235 microtome (Leica Microsystems, UK) in the sagittal plane. Blocks were trimmed until articular cartilage was evident. For each knee joint, sections of 3 µm thickness were obtained at 40 µm intervals through the joint from medial to lateral aspects until articular cartilage was no longer evident; this yielded 15-20 sections for each knee joint. Orientation of hip joints for mounting in blocks was standardised with the anterior aspect down and proximal extent positioned superior for subsequent sectioning in the coronal plane. Blocks were trimmed until articular cartilage was evident. For each hip joint, sections of 3 µm thickness were obtained at 40 µm intervals through the joint from anterior to posterior aspects until articular cartilage was no longer evident; this yielded 10-15 sections for each hip joint. Sections were mounted on slides, then incubated at 85^{o}C for 30 minutes, and then overnight at 55^{o}C. Hip and knee joint sections were deparaffinised and gradually hydrated to H_2O, stained in Toluidine Blue for 1 minute, washed in H_2O for 3 minutes, dehydrated in acetone twice for 3 minutes, cleared in xylene and re-mounted on slides.

Histological evaluation of the severity of OA in each joint section was performed with blinding to mouse genotype (only the study ID number of the mice was known) and according to the OARSI scoring system validated for histological assessments in the mouse (Table 2.6; Figure 1.3). Joint sections were reviewed by each assessor for microtomy artefacts; joint sections demonstrating microtomy artefacts were not included

in the scoring of OA severity, to avoid assessing slides with possible cutting artifacts. Microtomy artefacts were indicated by gross fragmented tissue, or incomplete joint sections on the slide. Joint sections were also reviewed by each assessor for iatrogenic surgical artefacts that would be indicated by coarse blade injury to the cartilage on slides corresponding to the anteromedial aspect of the knee joint and adjacent to the medial meniscal tibial ligament; no slides were excluded due to iatrogenic surgical artefacts. For knee joint sections, scores were generated separately for four regions of the joint: the medial tibial plateau (MTP), the medial femoral condyle (MFC), the lateral tibial plateau (LTP), and the lateral femoral condyle (LFC) (Figure 2.3). For hip joint sections, scores were generated from the articular surface of the femoral head only to determine the hip joint section score. As 15-20 sections were assessed in each knee joint, and 10-15 sections assessed for each hip joint, the most severe score of each region for each joint was used for further analyses. For each knee joint, the most severe scores were then summed from the tibial and femoral articular cartilage to provide a summed score for the medial and lateral compartments of the knee (ranging from a minimum possible score of 0 to a maximum possible score of 12). Finally, total scores for each whole knee joint were calculated by combining the scores for the medial and lateral compartments of each joint (ranging from a minimum possible score of 0 to a maximum possible score of 24). A second observer, who was also blinded to genotype, assessed a randomly selected sample of nine joints to test the inter-observer reproducibility of the scoring system.

Grade	Structural appearance of articular cartilage
0	Normal
1	Small fibrillations without loss of cartilage
2	Vertical clefts to beneath superficial layer; some loss of surface lamina
3	Vertical clefts/erosion to calcified cartilage affecting <25% of articular surface area
4	Vertical clefts/erosion to calcified cartilage affecting 25-50% of articular surface area
5	Vertical clefts/erosion to calcified cartilage affecting 50-75% of articular surface area
6	Vertical clefts/erosion to calcified cartilage affecting 75-100% of articular surface area

Table 2.6 – OARSI scoring system for assessment of OA in mice; the criteria for the nature and extent of structural changes associated with increasing severities of OA are shown; adapted from Glasson et al (383).

2.3.7 Nociception testing

Hypersensitivity to somatosensory stimuli was measured following DMM surgery in a second group of *Trim32* transgenic mice. DMM surgery was performed in female WT and *Trim32*$^{-/-}$ mice at eight weeks of age. Hypersensitivity to somatosensory stimuli, reflecting a reduced pain threshold due to chronic pain, was assessed by separately measuring the limb withdrawal threshold upon application of brief mechanical stimuli to the operated and non-operated hind limbs of mice eight weeks following the DMM surgery. Mice were placed on a wire-mesh floor within a cage. Von Frey filaments (bending force range used from 0.16 grams (g) to 8 g) were applied in ascending order of bending force at right angles to the mid-plantar surface of the hind paw through the mesh floor until limb withdrawal occurred. Each filament was applied to the hind paw until either filament bending or limb withdrawal occurred. Five-second time intervals between filament applications were used. The process was reported three times for the operated and non-operated limb of each animal, with intervals of 15 minutes between each set of tests. The lowest force recorded to induce withdrawal of each limb was used for analyses. A total of seven WT, and eight *Trim32*$^{-/-}$ mice were studied in nociception testing of operated and non-operated limbs in mice following induction of OA by DMM surgery. The operator performing nociception testing was blinded to mice genotype and limb of DMM surgery, with only the study ID number of the mice known.

2.3.8 Grip strength testing

The *Trim32*$^{-/-}$ mice have been reported to develop a mild skeletal myopathy after 5 months of age (295). To investigate any variation in muscle strength that may contribute to the development of OA, in addition to other mechanisms disrupted by deficiency of *Trim32*, limb grip strength testing was performed in each animal following completion of nociception testing (see 2.8.7). To measure limb grip strength, mice were assisted in grasping a pull bar of a grip strength meter with both fore limbs, and the peak force applied before loss of grasp was recorded (the animals could readily release the grip prior to any discomfort). The limb grip strength testing was performed in triplicate for each mouse, and mean scores for each animal used for further analyses. A total of seven WT, and eight *Trim32*$^{-/-}$ mice were studied in fore limb grip strength. The operator performing grip strength testing was blinded to mice genotype, with only the study ID number of the mice known.

2.3.9 Statistical analysis

All statistical analyses were performed using SPSS Statistics Version 19.0.0 (IBM; Armonk, New York, U.S.), and statistical significance was accepted at $p < 0.05$, unless specifically stated. Power calculations for the murine studies were performed using Minitab 17 (Minitab; State College, Pennsylvania, U.S.). All continuous dependent variables measured for independent groups were assessed for conformity with a normal distribution using the Shapiro-Wilk Test of Normality, with $p < 0.05$ indicating deviation from a normal distribution. Student's t-Test was performed to compare normally distributed continuous dependent variables for two independent groups. A Mann-Whitney *U* test was performed for comparison of continuous dependent variables for two independent groups in which the dependent variable did not conform to a normal distribution in either group, or of ordinal variables for two independent groups. One-way ANOVA with post-hoc Tukey tests was performed to compare a normally distributed variable between greater than two independent groups with differences between each group subsequently examined. Kruskal Wallis test with post-hoc Dunn's tests was

performed to compare ordinal variables, or dependent variables that did not conform to a normal distribution, between greater than two independent groups with differences between each group subsequently examined.

Comparison of number of cagemates and weight of mice between wild type and *Trim32* deficient mice were performed using Student's t-Test. Subchondral bone parameters were compared between WT and *Trim32* deficient mice by one-way ANOVA followed by post-hoc Tukey tests to further investigate significant differences between mice of different genotypes and to control for multiple comparisons.

Data for both hip and knee joint OARSI scores after DMM and ageing deviated from a normal distribution (Shapiro-Wilk tests: unoperated knee medial compartment OARSI scores, $p = 0.000008$; unoperated knee lateral compartment OARSI scores, $p = 0.00001$; operated knee medial compartment OARSI scores, $p = 0.02$; operated knee lateral compartment OARSI scores, $p = 0.01$; unoperated knee total joint scores, $p = 0.0001$; operated knee total joint OARSI scores, $p = 0.03$; aged knee medial compartment OARSI scores, $p = 0.001$; aged knee lateral compartment OARSI scores, $p = 0.01$; aged knee total joint scores, $p = 0.04$; and aged hip OARSI scores, $p = 0.00003$). Hip and knee joint OARSI scores were therefore compared between WT and *Trim32* deficient mice by Kruskal Wallis test with post-hoc Dunn's tests to further investigate significant differences between mice of different genotypes and to control for the effect of multiple comparisons. The inter-observer correlation of OARSI scores observed by independent observers was analysed using Spearman's rank correlation coefficient.

The covariate effect of mice weight on knee joint OARSI scores was investigated using a generalised linear model (GLM). Meta-analysis of hip and knee joint scores in WT and *Trim32* KO mice following ageing and DMM surgery was performed using Review Manager Version 5.3.5 software (The Cochrane Collaboration, Copenhagen). Nociception, measured by hind limb withdrawal thresholds, was compared between WT and *Trim32* KO mice using the Mann-Whitney *U* test (Shapiro-Wilk tests: WT operated limb, $p = 0.001$; KO operated limb, $p = 0.0003$; WT unoperated limb, $p = 0.001$; KO unoperated limb, $p = 0.001$). Grip strength was compared between

WT and *Trim32* KO mice using the Student's t-Test. All results are mean +/- standard deviation (SD).

Chapter 3

Variant screening of *TRIM32*

3.1 Summary

The aim of this chapter was to investigate genetic variation within *TRIM32* to identify novel or rare variants that are associated with OA of the hip in females. *TRIM32* is one of three protein-coding genes at the 9q33.1 susceptibility locus (tagged by the index SNP rs4836732) for hip OA in females. *TRIM32* encodes a protein with E3 ubiquitin ligase activity and may have biological relevance to OA through its role in ubiquitination, muscle regeneration, differentiation, proliferation, and ciliogenesis. Variant screening of *TRIM32* was performed by sequencing the proximal promoter, 5'UTR, both exons, and 3'UTR of *TRIM32* in the youngest 500 female patients with hip OA from the arcOGEN study patient cohort. Variants detected by screening of *TRIM32* were further evaluated by comparing their frequency in females with hip OA with a control population (data from 1000 Genomes Project), analysing LD with the index SNP rs4836732, assessing consequent amino acid and protein modifications, and bioinformatic analyses of transcription factors and regulatory motifs.

Nine variants were detected in female patients with hip OA: rs811457 located in the proximal promoter; rs12342207 located in the 5'UTR; rs141806013, rs3747835, and rs1661300 that reside within the coding region of exon 2; and rs3019, a novel variant (c.13277C>C/T), rs22816277, and rs761458746 that reside in the 3'UTR of *TRIM32*. None of the variants were in LD with the index SNP rs4836732. Two variants, rs811457 and rs3019 were detected in female patients with hip OA at disproportionate frequencies compared to the control population. The rs811457 variant was present at a reduced frequency in females with hip OA and may be protective against hip OA ($p = 0.001$; OR: 0.238 [0.092 – 0.617]). The rs3019 variant was present at an increased frequency in female patients with hip OA and was associated with an increased risk of hip OA in female patients ($p = 0.036$; OR: 1.512 [1.081 – 2.115].

The identification of rare variants in the proximal promoter and 3'UTR of *TRIM32* that are present at disproportionate frequencies in female patients with hip OA compared to the control population further implicates *TRIM32* in the genetic predisposition to OA and supports the further study of TRIM32 in the pathophysiology of OA.

3.2 Introduction

The overall aim of the experiments described in this chapter was to identify genetic variants within *TRIM32* and to identify novel or rare variants in *TRIM32* that are associated with OA of the hip in female patients. The *TRIM32* gene lies within the susceptibility locus with the greatest effect size identified by the arcOGEN GWAS of hip and knee OA, which was that on chromosome 9q33.1 (represented by the index genotyped SNP rs4836732; OR 1.20 [1.13 – 1.27], $p = 6.11 \times 10^{-10}$), and which was associated with the specific phenotype of hip OA in females (Figure 1.4 (229)). The top hit SNP rs4836732 may only be representative of true causal variants within this locus, and may be in LD with other causal SNPs at this locus. This locus contains three protein-coding genes (*ASTN2*, *PAPPA*, and *TRIM32*). Although variants in multiple genes may be represented by the previously identified association signal, the experiments in this chapter focused on detailed evaluation of *TRIM32*. *TRIM32* encodes a protein with E3 ubiquitin ligase activity, which may have biological relevance to the development of OA through its role in ubiquitination, musculoskeletal regeneration, and regulation of differentiation, proliferation, and ciliogenesis (281, 298, 301, 303).

Screening of *TRIM32* was performed by sequencing the proximal promoter, 5'UTR, both exons, and the 3'UTR in the youngest 500 female patients with hip OA from the arcOGEN study cohort. The youngest 500 female patients with hip OA were selected because the association of the index SNP rs4836732 was gender-specific, and the frequency of causal variants at this locus may be enriched in patients predisposed to the development of early-onset hip OA. Variants detected by screening of *TRIM32* in this cohort were then evaluated by comparing their frequency in female patients with OA with a control population (using data from the 1000 Genomes Project), analysing LD with the index SNP rs4836732, assessing consequent amino acid and protein modifications, and investigating if the variant was reported as an eQTL or located within a transcription factor binding site or regulatory motif.

3.3 Aims

The aims of the experiments described in this chapter were to:

1. Investigate the genetic variation of *TRIM32* to identify novel or rare variants in *TRIM32* that are associated with OA of the hip in females.
2. Investigate the biological implication of variants in *TRIM32* identified as associated with OA of the hip in females using bioinformatic analyses.

3.4 Results

3.4.1 Variants identified by DNA sequencing of *TRIM32*

To investigate the genetic variation of *TRIM32* to identify novel or rare variants in *TRIM32* that are associated with OA of the hip in females, TRIM32 was sequenced using DNA from the youngest available 500 female patients with hip OA from the arcOGEN study (229). The proximal promoter, 5'UTR, both exons, and 3'UTR of *TRIM32* were successfully amplified and sequenced in these patients. Variant screening was then performed and the frequency of any previously known variants from this cohort was compared against that of control population data retrieved from the 1000 Genomes Project (391). This enabled identification of any variants that are more or less prevalent in patients with hip OA, and associated with risk of developing hip OA. The identified variants are shown in Figure 3.1. Details of the nine variants identified in *TRIM32* in patients with hip OA, are shown in Table 3.1, including the location of each polymorphism within *TRIM32*, the Single Nucleotide Polymorphism database (dbSNP) identification number (if the variant has previously been reported), the associated genotypes and amino acid substitutions, genotype frequency, allele frequency in patients with hip OA and the control population, and estimation of the effect size of each variant in relation to the risk of developing hip OA. A schematic demonstrating the position of the identified variants within *TRIM32* is shown in Figure 3.2. Detailed description of the variants in each region of *TRIM32* is provided in the subsequent sections in this chapter (3.4.1.1 (5'UTR), 3.4.1.2 (Exon 2), 3.4.1.3 (3'UTR)). None of the nine identified variants deviated from Hardy-Weinberg equilibrium.

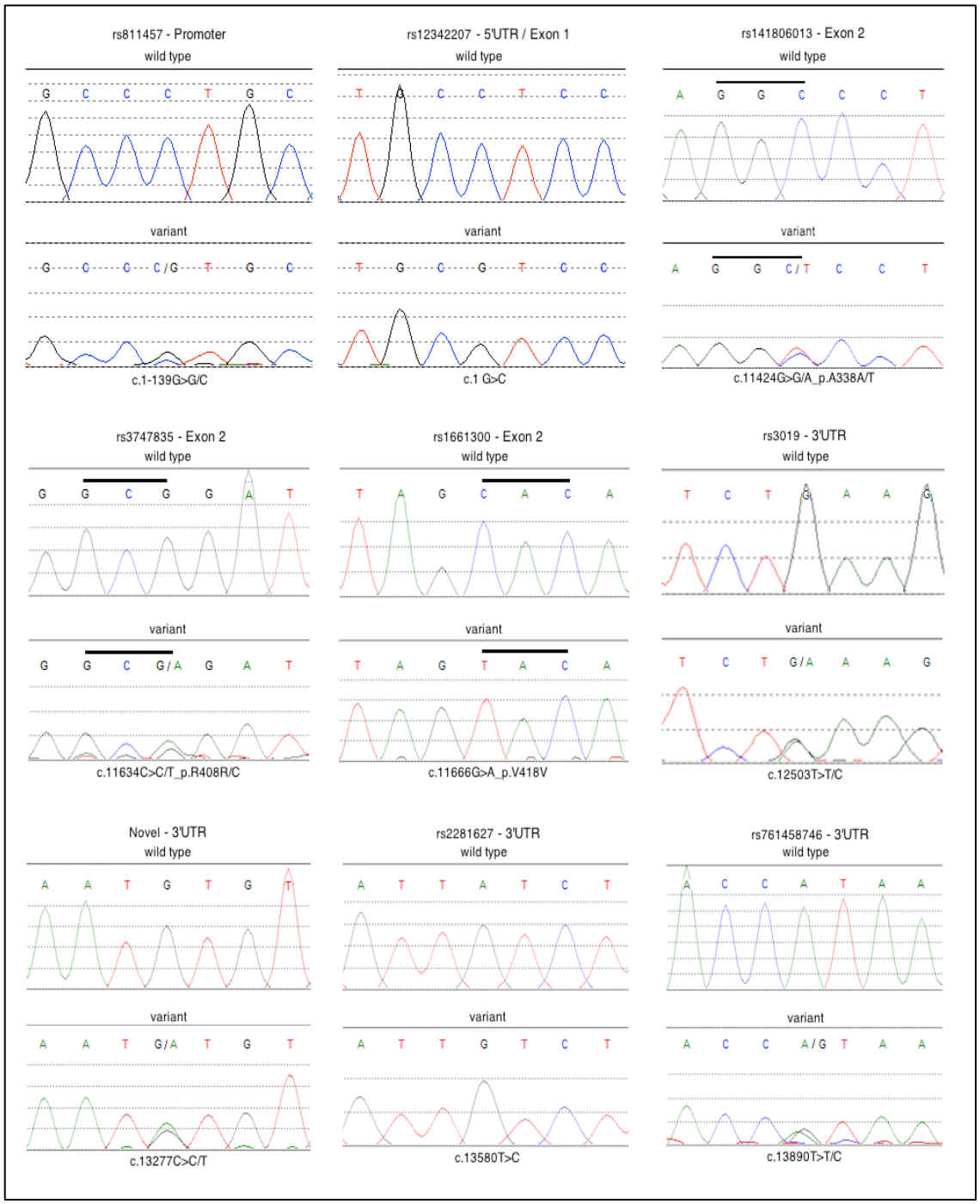

Figure 3.1 – Variants identified by DNA sequencing of *TRIM32*; variants identified by DNA sequencing of the proximal promoter, 5'UTR, both exons, and 3'UTR of *TRIM32* in the 500 youngest female patients with hip OA from the arcOGEN study cohort are shown; wild type and variant sequences are shown. Chromatogram images were generated using Mutation Surveyor® software (version 3.97; Softgenetics) with nucleotide sequences for the sense strand shown; adenine (green), cytosine (blue), guanine (black), thymine (red). Polymorphism identification (ID) numbers from dbSNP are shown for previously known variants, black bars indicate amino acid codons, and the variant *TRIM32* genotype and any corresponding amino acid change indicated beneath each chromatogram.

TRIM32 region	dbSNP identification number	Genotype	Genotype frequency in female hip OA cases (ratio (n))	Allele	Allele frequency in female hip OA cases (ratio)	MAF in control population	Chi-squared test p-value	Risk allele	Odds ratio [95 % CI]
Promoter	rs811457	c.1-139G>G/C	0.015 (5)	G	0.993	0.03	**0.001***	C	0.238 [0.092 - 0.617]
		c.1-139G>C	0.000 (0)	C	0.007				
5'UTR/Exon 1	rs12342207	c.1G>G/C	0.445 (153)	G	0.688	0.305	0.770	C	1.035 [0.839 - 1.276]
		c.1G>C	0.090 (31)	C	0.312				
Exon 2	rs141806013	c.11424G>G/A_p.A338A/T	0.005 (2)	G	0.997	0.001	0.563	A	2.724 [0.247 - 30.093]
		c.11424G>A_p.A338T	0.000 (0)	A	0.003				
Exon 2	rs3747835	c.11634C>C/T_p.R408R/C	0.002 (1)	C	0.999	0.001	0.563	T	0.607 [0.055 - 6.706]
		c.11634C>T_p.R408C	0.000 (0)	T	0.001				
Exon 2	rs1661300	c.11666G>G/A_p.V418V	0.162 (67)	G	0.907	0.115	0.147	A	0.787 [0.580 - 1.066]
		c.11666G>A_p.V418V	0.012 (5)	A	0.093				
3'UTR	rs3019	c.12503T>T/C	0.24 (63)	T	0.871	0.089	**0.036***	C	1.512 [1.081 - 2.115]
		c.12503T>C	0.008 (2)	C	0.129				
3'UTR	Novel	c.13277C>C/T	0.006 (2)	C	0.997	N/A	N/A	T	N/A
		c.13277C>T	0.000 (0)	T	0.003				
3'UTR	rs2281627	c.13580T>T/C	0.417 (134)	T	0.685	0.32	0.857	C	0.975 [0.788 - 1.206]
		c.13580T>C	0.106 (34)	C	0.315				
3'UTR	rs761458746	c.13890T>T/C	0.003 (1)	T	0.998	N/A	N/A	C	N/A
		c.13890T>C	0.000 (0)	C	0.002				

Table 3.1 – Variants identified by DNA sequencing of *TRIM32*; variants identified by DNA sequencing of the proximal promoter, 5'UTR, both exons, and 3'UTR of *TRIM32* in the 500 youngest female patients with hip OA from the arcOGEN study cohort are shown; consequent heterozygote and homozygote variant genotypes are shown with any associated amino acid changes. Polymorphism ID numbers from dbSNP are shown for previously known variants. Genotypes are shown for *TRIM32* sequence as the forward strand. The minor allele frequency (MAF) for the control population was retrieved from data from the 1000 Genomes Project for the CEU population of European ancestry (1000GENOMES:phase_3:EUR (391)). Statistical analysis was performed by chi-squared (χ^2) test to determine whether the minor allele frequencies observed among patients with hip OA were significantly different from those expected from the control population, and odds ratios were determined to estimate effect sizes of risk alleles; statistically significant results are annotated with (*) and presented in bold. OA: osteoarthritis; UTR: untranslated region; C: cytosine; G: guanine: T thymine: A: adenine; N/A: data not available; 95% CI: 95% confidence interval.

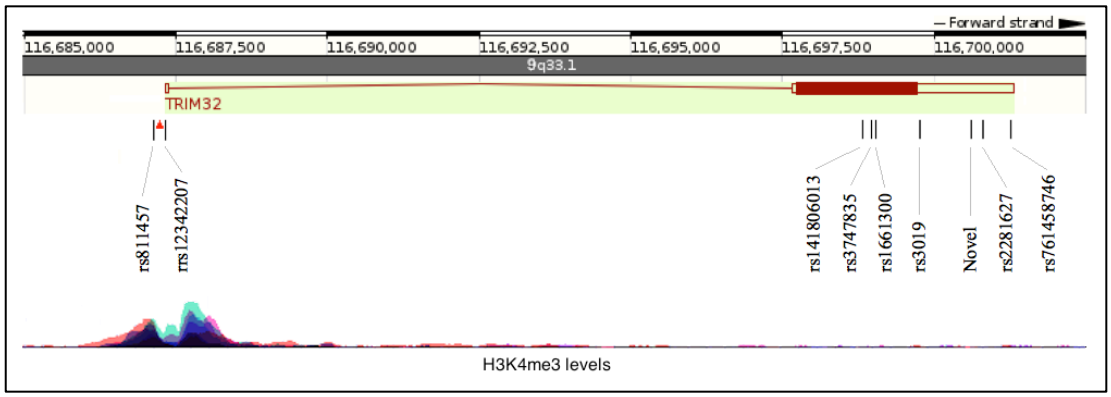

Figure 3.2 – Schematic of *TRIM32* demonstrating position of identified variants in female patients with hip OA; the position of the nine variants identified by DNA sequencing of *TRIM32* in the youngest 500 female patients from the arcOGEN study cohort are shown (229). The black bars indicate the position of the identified variants rs811457, rs12342207, rs141806013, rs3747835, rs1661300, rs3019, rs2291627, rs761458746, and the novel variant (c.13277C>C/T). The red triangle indicates the binding site for transcription factors TFAP2C and TFAP2A. The histogram beneath the *TRIM32* gene schematic shows the levels of enrichment of the H3K4me3 histone mark, often found near promoters, across *TRIM32* (the different colours indicate H3K4Me3 enrichment levels in different cell lines. The *TRIM32* schematic is adapted from data available using the Ensembl genome browser, using data from the GRCh38 genome build (407).

	TRIM32 region								
	Promoter	5'UTR	Exon 2			3'UTR			
Species	rs811457	rs12342207	rs141806013	rs3747835	rs1661300	rs3019	Novel	rs2281627	rs761458746
Human	G	G	A	R	V	T	C	T	T
Rhesus monkey	G	G	A	R	V	T	C	T	T
Mouse	A	A	A	R	V	T	C	T	T
Dog	N/A	N/A	A	R	V	T	C	N/A	T
Elephant	N/A	N/A	S	R	V	T	C	T	T
Chicken	N/A	N/A	T	R	V	T	N/A	N/A	N/A
Zebrafish	A	N/A	S	R	V	T	N/A	N/A	N/A
	Nucleotide		Amino acid			Nucleotide			

Table 3.2 – Species conservation for sites identified in variant screening of *TRIM32*; data was retrieved using the UCSC Human Genome Browser (408). The conservation of nucleotides across different species at the positions of the nine variants identified by sequencing *TRIM32* in 500 female patients with hip OA is shown. Comparison of the nucleotide at the position of each variant in the human genome is made with known nucleotides at each position for rhesus monkey, mouse, dog, elephant, chicken, and zebrafish genomes. N/A: data not available. For nucleotides, A = adenine, C = cytosine, G = guanine, and T = thymine. For amino acids, A = alanine, R = arginine, S = serine, T = threonine, and V = valine.

3.4.1.1 Variants in proximal promoter and 5'UTR of *TRIM32*

The proximal region of *TRIM32* was sequenced using DNA from the youngest available 500 female patients with hip OA from the arcOGEN study (229), including the proximal promoter and the 5'UTR of *TRIM32*. Mutation screening of the proximal promoter region identified the known SNP rs811457, c.1-139G>G/C (Figure 3.1 and Figure 3.2). This variant was identified in five HET patients with primary hip OA (Table 3.1). This variant results in a guanine to cytosine alteration and lies immediately proximal (-3 bp) to the CGI of the *TRIM32* promoter region. Although it is not itself reported to lie within a transcription factor binding site, it lies adjacent (-10 bp) to binding sites for transcription factor AP-2 gamma (TFAP2C) and transcription factor AP-2 alpha (TFAP2A) and in a region marked by very high levels of histone H3 lysine 4 methylation (H3K4me3; Figure 3.2). This variant, rs811457, was found to be present at a lower frequency in female patients with hip OA compared to the control population ($p = 0.001$; Table 3.1). The protective allele (C) for OA had an effect size of 0.238 [0.092 – 0.617] (Table 3.1). However, this variant was not in LD ($r^2 = 0.058$) with the index SNP (rs4836732) at the 9q33.1 locus identified as associated with hip OA in female patients in the arcOGEN study (Figure 1.4 (229)). This variant has not previously been reported as an eQTL for any genes in any tissues, and the polymorphism is not at a position that is highly conserved across species (Table 3.2). Furthermore, none of the remaining variants have been reported as an eQTL for any genes in any tissues.

Another variant, rs12342207, was identified that is located in the 5'UTR of *TRIM32* and which resulted in a change from guanine to cytosine (Figure 3.1 and Figure 3.2). This variant was identified at a relatively high frequency, but its frequency in female patients with OA did not differ significantly from the control population ($p = 0.770$; Table 3.1). Furthermore, this variant was only in moderate LD with the index SNP, rs4836732, at this susceptibility locus for OA ($r^2 = 0.431$).

Sequencing of the proximal promoter and 5'UTR of *TRIM32* in female patients with hip OA therefore identified two known variants, rs811457 and rs12342207. The rs12342207 variant was not present at significantly different frequencies between female patients with OA and the control population ($p = 0.770$). However, the rs811457 variant

was present at a lower frequency in female patients with OA compared to the control population (p = 0.001).

3.4.1.2 Variants in exon 2 of *TRIM32*

Exon 2 of *TRIM32* was also sequenced in 500 female patients with hip OA. Three variants were identified in exon 2, which contains the entire ORF for *TRIM32 (*Figure 3.1 and Figure 3.2). The rs141806013 variant results in an alanine to threonine amino acid change in exon 2, in a region of TRIM32 between the coiled-coil and NHL repeat domains (Figure 1.5). *In silico* assessment of the rs141806013 variant indicated that it is a benign and tolerated variant within the coding region of *TRIM32*. The rs3747835 variant results in an arginine to cysteine amino acid change within the NHL repeat domain of TRIM32 (Figure 1.5). *In silico* assessment of the rs3747835 variant indicated that it is a deleterious variant. However, neither rs141806013 nor rs3747835 were detected at a significantly different frequency in patients with hip OA compared to the control population (rs141806013: p = 0.563, rs3747835: p = 0.563; Table 3.1). LD data for rs141806013 and rs3747835 in relation to the index rs4836732 SNP were not available, as these variants were not covered by the available databases. The third variant identified in exon 2, rs1661300, is a synonymous mutation involving a guanine to adenine alteration (Table 3.1). This variant was not in LD with the index SNP rs4836732 (r^2 = 0.067), and was not present at a significantly different frequency in female patients with OA compared with the control population (p = 0.147). All three variants identified in exon 2 of *TRIM32* are at sites demonstrating high cross-species conservation (Table 3.2).

Sequencing of exon 2 of *TRIM32* in female patients with hip OA therefore identified three known variants, rs14180013, rs374785, and rs1661300. However, none of these variants were present at significantly different frequencies between female patients with hip OA and the control population.

3.4.1.3 Variants in 3'UTR of *TRIM32*

Finally, the 3'UTR region of *TRIM32* was sequenced in 500 female patients with hip OA. Four variants were identified in the 3'UTR of *TRIM32* (Figure 3.1 and Figure 3.2; Table 3.1). A novel variant, c.13277C>C/T, was identified that represents a cytosine to thymine alteration and which has not previously been reported. This novel variant was present in HET form in only two patients with hip OA. The rs2281627 variant results in a thymine to cytosine alteration in the 3'UTR of *TRIM32*. This variant was in moderate LD with the index SNP rs4836732 ($r^2 = 0.395$), but was present at a similar frequency in female patients with hip OA compared to the control population ($p = 0.857$). The rs761458746 variant represents a change from thymine to cytosine in the 3'UTR of *TRIM32* and was identified in HET form in a single female patient with hip OA; MAF and LD data for this SNP were also not available.

Finally, the rs3019 variant in the proximal 3'UTR of *TRIM32* was detected at a significantly higher frequency in female patients with hip OA compared to the control population ($p = 0.036$; Table 3.1). This variant, c.12503T>T/C, results in a thymine to cytosine alteration. The C risk allele was associated with an increased risk of hip OA in female patients, with an odds ratio of 1.512 (95% CI: [1.081 – 2.115]; Table 3.1). The rs3019 variant was not in LD with the previously reported index SNP rs4836732 at the 9q33.1 susceptibility locus for hip OA in females ($r^2 = 0.017$). However, the rs3019 variant is located at a site demonstrating high cross-species conservation (Table 3.2). None of the identified variants were in LD with each other.

Sequencing of the 3'UTR region in female patients with hip OA therefore identified four variants, rs3019, a novel variant (c.13277C>C/T), rs2281627, and rs76148746. However, only the rs3019 variant was identified as present at a significantly different frequency in female patients with hip OA compared to the control population. The rs3019 variant was detected at a significantly higher frequency in female patients with hip OA compared to the control population ($p = 0.036$).

3.5 Discussion

The experiments described in this chapter aimed to investigate the genetic variation of *TRIM32* to identify novel or rare variants in *TRIM32* that are associated with OA of the hip in females. Sequencing of the proximal promoter, 5'UTR, both exons, and 3'UTR of *TRIM32* in the youngest 500 females patients with hip OA from the arcOGEN patient cohort detected nine variants; two of which were present at disproportionate frequencies in female patients with hip OA compared to the control population, and may therefore contribute to the genetic predisposition to hip OA in females.

Sequencing of the proximal promoter and 5'UTR of *TRIM32* identified two known variants, rs811457 and rs12342207 (Figure 3.1). The rs12342207 variant is relatively common with a MAF of 0.312 in female patients with hip OA, though this was not significantly different from the control population (Table 3.1; $p = 0.770$). However, rs811457 was present at a reduced frequency in female patients with OA compared to the control population; the MAF in patients with OA was 0.007 (Table 3.1; $p = 0.001$). The variant C allele may therefore confer protection against OA compared to the more common G allele. The rs811457 variant (c.1-139G>G/C) lies adjacent to the CGI in the *TRIM32* promoter and in a region marked by very high levels of H3K4me3 (Figure 3.2). H3K4me3 is localised in close proximity to the transcriptional start sites of actively transcribed genes regulating transcription factor binding (409-411). The rs811457 variant also resides adjacent to the binding site for the transcription factors TFAP2A and TFAP2C, members of the AP-2 family of transcription factors. These factors, especially TFAP2A have important roles in chondrogenesis and skeletogenesis (412). TFAP2A is expressed in growth plate and articular cartilage and is a negative regulator of chondrocyte differentiation (412, 413). TFAP2A activity suppresses Col II expression, and also inhibits ACAN and Col X production (414). The rs811457 variant in the proximal promoter region of *TRIM32* may therefore be a functional variant affecting *TRIM32* expression in chondrocytes (415).

Three variants were identified in the protein-coding region of exon 2 of *TRIM32* (Figure 3.1). The two missense variants, rs3747835 and rs141806013 were both detected in HET form in one and two female patients with hip OA, respectively (Table 3.1). The

third variant, rs1661300, which is a synonymous variant, was detected more frequently (Table 3.1). However, the variants detected in exon 2 in female patients with hip OA are unlikely to have functional significance as their MAFs were similar to the control population, and none were in LD with the rs4836732 SNP that was associated with the development of hip OA in female patients in the arcOGEN GWAS (Table 3.1) (229).

Sequencing of the 3'UTR also identified four variants within *TRIM32* in female patients with hip OA (Figure 3.1, Table 3.1). Variants specifically in the 3'UTR may alter mRNA stability and translation through effects on polyadenylation and interactions between both regulatory proteins and mRNA, and microRNA and mRNA (416, 417). Polymorphisms in the 3'UTR region can lead to translational inhibition or mRNA degradation, and by altering miRNA binding sites can result in increased or decreased expression (418, 419). The novel variant, c.13277C>C/T, identified in the 3'UTR was only present in HET form in two patients with hip OA, while the rs761458746 variant was identified in HET form in a single patient. MAF and LD information for these variants was not available, though these variants are unlikely to have functional significance.

The rs3019 and rs2281627 variants detected in the 3'UTR may have relevance to the pathogenesis of OA (Figure 3.1). The rs2281627 variant is relatively common (MAF = 0.315) in female patients with hip OA and was in moderate LD ($r^2 = 0.395$) with the index SNP rs4836732 at the 9q33.1 locus for OA susceptibility. The rs3019 variant was detected at a significantly higher frequency in patients with OA compared to the control population ($p = 0.036$; Table 3.1), and resides at a site of high cross-species conservation, indicating that the variant could be deleterious (Table 3.2). Although the frequency of the rs3019 variant in female patients with hip OA was only just statistically significant ($p = 0.036$), this may still be a robust finding as sequencing was performed in the youngest cohort ($n = 500$) of female patients from the arcOGEN study and in whom variants associated with OA are likely to be enriched, and because the 9q33.1 locus within which *TRIM32* resides was previously demonstrates as associated with hip OA in females with genome-wide significance (229). *TRIM32* is targeted by miR-511; the rs3019 and rs2281627 variants occur at binding sites of miR-511. Haplotypes involving

the rs3019 and rs2281627 variants lead to disruption of seed sites for miR-511, resulting in impaired interactions of miR-511 with *TRIM32* (420). miR-511 is a potent regulator of the inflammatory response (421). miR-511 can target and regulate TLR4, inhibit the activation of TLR4-dependent inflammatory cytokine production, and control the activation and recruitment of macrophages (421, 422). A pathological role for miR-511 in joint inflammation has previously been demonstrated; miR-511 is upregulated in synovial monocytes in patients with rheumatoid arthritis (423). miR-511 is also associated with altered expression of several genes including *ALDH1A1*, a member of the *ALDH* gene superfamily, members of which are associated with altered chondrocyte phenotype and OA, and have fundamental roles in embryogenesis, RA signalling, limb development, and protection against oxidative stress (424-428). The identification of the rs3019 variant in the 3'UTR of *TRIM32* as being over-represented in female patients with hip OA therefore further implicates *TRIM32* in the pathogenesis of OA, especially as presence of the variant may alter interaction of *TRIM32* with microRNA involved in regulating joint inflammation.

Although none of the nine variants detected in *TRIM32* in female patients with hip OA were in significant LD with the rs4836732 polymorphism, such linkage could be further explored by conditional analysis of the rs3019 or rs811457 variants with rs4836732, or its immediately adjacent SNPs, for association with hip OA in female patients. The cohort examined in these experiments (n = 500) was relatively low compared to the arcOGEN study cohort that identified the 9q33.1 locus as associated with hip OA in female patients; examination of the polymorphisms in *TRIM32*, especially those under or over-represented in females with hip OA, in a larger cohort of patients or by comparison with a confirmed disease-free control population matched for age and gender could further validate these findings. It may also be informative to examine any association of the variants significantly associated with hip OA for association with other endophenotypes relevant to hip OA, such as radiographic parameters of hip morphology, which may indicate discrete developmental dysplasias, or joint space width as an indicator of early OA (254). Additional transcription factor binding sites have also been identified in more proximal regions of the *TRIM32* promoter (429). Further disease-associated variants could be identified by more

extensive sequencing of the promoter and intronic regions; the proximal promoter, 5'UTR, both exons, and 3'UTR of *TRIM32* were focused on in these experiments to prioritise regions of high functional relevance.

The rs811457 and rs3019 variants could also be investigated further by analysing the effect of these variants on chondrocyte function, which may help to identify the associated pathological molecular mechanisms. As the rs811457 variant lies adjacent to the TFAP2A/TFAP2C transcription factor binding site (Figure 3.2), the expression of TRIM32 in chondrocytes expressing this variant could be measured, as could the ability of the TFAP2A/TFAP2C transcription factors to bind the altered sequence in the proximal promoter of *TRIM32* by ChIP analysis. As the rs3019 variant in the 3'UTR of *TRIM32* may affect *TRIM32* expression by disrupting a binding site of miR-511, which can target TRIM32 in joint tissue, the expression of TRIM32 and miR-511 in chondrocytes expressing the rs3019 variant could be assessed (420, 423). Examining the effect of these two variants on the expression of TRIM32 and associated regulatory factors in chondrocytes may help to investigate the role of *TRIM32* in pathological mechanisms contributing to the OA disease process.

The Sanger sequencing and variant analysis methodology utilised in these experiments are effective for identification of SNPs, though it is acknowledged that other forms of variation such as insertions, deletions, CNVs, and epigenetic modifications could also contribute to the genetic predisposition to OA at this locus, as well could variants in other genes. The variants detected at disproportionate frequency in females with hip OA in these experiments could also be part of a larger haplotype conferring risk for hip OA.

The results of variant screening of *TRIM32* identified several variants. The rs811457 variant in the proximal promoter was under-represented in female patients with hip OA and may be protective against hip OA. The rs3019 variant was over-represented in female patients with hip OA and may be associated with increased risk of hip OA. The rs811457 and rs3019 variants may affect *TRIM32* expression and post-transcriptional regulation, respectively. Correlating the putative effect of these variants with studies of *in vitro* and *in vivo* altered expression of *TRIM32* in chondrocytes and

articular tissue may further validate *TRIM32* in the pathogenesis of OA. The role of *TRIM32* in articular tissue *in vitro* and the development of OA *in vivo* are investigated in subsequent chapters.

Chapter 4

The role of *TRIM32* in human and murine articular tissue *ex vivo*

4.1 Summary

This chapter aimed to investigate the role of TRIM32 in human and murine articular tissue *ex vivo*, by investigating TRIM32 expression in human articular cartilage, and the effect of *Trim32* knockout (*Trim32*$^{-/-}$) on both GAG release by murine femoral head explants and primary murine chondrocyte phenotype following stimulation with catabolic and anabolic cytokines.

Immunostaining for TRIM32 and ASTN2, the protein-coding genes within the recombination hotspot at the 9q33.1 locus associated with OA in female patients, demonstrated expression of TRIM32, but not ASTN2, in the superficial and mid zones of articular cartilage of the knee; TRIM32 expression was also observed in human femoral head cartilage. Western blot analysis demonstrated reduced expression of TRIM32 in human femoral head primary articular chondrocytes from patients with hip OA compared to control patients ($p = 0.03$).

The total GAG content of femoral head explants from WT and *Trim32*$^{-/-}$ mice was similar. Significantly greater GAG release occurred in femoral head explants from *Trim32*$^{-/-}$ mice after no stimulation ($p = 0.04$ WT *vs* KO) and IL1α treatment ($p = 0.02$ WT *vs* KO), but was most marked following treatment with RA ($p = 0.003$ WT *vs* KO).

Trim32 expression by WT primary murine chondrocytes was reduced following treatment with OSM ($p = 0.0002$) and IGF ($p = 7.92 \times 10^{-6}$), but not IL1α or TNFα. Unstimulated *Trim32*$^{-/-}$ primary murine chondrocytes expressed reduced *Col2a1* ($p = 8.53 \times 10^{-5}$ WT *vs* KO), and increased *Acan*, *Col10a1*, and *Sox9* compared to WT primary murine chondrocytes (*Acan*: $p = 0.001$; *Col10a1*: $p = 2.18 \times 10^{-5}$, *Sox9*: $p = 2.35 \times 10^{-6}$ WT *vs* KO). Upon treatment with IL1α, *Trim32*$^{-/-}$ primary murine chondrocytes expressed increased *Col10a1* mRNA ($p = 0.0003$ WT *vs* KO). Upon OSM and IGF1 stimulation, *Trim32*$^{-/-}$ primary murine chondrocytes expressed increased *Col2a1* (OSM: $p = 0.001$; IGF: $p = 0.0001$ WT *vs* KO). Following IGF1 stimulation, *Trim32*$^{-/-}$ primary murine chondrocytes expressed reduced *Sox9* (IGF: $p = 0.0007$ WT *vs* KO).

These results indicate that altered TRIM32 expression by primary human articular chondrocytes may be associated with OA, and that *Trim32* knockout may be

associated with increased GAG release in stimulated murine femoral head cartilage explants. Finally, *Trim32* deficiency may be associated with increased expression of genes associated with chondrocyte hypertrophy following catabolic cytokine stimulation, and dysregulation of *Col2a1* and *Sox9* expression upon anabolic cytokine stimulation.

4.2 Introduction

In Chapter 3, DNA sequencing studies identified genetic variants within *TRIM32* that are present at a disproportionate frequency in association with hip OA in female patients, implicating a role for TRIM32 in the aetiopathogenesis of OA in humans. The majority of genes studied following implication in the development of OA by GWAS (see Tables 1.1 and 1.2) have been demonstrated as expressed in human articular cartilage. However, the expression and role of *TRIM32* in articular tissue is not known. The overall aim of the experiments described in this chapter was to investigate the expression of *TRIM32* in human and murine articular tissue *ex vivo*, and to investigate the effect of *Trim32* knockout on both the integrity of murine articular cartilage and the response of *Trim32*-deficient primary murine chondrocytes to catabolic and anabolic cytokine stimulation.

The expression of *TRIM32* in human articular knee and femoral head cartilage is evaluated by immunostaining of cartilage sections from joint explants. The expression of *ASTN2*, the other protein-coding gene within the recombination hotspot at the 9q33.1 OA susceptibility locus, is also examined. Western blot analysis of TRIM32 expression by primary articular chondrocytes from femoral head cartilage from female patients with hip OA and control patients is evaluated to determine any alteration in TRIM32 expression associated with hip OA.

The effect of *Trim32* knockout on the integrity of articular cartilage is investigated by measuring GAG release, as a surrogate marker of aggrecanolysis, by femoral head explants from WT and *Trim32* KO mice. GAG content of femoral head explants and conditioned media are both measured to enable comparison of the percentage GAG release by femoral head explants from WT and *Trim32* KO mice. GAG release is assessed in response to no stimulation, and treatment with IL1α or RA, two potent inducers of aggrecanolysis.

Finally, the phenotype of primary articular chondrocytes from WT and *Trim32* KO mice is evaluated by measuring gene expression following stimulation with catabolic and anabolic cytokines. Expression of *Col2a1* and *Acan* (the main components

of healthy articular cartilage), *Col10a1* (a marker of hypertrophic chondrocytes in OA cartilage), and *Sox9* (a transcriptional regulator of the chondrocyte phenotype) is measured by qPCR in response to stimulation with catabolic cytokines, IL1α, TNFα, or OSM, and the anabolic cytokine IGF1.

4.3 Aims

The aims of the experiments described in this chapter were to:

1. Investigate the expression of TRIM32 in human articular cartilage, and to determine whether TRIM32 expression is altered in articular cartilage from female patients with OA of the hip.
2. Investigate the effect of TRIM32 on the integrity of articular cartilage *in vitro*, by measuring GAG release by femoral head explants from *Trim32* KO mice.
3. Evaluate the effect of *Trim32* knockout on chondrocyte phenotype *in vitro*, by measuring gene expression by primary chondrocytes from *Trim32* KO mice following catabolic and anabolic cytokine stimulation.

4.4 Results

4.4.1 Immunostaining for TRIM32 and ASTN2 in human articular cartilage

4.4.1.1 Immunostaining for TRIM32 in human knee joint cartilage

To investigate TRIM32 expression in human articular tissue, protein expression was initially investigated in human knee joint samples. To investigate whether or not TRIM32 protein was expressed in articular cartilage, immunostaining for TRIM32 was performed in archival human knee joint cartilage samples (Figure 4.1); TRIM32 expression was detected in knee joint cartilage. Positive staining was demonstrated in chondrocytes of the articular cartilage of the knee joint (indicated by arrows in Figures 4.1D and 4.1E).

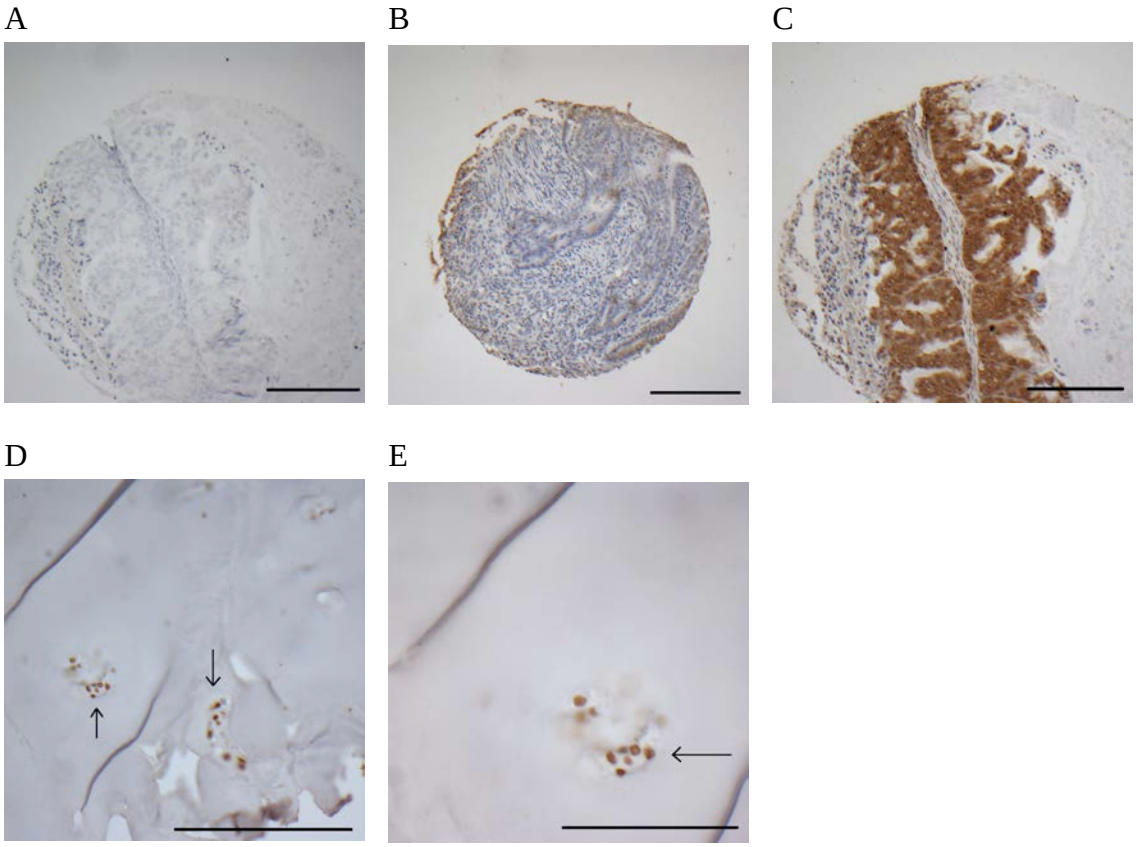

Figure 4.1 – Immunostaining of TRIM32 in human knee joint cartilage; TRIM32 protein expression was assessed in knee joint cartilage from human patients. Immunostaining signals for TRIM32 were visualised using DAKO Envision with HRP-linked secondary antibodies, and slides were counterstained with haematoxylin blue. Panel A shows negative control using murine serum in place of the primary antibody to demonstrate lack of non-specific staining, panel B demonstrates TRIM32 immunostaining of human renal tissue (negative control using primary antibody), panel C shows TRIM32 immunostaining of human ovarian tissue (positive control using primary antibody), panel D shows TRIM32 immunostaining of human knee cartilage, and panel E shows TRIM32 immunostaining of chondrocytes within human knee cartilage (high magnification). Arrows indicate positive staining for TRIM32 in photomicrographs of representative knee joint cartilage sections. Scale bars in panel A-D represent 50 μm, and the scale bar in panel E represents 25 μm.

4.4.1.2 Immunostaining for ASTN2 in human knee joint cartilage

ASTN2 resides on the opposite strand to *TRIM32* at the 9q33.1 locus in humans. It was therefore important to also determine the expression of ASTN2 in human articular tissue. ASTN2 expression was investigated using sections from the same human knee joint samples used to investigate the expression of TRIM32 (Figure 4.2). Positive immunostaining for ASTN2 was not identified in cartilage section from human knee joint samples (Figure 4.2D).

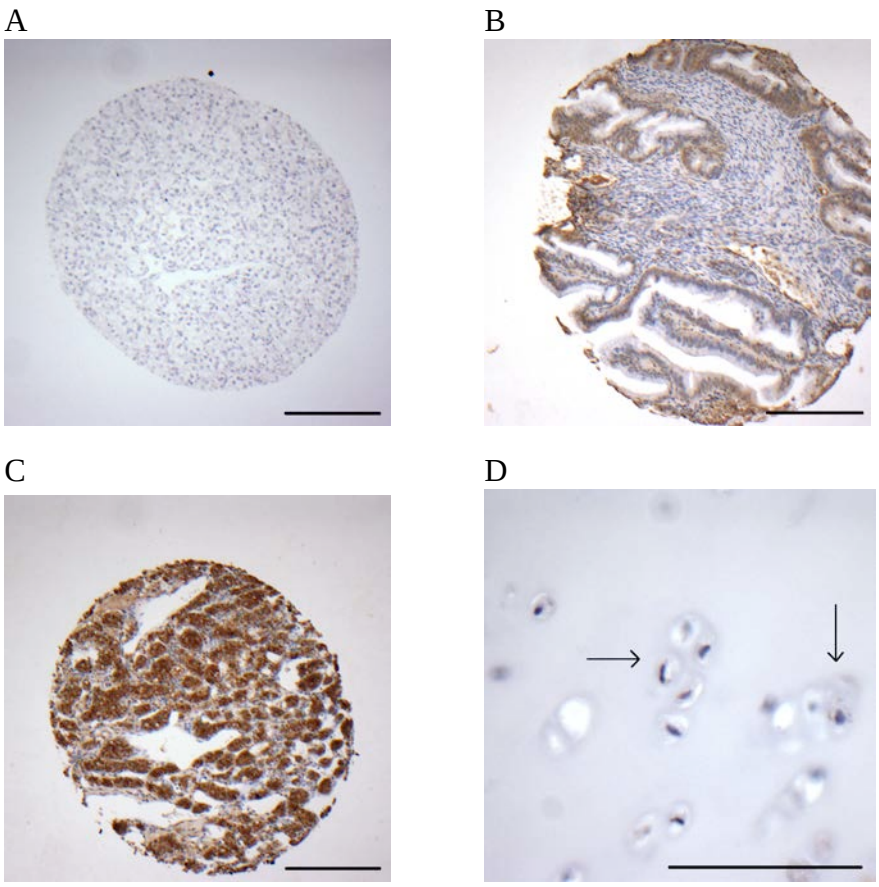

Figure 4.2 – Immunostaining for ASTN2 in human knee joint cartilage; ASTN2 protein expression was assessed in knee joint cartilage from human patients. Immunostaining signals for ASTN2 were visualised using DAKO Envision with HRP-linked secondary antibodies, and slides were counterstained with haematoxylin blue. Panel A shows negative control using murine serum in place of the primary antibody to demonstrate lack of non-specific staining, panel B demonstrates ASTN2 immunostaining of human colon tissue (negative control), panel C shows ASTN2 immunostaining of human renal tissue (positive control), and panel D shows ASTN2 immunostaining of human knee cartilage. Scale bars in panels A-C represent 50 μm, and the scale bar in panel D represents 25 μm.

4.4.1.3 Immunostaining for TRIM32 in human femoral head cartilage

As the 9q33.1 locus at which *TRIM32* resides in humans was associated with the development of hip OA in the arcOGEN study, TRIM32 expression was then assessed by immunostaining of human femoral head cartilage samples from the hip joint (Figure 4.3). Positive staining was also demonstrated in sections of femoral head cartilage, with positive staining for TRIM32 identified in primary articular chondrocytes (indicated by arrows in Figures 4.3D and 4.3E).

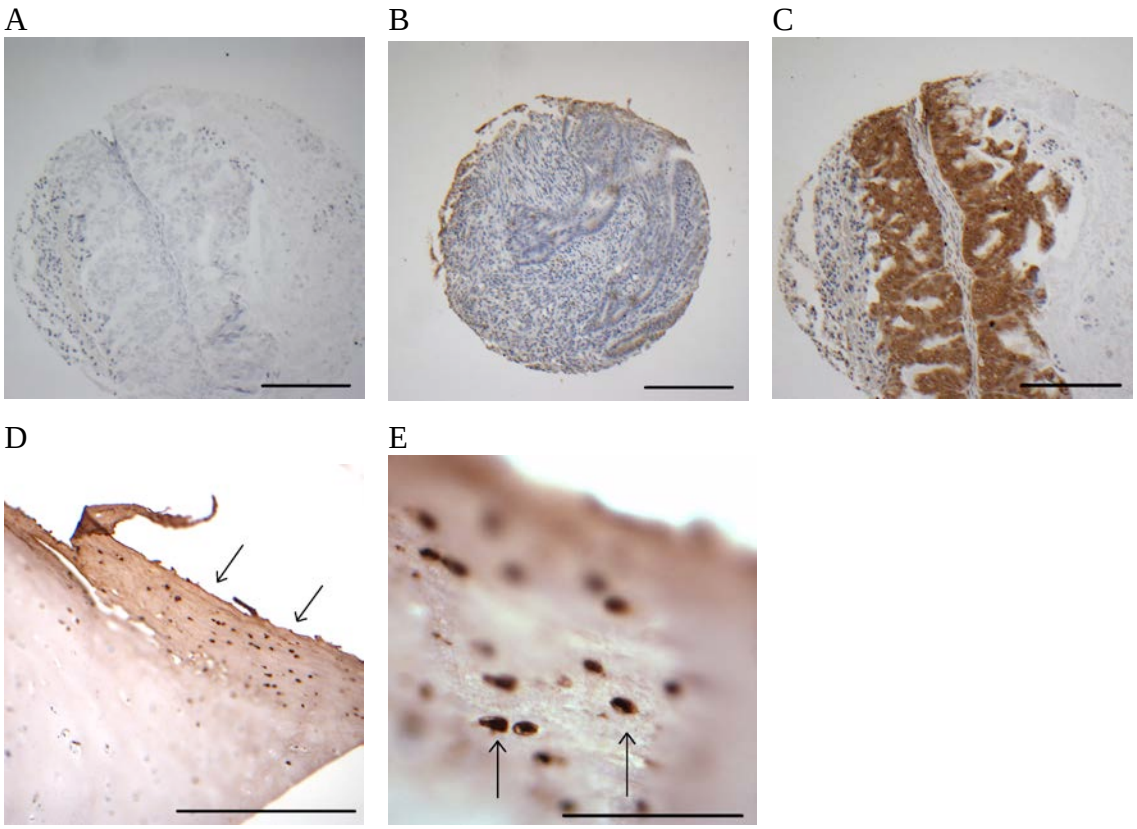

Figure 4.3 – Immunostaining for TRIM32 in human femoral head cartilage; TRIM32 protein expression was assessed in femoral head cartilage from human patients. Immunostaining signals for TRIM32 were visualised using DAKO Envision with HRP-linked secondary antibodies, and slides were counterstained with haematoxylin blue. Panel A shows negative control using murine serum in place of the primary antibody to demonstrate lack of non-specific staining, panel B demonstrates TRIM32 immunostaining of human colon tissue (negative control using primary antibody), panel C shows TRIM32 immunostaining of human ovarian tissue (positive control using primary antibody), panel D shows positive TRIM32 immunostaining of femoral head articular cartilage (arrows) in human hip cartilage sections, and panel E show TRIM32 immunostaining of chondrocytes within human femoral head cartilage (high magnification). Arrows indicate positive staining for TRIM32 in photomicrographs of representative femoral head cartilage sections. Scale bars in panel A-D represent 50 μm, and the scale bar in panel E represents 25 μm.

4.4.2 Western blot analysis of TRIM32 expression in human femoral head primary articular chondrocytes

To further evaluate the expression of TRIM32 protein in human articular cartilage, the expression levels of TRIM32 in cultured human femoral head primary articular chondrocytes was assessed by Western blot analysis. The expression levels of TRIM32 were compared between cultured femoral head primary articular chondrocytes from control patients (patients undergoing hip arthroplasty for acute fractured neck of femur and without previous hip pain, or medical comorbidities or treatments that may affect chondrocyte metabolism (see section 2.2.1)) and patients with severe hip OA undergoing total hip arthroplasty (Figure 4.4). Patients were matched for age (control patients 72.3 ± 7.76 years, hip OA patients 67.7 years ± 8.66 years; $p = 0.35$) and gender (all patients were female).

TRIM32 expression was detected in primary femoral head articular chondrocytes from both control patients and patients with hip OA (Figure 4.4A). Densitometry analysis demonstrated that TRIM32 protein expression was significantly lower in primary femoral head articular chondrocytes from patients with hip OA compared to control patients (control patients 12.2 ± 6.1% relative to β-Actin expression, hip OA patients 6.5 ± 3.0%; $p = 0.03$). However, this should be reviewed with caution as the intensity of detected β-Actin appeared stronger in some samples from patients with OA (Figure 4.4A).

A

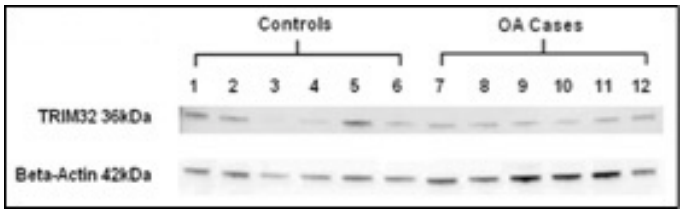

B

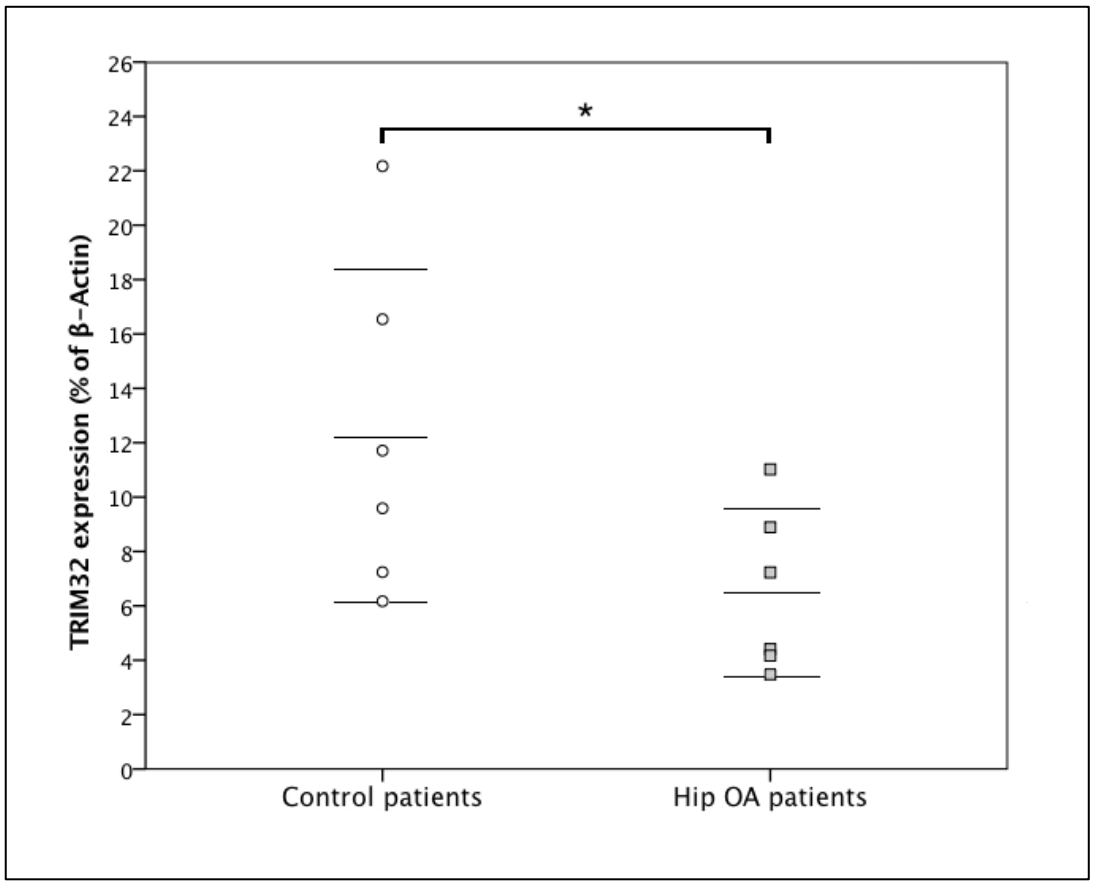

Figure 4.4 – TRIM32 protein expression in human femoral head primary articular chondrocytes; protein detection by chemiluminescence following Western blotting of protein extracts from cultured human femoral head primary articular chondrocytes. Panel A shows images captured upon chemiluminescent detection of TRIM32 (36 kDa) and β-Actin (42 kDa) in patients without OA (controls; n = 6) and patients with hip OA (OA cases; n = 6). Panel B shows densitometry analysis of TRIM32 expression by human femoral head primary articular chondrocytes detected in Panel A, normalised against β-Actin expression levels. Lines represent mean ± SD. Statistical analysis of relative TRIM32 expression levels in human femoral head primary articular chondrocytes between control patients and hip OA patients was performed by Student's t-Test, with statistical significance accepted at $p < 0.05$: *$p = 0.03$ compared to control patients.

4.4.3 Aggrecanolysis in femoral head explants from *Trim32* knockout mice

Proteolytic cleavage of ACAN, the most abundant species of proteoglycan in cartilage, is a key event in the pathogenesis of OA. To investigate any effect of *Trim32* knockout on enzymatic degradation of ACAN *in vitro*, aggrecanolysis was estimated using femoral head explants from 3-week old WT and *Trim32* KO mice after treatment with no stimulation, IL-1α, or RA (see section 2.2.6); murine proximal femoral epiphyses are entirely cartilaginous at this age. GAG release was measured, as a surrogate marker of aggrecanolysis, in femoral head explant cultures from WT and *Trim32* KO mice. The total GAG content of femoral head explants from WT and *Trim32* KO mice was determined by measuring and summing the GAG content of femoral head explants and the quantity of GAG released into culture media after each treatment. Finally, the proportion of GAG released into media as a percentage of the total GAG content of femoral heads was calculated for explants from WT and *Trim32* mice after treatment with no stimulation, IL-1α, or RA (see sections 2.2.6, 2.2.7, and 2.2.8).

4.4.3.1 Total glycosaminoglycan content of femoral head explants from *Trim32* knockout mice

To determine whether or not GAG release upon cytokine stimulation by femoral head explants was different between WT and *Trim32* KO mice, it was important to first establish whether or nor there was any difference in the initial total GAG content of femoral head explants from WT and *Trim32* KO mice. The total GAG content of femoral heads from WT and *Trim32*$^{-/-}$ mice was determined by summing the GAG content of femoral head explants with the corresponding values for quantity of GAG released into culture media for each sample. Importantly, there was no difference in the total GAG content of unstimulated femoral heads from WT and *Trim32*$^{-/-}$ mice (WT 100.6 ± 10.7 μg, KO 101.2 ± 11.3 μg; p = 0.94 (Figure 4.5)). There was also no significant difference in the total GAG content of femoral heads from WT and *Trim32*$^{-/-}$ mice after treatment with either IL1α (WT 89.3 ± 2.4 μg, KO 107.8 ± 20.1 μg; p = 0.12) or RA (WT 94.1 ± 14.7 μg, KO 87.5 ± 7.7 μg; p = 0.45 (Figure 4.5). This indicates that

the GAG content of femoral head explants from immature *Trim32*$^{-/-}$ mice is equivalent to that of WT mice.

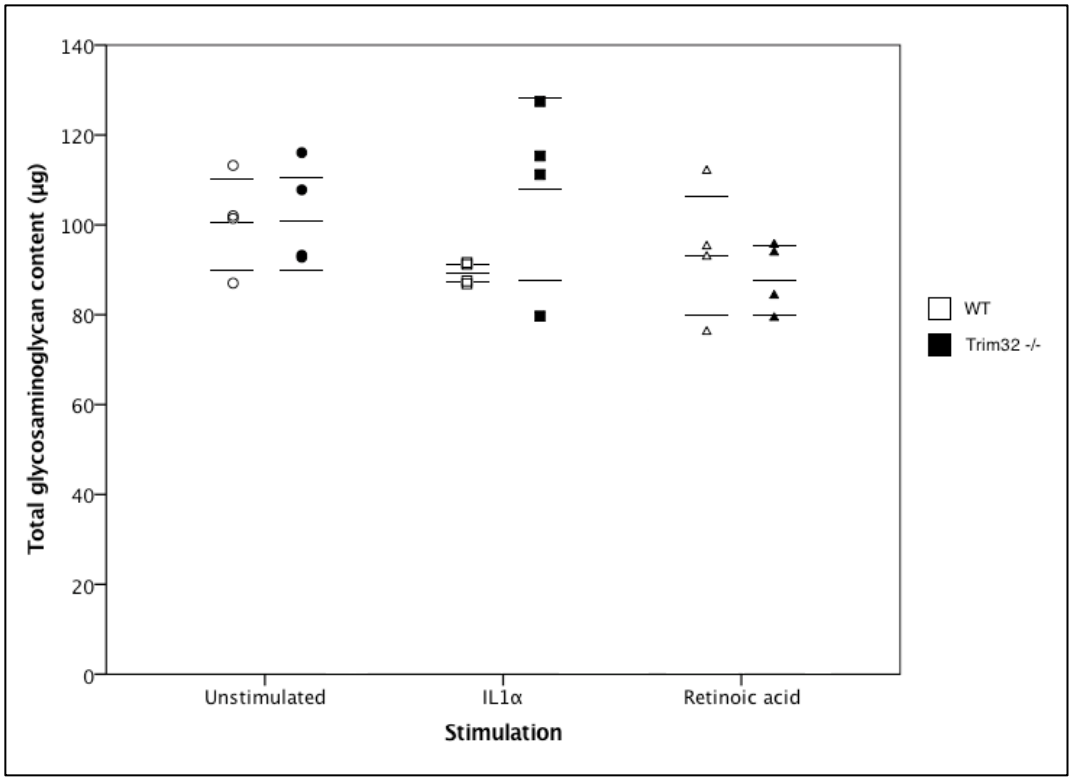

Figure 4.5 – Total glycosaminoglycan content of femoral heads from wild type (WT) and *Trim32*$^{-/-}$ (KO) mice following treatment with no stimulation, IL1α or retinoic acid; total glycosaminoglycan (GAG) content of pairs of femoral heads was assessed in WT (n = 4) and *Trim32*$^{-/-}$ mice (n =4). Absolute values (lines represent mean ± SD) for total GAG content of femoral heads from WT and *Trim32*$^{-/-}$ mice are shown, as assessed using the DMMB dye-binding assay. Total GAG content of femoral heads was determined by summing the GAG content of femoral head explants with GAG released into media by femoral head explants, for each sample. Total GAG content of femoral heads was assessed following treatment with no stimulation (unstimulated), 10 ng/ml IL1α, or 10 µM retinoic acid for 72 hours. Statistical analysis of total GAG content of femoral heads between WT and *Trim32*$^{-/-}$ mice groups was performed by two-tailed Student's t-Test, with statistical significance accepted at $p < 0.05$.

4.4.3.2 Glycosaminoglycan retention and release by femoral head explants from *Trim32* knockout mice

To establish the proportion of GAG release upon cytokine stimulation by femoral head explants from WT and *Trim32* KO mice, the quantity of GAG retained and released by femoral head explants from WT and *Trim32* KO mice was measured. The quantity of GAG retained by femoral head explants from WT and *Trim32* KO (*Trim32*$^{-/-}$) mice was assessed following treatment with no stimulation, IL-1α, or RA. There was no difference in the quantity of GAG retained by femoral head explants from WT or *Trim32*$^{-/-}$ mice, either after no stimulation (mean ± SD: WT 88.4 ± 10.4 μg, KO 78.4 ± 4.3 μg; p = 0.13) or treatment with IL-1α (WT 42.6 ± 1.6 μg, KO 35.7 ± 8.1 μg; p = 0.15 (Figure 4.6A)). However, GAG retention by femoral head explants from *Trim32*$^{-/-}$ mice was significantly lower compared to that of WT mice, after treatment with RA (WT 66.7 ± 15.5 μg, KO 30.9 ± 8.7 μg; Mann-Whitney *U* test p = 0.03 (Shapiro-Wilk Test for GAG content in WT group p = 0.04; Figure 4.6A)).

The quantity of GAG released into culture media by femoral head explants from WT and *Trim32* KO (*Trim32*$^{-/-}$) mice was then assessed following treatment with no stimulation, IL-1α, or RA. There was no difference in the quantity of GAG released by femoral head explants from WT and *Trim32*$^{-/-}$ following no stimulation (WT 12.3 ± 0.7 μg, KO 22.8 ± 10.0 μg; p = 0.08 (Figure 4.6B)), or following stimulation with IL1α (WT 46.8 ± 1.3 μg, KO 72.1 ± 18.6 μg; Mann-Whitney *U* test p = 0.34 (Shapiro-Wilk Test for GAG release in KO group p = 0.016; Figure 4.6B)). The quantity of GAG released by femoral head explants from both WT and *Trim32*$^{-/-}$ mice was greater following treatment with RA, compared with no stimulation (Figure 4.6B). GAG release was significantly greater by femoral head explants from *Trim32*$^{-/-}$ mice compared to WT mice after treatment with RA (WT 27.4 ± 7.1 μg, KO 56.6 ± 4.7 μg; p = 0.0005 (Figure 4.6B)).

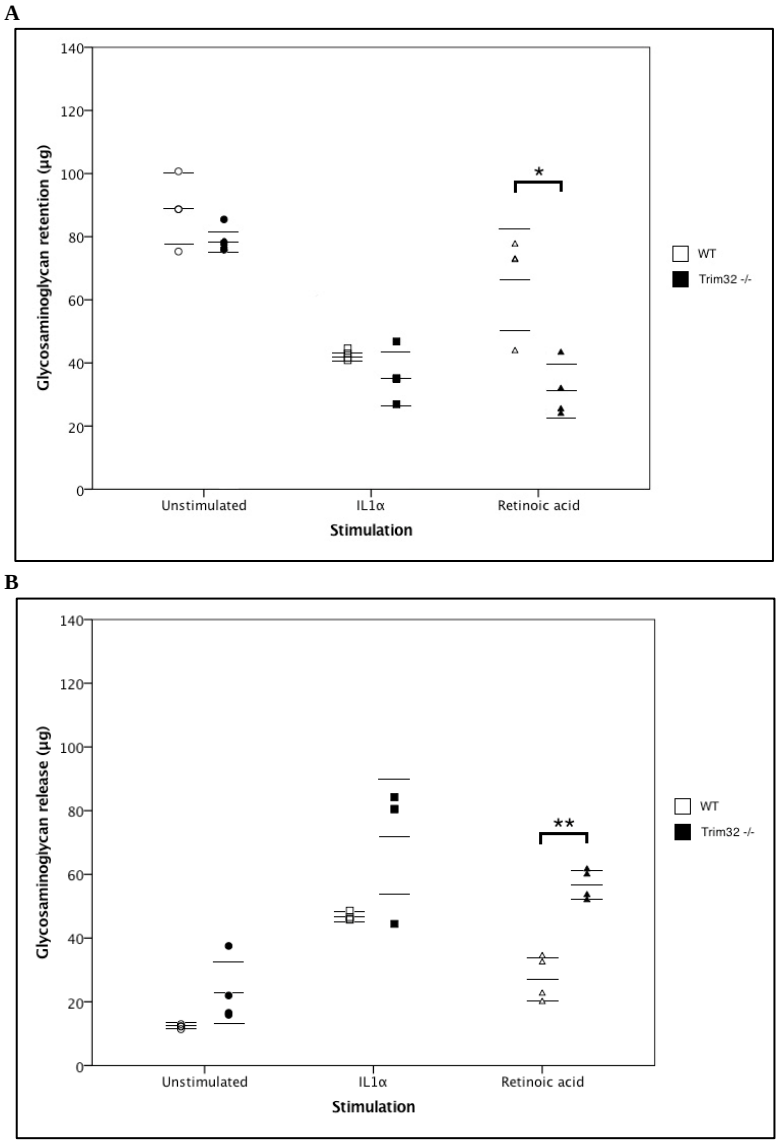

Figure 4.6 – Glycosaminoglycan retention and release by femoral head explants from wild type (WT) and *Trim32*$^{-/-}$ (KO) mice following treatment with no stimulation, IL1α or retinoic acid; glycosaminoglycan (GAG) retention (panel A) and release (panel B) by pairs of femoral head explants were assessed in WT (n = 4) and *Trim32*$^{-/-}$ mice (n =4). Absolute values (lines represent mean ± SD) for GAG quantity retained and released by femoral head explants from WT and *Trim32*$^{-/-}$ mice are shown, as assessed using the DMMB dye-binding assay. Femoral head explants and conditioned media were assessed for GAG content following treatment with no stimulation (unstimulated), 10 ng/ml IL1α, or 10 µM retinoic acid (RA) for 72 hours. Statistical analysis of GAG retention and release by femoral head explants between WT and *Trim32*$^{-/-}$ mice groups was performed by two-tailed Student's t-Test, except for comparison of GAG content of femoral head explants between WT and *Trim32*$^{-/-}$ mice groups following treatment with RA as data for the WT group deviated from normal distribution (Shapiro-Wilk Test p = 0.044) and comparison of GAG release by femoral head explants between WT and *Trim32*$^{-/-}$ mice groups following treatment with IL1α that was analysed by Mann-Whitney *U* test as data for the *Trim32*$^{-/-}$ group deviated from normal distribution (Shapiro-Wilk Test p = 0.016): statistical significance was accepted at $p < 0.05$, *p = 0.03 compared to WT mice; **p = 0.0005 compared to WT mice.

4.4.3.3 Relative glycosaminoglycan release by femoral head explants from *Trim32* knockout mice

The quantity of GAG retained and released upon cytokine stimulation by femoral head explants from WT and *Trim32* KO mice was then used to determine the proportion of GAG release into culture media by the femoral head explants after each stimulation. The proportion of GAG released into culture media by femoral head explants upon treatment with no stimulation, IL1α, or RA was compared between WT and *Trim32*$^{-/-}$ mice (Figure 4.7). Significantly greater GAG was released by unstimulated femoral head explants from *Trim32*$^{-/-}$ compared with WT mice (WT 12.3 ± 1.0 %, KO 22.0 ± 7.1 %; p = 0.04). Significantly greater GAG release by femoral head explants from *Trim32*$^{-/-}$ compared with WT mice, was also identified following treatment with IL1α (WT 52.4 ± 0.9 %, KO 66.2 ± 8.5 %; p = 0.02). Significantly greater GAG release was also demonstrated in femoral head explants from *Trim32*$^{-/-}$ compared with WT mice, upon treatment with RA (WT 29.6 ± 9.5 %, KO 65.1 ± 7.3 %; p = 0.003 (Figure 4.7)).

The increased proportion of GAG released by femoral head explants from *Trim32*$^{-/-}$ compared with WT mice was particularly exaggerated following treatment with RA (Figure 4.7). The difference between the percentage GAG release by femoral head explants from *Trim32*$^{-/-}$ mice compared with WT mice was more significant in response to treatment with RA compared to unstimulated controls or following IL1α stimulation (WT v KO, unstimulated p = 0.04; WT v KO, IL1α stimulation p = 0.02; WT v KO, RA stimulation p = 0.003).

These results indicate that GAG loss, as an indicator of aggrecanolysis and a key event in the pathogenesis of OA, is significantly greater in *Trim32*$^{-/-}$ mice compared with WT mice *in vitro*. These results also indicate that the increased GAG release by femoral heads from *Trim32*$^{-/-}$ mice is particularly exacerbated in response to stimulation by RA.

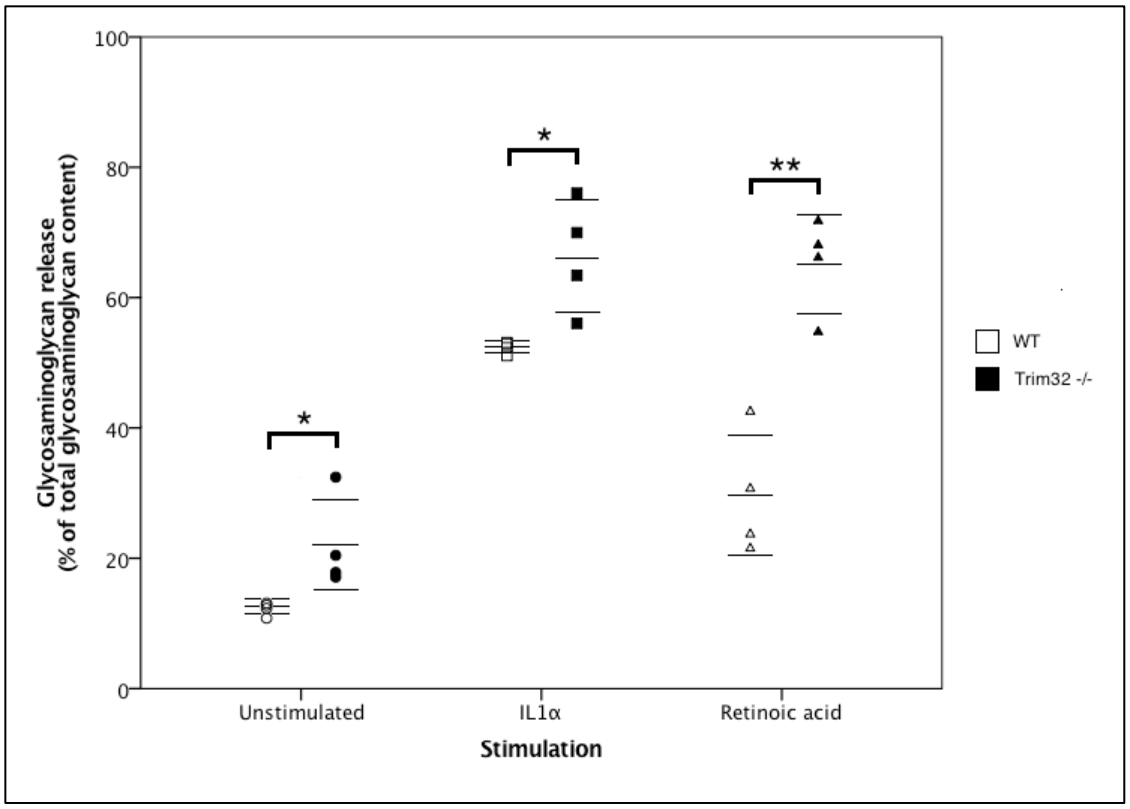

Figure 4.7 – Percentage glycosaminoglycan release by femoral head explants from wild type (WT) and *Trim32*$^{-/-}$ (KO) mice following treatment with no stimulation, IL1α or retinoic acid; percentage glycosaminoglycan (GAG) release by pairs of femoral head explants was assessed in WT (n = 4) and *Trim32*$^{-/-}$ mice (n =4). Absolute values (lines represent mean ± SD) for percentage GAG release by femoral heads from WT and *Trim32*$^{-/-}$ mice are shown, as assessed using the DMMB dye-binding assay. Percentage GAG release was determined by dividing the GAG content of conditioned media by the total GAG content of femoral head explants, for each sample. Percentage GAG release by femoral head explants was assessed following treatment with no stimulation (unstimulated), 10 ng/ml IL1α, or 10 μM retinoic acid for 72 hours. Statistical analysis of percentage GAG release by femoral head explants between WT and *Trim32*$^{-/-}$ mice groups and treatment groups was performed by two-way ANOVA with post-hoc Tukey tests: statistical significance was accepted at $p < 0.05$, * $p = 0.04$ (Unstimulated WT *vs* KO), *$p = 0.02$ (IL1α stimulation, WT *vs* KO); ** $p = 0.003$ (RA stimulation, WT vs KO).

4.4.4 *Trim32* expression in primary chondrocytes from wild type mice following catabolic and anabolic cytokine stimulation

To further investigate whether or not *Trim32* has a role in chondrocyte metabolism, the expression of *Trim32* in primary chondrocytes from WT mice was investigated following stimulation with catabolic and anabolic cytokines. In OA cartilage, chondrocytes show a dysregulated expression of catabolic and anabolic genes, resulting in imbalanced homeostasis. IL1, TNFα, and OSM are particularly implicated in the degradation of articular cartilage in OA and induction of catabolic responses by chondrocytes (159, 430). IGF1 is an anabolic cytokine that stimulates proteoglycan production by chondrocytes (431). The expression of *Trim32* mRNA by primary chondrocytes from WT mice was assessed in response to no stimulation, and following stimulation with catabolic (IL1α, TNFα, and OSM) and anabolic (IGF1) cytokines.

The expression of *Trim32* in primary chondrocytes from WT mice following treatment with IL1α, TNFα, OSM, and IGF1 was compared to *Trim32* expression in unstimulated primary chondrocytes from WT mice (Figure 4.8). There was no difference in *Trim32* mRNA expression in primary chondrocytes from WT mice after treatment with either IL1α ($p = 0.78$) or TNFα ($p = 0.58$). Significantly reduced *Trim32* mRNA expression by primary chondrocytes from WT mice was demonstrated following treatment with both OSM (Figure 4.8, $p = 0.0002$; mean ± SD: 70.33 ± 4.04% compared to unstimulated controls) and IGF1 ($p = 7.92 \times 10^{-6}$; 66.00 ± 2.00% compared to unstimulated controls).

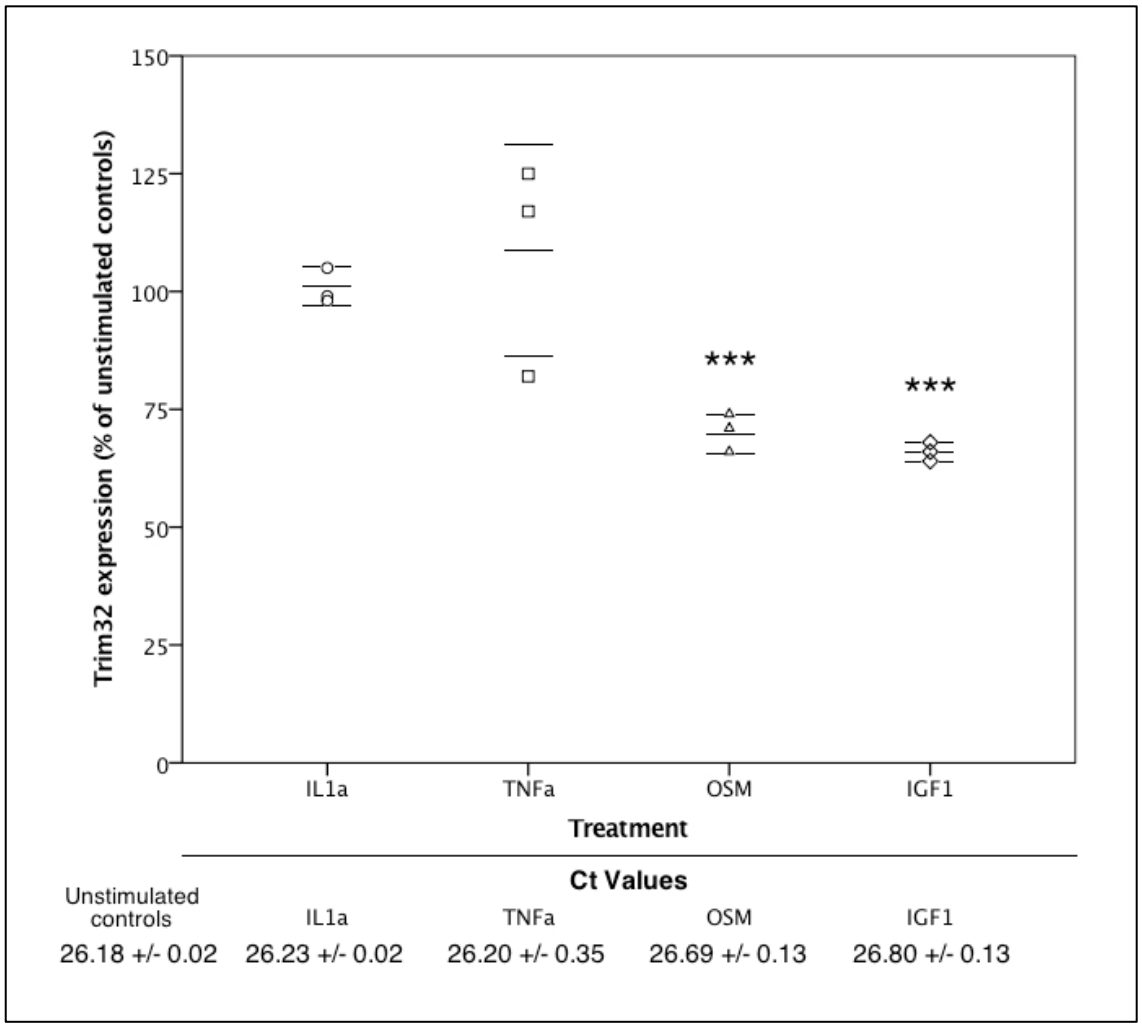

Figure 4.8 – *Trim32* mRNA expression in primary chondrocytes from wild type mice following treatment with IL1α, TNFα, Oncostatin-M (OSM), or IGF1; quantitative reverse transcription-polymerase chain reaction was used to measure *Trim32* mRNA expression in primary murine chondrocytes from wild-type (WT) mice following treatment with IL1α (10 ng/ml), TNFα (100 ng/ml), OSM (100 ng/ml), or IGF1 (100 ng/ml) for 48 hours. *Trim32* mRNA expression levels are expressed relative to *Trim32* mRNA levels in unstimulated primary murine chondrocytes (controls) after 48 hours' culture and were calculated from $\Delta\Delta C_t$ values. Absolute values (lines represent mean ± SD) for percentage *Trim32* mRNA expression compared to unstimulated controls are shown for each experiment (n = 3 replicates from independent experiments for each group). Ct values are shown (mean ± SD). Statistical analysis of *Trim32* expression levels between cytokine-treated and unstimulated primary chondrocytes was performed by two-tailed Student's t-Test: after Bonferroni correction for multiple tests, statistical significance was accepted at $p < 0.0025$, ***$p = 0.0002$ (OSM stimulation, compared to unstimulated controls), ***$p = 7.92 \times 10^{-6}$ (IGF1 stimulation, compared to unstimulated controls).

4.4.5 Gene expression by primary chondrocytes from *Trim32* knockout mice following catabolic and anabolic cytokine stimulation

In previous sections 4.4.3 and 4.4.4, increased GAG release by femoral head cartilage explants, and reduced expression of *Trim32* by primary chondrocytes in response to catabolic and anabolic cytokines from *Trim32* KO mice compared to WT mice in response to catabolic and anabolic cytokines, was demonstrated. To investigate whether or not *Trim32* deficiency affects the phenotype of primary chondrocytes, the expression of *Col2a1*, *Acan*, *Col10a1*, and *Sox9* mRNA was assessed in comparison to that by primary chondrocytes from WT mice, following treatment with no stimulation, catabolic (IL1α, TNFα, and OSM), and anabolic (IGF1) cytokines. *Col2a1* and *Acan* encode Col II and ACAN, respectively, which are the two major macromolecules in the ECM synthesised by healthy mature chondrocytes (432). *Col10a1* encodes Col X, which is a marker of hypertrophic chondrocytes present in the growth plate and osteoarthritic cartilage (433). *Sox9* encodes a transcription factor that regulates the chondrocyte phenotype and controls the expression of genes encoding important proteins of the ECM, including Col II, ACAN, and COMP (434).

4.4.5.1 Gene expression by unstimulated primary chondrocytes from *Trim32* knockout mice

The expression of *Col2a1*, *Acan*, *Col10a1*, and *Sox9* by unstimulated primary chondrocytes from WT and *Trim32*$^{-/-}$ mice was assessed. This permitted analysis of gene expression in unstimulated basal conditions, and also provided baseline gene expression levels from which changes in gene expression, after cytokine stimulation of primary chondrocytes from WT and *Trim32*$^{-/-}$ mice, could subsequently be compared. Gene expression by unstimulated primary chondrocytes from WT and *Trim32*$^{-/-}$ KO mice is shown in Figure 4.9; the expression of *Col2a1*, *Acan*, *Col10a1*, and *Sox9* are normalised to the expression of GAPDH, a stable reference gene in chondrocyte cultures (435). In unstimulated conditions, *Col2a1* mRNA expression was significantly lower by chondrocytes from *Trim32*$^{-/-}$ mice compared to the expression by chondrocytes from WT mice (Figure 4.9, WT 119 ± 12.69 %, KO 0.98 ± 0.16 %; $p = 8.53 \times 10^{-5}$ WT *vs*

KO). The expression of *Acan*, *Col10a1*, and *Sox9* mRNA were all significantly greater by chondrocytes from *Trim32*$^{-/-}$ mice compared to their expression by chondrocytes from WT mice, as shown in Figure 4.9 (*Acan*: WT 1.63 ± 0.33 %, KO 5.46 ± 0.84 %, p = 0.001 WT *vs* KO; *Col10a1*: WT 3.19 ± 0.50 %, KO 28.73 ± 1.87 %, p = 2.18 x 10^{-5} WT *vs* KO; *Sox9*: WT 42 ± 1.15 %, KO 103.64 ± 2.41 %, p = 2.35 x 10^{-6} WT *vs* KO). These results indicate that immature primary chondrocytes harvested from femoral head epiphyses from *Trim32* KO mice may express significantly different levels of *Col2a1*, *Acan, Col10a1*, and *Sox9*, compared to those from WT mice (Figure 4.9).

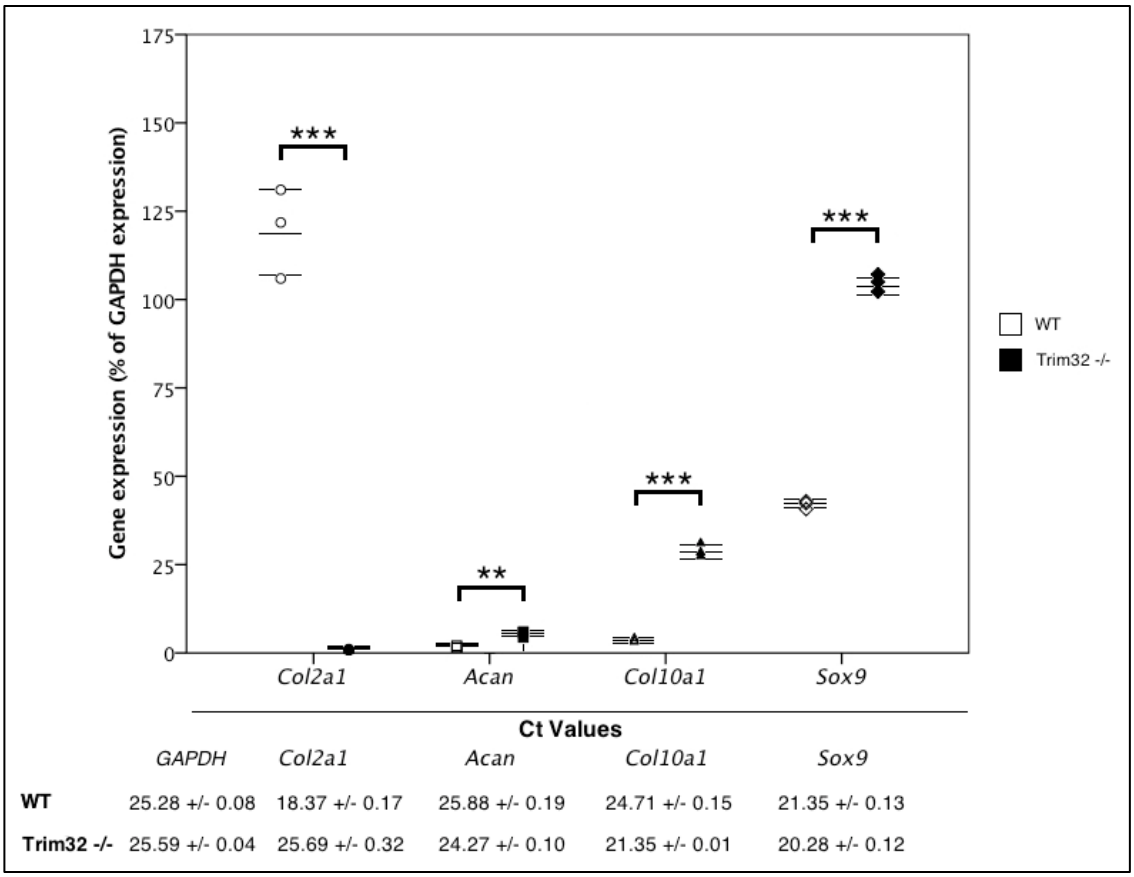

	GAPDH	*Col2a1*	*Acan*	*Col10a1*	*Sox9*
WT	25.28 +/- 0.08	18.37 +/- 0.17	25.88 +/- 0.19	24.71 +/- 0.15	21.35 +/- 0.13
Trim32 -/-	25.59 +/- 0.04	25.69 +/- 0.32	24.27 +/- 0.10	21.35 +/- 0.01	20.28 +/- 0.12

Figure 4.9 – Gene expression by unstimulated primary chondrocytes from wild type (WT) and *Trim32*$^{-/-}$ (KO) mice; quantitative reverse transcription-polymerase chain reaction was used to measure *Col2a1*, *Acan*, *Col10a1*, and *Sox9* mRNA expression by primary chondrocytes from WT and *Trim32*$^{-/-}$ mice following treatment with no stimulation for 48 hours. *Col2a1*, *Acan*, *Col10a1*, and *Sox9* mRNA expression are displayed relative to GAPDH mRNA expression levels in primary chondrocytes from wild type and *Trim32*$^{-/-}$ mice treated with no stimulation for 48 hours, and were calculated from $\Delta\Delta C_t$ values. Values (lines represent mean ± SD) for mRNA expression compared to *GAPDH* mRNA expression levels are shown for each experiment (n = 3 replicates from independent experiments for each group). Ct values are shown (mean ± SD). Statistical analysis of mRNA expression of differentiation markers between primary chondrocytes from WT and *Trim32*$^{-/-}$ mice was performed by two-tailed Student's t-Test: after Bonferroni correction for multiple tests, statistical significance was accepted at $p < 0.0025$, **$p = 0.001$ (*Acan*, WT *vs* KO), ***$p = 8.53 \times 10^{-5}$ (*Col2a1*, WT *vs* KO), ***$p = 2.18 \times 10^{-5}$ (*Col10a1*, WT *vs* KO), ***$p = 2.35 \times 10^{-6}$ (*Sox9*, WT *vs* KO).

4.4.5.2 Gene expression by primary chondrocytes from *Trim32* knockout mice following treatment with IL1α

In the previous section 4.4.5.1, significantly different expression of *Col2a1*, *Acan*, *Col10a1*, and *Sox9* was demonstrated by primary chondrocytes from *Trim32* KO mice, compared to those isolated from WT mice. To investigate whether or not *Trim32* deficiency affects the change in chondrocyte phenotype in response to catabolic or anabolic cytokines, the change in expression of these genes was measured by qPCR following stimulation with IL1α, TNFα, OSM, and IGF1 in primary chondrocytes from *Trim32* KO mice and WT mice. To control for basal gene expression levels following different stimulations, changes in target gene expression, established using the 'delta-delta Ct' method, were normalised to any changes in expression of the stable house-keeping gene GAPDH following different stimulations (435).

The change in gene expression by primary chondrocytes from WT and *Trim32* KO mice following treatment with IL1α was compared (Figure 4.10). There was no significant difference in the change of expression of *Col2a1* (Mann-Whitney *U* test p = 0.05 (Shapiro-Wilk Tests: WT *Col2a1*, $p = 8.5 \times 10^{-16}$; KO *Col2a1*, $p = 4.2 \times 10^{-16}$)), *Acan* (Mann-Whitney *U* test p = 0.99 (Shapiro-Wilk Tests: WT *Acan*, $p = 8.5 \times 10^{-16}$; KO *Acan*, $p = 8.5 \times 10^{-16}$)), or *Sox9* (Mann-Whitney *U* test p = 0.08 (Shapiro-Wilk Test: KO *Sox9*, $p = 4.2 \times 10^{-16}$)) mRNA between primary chondrocytes from WT and *Trim32*$^{-/-}$ mice following treatment with IL1α (Figure 4.10). However, primary chondrocytes from *Trim32*$^{-/-}$ mice demonstrated a significantly greater expression of *Col10a1* following treatment with IL1α, compared to those from WT mice (Figure 4.10; WT 5.33 ± 1.53 %, KO 22.33 ± 2.08 %; p = 0.0003 WT *vs* KO).

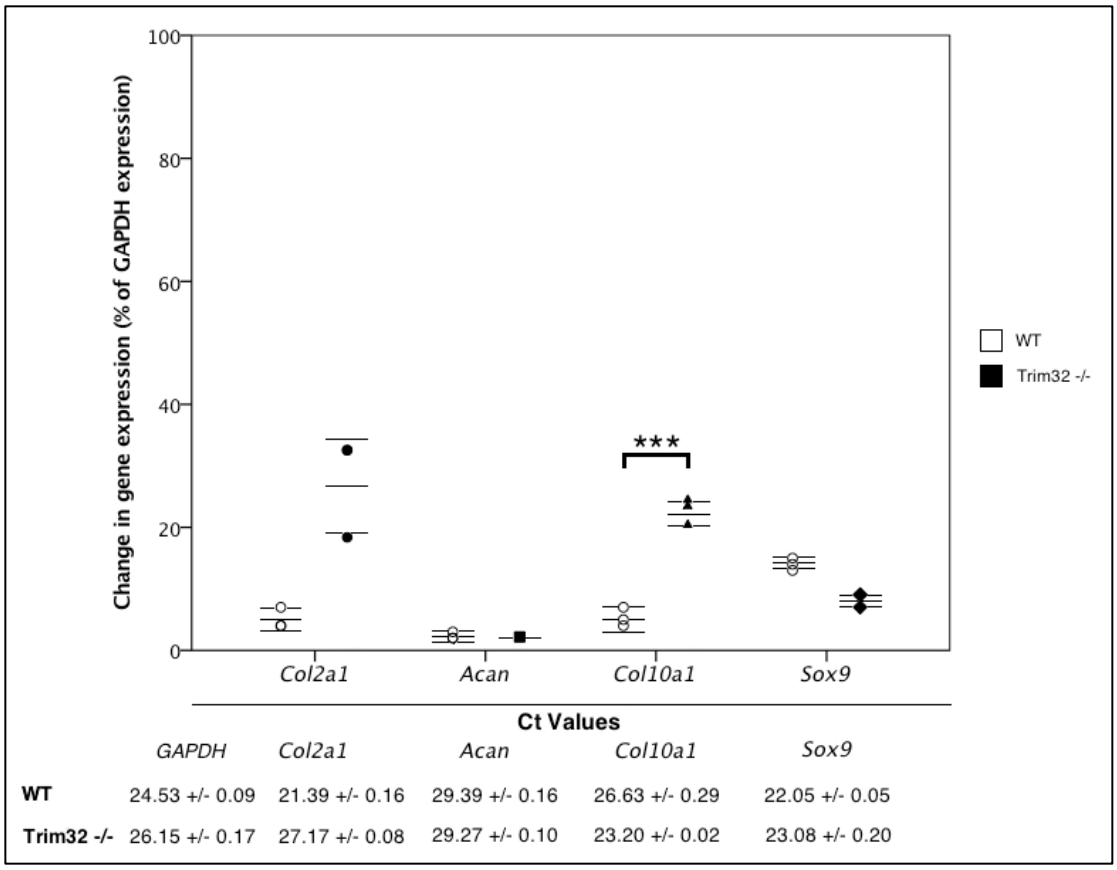

	GAPDH	Col2a1	Acan	Col10a1	Sox9
WT	24.53 +/- 0.09	21.39 +/- 0.16	29.39 +/- 0.16	26.63 +/- 0.29	22.05 +/- 0.05
Trim32 -/-	26.15 +/- 0.17	27.17 +/- 0.08	29.27 +/- 0.10	23.20 +/- 0.02	23.08 +/- 0.20

Figure 4.10 – Gene expression by primary chondrocytes from wild type (WT) and *Trim32*$^{-/-}$ (KO) mice following treatment with IL1α; quantitative reverse transcription-polymerase chain reaction was used to measure *Col2a1*, *Acan*, *Col10a1*, and *Sox9* mRNA expression by primary chondrocytes from WT and *Trim32*$^{-/-}$ mice following treatment with IL1α (10 ng/ml) for 48 hours. The change in *Col2a1*, *Acan*, *Col10a1*, and *Sox9* mRNA expression levels following IL1α treatment of primary chondrocytes from WT and *Trim32*$^{-/-}$ mice are displayed relative to unstimulated primary chondrocytes from wild type and *Trim32*$^{-/-}$ mice, normalised against the change in the housekeeping gene *GAPDH* mRNA expression upon IL1α treatment of primary chondrocytes from WT mice and *Trim32*$^{-/-}$ mice, and were calculated from $\Delta\Delta C_t$ values. Values (lines represent mean ± SD) for mRNA expression compared to *GAPDH* mRNA expression levels are shown for each experiment (n = 3 replicates from independent experiments for each group). Ct values are shown (mean ± SD). Statistical analysis of mRNA expression of differentiation markers between primary chondrocytes from WT and *Trim32*$^{-/-}$ mice was performed by two-tailed Student's t-Test, except for comparisons of groups of data deviating from a normal distribution that were analysed by Mann-Whitney *U* test including mRNA expression of *Col2a1* (Shapiro-Wilk Tests: WT $p = 8.5 \times 10^{-16}$, KO $p = 4.2 \times 10^{-16}$), *Acan* (Shapiro-Wilk Tests: WT $p = 8.5 \times 10^{-16}$, KO $p = 8.5 \times 10^{-16}$), and *Sox9* (Shapiro-Wilk Tests: KO $p = 4.2 \times 10^{-16}$): after Bonferroni correction for multiple tests, statistical significance was accepted at $p < 0.0025$, ***$p = 0.0003$ (*Col10a1*, WT *vs* KO).

4.4.5.3 Gene expression by primary chondrocytes from *Trim32* knockout mice following treatment with TNFα

The change in gene expression by primary chondrocytes from WT and *Trim32* KO mice following treatment with the catabolic cytokine TNFα was also compared (Figure 4.11). There was no significant difference in the change in expression of *Acan* (Mann-Whitney *U* test p = 0.06 (Shapiro-Wilk Tests: WT *Acan*, p = 8.5 x 10^{-16}; KO *Acan*, p = 8.5 x 10^{-16})), or *Sox9* (Mann-Whitney *U* test p = 0.08 (Shapiro-Wilk Test: WT *Sox9*, p = 4.2 x 10^{-16})) mRNA between primary chondrocytes from WT and *Trim32*$^{-/-}$ mice following treatment with TNFα (Figure 4.11). There was a near 50-fold increase in *Col2a1* mRNA expression by primary chondrocytes from *Trim32*$^{-/-}$ mice following treatment with TNFα, but this did not surpass the significance threshold following Bonferroni correction (WT 15.33 ± 1.53 %, KO 4982 ± 1796 %; p = 0.009 WT *vs* KO). In contrast to the changes following stimulation with IL1α, another catabolic cytokine, no significant difference was demonstrated in the change of expression of *Col10a1* by primary chondrocytes from *Trim32*$^{-/-}$ mice following treatment with TNFα compared to those from WT mice (Figure 4.11; p = 0.02).

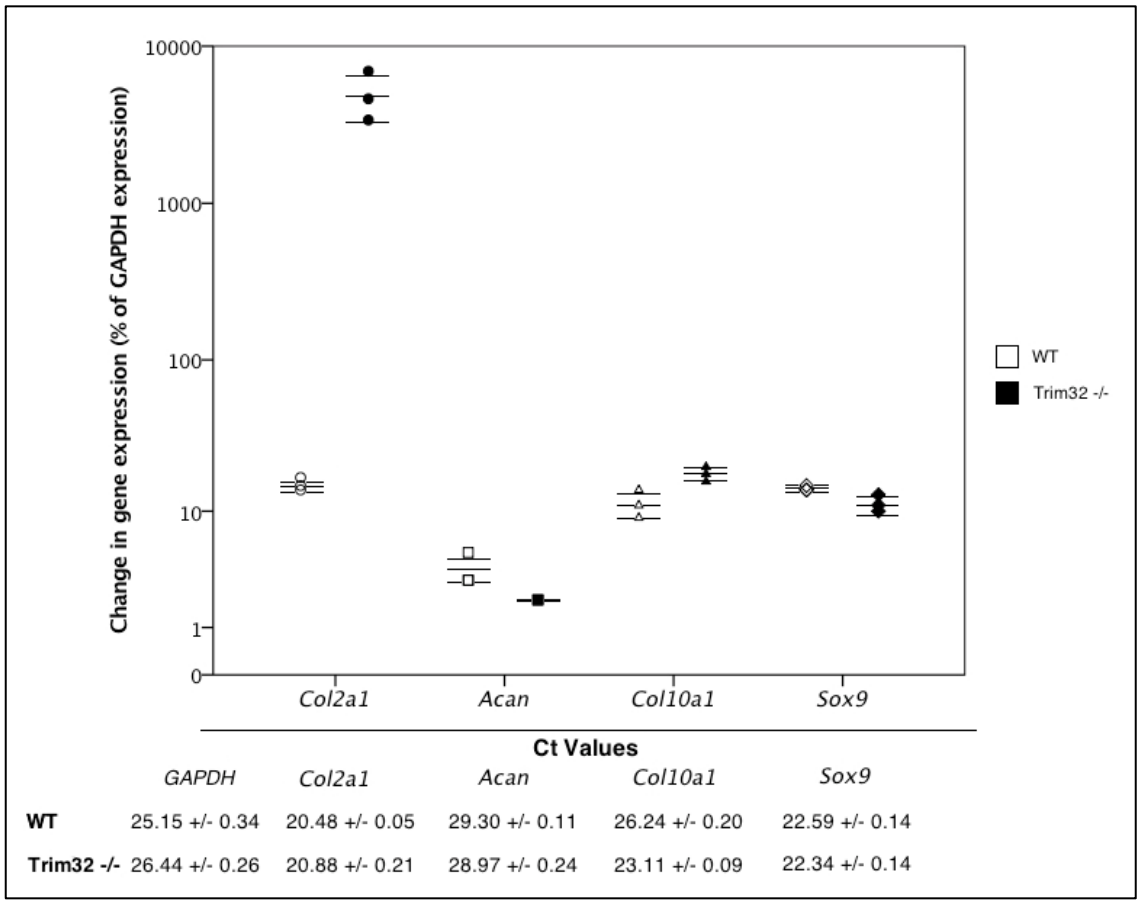

	GAPDH	Col2a1	Acan	Col10a1	Sox9
WT	25.15 +/- 0.34	20.48 +/- 0.05	29.30 +/- 0.11	26.24 +/- 0.20	22.59 +/- 0.14
Trim32 -/-	26.44 +/- 0.26	20.88 +/- 0.21	28.97 +/- 0.24	23.11 +/- 0.09	22.34 +/- 0.14

Figure 4.11 – Gene expression by primary chondrocytes from wild type (WT) and *Trim32*$^{-/-}$ (KO) mice following treatment with TNFα; quantitative reverse transcription-polymerase chain reaction was used to measure *Col2a1*, *Acan*, *Col10a1*, and *Sox9* mRNA expression by primary chondrocytes from WT and *Trim32*$^{-/-}$ mice following treatment with TNFα (100 ng/ml) for 48 hours. The change in *Col2a1*, *Acan*, *Col10a1*, and *Sox9* mRNA expression levels following TNFα treatment of primary chondrocytes from WT and *Trim32*$^{-/-}$ mice are displayed relative to unstimulated primary chondrocytes from WT and *Trim32*$^{-/-}$ mice, normalised against the change in the housekeeping gene *GAPDH* mRNA expression upon TNFα treatment of primary chondrocytes from WT mice and *Trim32*$^{-/-}$ mice, and were calculated from $\Delta\Delta C_t$ values. Values (lines represent mean ± SD) for mRNA expression compared to *GAPDH* mRNA expression levels are shown for each experiment (n = 3 replicates from independent experiments for each group). Ct values are shown (mean ± SD). Statistical analysis of mRNA expression of differentiation markers between primary chondrocytes from WT and *Trim32*$^{-/-}$ mice was performed by two-tailed Student's t-Test, except for comparisons of groups of data deviating from a normal distribution that were analysed by Mann-Whitney *U* test including mRNA expression of *Acan* (Shapiro-Wilk Tests: WT $p = 8.5 \times 10^{-16}$, KO $p = 8.5 \times 10^{-16}$), and *Sox9* (Shapiro-Wilk Test: WT $p = 4.2 \times 10^{-16}$); after Bonferroni correction for multiple tests, statistical significance was accepted at $p < 0.0025$.

4.4.5.4 Gene expression by primary chondrocytes from *Trim32* knockout mice following treatment with OSM

The change in gene expression by primary chondrocytes from WT and *Trim32* KO mice following treatment with the catabolic cytokine OSM was assessed (Figure 4.12).

No significant difference was observed in the change in *Acan* ($p = 0.006$), *Col10a1* (Mann-Whitney *U* test $p = 0.99$ (Shapiro-Wilk Test: WT *Col10a1*, $p = 8.5 \times 10^{-16}$)) or *Sox9* (Mann-Whitney *U* test $p = 0.08$ (Shapiro-Wilk Test: KO *Sox9*, $p = 4.2 \times 10^{-16}$)) mRNA expression by primary chondrocytes from *Trim32*$^{-/-}$ mice following treatment with OSM, compared to the change seen in expression by primary chondrocytes from WT mice (Figure 4.12).

There was a significantly greater change in the expression of *Col2a1* mRNA by primary chondrocytes from *Trim32*$^{-/-}$ mice following treatment with OSM, compared to that seen in primary chondrocytes from WT mice (Figure 4.12; WT 27.33 ± 4.73 %, KO 4507 ± 963 %; $p = 0.001$).

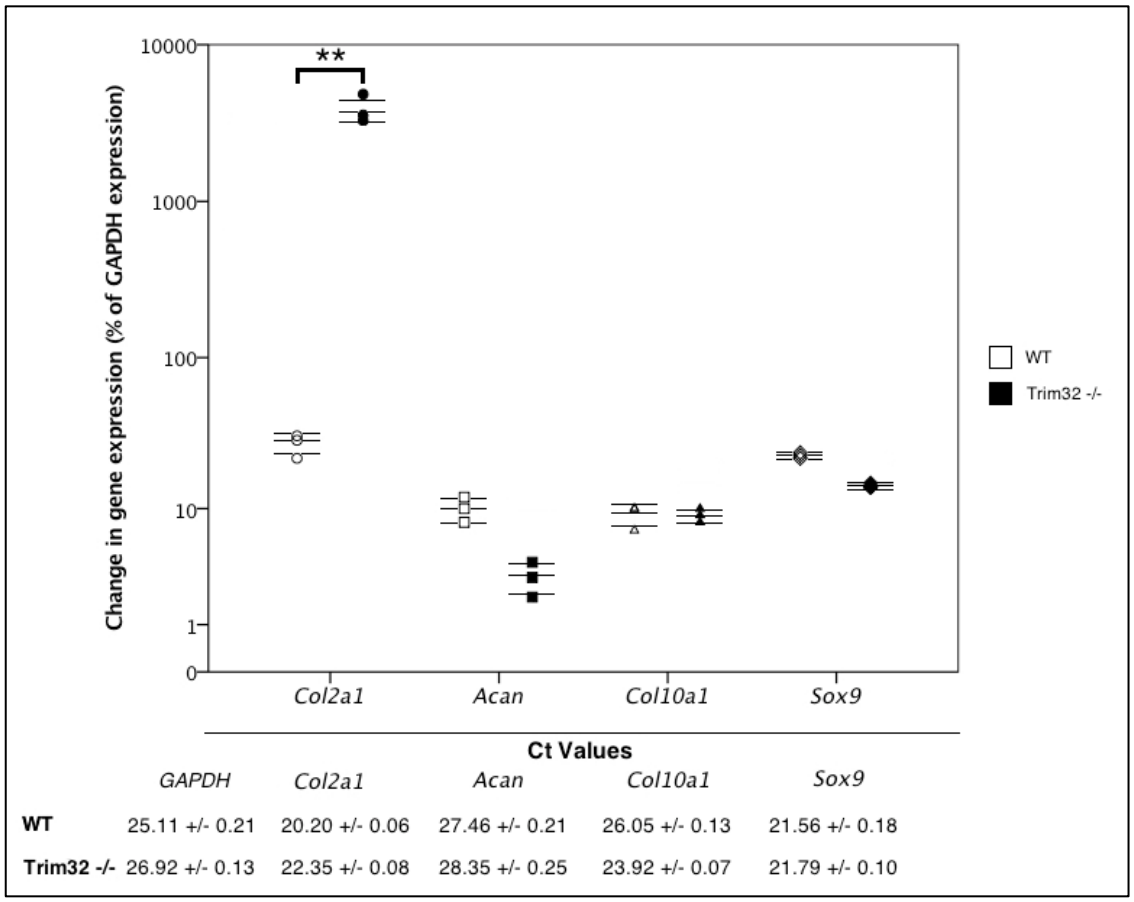

	GAPDH	Col2a1	Acan	Col10a1	Sox9
WT	25.11 +/- 0.21	20.20 +/- 0.06	27.46 +/- 0.21	26.05 +/- 0.13	21.56 +/- 0.18
Trim32 -/-	26.92 +/- 0.13	22.35 +/- 0.08	28.35 +/- 0.25	23.92 +/- 0.07	21.79 +/- 0.10

Figure 4.12 – Gene expression by primary chondrocytes from wild type (WT) and *Trim32*$^{-/-}$ (KO) mice following treatment with Oncostatin-M (OSM); quantitative reverse transcription-polymerase chain reaction was used to measure *Col2a1*, *Acan*, *Col10a1*, and *Sox9* mRNA expression by primary chondrocytes from WT and *Trim32*$^{-/-}$ mice following treatment with OSM (100 ng/ml) for 48 hours. The change in *Col2a1*, *Acan*, *Col10a1*, and *Sox9* mRNA expression levels following OSM treatment of primary chondrocytes from WT and *Trim32*$^{-/-}$ mice are displayed relative to unstimulated primary chondrocytes from WT and *Trim32*$^{-/-}$ mice, normalised against the change in the housekeeping gene *GAPDH* mRNA expression upon OSM treatment of primary chondrocytes from WT mice and *Trim32*$^{-/-}$ mice, and were calculated from $\Delta\Delta C_t$ values. Values (lines represent mean ± SD) for mRNA expression compared to *GAPDH* mRNA expression levels are shown for each experiment (n = 3 replicates from independent experiments for each group). Ct values are shown (mean ± SD). Statistical analysis of mRNA expression of differentiation markers between primary chondrocytes from WT and *Trim32*$^{-/-}$ mice was performed by two-tailed Student's t-Test, except for comparisons of groups of data deviating from a normal distribution that were analysed by Mann-Whitney *U* test including mRNA expression of *Col10a1* (Shapiro-Wilk Test: WT $p = 8.5 \times 10^{-16}$), and *Sox9* (Shapiro-Wilk Test: KO $p = 4.2 \times 10^{-16}$); after Bonferroni correction for multiple tests, statistical significance was accepted at $p < 0.0025$, **$p = 0.001$ (*Col2a1*, WT *vs* KO).

4.4.5.5 Gene expression by primary chondrocytes from *Trim32* knockout mice following treatment with IGF1

The change in gene expression by primary chondrocytes from WT and *Trim32* KO mice following treatment with the anabolic cytokine IGF1, was also assessed (Figure 4.13).

There was also no significant difference in the change in *Acan* ($p = 0.03$) or *Col10a1* ($p = 0.01$) mRNA expression by primary chondrocytes from *Trim32*$^{-/-}$ mice following treatment with IGF1, compared to the change seen in expression by primary chondrocytes from WT mice (Figure 4.13).

There was a significantly increased expression of *Col2a1* mRNA by primary chondrocytes from *Trim32*$^{-/-}$ mice following treatment with IGF1 (approximate 250-fold increase), compared to that seen in primary chondrocytes from WT mice (Figure 4.13; WT 119.67 ± 13.05 %, KO 25974 ± 3114 %; $p = 0.0001$). There was also a significantly greater decrease in the expression of *Sox9* mRNA by primary chondrocytes from *Trim32*$^{-/-}$ mice following treatment with IGF1, compared to that seen in primary chondrocytes from WT mice (Figure 4.13; WT 73 ± 3.61 %, KO 47 ± 3 %; $p = 0.0007$).

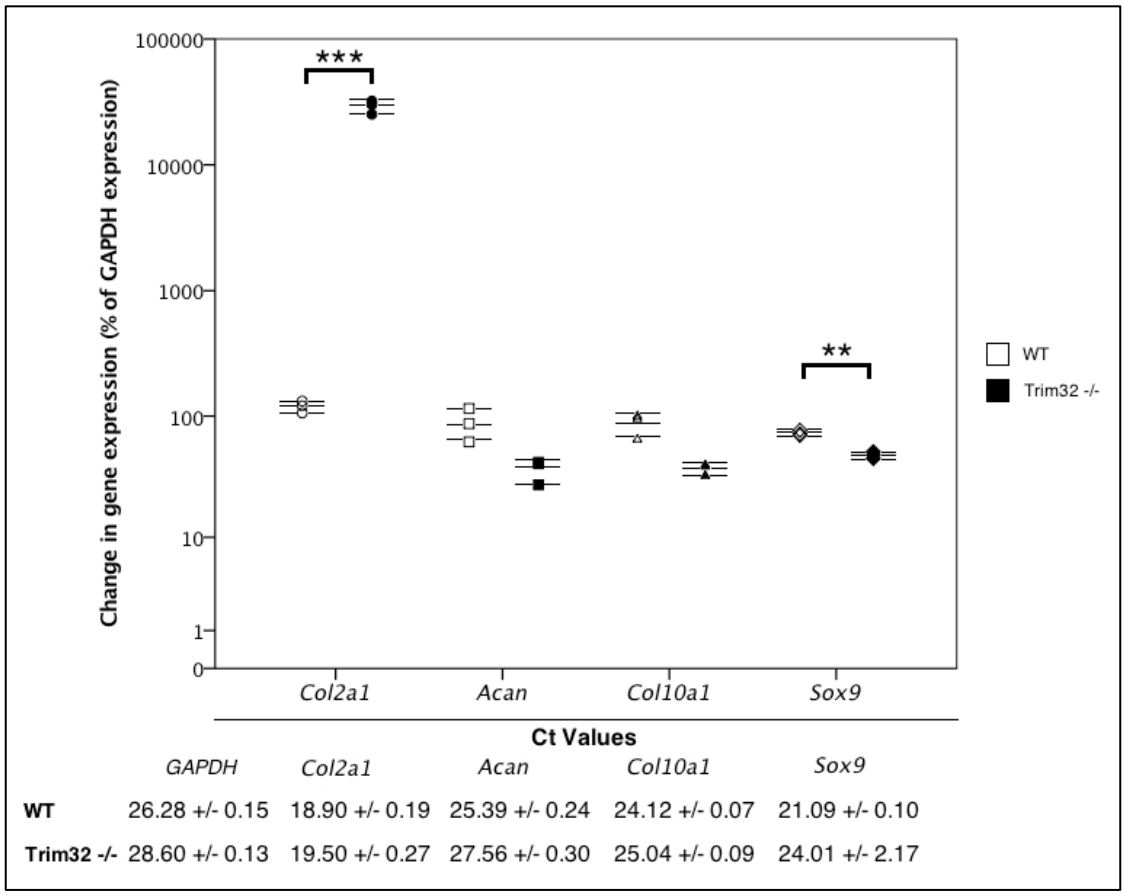

	GAPDH	*Col2a1*	*Acan*	*Col10a1*	*Sox9*
WT	26.28 +/- 0.15	18.90 +/- 0.19	25.39 +/- 0.24	24.12 +/- 0.07	21.09 +/- 0.10
Trim32 -/-	28.60 +/- 0.13	19.50 +/- 0.27	27.56 +/- 0.30	25.04 +/- 0.09	24.01 +/- 2.17

Figure 4.13 – Gene expression by primary chondrocytes from wild type (WT) and *Trim32*$^{-/-}$ (KO) mice following treatment with IGF1; quantitative reverse transcription-polymerase chain reaction was used to measure *Col2a1*, *Acan*, *Col10a1*, and *Sox9* mRNA expression by primary chondrocytes from WT and *Trim32*$^{-/-}$ mice following treatment with IGF1 (100 ng/ml) for 48 hours. The change in *Col2a1*, *Acan*, *Col10a1*, and *Sox9* mRNA expression levels following IGF1 treatment of primary chondrocytes from WT and *Trim32*$^{-/-}$ mice are displayed relative to unstimulated primary chondrocytes from WT and *Trim32*$^{-/-}$ mice, normalised against the change in the housekeeping gene *GAPDH* mRNA expression upon IGF1 treatment of primary chondrocytes from WT mice and *Trim32*$^{-/-}$ mice, and were calculated from $\Delta\Delta C_t$ values. Values (lines represent mean ± SD) for mRNA expression compared to *GAPDH* mRNA expression levels are shown for each experiment (n = 3 replicates from independent experiments for each group). Ct values are shown (mean ± SD). Statistical analysis of mRNA expression of differentiation markers between primary chondrocytes from WT and *Trim32*$^{-/-}$ mice was performed by two-tailed Student's t-Test; after Bonferroni correction for multiple tests, statistical significance was accepted at $p < 0.0025$, **p = 0.0007 (*Sox9*, WT *vs* KO), ***p = 0.0001 (*Col2a1*, WT *vs* KO).

The results of gene expression studies by primary chondrocytes from WT and *Trim32* KO mice have identified that *Trim32* expression was reduced in WT chondrocytes following OSM and IGF stimulation. Murine chondrocytes deficient of *Trim32* expressed reduced *Col2a1* and increased *Acan*, *Col10a1*, and *Sox9*. Finally, in *Trim32* deficient chondrocytes, treatment with IL1α resulted in increased *Col10a1* expression, treatment with OSM resulted in increased *Col2a1* expression, and treatment with IGF resulted in increased *Col2a1* and reduced *Sox9* expression.

4.5 Discussion

The experiments in this chapter aimed to investigate the expression of TRIM32 in human and murine articular tissue *ex vivo*, and to investigate the effect of *Trim32* knockout on both the integrity of murine articular cartilage and the response of primary murine chondrocytes to catabolic and anabolic cytokine stimulation.

Immunostaining for TRIM32 in human articular cartilage from femoral head and knee joint tissue demonstrated expression within chondrocytes and predominantly at the superficial and mid zones of articular cartilage (Figures 4.1 and 4.3). ASTN2 was not detected in cartilage (Figure 4.2). This is consistent with the known expression of ASTN2, which is expressed in brain, eye, heart, lung, liver and kidney tissue, but minimally expressed in other tissues including connective tissue and musculoskeletal tissue (231). Immunostaining intensity in cartilage may often be influenced by proteoglycan content of cartilage; it is not likely that proteoglycan content affected ASTN2 immunostaining intensity as the same cartilage samples were used for detection of TRIM32. *PAPPA* is a third protein-coding gene at the periphery of the recombination hotspot at the 9q33.1 OA susceptibility locus; it was not possible to detect PAPPA by immunostaining; the large heterotetrameric glycoprotein product (~500 kilodaltons (kDa)) is only recognised in an unreduced form, which is disrupted by antigen retrieval techniques (436).

The results of immunostaining for TRIM32 provide semi-quantitative evidence of the expression of TRIM32 in human articular cartilage, indicating expression by chondrocytes in the superficial and middle zones of articular cartilage (Figure 1.2). The abundance of chondrocytes is high in these regions, with chondrocytes more elongated and parallel to the articular surface in the superficial zone, whereas more typical spherical chondrocytes are present in the middle zones. The superficial and middle zones also express high levels of Col II and ACAN, respectively.

TRIM32 was also detected by Western blot analysis of protein extracts from cultured femoral head articular chondrocytes from patients with hip OA undergoing total hip arthroplasty surgery, and from patients without hip OA (Figure 4.4A and

Figure 4.4B). That TRIM32 was detected in cartilage tissue by both immunostaining and Western blot analysis supports the finding that TRIM32 is expressed in human articular cartilage. Comparison of the expression levels of TRIM32, detected by Western blotting, by femoral head articular chondrocytes indicated that TRIM32 expression may be reduced in articular chondrocytes from patients with hip OA compared to patients without hip OA ($p = 0.03$; Figure 4.4A and Figure 4.4B). However, the detected intensity of β-actin expression appeared stronger in some samples from patients with OA compared to control patients (Figure 4.4A). This could confound any detected differences in expression of TRIM32 when the results are normalised to β-actin expression levels as a control, despite standardising the quantity of protein in each sample and controlling for background staining intensities. β-actin protein expression levels have previously been reported as stable between cultured human primary chondrocytes from normal and OA cartilage (437). Alternative reference proteins that may also be expressed at a consistent level by cultured human chondrocytes could include beta2-microglobulin (438). Alternatively, a combination of reference control proteins could be used (439). Therefore, although the difference in TRIM32 expression, as detected by Western blotting, between femoral head chondrocytes from patients with and without hip OA was statistically significant, these results should be viewed with caution.

TRIM32 is ubiquitously expressed, and its broad range of substrate specificity permits a variety of functions in different tissues (440, 441). TRIM32 has been identified in nuclear and cytoplasmic compartments, and extracellular vesicles (442, 443). Cell types differ in their intracellular distribution of TRIM32 expression, with some preferentially expressing TRIM32 in the nucleus or cytoplasm (444, 445). TRIM32 is recognised to migrate between intracellular compartments, though the nuclear import and export mechanisms for TRIM32 remain largely undetermined. In addition to its role as an E3 ubiquitin ligase, TRIM32 can self-associate to form cytoplasmic bodies that may act as a reservoir of TRIM32 to maintain appropriate levels of soluble free TRIM32 protein (446). TRIM32 may also autoubiquitinate to regulate its own intracellular availability (299). TRIM32 can control cell proliferation, motility, and apoptosis (447). The identification of TRIM32 expression by cultured human

chondrocytes, the level of which may be different between chondrocytes isolated from normal and OA cartilage (Figure 4.4), is an interesting finding, and further studies will be required to determine the role of TRIM32 in cartilage, and its mechanisms of action.

Proteolytic cleavage of ACAN within cartilage is a fundamental step in the pathogenesis of OA. GAG loss, as an indicator of aggrecanolysis, was measured in femoral head explants from WT and *Trim32* KO mice following treatment with no stimulation, IL1α, or RA (Figure 4.5, Figure 4.6, and Figure 4.7). The concentrations of IL1α and RA used were selected for maximal induction of aggrecanolysis (402). GAGs comprise 90% of the mass of ACAN, the most abundant of which is chondroitin sulphate (448). ACAN is the most abundant proteoglycan in cartilage by weight; in consort with Col II it provides cartilage with resistance to mechanical load (448). The protein core of ACAN comprises G1 and G2 globular domains at the N terminus, and a G3 domain at the C terminus. ACAN is stabilised in the cartilage matrix by binding HA through its G1 domain (449). The interval between the G2 and G3 domains contains hydrophilic GAGs, providing osmotic swelling pressure that confers cartilage with its compressive strength (449).

Aggrecanolysis occurs most significantly at the interval between the G1 and G2 domains of ACAN, termed the interglobular domain (IGD) (448). Aggrecanolysis is primarily mediated by neutral proteinases including MMPs such as MMP3 and MMP13, and the aggrecanases ADAMTS4 and ADAMTS5. The MMPs and aggrecanases preferentially act at distinct sites within the IGD of ACAN. However, the processes that activate MMPs and aggrecanases in osteoarthritic cartilage are not fully known.

The results of GAG release by femoral head explants from *Trim32* KO mice indicate greater loss of GAG associated with *Trim32* deficiency in unstimulated conditions, and following IL1α stimulation, but most marked upon stimulation with RA (Figure 4.7). That the total GAG content of femoral heads from WT and *Trim32* KO mice was similar in each experiment indicates that GAG synthesis is not affected by *Trim32* KO (Figure 4.5). Furthermore, that relative GAG release by femoral head explants was significantly greater for explants from *Trim32* KO mice after each

stimulation may indicate that *Trim32* deficiency is associated with dysregulation of GAG turnover (Figure 4.7). These results complement the findings from the Western blot analysis of TRIM32 expression by femoral head chondrocytes from patients with hip OA, in which reduced TRIM32 expression was demonstrated in samples from patients with OA (Figure 4.4).

It is interesting that relative GAG release was most marked following RA stimulation, as *Trim32* has previously been shown to function as a co-activator for RARα-mediated transcription (450). TRIM32 physically interacts with RARα and enhances RA-dependent RARα-mediated transcriptional activity in a dose-dependent manner. Nuclear RARs are both positively and negatively influenced by Wnt/β-catenin signalling in a variety of cell types. RA signalling is an established mechanism regulating skeletogenesis and cartilage homeostasis ((451-453). During chondrogenesis, genes encoding RARs demonstrate specific spatiotemporal expression patterns (454). RA may significantly influence cartilage matrix homeostasis by stimulating its synthesis or degradation, and also chondrocyte phenotype (452, 455, 456). Dysregulation of RA signalling can therefore lead to cartilage degradation.

RA stimulates Wnt/β-catenin signalling in chondrocytes and thereby increases the expression of Wnt proteins and receptors. Wnt/β-catenin signalling is another regulator of cartilage matrix synthesis and degradation by chondrocytes (457). Stimulation of Wnt/β-catenin signalling downregulates expression of ACAN, Col II and Col IX by chondrocytes and increases their production of matrix proteases, resulting in matrix loss in cartilage (458), RARγ can differentially regulate Wnt/β-catenin signalling in chondrocytes dependent upon RA ligand availability (459, 460). Wnt/β-catenin and RA signalling may therefore act together to mediate chondrocyte function and phenotype.

The Wnt/β-catenin signalling pathway is also a key pathway mediated by protein-inhibitor of activated STAT3 (Pias3). Mammalian cells contain four members of the Pias family. These ligases bring reactants in close proximity and promote increased isopeptide bond formation. In mammalian cells, S-nitrosation by nitric oxide promotes

Pias3 degradation by facilitating its interaction with TRIM32 (461, 462). Pias3 degradation is protective against joint destruction in arthritis by reducing activation of fibroblast-like synoviocytes and reducing their expression of MMP3, MMP9, and MMP13. It is unknown whether similar mechanisms exist in chondrocytes. The results described in this chapter, whereby reduced *Trim32* expression was associated with increased GAG release may support similar mechanisms in chondrocytes and cartilage.

There are strengths and limitations of assessing aggrecanolysis in cartilage by measuring GAG loss using the DMMB dye-binding assay. GAGs comprise approximately 90% of the mass of ACAN, of which chondroitin sulphate is the most abundant. ACAN concentration is most commonly estimated by measuring sulphated GAG concentration of cartilage and media as surrogate markers of ACAN concentration. The DMMB assay has the advantage of measuring the concentration of sulphated GAGs and does not detect unsulphated GAGs such as HA, which is also relatively abundant in cartilage. One limitation of the DMMB assay is the gradual precipitation of dye/GAG complexes; this was avoided by immediate analysis of reactions. The DMMB assay is usually normalised to wet weight of the tissue under investigation if large tissue volumes are utilised. However, with murine cartilage, very small volumes of residual liquid can alter the tissue weight significantly, leading to detection errors. Therefore, normalisation of murine cartilage in the experiments in this chapter was performed as a proportion of total GAG content; this is more accurate than using wet weight as a denominator for tissue such as murine cartilage (402).

Aggrecanolysis can also be measured by other methods. The uronic acid assay and alcian blue assay may be used to estimate GAG content. However, these assays may also detect HA, and are more labour intensive (463). The traditional DMMB assay measures the concentration of sulphated GAGs as an indication of the actual ACAN concentration. Comparison of the results of the DMMB assay between the conditioned media and cartilage explants, therefore, measures relative GAG concentration, and does not directly measure aggrecanolysis. A more accurate determination of aggrecanolysis in cartilage explant cultures can be achieved by Western blotting to identify ACAN fragments following ADAMTS-mediated aggrecanolysis using neoepitope antibodies,

which have been validated in murine cartilage (402). Neoepitope antibodies recognise the newly generated N-terminus and C-terminus of ACAN fragments following proteolysis. To achieve a comprehensive analysis of ADAMTS-mediated activity in stimulated femoral head explant cultures, detection of a range of neoepitopes from both the chondroitin sulphate and interglobular domains of ACAN can be performed, such as VTEGE$_{373}$, $_{374}$ALGSV, SSELE$_{1279}$, FREEE$_{1467}$, $_{1468}$GLGSV, $_{1573}$AGEGP, and $_{1673}$LGHGP (402). The findings described in this chapter of altered GAG release from stimulated femoral head explants from *Trim32* KO mice compared to WT mice, could be examined further in future studies by performing Western blotting for the full length ACAN protein, and for a range of ACAN fragments using neoepitope antibodies. This could be performed in the media and femoral head explants from WT and *Trim32* KO mice following treatment with IL1α and RA to examine the effect of *Trim32* knockout on aggrecanolysis in more detail. The GAG assays using pairs of femoral head explants from WT and *Trim32* KO mice were only performed in independent replicates of three pairs of femoral heads for each genotype group of mice. Although significant differences were identified between GAG assay results between WT and *Trim32* KO mice, an increased number of replicates in each group could lead to more robust findings.

The effect of *Trim32* KO on chondrocyte phenotype was then assessed in response to catabolic and anabolic cytokine stimulation. *Trim32* mRNA levels were found to decrease in chondrocytes from WT mice in response to OSM and IGF1 stimulation but not IL1α or TNFα stimulation (Figure 4.8). Primary chondrocytes from *Trim32* KO mice demonstrated reduced *Col2a1* expression and increased expression of *Acan, Col10a1,* and *Sox9* compared to WT primary murine chondrocytes (Figure 4.9). The relative levels of *Col2a1* and *GAPDH* expression were comparable to those previously reported for primary murine chondrocytes *in vitro* (403, 464, 465). These results may indicate a significant alteration of the normal phenotype of chondrocytes from *Trim32* KO mice *in vitro* compared to WT primary murine chondrocytes, with a relatively reduced expression of markers of mature chondrocytes, and an increased expression of *Col10a1,* a marker of hypertrophic chondrocytes, and *Sox9,* a transcriptional regulator of chondrogenesis.

In *Trim32* KO murine primary chondrocytes, a greater expression of *Col10a* was detected in response to IL1α; a similar direction of effect was seen following stimulation with TNFα, though this was not significant (Figures 4.10 and 4.11). These findings are consistent with previous studies demonstrating an increased potency of IL1α compared to TNFα in inducing catabolic responses in primary chondrocytes (466). This may indicate an increased shift towards a hypertrophic chondrocyte phenotype in *Trim32* KO primary chondrocytes in response to pro-inflammatory cytokine stimulation (467, 468). Upon stimulation with OSM, another catabolic cytokine, and IGF1, an anabolic cytokine, there was a significant increase of *Col2a1* expression; following IGF1 stimulation, a reduced expression of *Sox9* by *Trim32* KO primary murine chondrocytes was also identified (Figure 4.12 and Figure 4.13) (469-473). *Col2a1* expression is significantly increased by activated mature chondrocytes in osteoarthritic cartilage (Figures 4.11, 4.12 and 4.13; (474)). It is uncertain whether this increase in *Col2a1* expression by *Trim32*-deficient chondrocytes represents an exaggerated shift towards a mature chondrocyte phenotype, or also represents a predisposition to an activated state typical of osteoarthritic cartilage (475, 476).

There are limitations to the gene expression studies performed in immature primary murine chondrocytes described in this chapter. The large apparent relative increase in *Col2a1* expression in chondrocytes from *Trim32* KO mice following OSM and IGF1 stimulation (Figure 4.12 and Figure 4.13) may be due to the comparison with low levels of *Col2a1* expression in unstimulated *Trim32*-deficient chondrocytes (Figure 4.9; *Col2a1* Ct values WT 18.37, *Trim32* KO 25.69), though the GAPDH expression levels were similar between unstimulated chondrocytes from WT and *Trim32* KO mice (Figure 4.9; GAPH Ct values WT 25.28, *Trim32* KO 25.59). Caution is also required in interpreting the gene expression results as each experiment was performed in replicates of only three. Furthermore, the findings from *in vitro* studies of immature primary murine chondrocytes cannot be directly extrapolated to pathological mechanisms occurring in OA in humans. These experiments utilised immature primary murine chondrocytes from femoral head epiphyseal cartilage. Histological analysis or phenotyping was not performed to compare the femoral head epiphyses from WT and

Trim32 KO mice. Although the murine femoral head epiphyses was cartilaginous at the time of harvest in these experiments (3 weeks), the epiphyseal region of the femoral head explants contains a heterogeneous population of cells, including resting chondrocytes, hypertrophic chondrocytes, chondroclasts, osteoclasts, and osteoblasts (477, 478). The changes in gene expression between cells harvested from femoral epiphyses of WT and *Trim32* KO mice could therefore reflect changes in individual cell types or changes in proportion of cell types. This could be investigated further in future studies, for example by examining the immunohistochemical localisation of markers such as Col II and Col X in epiphyseal cartilage from WT and *Trim32* KO mice. Finally, although seeded immature chondrocytes were not passaged in these experiments, cultured chondrocytes may lose their phenotype upon monolayer culture with change from a polygonal to a flattened shape, and reduce Col II, and increased Col X, expression (479).

Measuring gene expression by quantitative reverse transcription-PCR also has several advantages and limitations. Chondrocyte phenotype in response to subsequent cytokine stimulations was assessed by mRNA expression levels of chondrocyte markers of differentiation relative to unstimulated controls and normalised to *GAPDH* mRNA expression within each experiment using the $\Delta\Delta C_t$ method, thereby accounting for efficiency and basal expression levels. The interval between stimulation and detection of mRNA expression can be important; the interval of 48 hours used in these experiments is a reliable time-point at which to assess the response of chondrocytes to stimulation by cytokines at the chosen concentrations (480-483). These results represent relative changes in expression and not absolute mRNA expression levels. There are also several factors that preclude direct translation of results of *in vitro* mRNA analysis of gene expression to the *in vivo* environment; mRNA may not be translated efficiently, post-translational modifications may regulate protein activity, and a variety of inhibitors and enhancers may ameliorate or potentiate protein activity.

The results from the analysis of gene expression by immature primary murine chondrocytes from WT and *Trim32* KO mice indicate that *Trim32* deficiency may be associated with increased expression of genes associated with chondrocyte hypertrophy

following catabolic cytokine stimulation, and dysregulation of *Col2a1* and *Sox9* expression upon anabolic cytokine stimulation (Figure 4.9 to Figure 4.13). These results may support the findings from analysis of TRIM32 protein expression by human primary chondrocytes, in which lower TRIM32 expression was associated with an osteoarthritic phenotype, and also the findings from GAG release, as an indicator of aggrecanolysis, in murine femoral head explants, in which increased GAG release occurred in explants from *Trim32* KO mice (Figures 4.4 to 4.7). Further studies are required to determine in more detail the role of TRIM32 in immature and mature articular cartilage, other joint tissues, and the potential effects of TRIM32 in pathological mechanisms occurring in OA.

Chapter 5

The role of *Trim32* in the development of OA *in vivo*: surgically induced and ageing induced OA in *Trim32* knockout mice

5.1 Summary

The aim of this chapter was to evaluate the effect of *Trim32* knockout on the development of OA *in vivo* in mice following ageing to 10 months or surgically induced joint instability (DMM surgery). Following DMM surgery, muscle strength and nociception testing were also performed.

Cartilage degradation was measured histologically using the OARSI score and subchondral bone changes were assessed by μCT 8 weeks after DMM surgery in female WT (n = 14), *Trim32*$^{+/-}$ (HET; n = 14), and *Trim32*$^{-/-}$ (KO; n =13) mice. Muscle strength and nociception were assessed using a grip strength meter and von Frey filaments, respectively, in WT (n = 7) and *Trim32*$^{-/-}$ mice (n = 8). Knee joint histomorphometry was also analysed in aged female WT (n = 12), *Trim32*$^{+/-}$ (n = 12), and *Trim32*$^{-/-}$ mice (n = 13).

Joint OARSI scores and subchondral bone parameters were similar in control unoperated contralateral knees from WT, *Trim32*$^{+/-}$, and *Trim32*$^{-/-}$ mice after DMM and ageing. After DMM, a greater increase in tibial epiphyseal trabecular volume ($p = 5{\cdot}0 \times 10^{-5}$ WT *vs* KO) and number ($p = 8{\cdot}97 \times 10^{-7}$ WT *vs* KO) occurred in *Trim32*$^{-/-}$ than WT mice. In aged mice, tibial medial bone plate thickness (p = 0·004 WT *vs* KO), and femoral epiphyseal trabecular volume (p = 0·032 WT *vs* KO) and thickness (p = 0·001 WT *vs* KO), and medial bone plate thickness (p = 0·001 WT *vs* KO) were greater in *Trim32*$^{-/-}$ than in WT mice.

After DMM, total knee joint OARSI scores were more severe in *Trim32*$^{+/-}$ and *Trim32*$^{-/-}$ mice than in WT mice (p = 0.005 WT *vs* HET, $p = 7.0 \times 10^{-6}$ WT *vs* KO). In aged mice, knee joint medial compartment OARSI scores were more severe in *Trim32* deficient mice; the trend was approaching statistical significance (p = 0.06). In aged mice, total hip joint OARSI scores were not significantly different between WT, *Trim32*$^{+/-}$, and *Trim32*$^{-/-}$ mice. Meta-analysis of knee and hip joint OARSI scores showed increased cartilage degradation in *Trim32*$^{-/-}$ compared to WT mice. Mechanical allodynia was more severe (p = 0.0008), and grip strength lower (p = 0.03), in *Trim32*$^{-/-}$ compared to WT mice.

These results demonstrate increased cartilage degradation and tibial epiphyseal bone changes after DMM, and a trend towards increased cartilage degradation and medial knee subchondral bone changes upon ageing in *Trim32* KO mice. These findings were associated with lower pain thresholds in *Trim32* KO mice and indicate a protective role for TRIM32 in the maintenance of cartilage integrity *in vivo*.

5.2 Introduction

In Chapter 4 it was demonstrated that TRIM32 significantly influences the response of chondrocytes and cartilage to anabolic and catabolic stimuli *in vitro*. Interpretation of the overall impact of such effects is restricted by the limitations of the cell and tissue culture environments. Analysing the effect of deficiency of a gene implicated in the development of OA using *in vivo* models provides an environment that better represents the true disease process. Several murine models of OA exist and their appropriate application depends upon the experimental objectives. The overall aim of the experiments described in this chapter was to investigate the effect of *Trim32* knockout on the development of OA *in vivo* following ageing or surgically induced joint instability (DMM surgery) murine models of OA.

In this chapter, the effect of DMM surgery on the development of OA in WT mice, mice with *Trim32* haploinsufficiency, and *Trim32* KO mice is evaluated through analysis of subchondral bone and epiphyseal trabecular bone changes at the distal femur and proximal tibia at the knee joint as assessed by μCT, and through analysis of histological degenerative changes of the articular cartilage in the medial and lateral compartments of the knee joint, and the knee joint as a whole. DMM surgery was performed in mice at 8 weeks of age, and joint histomorphometry was analysed 8 weeks following the DMM procedure.

The effect of natural ageing on the development of spontaneous OA in WT mice, mice with *Trim32* haploinsufficiency, and *Trim32* KO mice is also evaluated through analysis of subchondral bone and epiphyseal trabecular bone of both the knee joint and proximal femur at the hip joint as assessed by μCT, and through analysis of histological changes of the articular cartilage in the medial and lateral compartments of the knee joint, the knee joint as a whole, and of the proximal femur of the hip joint. Mice were aged to 10 months prior to analysis of joint histomorphometry.

The osteoarthritic changes of the articular cartilage following DMM surgery and ageing in WT and *Trim32* KO mice are assimilated in a meta-analysis to evaluate the

overall effect of *Trim32* knockout on the development of degenerative osteoarthritic changes of the articular cartilage in mice.

Finally, in addition to the osteoarticular changes assessed, the effect of the development of OA following DMM surgery on pain behaviour and muscle strength were also investigated in WT and *Trim32* KO mice by evaluating hypersensitivity to mechanical stimulation and limb grip strength.

5.3 Aims

The aims of the experiments described in this chapter were to:

1. Investigate the effect of *Trim32* knockout on the development of OA *in vivo*, by assessing knee joint histology and histomorphometry, in response to DMM surgery in mice.
2. Investigate the effect of *Trim32* knockout on the development of OA *in vivo*, by assessing knee and hip histology and histomorphometry, in response to natural ageing in mice.
3. Evaluate the effect of *Trim32* knockout on the development of pain and muscle strength *in vivo*, by assessing mechanical allodynia and limb grip strength, in response to DMM surgery in mice.

5.4 Results

5.4.1 MicroCT analysis of knee joints of *Trim32* knockout mice after DMM

To investigate the effect of *Trim32* deficiency on the development of OA *in vivo*, the DMM surgical procedure was performed in WT, *Trim32*$^{+/-}$, and *Trim32*$^{-/-}$ mice at 8 weeks of age to induce the development of OA. Eight weeks following the DMM procedure, mice were culled and operated (right) and unoperated control (left) joints were retrieved for analysis of subchondral bone by microCT and cartilage degradation by histological scoring. To determine if any alteration in the susceptibility to knee OA following DMM surgery in *Trim32* KO mice was associated with abnormalities of subchondral bone, microCT analysis of both tibial and femoral subchondral bone at the knee joint was performed in WT, *Trim32*$^{+/-}$ (HET), and *Trim32*$^{-/-}$ (KO) mice. The number of cage mates was controlled throughout: there were no significant differences in the mean number of cage mates of WT, *Trim32*$^{+/-}$, or *Trim32*$^{-/-}$ mice undergoing DMM surgery (WT 1.67, HET 2.0, KO 2.0; p = 0.46 WT *vs* HET, p = 0.39 WT *vs* KO). There were no significant differences in the weight of WT, *Trim32*$^{+/-}$, or *Trim32*$^{-/-}$ mice either at time of surgery aged 8 weeks (WT 18.9 g, HET 18.8 g, KO 19.6 g; p = 0.75 WT vs HET, p = 0.21 WT vs KO) or at time of analysis aged 16 weeks (WT 22.4 g, HET 22.5 g, KO 23.7 g; p = 0.78 WT vs HET, p = 0.09 WT vs KO).

The absolute values of subchondral bone parameters of the tibia and femur at the knee joint are summarised in Table 5.1 and Table 5.2, respectively. There were no significant differences in either the tibial or femoral subchondral bone parameters of either the operated or unoperated control knee between WT and *Trim32*$^{+/-}$ mice following DMM surgery. Several differences in the absolute values of subchondral bone parameters were identified in both the tibial and femoral subchondral bone between WT and *Trim32*$^{-/-}$ mice following DMM surgery. In the tibial subchondral bone of the unoperated knee, trabecular thickness was greater (p = 0.015), and trabecular number lower (p = 0.02) in the *Trim32*$^{-/-}$ mice (Table 5.1). In the tibial subchondral bone of the operated knee, bone volume (p = 0.003), trabecular thickness (p = 0.02), medial bone plate thickness (p = 0.04), and lateral bone plate thickness (p = 0.004) were all greater in the *Trim32*$^{-/-}$ mice compared to WT mice (Table 5.1). In the femoral subchondral bone

of the control knee, only trabecular thickness ($p = 0.03$) was greater in the *Trim32*$^{-/-}$ mice compared to WT mice (Table 5.2). In the femoral subchondral bone of the operated knee, bone volume ($p = 0.03$), trabecular thickness ($p = 0.0003$), and lateral bone plate thickness ($p = 0.03$) were all greater in the *Trim32*$^{-/-}$ mice compared to WT mice, and medial bone plate thickness was non-significantly increased (Table 5.2; $p = 0.052$).

MicroCT analysis of the subchondral bone of the knee joints of WT, *Trim32*$^{+/-}$, and *Trim32*$^{-/-}$ mice following DMM surgery identified increased trabecular thickness of the tibia and femur, and reduced trabecular number in control unoperated knee joints from *Trim32*$^{-/-}$ mice compared to WT mice (Table 5.1 and Table 5.2). Further changes were identified in the subchondral bone of operated knee joints from *Trim32*$^{-/-}$ mice compared to WT mice following DMM surgery. In addition to increased trabecular thickness of the subchondral bone of operated knee joints from *Trim32*$^{-/-}$ compared to WT mice as seen in the control unoperated knee joints, there was a significant increase in tibial subchondral bone volume, and medial and lateral bone plate thickness, and increased femoral subchondral bone volume and increased lateral bone plate thickness in *Trim32*$^{-/-}$ mice compared to WT mice after DMM surgery. Significant increases in the subchondral trabecular bone and subchondral bone plates of knee joints in *Trim32*$^{-/-}$ mice compared to WT mice may signify increased subchondral bone sclerosis following DMM surgery in *Trim32*$^{-/-}$ mice compared to WT mice.

Control (Left Knee)	TRIM32 Genotype			WT v HET	WT v KO
TIBIA	WT (n=14)	HET (n=14)	KO (n=13)	p-value	p-value
BV/TV (%)	28.04 +/- 2.99	28.39 +/- 1.99	27.81 +/- 1.99	0.921	0.964
Tb.Th (µm)	47.75 +/- 3.89	49.10 +/- 2.67	51.42 +/- 2.97	0.520	**0.015***
Tb.Sp (µm)	177.30 +/- 14.33	175.55 +/- 16.27	183.53 +/- 11.41	0.943	0.497
Tb.N (1/mm)	5.87 +/- 0.36	5.80 +/- 0.47	5.42 +/- 0.41	0.886	**0.021***
Medial Bone Plate Thickness (µm)	54.32 +/- 5.59	58.23 +/- 3.28	58.09 +/- 5.20	0.091	0.115
Lateral Bone Plate Thickness (µm)	54.53 +/- 3.99	58.48 +/- 4.67	58.00 +/- 4.74	0.063	0.122
DMM (Right Knee)	**TRIM32 Genotype**			**WT v HET**	**WT v KO**
TIBIA	WT (n=14)	HET (n=14)	KO (n=13)	p-value	p-value
BV/TV (%)	29.65 +/- 4.09	31.70 +/- 3.62	34.18 +/- 1.81	0.253	**0.003****
Tb.Th (µm)	52.19 +/- 5.17	55.11 +/- 3.73	56.54 +/- 3.04	0.157	**0.024***
Tb.Sp (µm)	188.34 +/- 18.33	180.49 +/- 15.10	190.09 +/- 12.68	0.756	0.975
Tb.N (1/mm)	5.68 +/- 0.47	5.41 +/- 0.53	6.02 +/- 0.43	0.912	0.108
Medial Bone Plate Thickness (µm)	58.40 +/- 6.38	60.24 +/- 4.94	64.09 +/- 6.28	0.244	**0.043***
Lateral Bone Plate Thickness (µm)	59.09 +/- 7.42	63.01 +/- 5.11	66.92 +/- 4.78	0.171	**0.004****

Table 5.1 - MicroCT analysis of tibial subchondral bone of DMM-operated and control joints from wild-type (WT), *Trim32*$^{+/-}$ mice (HET), and *Trim32*$^{-/-}$ mice (KO); WT (n=14), *Trim32*$^{+/-}$ (n=14), and *Trim32*$^{-/-}$ (n=13) mice underwent the DMM procedure at 8 weeks of age, and operated (right) knee joints and unoperated control (left) knee joints were harvested at 16 weeks of age for analysis by microCT of subchondral trabecular bone parameters (BV/TV: trabecular volume; Tb.Th: trabecular thickness; Tb.Sp: trabecular separation; Tb.N: trabecular number) and subchondral medial and lateral bone plate thickness. Values are mean +/- SD. Statistical analysis was performed by one-way ANOVA with post-hoc Tukey test, with statistical significance accepted at $p < 0.05$ and annotated with (*) and presented in bold.

Control (Left Knee)	TRIM32 Genotype			WT v HET	WT v KO
FEMUR	WT (n=14)	HET (n=14)	KO (n=13)	p-value	p-value
BV/TV (%)	24.54 +/- 3.07	26.18 +/- 1.55	26.37 +/- 2.15	0.167	0.120
Tb.Th (µm)	45.54 +/- 3.62	47.76 +/- 1.70	48.57 +/- 2.90	0.151	**0.033***
Tb.Sp (µm)	185.68 +/- 14.74	181.11 +/- 13.97	187.39 +/- 10.79	0.640	0.941
Tb.N (1/mm)	5.35 +/- 0.42	5.48 +/- 0.29	5.43 +/- 0.42	0.645	0.842
Medial Bone Plate Thickness (µm)	47.45 +/- 4.18	49.64 +/- 3.13	50.42 +/- 3.86	0.307	0.128
Lateral Bone Plate Thickness (µm)	66.83 +/- 4.44	69.69 +/- 6.84	69.02 +/- 3.96	0.332	0.532
DMM (Right Knee)	**TRIM32 Genotype**			**WT v HET**	**WT v KO**
FEMUR	WT (n=14)	HET (n=14)	KO (n=13)	p-value	p-value
BV/TV (%)	24.45 +/- 3.28	25.90 +/- 2.77	28.72 +/- 2.10	0.244	**0.003****
Tb.Th (µm)	50.53 +/- 4.09	52.43 +/- 2.55	56.18 +/- 2.18	0.171	**0.0003*****
Tb.Sp (µm)	198.98 +/- 14.88	199.53 +/- 9.98	192.92 +/- 10.63	0.999	0.419
Tb.N (1/mm)	4.84 +/- 0.51	4.94 +/- 0.46	5.11 +/- 0.38	0.748	0.371
Medial Bone Plate Thickness (µm)	52.08 +/- 4.06	54.71 +/- 6.56	56.83 +/- 4.18	0.368	0.052
Lateral Bone Plate Thickness (µm)	69.38 +/- 7.46	72.89 +/- 7.32	76.34 +/- 5.65	0.375	**0.031***

Table 5.2 - MicroCT analysis of femoral subchondral bone of DMM-operated and control joints from wild-type (WT), *Trim32*$^{+/-}$ mice (HET), and *Trim32*$^{-/-}$ mice (KO); WT (n=14), *Trim32*$^{+/-}$ (n=14), and *Trim32*$^{-/-}$ (n=13) mice underwent the DMM procedure at 8 weeks of age, and operated (right) knee joints and unoperated control (left) knee joints were harvested at 16 weeks of age for analysis by microCT of subchondral trabecular bone parameters (BV/TV: trabecular volume; Tb.Th: trabecular thickness; Tb.Sp: trabecular separation; Tb.N: trabecular number) and subchondral medial and lateral bone plate thickness. Values are mean +/- SD. Statistical analysis was performed by one-way ANOVA with post-hoc Tukey test, with statistical significance accepted at $p < 0.05$ and annotated with (*) and presented in bold.

To better evaluate the response of the subchondral bone of the knee joint in *Trim32* KO mice to surgically induced joint instability, the change in absolute values of subchondral bone parameters between the operated (DMM) and unoperated (control) knees were compared between WT, *Trim32*$^{+/-}$, and *Trim32*$^{-/-}$ mice. There were no significant differences in the change in either tibial or femoral subchondral bone parameters following DMM surgery in the *Trim32*$^{+/-}$ mice compared to WT mice (Figure 5.1 and Figure 5.2). Several significant changes were identified in the tibial subchondral bone parameters following DMM surgery in the *Trim32*$^{-/-}$ mice compared to WT mice. A greater increase in tibial subchondral bone volume (WT +5.89%, KO +23.1%; $p = 5.0 \times 10^{-5}$ WT *vs* KO) was demonstrated in *Trim32*$^{-/-}$ mice following DMM surgery, compared to WT mice (Figure 5.1A). This was associated with a correspondingly greater increase in trabecular number in the *Trim32*$^{-/-}$ mice following DMM surgery (WT -3.22%, KO +12.01%; $p = 8.97 \times 10^{-7}$ WT *vs* KO; Figure 5.1A). A non-significant greater increase in lateral tibial subchondral bone plate thickness was also demonstrated in *Trim32*$^{-/-}$ mice following DMM surgery, compared to WT mice (WT +8.61%, KO +16.08%; p = 0.268 WT *vs* KO), though this effect was not as marked in the medial tibial subchondral bone plate (Figure 5.1B).

At the femoral subchondral bone, a greater increase in bone volume was observed in *Trim32*$^{-/-}$ mice following DMM surgery compared to WT mice, which was approaching statistical significance (WT +0.07%, KO +10.33%; p = 0.07 WT *vs* KO; Figure 5.2A). This was also associated with a non-significant increase in trabecular thickness in the *Trim32*$^{-/-}$ mice (Figure 5.2A). Similar to the changes identified in the tibia, a non-significant greater increase in lateral femoral subchondral bone plate thickness was demonstrated in *Trim32*$^{-/-}$ mice following DMM surgery, compared to WT mice (WT +3.78%, KO +10.96%; p = 0.08 WT *vs* KO (Figure 5.2B)).

A

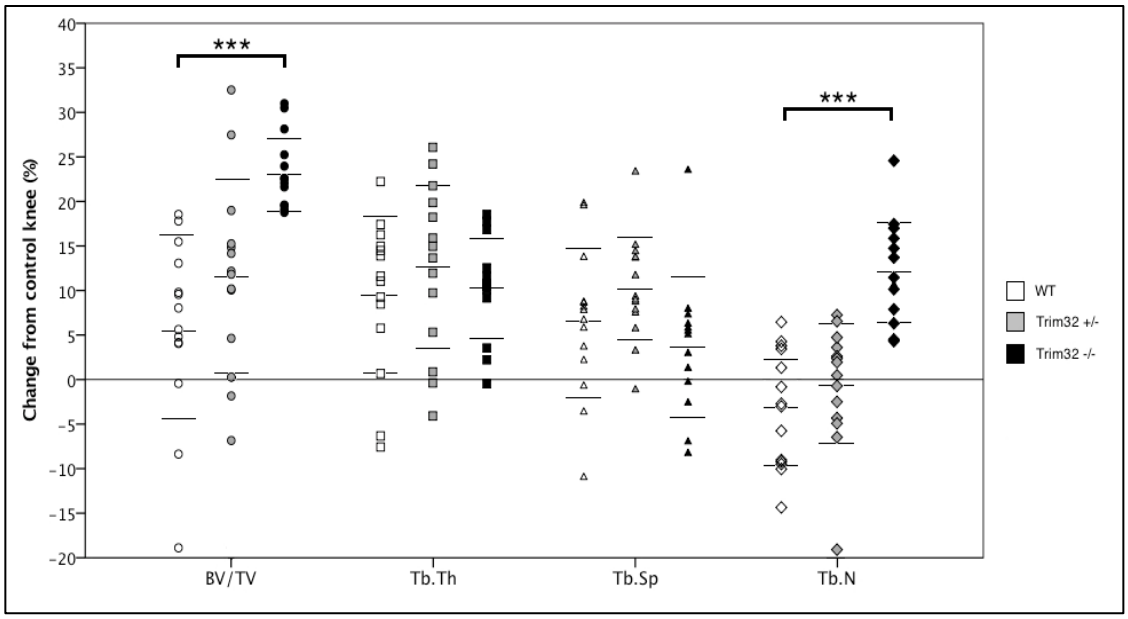

B

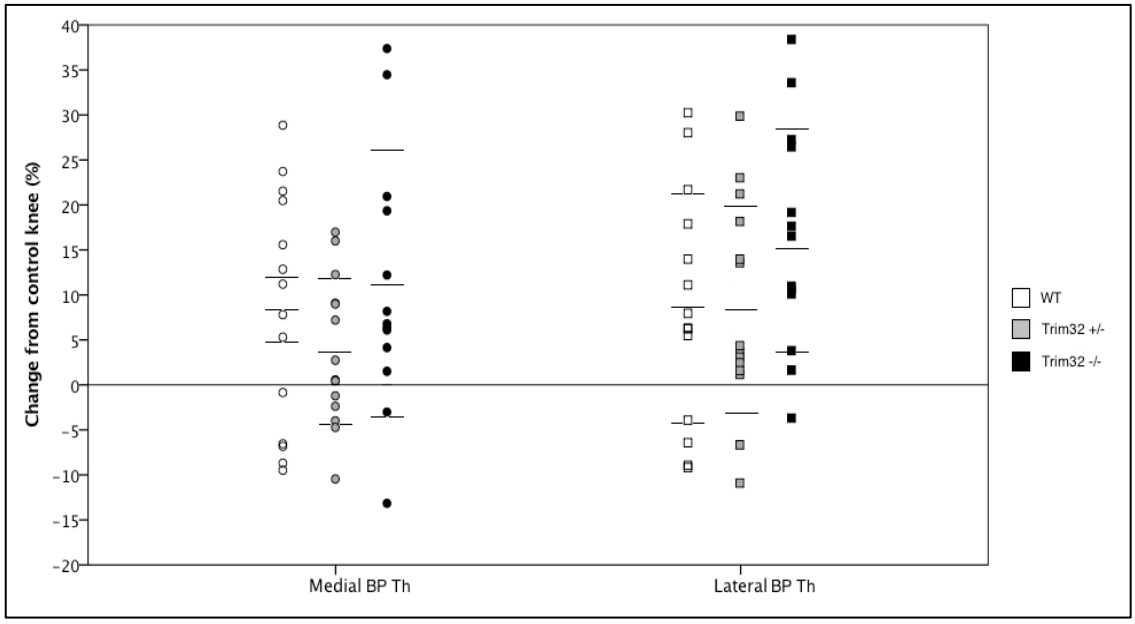

Figure 5.1 – Percentage change in microCT parameters of tibial subchondral bone of DMM-operated compared to control joints in wild-type (WT), *Trim32*$^{+/-}$ mice (HET), and *Trim32*$^{-/-}$ mice (KO); 14 WT, 14 *Trim32*$^{+/-}$ (HET), and 13 *Trim32*$^{-/-}$ (KO) mice underwent the DMM procedure at 8 weeks of age, and operated (right) and unoperated control (left) knee joints were harvested at 16 weeks of age for analysis by microCT of subchondral trabecular bone parameters (BV/TV: trabecular volume; Tb.Th: trabecular thickness; Tb.Sp: trabecular separation; Tb.N: trabecular number) and subchondral medial and lateral bone plate thickness. Values for percentage change (lines represent mean +/- SD) in microCT parameters of tibial subchondral bone of DMM operated compared to control joints are shown for A) trabecular bone, and B) medial and lateral subchondral bone plates. Statistical analysis was performed by one-way ANOVA with post-hoc Tukey test, with statistical significance accepted at $p < 0.05$: *$p = 5.0 \times 10^{-5}$; **$p = 8.97 \times 10^{-7}$.

A

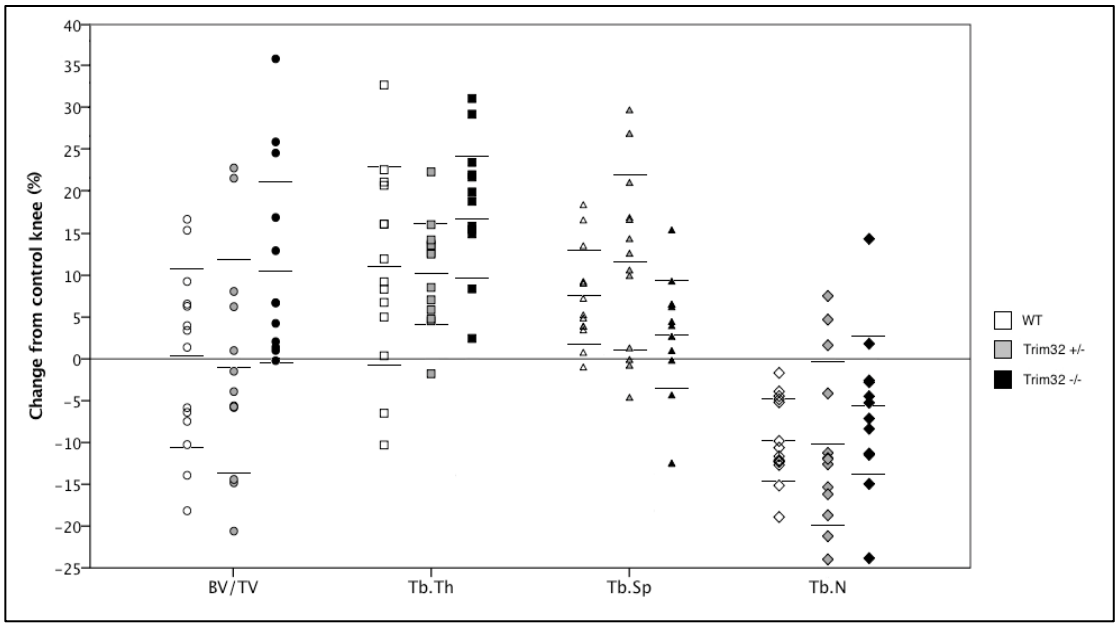

B

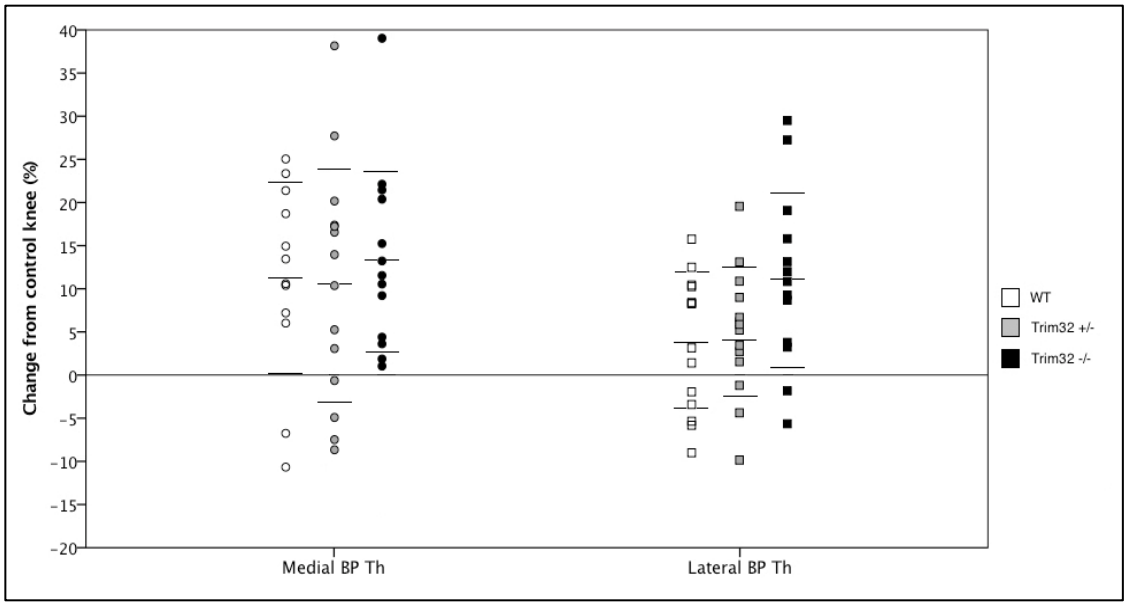

Figure 5.2 – Percentage change in microCT parameters of femoral subchondral bone of DMM-operated compared to control joints in wild-type (WT), *Trim32*$^{+/-}$ mice (HET), and *Trim32*$^{-/-}$ mice (KO); 14 WT, 14 *Trim32*$^{+/-}$ (HET), and 13 *Trim32*$^{-/-}$ (KO) mice underwent the DMM procedure at 8 weeks of age, and operated (right) and unoperated control (left) knee joints were harvested at 16 weeks of age for analysis by microCT of subchondral trabecular bone parameters (BV/TV: trabecular volume; Tb.Th: trabecular thickness; Tb.Sp: trabecular separation; Tb.N: trabecular number) and subchondral medial and lateral bone plate thickness. Values for percentage change (lines represent mean +/- SD) in microCT parameters of femoral subchondral bone of DMM-operated compared to control joints are shown for A) trabecular bone, and B) medial and lateral subchondral bone plates. Statistical analysis was performed by one-way ANOVA with post-hoc Tukey test, with statistical significance accepted at $p < 0.05$.

5.4.2 MicroCT analysis of knee joints of *Trim32* knockout mice after ageing

To investigate the effect of *Trim32* deficiency on the development of spontaneous OA *in vivo*, WT, *Trim32*$^{+/-}$, and *Trim32*$^{-/-}$ mice were also aged to 10 months, after which hip and knee joints were retrieved for analysis of subchondral bone by microCT and cartilage degradation by histological scoring. To investigate any alteration in subchondral bone changes representative of knee OA upon ageing of *Trim32* KO mice, μCT analysis of both tibia and femoral subchondral bone at the knee joint was performed in aged WT, *Trim32*$^{+/-}$, and *Trim32*$^{-/-}$ mice. The mean number of cage mates was similar throughout the 10 months' of ageing for WT, *Trim32*$^{+/-}$, and *Trim32*$^{-/-}$ mice (WT 4.75, HET 4.5, KO 5.2; p = 0.64 WT *vs* HET, p = 0.06 WT *vs* KO). There was no significant difference in the mean final weight between WT and *Trim32*$^{+/-}$ mice, although *Trim32*$^{-/-}$ mice were heavier than WT mice (WT 28.1 g, HET 29.9 g, KO 37.3 g; p = 0.20 WT *vs* HET, p = 0.0002 WT *vs* KO).

The absolute values of subchondral bone parameters of the tibia and femur at the knee joint of aged mice are shown in Table 5.3. The only significant difference between the aged WT and *Trim32*$^{+/-}$ mice was observed in the trabecular thickness of the femoral subchondral bone (WT 54.15 μm, HET 59.32 μm; p = 0.021 WT *vs* HET); all other measured subchondral bone parameters at the knee were similar between aged WT and *Trim32*$^{+/-}$ mice.

Several significant differences in subchondral bone parameters at the knee were identified between aged WT and *Trim32*$^{-/-}$ mice (Table 5.3). After ageing, *Trim32*$^{-/-}$ mice demonstrated significantly increased medial tibial bone plate thickness compared to WT mice (WT 68.55 μm, KO 79.70 μm; p = 0.004 WT *vs* KO), and increased lateral bone plate thickness, which was approaching statistical significance (WT 64.08 μm, KO 70.07 μm; p = 0.064 WT *vs* KO; Table 5.3). At the femoral subchondral bone, *Trim32*$^{-/-}$ mice developed increase bone volume (WT 22.46 μm, KO 25.63 μm; p = 0.03 WT *vs* KO), trabecular thickness (WT 54.15 μm, KO 61.34 μm; p = 0.001 WT *vs* KO), and medial bone plate thickness (WT 58.72 μm, KO 67.71 μm; p = 0.001 (Table 5.3)) after ageing compared to WT littermates.

Right Knee	TRIM32 Genotype			WT v HET	WT v KO
TIBIA	WT (n=12)	HET (n=12)	KO (n=13)	p-value	p-value
BV/TV (%)	25.20 +/- 2.31	27.35 +/- 2.59	25.58 +/- 2.19	0.086	0.925
Tb.Th (µm)	59.49 +/- 3.30	60.66 +/- 4.26	62.02 +/- 2.55	0.677	0.170
Tb.Sp (µm)	241.77 +/- 19.41	228.67 +/- 14.49	242.77 +/- 21.98	0.205	0.994
Tb.N (1/mm)	4.24 +/- 0.46	4.19 +/- 0.33	4.13 +/- 0.34	0.192	0.707
Medial Bone Plate Thickness (µm)	68.55 +/- 7.54	70.86 +/- 9.39	79.70 +/- 7.15	0.763	**0.004****
Lateral Bone Plate Thickness (µm)	64.08 +/- 6.10	70.41 +/- 7.00	70.07 +/- 5.61	0.053	0.064
Right Knee	**TRIM32 Genotype**			**WT v HET**	**WT v KO**
FEMUR	WT (n=12)	HET (n=12)	KO (n=13)	p-value	p-value
BV/TV (%)	22.46 +/- 3.23	24.89 +/- 2.41	25.63 +/- 3.25	0.128	**0.032***
Tb.Th (µm)	54.15 +/- 5.14	59.32 +/- 3.31	61.34 +/- 4.20	**0.021***	**0.001****
Tb.Sp (µm)	245.49 +/- 17.55	235.02 +/- 15.61	235.09 +/- 19.05	0.312	0.315
Tb.N (1/mm)	4.16 +/- 0.57	4.20 +/- 0.36	4.17 +/- 0.37	0.964	0.996
Medial Bone Plate Thickness (µm)	58.72 +/- 5.96	60.23 +/- 5.20	67.71 +/- 6.13	0.789	**0.001****
Lateral Bone Plate Thickness (µm)	83.13 +/- 12.89	82.86 +/- 8.15	88.36 +/- 9.28	0.997	0.386

Table 5.3 - Absolute values of microCT analysis of tibial and femoral subchondral bone of knee joints from aged wild-type (WT), *Trim32*$^{+/-}$ mice (HET), and *Trim32*$^{-/-}$ mice (KO); WT (n=12), *Trim32*$^{+/-}$ (n=12), and *Trim32*$^{-/-}$ (n=13) mice were aged to 10 months after which knee joints were harvested for analysis by microCT of tibial and femoral subchondral trabecular bone parameters (BV/TV: trabecular volume; Tb.Th: trabecular thickness; Tb.Sp: trabecular separation; Tb.N: trabecular number) and subchondral medial and lateral bone plate thickness. Values are mean +/- SD. Statistical analysis was performed by one-way ANOVA with post-hoc Tukey test, with statistical significance accepted at $p < 0.05$; statistically significant results are annotated with (*) and presented in bold.

In aged mice, microCT analysis of subchondral bone parameters identified a significant increase in medial bone plate thickness of the tibial and femoral aspects of the knee joints of *Trim32*$^{-/-}$ compared to WT mice, and also increased trabecular bone thickness at the femoral aspect of the knee joint in *Trim32* deficient mice, compared to WT mice (Table 5.3).

5.4.3 MicroCT analysis of hip joints of *Trim32* knockout mice after ageing

To investigate any alteration in subchondral bone changes representative of hip OA upon ageing of *Trim32* KO mice, μCT of femoral head subchondral bone at the hip joint was performed in WT, *Trim32*$^{+/-}$, and *Trim32*$^{-/-}$ mice. Hip joints were harvested from the same mice utilised to analyse subchondral bone parameters at the knee joint and thus the number of cage mates were similar across genotype groups (see section 5.4.2); *Trim32*$^{-/-}$ mice were heavier than WT mice at age 10 months, but *Trim32*$^{+/-}$ mice were similar in weight to WT mice (see section 5.4.2). The absolute values of subchondral bone parameters of the femoral head of the hip joint are summarised in Table 5.4. No significant differences were identified between WT, *Trim32*$^{+/-}$, and *Trim32*$^{-/-}$ mice in the measured subchondral bone parameters at the femoral head after natural ageing (Table 5.4).

Right Hip	TRIM32 Genotype			WT v HET	WT v KO
Femoral Head	WT (n=12)	HET (n=12)	KO (n=13)	p-value	p-value
BV/TV (%)	34.33 +/- 5.23	35.20 +/- 3.27	37.93 +/- 5.09	0.880	0.118
Tb.Th (μm)	48.48 +/- 8.49	48.50 +/- 5.48	53.38 +/- 6.89	1.000	0.182
Tb.Sp (μm)	135.59 +/- 10.97	135.92 +/- 9.22	133.46 +/- 11.81	0.993	0.898
Tb.N (1/mm)	7.18 +/- 1.28	6.81 +/- 0.65	7.13 +/- 0.73	0.945	0.988
Subchondral Bone Plate Thickness (μm)	42.29 +/- 21.24	32.75 +/- 19.53	35.86 +/- 22.01	0.519	0.731

Table 5.4 - Absolute values of microCT analysis of subchondral bone of the femoral head from aged wild-type (WT), *Trim32*$^{+/-}$ mice (HET), and *Trim32*$^{-/-}$ mice (KO); WT (n=12), *Trim32*$^{+/-}$ (n=12), and *Trim32*$^{-/-}$ (n=13) mice were aged to 10 months after which hip joints were harvested for analysis by microCT of femoral head subchondral trabecular bone parameters (BV/TV: trabecular volume; Tb.Th: trabecular thickness; Tb.Sp: trabecular separation; Tb.N: trabecular number) and subchondral bone plate thickness. Values are mean +/- SD. Statistical analysis was performed by one-way ANOVA with post-hoc Tukey test, with statistical significance accepted at $p < 0.05$; statistically significant results are annotated with (*) and presented in bold.

5.4.4 Histological analysis of knee joints of *Trim32* knockout mice after DMM

In addition to analysis of knee joints from WT, *Trim32*$^{+/-}$, and *Trim32*$^{-/-}$ mice by microCT following the DMM procedure, knee joints were also assessed for cartilage degradation by histological scoring of sagittal joint sections using the OARSI scoring system (383). The reproducibility of the OARSI histological scoring system to assess cartilage degradation following joint sectioning and staining with Toluidine Blue was evaluated by comparing scores assigned by two observers independently examining 153 sections from nine randomly selected knee joints. This resulted in an inter-observer correlation coefficient (r_s) of 0.334 ($p = 0.047$). This represents a significant positive correlation between independent observers scoring OA severity of joint sections and supports reproducibility of the histological analysis undertaken.

To determine any alteration in susceptibility to knee OA following DMM surgery in *Trim32* KO mice, grading of OA severity using the OARSI scoring system was performed for knee joints harvested from WT, *Trim32*$^{+/-}$, and *Trim32*$^{-/-}$ mice following DMM surgery. Knee joints were harvested from the same mice utilised to analyse μCT subchondral bone parameters; there were no significant differences in number of cage mates or weight of mice across genotype groups (see section 5.4.1).

There were no significant differences in the OARSI scores of the medial or lateral compartments of unoperated (control) knee joints between WT, *Trim32*$^{+/-}$, and *Trim32*$^{-/-}$ mice, as shown in Figure 5.3A (medial compartment $p = 0.240$ WT *vs* HET *vs* KO; lateral compartment $p = 0.182$ WT *vs* HET *vs* KO). There were also no significant differences on summing medial and lateral compartment scores to compare total knee joint OARSI scores of unoperated knee joints between WT, *Trim32*$^{+/-}$, and *Trim32*$^{-/-}$ mice, as shown in Figure 5.4 (total knee joint OARSI score $p = 0.136$ WT *vs* HET *vs* KO). Representative photomicrographs of histological sections from unoperated knee joints of WT, *Trim32*$^{+/-}$, and *Trim32*$^{-/-}$ mice are shown in Figure 5.3 C-E. These results indicate that there is no significant difference in OA severity of unoperated knee joints of WT, *Trim32*$^{+/-}$, and *Trim32*$^{-/-}$ mice by 16 weeks of age.

The DMM operated knee joints of *Trim32*$^{-/-}$, but not *Trim32*$^{+/-}$ mice demonstrated significantly increased OARSI scores of the medial compartment compared to WT mice, as shown in Figure 5.3B. Medial compartment OARSI scores were (mean ± SD) 3.1 ± 0.9 in WT mice, 4.1 ± 1.3 in *Trim32*$^{+/-}$ mice, and 5.2 ± 1.1 in *Trim32*$^{-/-}$ mice (Kruskal Wallis p = 0.0003 WT *vs* HET *vs* KO; post-hoc Dunn's tests p = 0.157 WT *vs* HET, p = 5.0 x 10^{-5} WT *vs* KO). The DMM operated knee joints of both *Trim32*$^{+/-}$ and *Trim32*$^{-/-}$ mice demonstrated significantly increased OARSI scores of the lateral compartment compared to WT mice, as shown in Figure 5.3B. Lateral compartment OARSI scores were 2.3 ± 1.3 in WT mice, 4.1 ± 1.3 in *Trim32*$^{+/-}$ mice, and 4.9 ± 1.4 in *Trim32*$^{-/-}$ mice (Kruskal Wallis p = 0.0002 WT vs HET vs KO; post-hoc Dunn's tests p = 0.004 WT vs HET, p = 7.0 x 10^{-5} WT vs KO). The summed total knee joint OARSI scores of DMM operated joints were also significantly greater in *Trim32*$^{+/-}$ and *Trim32*$^{-/-}$ mice compared to WT mice (Figure 5.4). Total knee joint OARSI scores were 5.4 ± 1.6 in WT mice, 8.1 ± 2.1 in *Trim32*$^{+/-}$ mice, and 10.1 ± 2.3 in *Trim32*$^{-/-}$ mice (Kruskal Wallis p = 3.0 x 10^{-5} WT *vs* HET *vs* KO; post-hoc Dunn's tests p = 0.005 WT *vs* HET, p = 7.0 x 10^{-6} WT *vs* KO). Representative photomicrographs of histological sections from DMM operated knee joints of WT, *Trim32*$^{+/-}$, and *Trim32*$^{-/-}$ mice demonstrating degenerate cartilage lesions are shown in Figure 5.3 F-H. As the mean weight of the *Trim32*$^{-/-}$ mice was non-significantly greater than the WT mice (mean weight WT 22.4 g, KO 23.7 g; p = 0.09 WT *vs* KO), the potential confounding effect of weight on the joint cartilage degradation scores was investigated using a generalised linear model (GLM). Weight did not have a significant covariate effect on OARSI scores when comparing WT and *Trim32*$^{-/-}$ mice (GLM; p = 0.56).

These results indicate that cartilage degradation scores were significantly greater in *Trim32* KO mice compared to WT mice following DMM surgery (Figure 5.3 and Figure 5.4). These results also indicate that mice with *Trim32* haploinsufficiency may be susceptible to increased cartilage degradation after DMM surgery in mice, but the effect is greatest in complete *Trim32* KO mice.

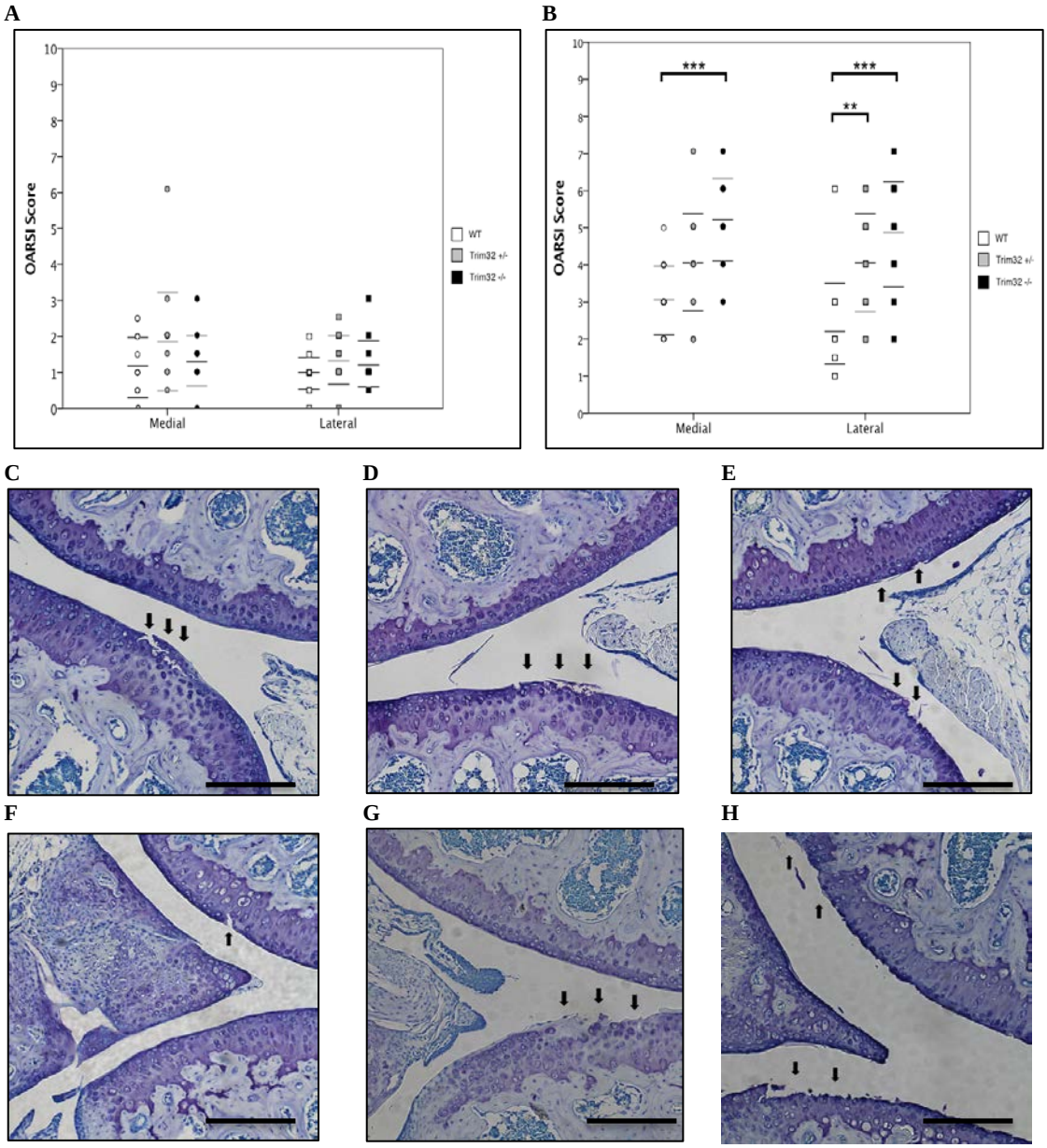

Figure 5.3 – Response to DMM in wild-type (WT), *Trim32*$^{+/-}$ (HET), and *Trim32*$^{-/-}$ (KO) mice: medial and lateral knee compartment osteoarthritis scores; summed osteoarthritis scores from femoral and tibial joint surfaces in medial and lateral compartments of knee joints left unoperated (control; panel A), or underwent DMM (panel B) in WT, (n = 14), HET (*Trim32*$^{+/-}$, n = 14), and KO (*Trim32*$^{-/-}$, n = 13) mice. Absolute values are shown (lines represent mean ± SD). Statistical analysis between groups was by Kruskal Wallis test with post-hoc Dunn's tests, with statistical significance accepted at $p < 0.05$. In panel B: medial compartment Kruskal Wallis test p = 0.0003 WT *vs* HET *vs* KO (post-hoc Dunn's test ***p = 5.0 x 10^{-5} WT *vs* KO); lateral compartment Kruskal Wallis test p = 0.0002 WT *vs* HET *vs* KO (post-hoc Dunn's tests **p = 0.004 WT *vs* HET, ***p = 7.0 x 10^{-5} WT *vs* KO). Panels C, D, and E show representative photomicrographs (sagittal sections) from control knee joints of WT, HET, and KO mice, respectively. Panels F, G, and H show representative photomicrographs (sagittal sections) from operated knee joints of WT, HET, and KO mice, respectively. Arrows show cartilage lesions. OARSI scores (first score for femoral aspect, second score for tibial aspect for the photomicrographs are: (C) 0, 2; (D) 0, 2; (E) 1, 2; (F) 2, 0; (G) 0, 3; (H) 2, 4. Scale bars for panels C-H represent 300 μm.

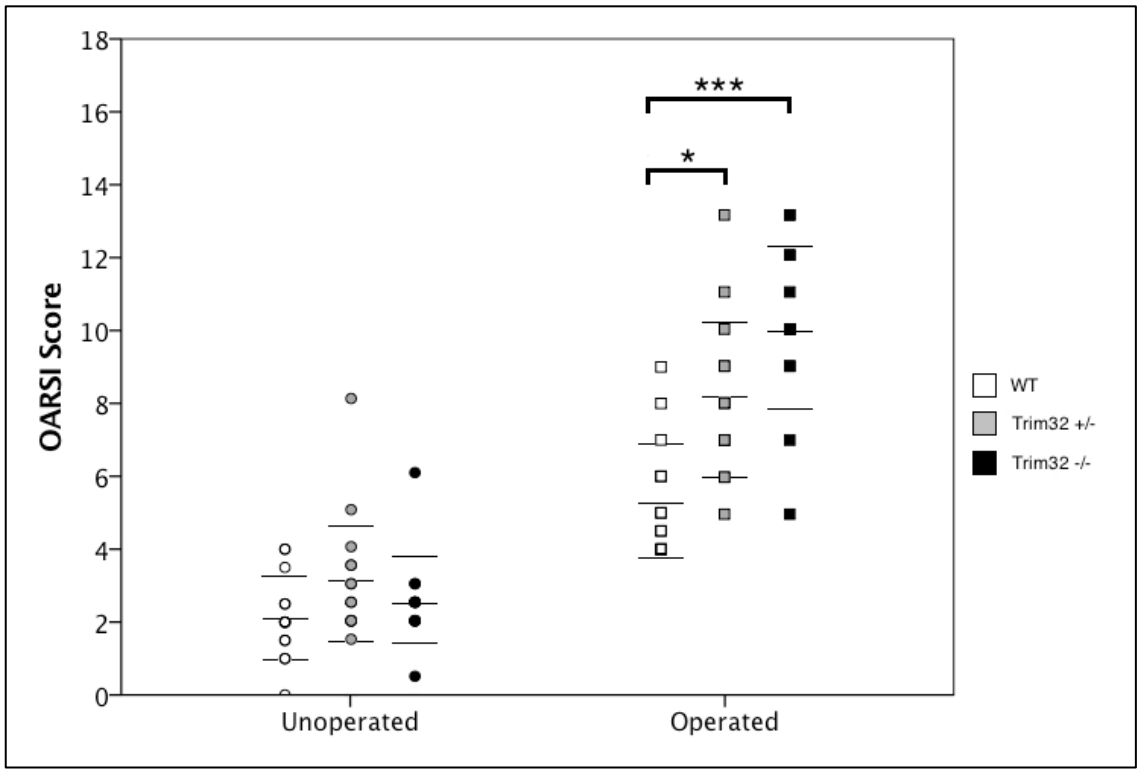

Figure 5.4 – Response to DMM in wild-type (WT), *Trim32*$^{+/-}$ (HET), and *Trim32*$^{-/-}$ (KO) mice: total knee joint osteoarthritis scores; summed osteoarthritis scores from the medial and lateral compartments of knee joints that were left unoperated (control), or underwent DMM (operated) in wild type (WT, n = 14), heterozygous (*Trim32*$^{+/-}$, n = 14), and knockout (*Trim32*$^{-/-}$, n = 13) mice are shown. In all mice, the DMM procedure was performed at 8 weeks of age, and knee joints from mice were harvested for analysis at 1 week of age. Histological analysis of cartilage degradation in each knee joint was performed using the OARSI histological scoring system to grade severity of cartilage degradation in the medial and lateral compartments of both the tibial and femoral aspects of each knee joint. For each knee joint, scores for these four compartments were summed to produce a total joint OARSI score. Absolute values for the total knee joint OARSI score for each joint are shown (lines represent mean ± SD). Statistical analysis between groups was performed by Kruskal Wallis test with post-hoc Dunn's tests, with statistical significance accepted at $p < 0.05$. For operated groups, Kruskal Wallis test $p = 3.0 \times 10^{-5}$ WT *vs* HET *vs* KO (post-hoc Dunn's tests *p = 0.005 WT vs HET, ***$p = 7.0 \times 10^{-5}$ WT vs KO).

5.4.5 Histological analysis of knee joints of *Trim32* knockout mice after ageing

To investigate any alteration in the susceptibility to spontaneous primary knee OA, grading of OA severity using the OARSI scoring system was performed for knee joints harvested from WT, *Trim32*$^{+/-}$, and *Trim32*$^{-/-}$ mice after natural ageing to 10 months. Knee joints were harvested from the same mice used to analyse μCT subchondral bone parameters in aged WT, *Trim32*$^{+/-}$, and *Trim32*$^{-/-}$ mice (see section 5.4.3). Histological analysis demonstrated no significant differences in OARSI scores of the medial compartment, lateral compartment, or total knee joint for *Trim32*$^{+/-}$ mice compared to WT mice (Figure 5.5A and Figure 5.6). OARSI scores were more severe in the medial compartment, but not the lateral compartment, of the knee in aged *Trim32*$^{-/-}$ mice compared to WT mice, though the difference was only approaching statistical significance (Figure 5.5A). Medial compartment OARSI scores were 3.4 ± 1.1 in WT mice, 3.3 ± 1.4 in *Trim32*$^{+/-}$ mice, and 4.7 ± 1.7 in *Trim32*$^{-/-}$ mice (Kruskal Wallis p = 0.06 WT *vs* HET *vs* KO). Lateral compartment OARSI scores were 4.6 ± 1 in WT mice, 4.8 ± 1.8 in *Trim32*$^{+/-}$ mice, and 5.2 ± 1.4 in *Trim32*$^{-/-}$ mice (Kruskal Wallis p = 0.44 WT *vs* HET *vs* KO). The summed total knee joint OARSI scores upon ageing were increased in *Trim32*$^{-/-}$ mice compared to WT mice, though the difference was not statistically significant (Figure 5.6): total knee joint OARSI scores were 8.0 ± 1.7 in WT mice, 8.2 ± 1.9 in *Trim32*$^{+/-}$ mice, and 9.9 ± 2.6 in *Trim32*$^{-/-}$ mice (Kruskal Wallis p = 0.09 WT *vs* HET *vs* KO). There was, therefore, a trend for more severe cartilage degradation OARSI scores in the medial compartment and whole joint in aged *Trim32*$^{-/-}$ mice, compared to WT mice, but these did not reach statistical significance. Representative photomicrographs of histological sections from knee joints of WT, *Trim32*$^{+/-}$, and *Trim32*$^{-/-}$ mice aged to 10 months are shown in Figure 5.5 B-D.

As the mean weight of the *Trim32*$^{-/-}$ mice was significantly greater than WT mice (mean weight WT 28.1 g, KO 37.3 g; $p = 2.7 \times 10^{-4}$), any confounding effect of weight on knee joint cartilage degradation scores in aged *Trim32* KO mice was investigated using a GLM analysis. Weight did not have a significant covariate effect on the OARSI score in aged *Trim32*$^{-/-}$ mice compared to WT mice (GLM; p = 0.05). Although the covariate effect of weight using the GLM analysis was approaching

significance, the majority of the difference in the joint OARSI score was attributable to difference in genotype (GLM corrected model effect 46.2 units; 46.0 units attributable to *Trim32* genotype). Increased cartilage degradation scores in the medial compartment and whole joint of *Trim32*$^{-/-}$ mice did not reach statistical significance. Although a trend for increased cartilage degradation OARSI scores was identified in the medial compartment and whole joint of *Trim32* KO mice compared to WT mice, these results are inconclusive regarding the susceptibility of *Trim32* deficient mice to spontaneous OA of the knee joint, as the trends were not statistically significant (Figure 5.5 and Figure 5.6).

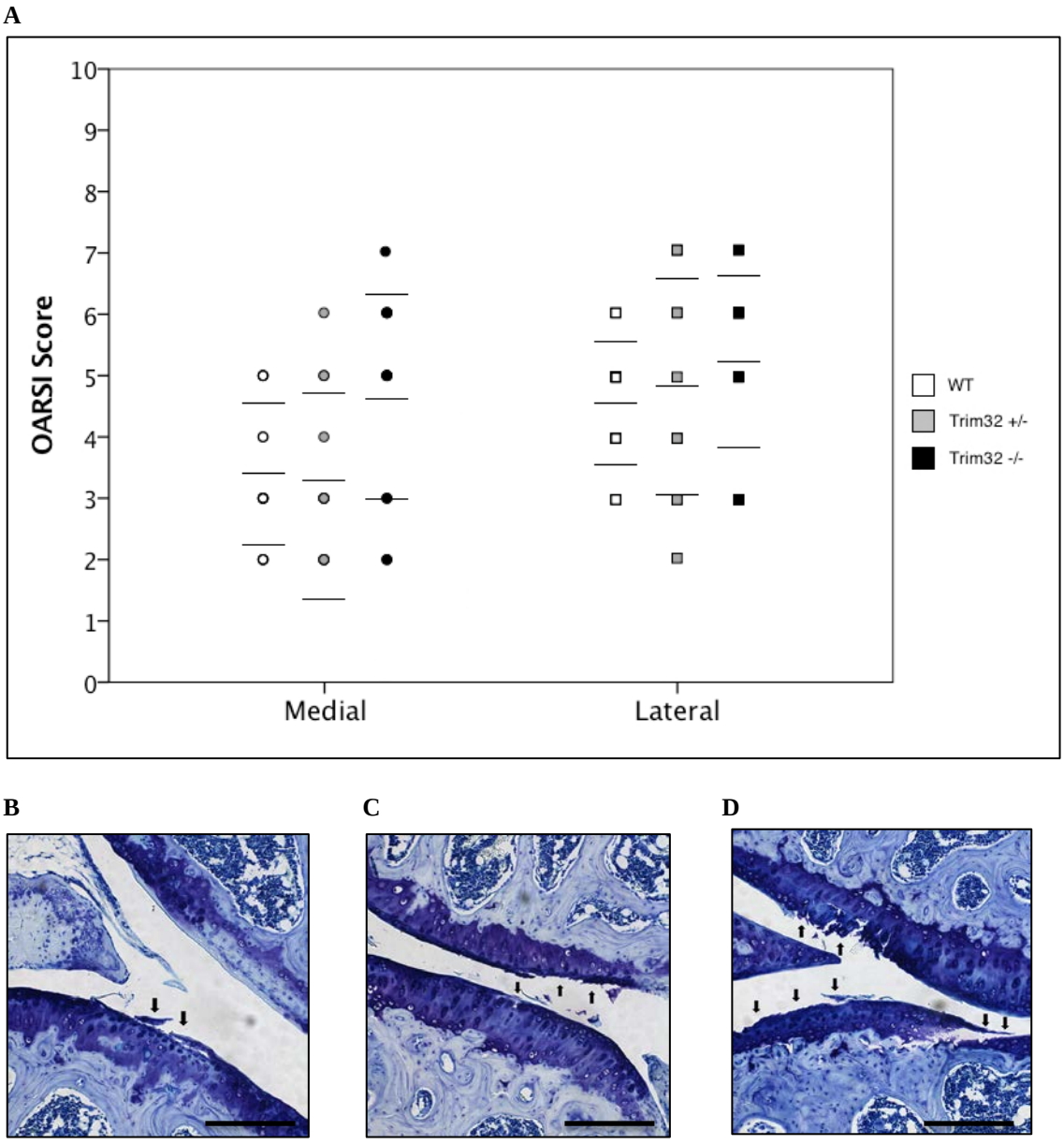

Figure 5.5 – Age-related knee osteoarthritis in wild-type (WT), *Trim32*$^{+/-}$ (HET), and *Trim32*$^{-/-}$ (KO) mice: medial and lateral knee compartment osteoarthritis scores; panel A shows summed osteoarthritis scores from the femoral and tibial joint surfaces in the medial and lateral compartments of the knee joints from wild type (WT, n = 12), heterozygous (*Trim32*$^{+/-}$, n = 12), and knockout (*Trim32*$^{-/-}$, n = 13) mice aged to 10 months. Histological analysis of cartilage degradation in each compartment was performed using the OARSI scoring system. Absolute values are shown (lines represent mean ± SD). Statistical analysis between groups was performed by Kruskal Wallis test with post-hoc Dunn's tests, with statistical significance accepted at $p < 0.05$. For the medial compartment, Kruskal Wallis test $p = 0.06$ WT *vs* HET *vs* KO, and for the lateral compartment, Kruskal Wallis $p = 0.44$ WT *vs* HET *vs* KO. Panels B, C, and D show representative photomicrographs (sagittal sections) from the knee joints of WT, HET, and KO mice aged to 10 months, respectively. Arrows indicate cartilage lesions. OARSI scores (first score for femoral aspect, second score for tibial aspect for the photomicrographs are: (B) 0, 2; (C) 2, 2; (D) 3, 4. Scale bars for panels C-D represent 300 μm.

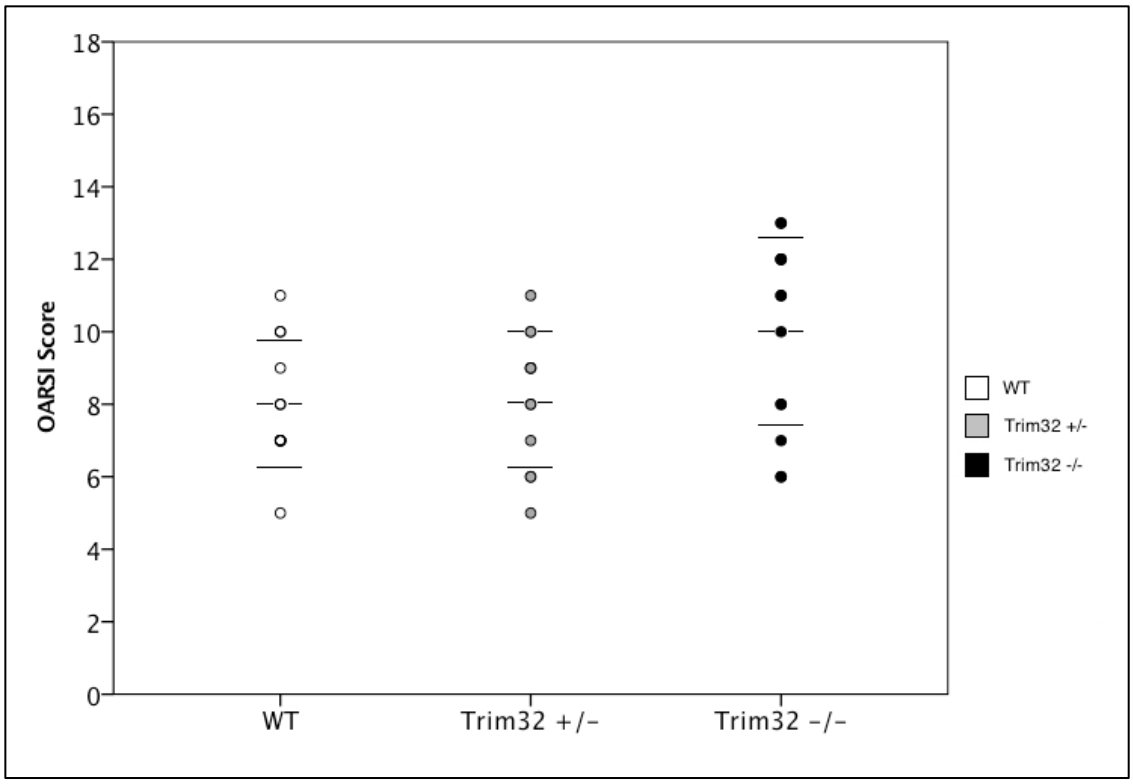

Figure 5.6 – Age-related knee osteoarthritis in wild-type (WT), *Trim32*$^{+/-}$ (HET), and *Trim32*$^{-/-}$ (KO) mice: total knee joint osteoarthritis scores; summed osteoarthritis scores from the medial and lateral compartments of knee joints from wild type (WT, n = 12), heterozygous (*Trim32*$^{+/-}$, n = 12), and knockout (*Trim32*$^{-/-}$, n = 13) mice aged to 10 months are shown. In all mice, knee joints were harvested for analysis at 10 months of age. Histological analysis of cartilage degradation in each knee joint was performed using the OARSI histological scoring system to grade severity of cartilage degradation in the medial and lateral compartments of both the tibial and femoral aspects of each knee joint. For each knee joint, scores for these four compartments were summed to produce a total joint OARSI score. Absolute values for the total knee joint OARSI score for each joint are shown (lines represent mean ± SD). Statistical analysis between groups was performed by Kruskal Wallis test with post-hoc Dunn's tests, with statistical significance accepted at $p < 0.05$. For total knee joint OARSI scores in aged mice, Kruskal Wallis test $p = 0.09$ WT *vs* HET *vs* KO.

5.4.6 Histological analysis of hip joints of *Trim32* knockout mice after ageing

To investigate any alteration in the susceptibility to spontaneous primary hip OA, grading of OA severity using the OARSI scoring system was performed for femoral head cartilage of hip joints harvested from WT, *Trim32*$^{+/-}$, and *Trim32*$^{-/-}$ mice after natural ageing to 10 months. Hip joints were harvested from the same mice used to analyse μCT subchondral bone parameters in aged WT, *Trim32*$^{+/-}$, and *Trim32*$^{-/-}$ mice (see section 5.4.3). No significant difference was observed in OARSI scores of femoral head cartilage between aged *Trim32*$^{+/-}$ mice and WT mice (Figure 5.7A). A non-significant increase in femoral head OA severity was observed for the aged *Trim32*$^{-/-}$ mice compared to the WT mice (Figure 5.7A). The hip joint OARSI scores upon ageing were 0.8 ± 0.5 in WT mice, 0.9 ± 0.5 in *Trim32*$^{+/-}$ mice, and 1.2 ± 0.6 in *Trim32*$^{-/-}$ mice (Kruskal Wallis p = 0.28 WT *vs* HET *vs* KO). Representative photomicrographs of histological sections from hip joints of WT, *Trim32*$^{+/-}$, and *Trim32*$^{-/-}$ mice aged to 10 months are shown in Figure 5.7 B-D.

The results of histological analysis of hip joints from aged WT, *Trim32*$^{+/-}$, and *Trim32*$^{-/-}$ mice therefore demonstrated no significant difference in hip cartilage degradation between WT and *Trim32* deficient mice.

A

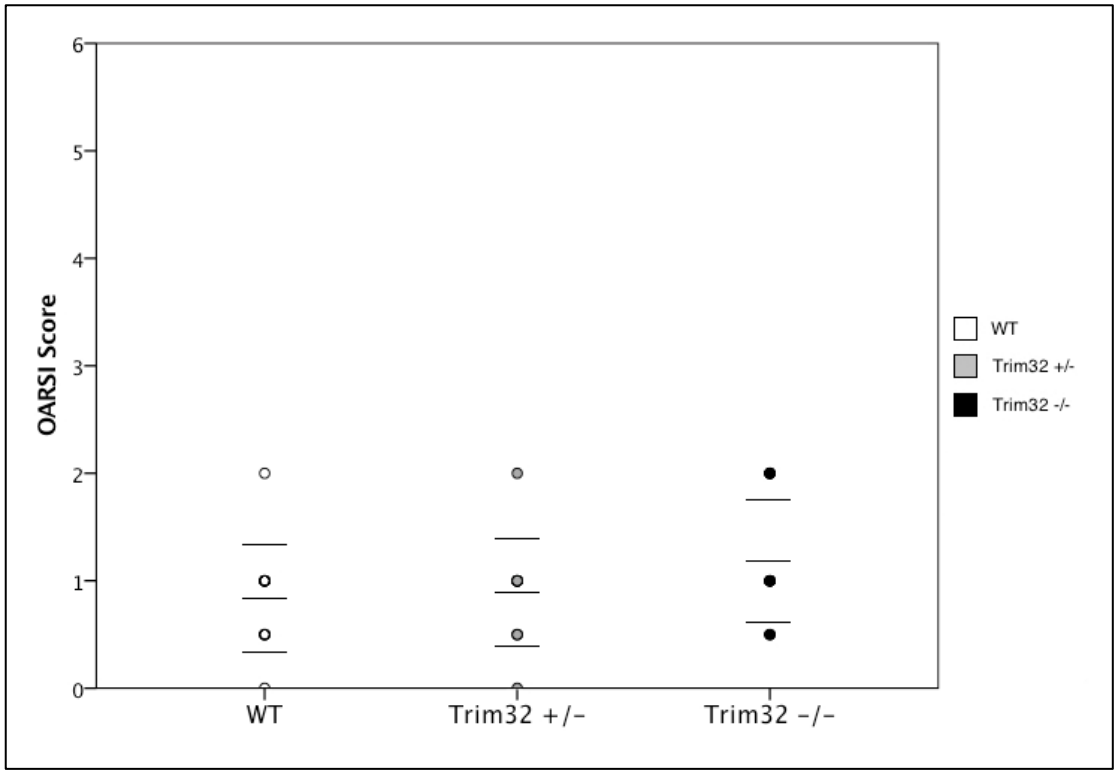

B **C** **D**

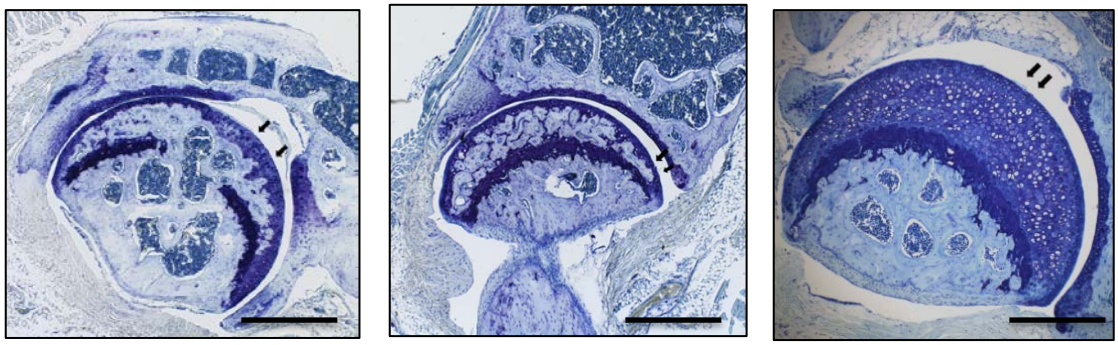

Figure 5.7 – Age-related hip osteoarthritis in wild-type (WT), *Trim32*$^{+/-}$ (HET), and *Trim32*$^{-/-}$ (KO) mice; panel A shows summed osteoarthritis scores from the femoral head of hip joints from wild type (WT, n = 12), heterozygous (*Trim32*$^{+/-}$, n = 12), and knockout (*Trim32*$^{-/-}$, n = 13) mice aged to 10 months. Histological analysis of cartilage degradation in each compartment was performed using the OARSI scoring system. Absolute values are shown (lines represent mean ± SD). Statistical analysis between groups was performed by Kruskal Wallis test with post-hoc Dunn's tests, with statistical significance accepted at $p < 0.05$. For hip joint OARSI scores in aged mice, Kruskal Wallis test $p = 0.28$ WT *vs* HET *vs* KO. Panels B, C, and D show representative photomicrographs (sagittal sections) from the femoral head from hip joints of WT, HET, and KO mice aged to 10 months, respectively. Arrows indicate cartilage lesions. OARSI scores for femoral head cartilage in photomicrographs are: (B) 0.5; (C) 1; (D) 2. Scale bars for panels A and B represent 300 μm; scale bar in panel C represent 200 μm.

5.4.7 Meta-analysis of hip and knee joint histological changes in *Trim32* knockout mice after DMM and ageing

A meta-analysis was performed to collate the findings from histological analyses of OA severity in *Trim32* KO mice compared to WT mice following DMM surgery and ageing. This would enable an interpretation of the overall effect of *Trim32* deficiency on OA severity from the murine disease models. A summary table and forest plot of the results of the meta-analysis is shown in Figure 5.8. The overall direction of effect suggests a protective role for TRIM32 in maintenance of cartilage integrity, as shown in the forest plot. The detected protective effect of TRIM32 in maintenance of cartilage integrity was greater in the knee joint compared to the hip joint. This difference is reflected by greater mean differences in OARSI scores between WT and *Trim32*$^{-/-}$ mice of 1.92 [95% CI: 0.21 – 3.63] for aged knee joints, and 4.72 [95% CI: 3.21 – 6.23] for DMM operated knee joints, compared to a mean difference of 0.36 [95% CI: -0.07 – 0.79] for aged hip joints (Figure 5.8).

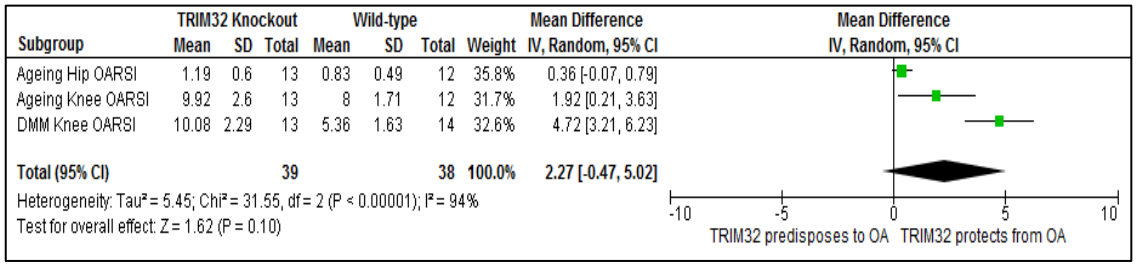

Figure 5.8 – Meta-analysis of hip and knee joint osteoarthritis scores in wild-type (WT) and *Trim32*$^{-/-}$ (KO) mice; results of histological knee cartilage degradation (OARSI) scores following the DMM surgery, and both hip and knee cartilage degradation (OARSI) scores following ageing to 10 months, of both WT and *Trim32* KO mice were collated in a meta-analysis. Meta-analysis of OARSI scores was performed using Review Manager Version 5.3.5 software (The Cochrane Collaboration, Copenhagen). Mean scores with standard deviations (SD) are shown, along with 95% confidence intervals (95% CI).

5.4.8 Nociception analysis of *Trim32* knockout mice after DMM

Chronic joint pain is the predominant clinical symptom associated with OA. To investigate whether any alteration in the susceptibility to OA in *Trim32* KO mice was associated with the development of chronic pain as a behavioural sequelae, nociception testing was performed in WT and *Trim32*$^{-/-}$ mice following DMM surgery. Nociception was assessed by measuring hind limb withdrawal thresholds following application of von Frey filaments of increasing bending strength to the paw of the unoperated and operated hind limbs of WT and *Trim32*$^{-/-}$ mice following DMM surgery.

There was no significant difference in the limb withdrawal thresholds in the contralateral unoperated (control) limb of *Trim32*$^{-/-}$ mice and WT mice after DMM surgery, as shown in Figure 5.9. The limb withdrawal thresholds in unoperated limbs were (mean ± SD) 6.8 ± 1 g for WT mice and 6.9 ± 1 g for *Trim32*$^{-/-}$ mice (Shapiro-Wilk tests p = 0.001 WT, p = 0.001 KO; Mann-Whitney *U* test p = 0.89 WT *vs* KO). However, the limb withdrawal thresholds in operated (DMM surgery) limbs were significantly lower in *Trim32*$^{-/-}$ mice compared to WT mice (Figure 5.9). The limb withdrawal thresholds for operated limbs were 0.8 ± 0.3 g for WT mice, compared to 0.2 ± 0.1 g for *Trim32*$^{-/-}$ mice (Shapiro-Wilk tests p = 0.001 WT, p = 0.0003 KO; Mann-Whitney *U* test p = 0.0008 WT *vs* KO).

The reduced limb withdrawal thresholds in the operated limbs of *Trim32*$^{-/-}$ mice compared to WT mice may indicate the development of increased mechanical allodynia in *Trim32* KO mice following DMM surgery (Figure 5.9). This is associated with increased OARSI scores observed in the knee joints of *Trim32* KO mice compared to WT mice following DMM surgery and may reflect the development of more severe joint degeneration in *Trim32* KO mice.

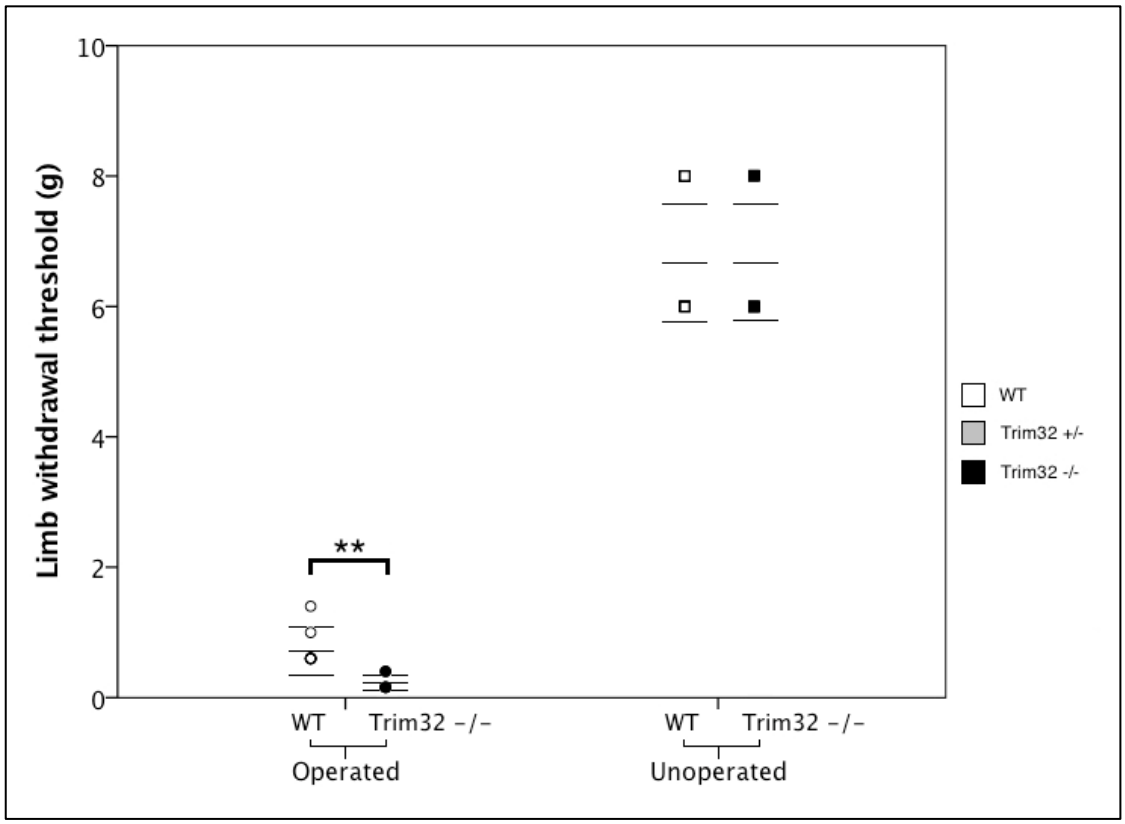

Figure 5.9 – Hind limb pain thresholds following DMM surgery in wild-type (WT) and *Trim32*$^{-/-}$ (KO) mice; nociception thresholds were assessed in WT and *Trim32*$^{-/-}$ mice eight weeks after undergoing DMM knee surgery. Nociception thresholds were measured by the application of range of von Frey filaments to the hind limbs to assess hind limb hypersensitivity following the DMM surgery. Von Frey filaments were applied to both the operated and unoperated hind limb of WT (n = 7) and *Trim32*$^{-/-}$ (n = 8) mice, and limb withdrawal thresholds measured. Absolute values are shown (lines represent mean ± SD). Statistical analysis of withdrawal thresholds for each limb between WT and KO mice groups was performed by Mann-Whitney *U* tests, with statistical significance accepted at $p < 0.05$. For operated groups, Mann-Whitney *U* test p = **0.0008 WT *vs* KO; for unoperated groups, Mann-Whitney *U* test p = 0.89 WT *vs* KO.

5.4.9 Grip strength analysis of *Trim32* knockout mice

Trim32 KO mice have previously been reported to develop a mild skeletal myopathy after five months of age (295). In previous experiments to determine any alteration in susceptibility to knee OA following DMM surgery in *Trim32* KO mice, WT and *Trim32* deficient mice were analysed for changes in subchondral bone parameters by microCT and for histological cartilage degradation at 16 weeks of age (see section 5.4.1 and section 5.4.4). To investigate any variation in muscle strength that may have also contributed to the development of OA in *Trim32* deficient mice, forelimb grip strength was also measured in both WT and *Trim32* KO mice following DMM surgery, at 16 weeks of age (see section 2.3.8). Forelimb grip strength testing was performed as in indication of general skeletal muscle strength.

Grip strength was significantly lower in *Trim32*$^{-/-}$ mice compared to WT mice (Figure 5.10). The limiting grip strength (mean ± SD) was 78.9 ± 8 g in WT mice compared to 69.1 ± 7 g in *Trim32*$^{-/-}$ mice, representing a mean 12% reduction in mean grip strength in *Trim32* KO mice ($p = 0.03$, WT *vs* KO). These results indicate the development of a mild skeletal myopathy in *Trim32* KO mice and that skeletal muscle strength is lower in *Trim32* KO mice compared to WT mice by 16 weeks of age; this is the time point at which microCT and histological assessments were performed in previous experiments examining the susceptibility to knee OA following DMM surgery in *Trim32* KO mice (see section 5.4.1 and section 5.4.4).

Mild skeletal myopathy in *Trim32* KO mice may, therefore, also contribute to the development of increased cartilage degradation and subchondral bone changes after DMM in the *Trim32* KO mice (Figure 5.10). Grip strength testing was not performed in mice with *Trim32* haploinsufficiency, or in aged mice with *Trim32* deficiency.

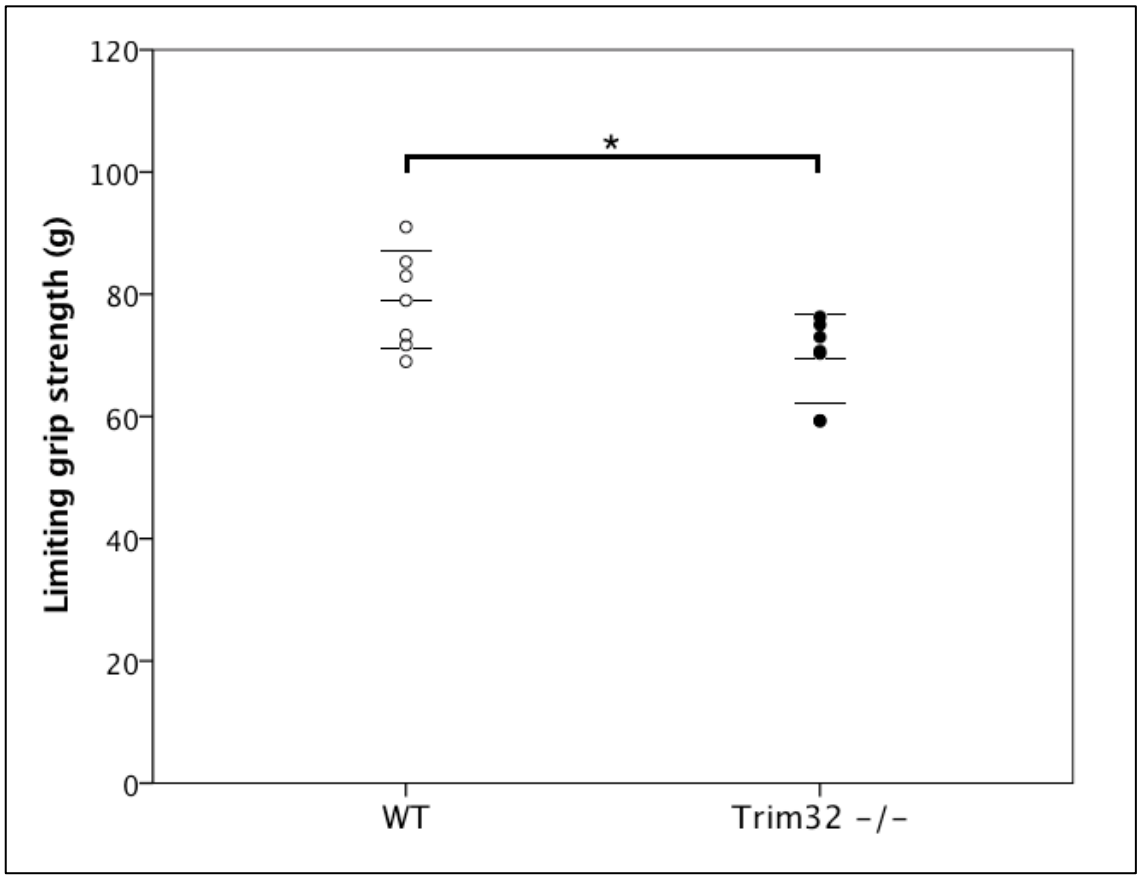

Figure 5.10 – Grip strength testing following DMM surgery in wild-type (WT) and *Trim32*$^{-/-}$ (KO) mice; forelimb grip strength was assessed, as an indicator of skeletal muscle strength, by measuring the ability of mice to maintain grip on a grip strength meter. Forelimb grip strength testing was performed to investigate whether or not any skeletal myopathy that may develop in *Trim32*$^{-/-}$ mice could confound any changes identified by histological and microCT analysis of knee joint following the DMM procedure. DMM surgery was performed in WT (n = 7) and *Trim32*$^{-/-}$ (n = 8) mice at eight weeks of age, and forelimb *g*rip strength testing was measured at eight weeks following DMM surgery (the same time point at which histological and microCT assessments of knee joints were performed). Increased resistance weight was applied through the grip strength meter and the limiting grip strength at which forelimb disengagement from the meter occurred was recorded. Absolute values are shown (lines represent mean ± SD). Statistical analysis of forelimb limiting grip strengths between WT and KO mice groups was performed by two-tailed Student's T-test, with statistical significance accepted at $p < 0.05$: *$p = 0.03$ compared to WT mice.

5.5 Discussion

The experiments described in this chapter aimed to investigate the effect of *Trim32* knockout on the development of OA *in vivo* utilising murine models of OA. The models studied were the DMM model and ageing model of OA, both performed in WT and *Trim32* KO mice.

The DMM model was performed to evaluate the effect of *Trim32* knockout on the development of accelerated degenerative OA following surgically induced joint instability. The results following DMM surgery in WT mice and mice with *Trim32* deficiency have provided several insights into the utilisation of the DMM surgical procedure to model OA in mice, in addition to evaluating the effects of *Trim32* deficiency on the development of OA *in vivo*.

The DMM procedure was selected as it is the most validated model of surgically induced OA in mice. The ACLT model is another commonly used model of surgically induced OA in mice, but it is associated with acute severe knee instability that does not usually occur in primary human OA (349). There is a risk of inadvertently damaging the cruciate ligaments of the knee and other structures during the DMM procedure (484). Particular care was taken during the DMM surgical procedures in this study to only transect the MMTL and to avoid damaging the cruciate ligaments. By avoiding damage to further structures, the procedure induces a localised post-traumatic arthritis rather than gross instability in association with an inflammatory arthritis (349). Indeed, the cruciate ligaments were intact on subsequent histological sections in this study, and no wound complications or further postoperative morbidity occurred in any experimental animals.

The majority of studies utilising the DMM surgical procedure to induce OA in mice have performed sham surgery as a control procedure. The sham surgery can either be performed in the hind limb contralateral to that in which the DMM surgery is performed (485-487), or can be performed in a further control group of mice (465, 488, 489). Recent studies have demonstrated that no significant histological changes occur in the contralateral unoperated knee in response to the DMM procedure in mice (484, 490).

Sham surgery was therefore not performed for DMM experiments, and the contralateral knee was used as a control based on the absence of significant differences demonstrated in previous studies, and to safeguard animal welfare.

The majority of studies assessing the effects of DMM surgery in KO mice have also used male mice. It has previously been reported that the development of OA is more severe in male than female mice following DMM surgery (376). This gender effect was particularly marked in mice of the 129SvEv strain, which are also particularly susceptible to cartilage degradation following surgically induced instability. The severity of histological changes of knee joint cartilage following DMM surgery has been evaluated further in different strains of experimental mice; C57Bl/6 mice demonstrate a moderate response to DMM surgery (349). Furthermore, several studies, including those examining transgenic mice on C57Bl/6 background, have demonstrated no significant difference between male and female mice in response to DMM surgery (489, 491). Therefore, as the 9q33.1 locus at which *TRIM32* resides was identified as associated with OA specifically in female patients in the arcOGEN study, the effect of knockout of *Trim32* was examined in female mice only. The relatively moderate response of performing DMM surgery on mice of C57Bl/6 background strain permitted the identification of either a decrease or increase in OA severity in *Trim32* deficient mice, in whom the direction of effect of TRIM32 deficiency on the development of OA was not previously known. The number of mice included in the WT, *Trim32*$^{+/-}$, and *Trim32*$^{-/-}$ groups in the DMM experiments provided reasonable power (80%) to detect a significant difference in the histological total knee joint cartilage degradation scores (see section 2.3.3).

The femoral aspect of the knee joint is less commonly assessed in murine studies utilising the DMM procedure, and descriptions of subchondral bone changes of the distal femur following DMM surgery are particularly limited. Analysis of subchondral bone changes following DMM surgery in the WT and *Trim32* KO mice demonstrated that subchondral bone changes may occur throughout both the proximal tibia and distal femur at the knee joint, indicating that changes may occur throughout the knee joint following the DMM procedure in which the surgical lesion is induced on the medial

meniscus overlying the medial tibial plateau (Table 5.1 and Table 5.2; Figure 5.1 and Figure 5.2).

To assess the development of chronic pain following DMM surgery in the *Trim32* KO mice, von Frey filament testing was performed to measure hypersensitivity to mechanical stimulation of the hind limbs. The demonstration of similar limb withdrawal thresholds in the unoperated limbs, despite the development of cartilage lesions in the operated limb, further supports the use of the contralateral limb as an internal control in experiments using the DMM procedure (Figure 5.9). Few studies have examined nociception and pain behaviour following DMM surgery in mice. The von Frey testing is particularly suitable for assessing the development of chronic pain following DMM surgery as mechanical allodynia can be detected as soon as eight weeks after DMM, which correlates with the interval required to reliably detect histological and histomorphometric changes following DMM surgery (489). Other measures of chronic pain such as gait pattern and activity level require greater intervals postoperatively for changes to become reliably detectable between operated and unoperated hind limbs (492). These studies in mice with targeted deletion of *Trim32* demonstrate that increased cartilage degradation may be associated with an increase in chronic pain in the affected limb on assessing mechanical allodynia (Figure 5.9). It is possible that a sensory or neurological deficit may also contribute to the development of OA, though this cannot be determined from these results as the significant difference was only demonstrated after DMM surgery and was not observed in the unoperated contralateral hind limb between WT and *Trim32* KO mice. No gross alterations in gait or activity level were observed; these usually develop later following DMM surgery, and would require formal assessment to be addressed accurately (492). That significantly different levels of chronic pain may be detected using von Frey filament testing after DMM surgery provides some validation for this modality for the evaluation of potential novel disease modifying therapies for OA.

Grip strength in *Trim32* KO mice has previously been reported as reduced by 17% by age 5-9 months compared to WT littermates, but mice with *Trim32* haploinsufficiency exhibit preserved skeletal muscle strength (295). In previous studies,

Trim32 deficient mice also developed increased weight after several months of age compared to WT littermates, but no further developmental abnormalities have been reported (295). The developmental phenotype of *Trim32* deficient mice was not assessed in the experiments in this thesis, although the weight and grip strength of WT and *Trim32* deficient mice were measured during the DMM experiments, and the weight of mice was measured during the ageing experiments, to assess for any confounding effects on joint histological changes, bone histomorphometry, and nociception results. In the experiments described in this chapter, forelimb grip strength was reduced by 12% in the *Trim32* KO mice compared to WT mice when measured following the DMM procedure at age 16 weeks, indicating development of a mild skeletal myopathy (Figure 5.10). In the experiments investigating the development of OA in WT and *Trim32* deficient mice in this chapter, grip strength was only evaluated in mice following the DMM procedure, and not upon ageing. The differences in the identified severity of mild skeletal myopathy in these experiments and previous studies reflects the relative ages at which skeletal muscle strength was measured in previous studies and in these experiments (295). The mild skeletal myopathy in *Trim32* KO mice may have a confounding effect on the development of increased cartilage degradation and subchondral bone changes after DMM in the *Trim32* KO mice. However, *Trim32*$^{+/-}$ mice, which have preserved skeletal muscle strength, also demonstrated significantly increased total knee joint OA scores in response to DMM surgery, suggesting that increased cartilage degeneration may occur in *Trim32* deficient mice following the DMM procedure, independent of any alteration in skeletal muscle strength (Figure 5.4). To better understand whether or not development of mild skeletal myopathy significantly contributed to the development of subchondral bone and cartilage changes in the *Trim32* KO mice after the DMM procedure would require performing grip strength testing, microCT analysis of subchondral bone, and histological analysis of cartilage in WT and *Trim32* KO mice at multiple time points following the DMM procedure and upon ageing, and could be addressed in future studies. It is a limitation of the experiments investigating the development of OA in *Trim32* deficient mice following the DMM procedure described in this chapter that further time points for analysis of subchondral bone, cartilage, nociception, and grip strength were not performed following the DMM procedure.

Analysis of WT and *Trim32* deficient mice at only one time point following DMM surgery also limits interpretation of the histological changes occurring in the joint after DMM surgery. Analysis of several time points may permit more detailed analysis of whether changes occur first in the cartilage, subchondral bone or synovium, and the subsequent sequence of involvement, and progression of, degenerative or inflammatory changes in other joint tissues (374, 493). Nociception testing was also performed at only a single time point (eight weeks) following DMM surgery in female WT and *Trim32* KO mice. Assessment of mechanical allodynia at multiple time points following DMM surgery may better inform the understanding of pathways involved in generation of mechanical allodynia during lesion development (489). Mechanical allodynia was also only measured in female WT and *Trim32* KO C57Bl/6 mice. Caution is required in interpreting the findings of increased mechanical allodynia in the operated hind limb of female *Trim32* KO mice compared to WT mice following DMM surgery, as there is limited published data regarding the time course of development of mechanical allodynia in female mice following DMM surgery, different mouse strains display variability between the development of mechanical allodynia in the ipsilateral operated hind limb and the contralateral unoperated hind limb, and because variability exists between male and female mice in the development of pain-relevant parameters, including mechanical allodynia (Figure 5.9) (489, 494, 495). Further pain-relevant parameters that could be assessed to provide a more comprehensive analysis of the development of pain in mice following DMM include thermal allodynia, locomotor activity, gait analysis, and response to analgesia (489, 496, 497).

Another potential confounding factor on the development of OA in *Trim32* KO mice is their increased weight after several months of age compared to WT littermates (295). At the time of analysis of joint histology and histomorphometry following DMM surgery (aged 16 weeks), *Trim32* KO mice were non-significantly heavier than WT littermates in this study. Further evaluation by GLM analysis supported an absence of a confounding effect of weight on histological grade of OA following DMM surgery in *Trim32* KO mice (see section 5.4.4). The aged mice were significantly heavier but there was no significant covariate effect on GLM analysis (see section 5.4.5). This suggests that increased cartilage degradation in *Trim32* KO mice was not dependent on their

increased weight. Previous studies have also demonstrated that obesity itself is not directly correlated with increased susceptibility to OA in mice (498). Leptin-deficient and leptin-receptor deficient mice both develop extreme obesity without an increased incidence of knee OA (364). Furthermore, increased joint loading is not sufficient to cause increased incidence of knee OA with obesity in C57Bl/6 mice (363). However, adipose tissue is a significant source of pro-inflammatory and anti-inflammatory cytokines, which may promote catabolic processes to predispose to OA in the presence of obesity (499-501). Mice that develop obesity induced by a very high-fat diet do develop OA and systemic inflammation in proportion to body fat, further supporting a predominant mechanism by which obesity induced by exposure to a high fat diet and a pro-inflammatory state predisposes to OA, rather than by increased mechanical loading (363). Furthermore, following surgically induced knee OA, C57Bl/6 mice fed a short-term high fat diet develop increased OA in the absence of weight gain, compared to mice fed a lean diet (502). Diet was consistent for the *Trim32* KO and WT mice throughout this study. Circulating adipokines levels were not assayed in *Trim32* KO mice in this study, but this could be insightful if further studies indicate the involvement of related molecular pathways.

Following DMM surgery in *Trim32* KO mice, increased tibial subchondral bone density and trabecular number were observed, compared to WT mice (Figure 5.1). Similar, non-significant, changes were identified in the femoral subchondral bone in the *Trim32* KO mice. Subchondral bone sclerosis was associated with increased cartilage degeneration in both the medial and lateral aspects of the operated knee joint in *Trim32* KO mice compared to WT mice (Figure 5.3). This pattern of cartilage degeneration and subchondral bone changes, with the more severe cartilage degeneration in the medial than lateral compartment, and the tibial subchondral bone altered to a greater extent than the femoral subchondral bone, is consistent with findings from studies of other KO mice predisposed to OA following DMM surgery (484, 503, 504). The increased severity of cartilage degeneration was exaggerated in *Trim32*$^{-/-}$ mice compared to *Trim32*$^{+/-}$ mice (Figure 5.4). The development of increased cartilage degeneration in both *Trim32*$^{-/-}$ and *Trim32*$^{+/-}$ mice, but significantly altered subchondral bone changes only in *Trim32*$^{-/-}$ mice may indicate that cartilage lesions were the primary event following the DMM

surgery, with subchondral bone changes occurring secondarily. To definitively establish the temporality of changes in cartilage and subchondral bone in *Trim32* KO mice would, however, require evaluation of subchondral bone changes and histological changes at several time intervals following DMM surgery.

There are limitations to the animal models of OA used in these experiments. In evaluating the *in vivo* effect of targeted gene deletion on the development of OA using animal disease models, it is beneficial to assess more than one model as no single model can fully replicate the pathological processes leading to OA in humans. The DMM and the ageing models of OA in mice were selected to investigate the effect of *Trim32* deficiency on the development of OA *in vivo*. Findings from variant screening of *TRIM32* in patients with hip OA implicated genetic variation in *TRIM32* as associated with the development of hip OA in humans (see section 3.5), and *TRIM32* is the most biologically plausible candidate gene for OA risk at the 9q33.1 locus (see section 1.3.2.2). The DMM model induces the accelerated development of knee OA and represents a secondary post-traumatic type of OA. Performing DMM surgery in mice aged 8 weeks with subsequent knee joint analysis at age 16 weeks also permitted assessment of severity of OA before the development of other significant phenotypes that occur upon ageing in *Trim32* deficient mice, such as increased weight and skeletal myopathy (295). However, caution needs to be applied in translating results from the DMM model of knee OA in the study of genetic association with hip OA in humans.

The DMM model of knee OA was selected, as it is the most validated model of accelerated OA in mice. Accelerated models of hip OA have been reported in larger animals such as dogs, rabbits, rats, and sheep, including intra-articular injection of MIA, NGF, papain, and sodium urate, and surgical models including debridement of femoral head cartilage, femoral neck osteotomy, gluteal muscle excision, and induction of developmental dislocation of the hip or femoroacetabular impingement (505-514). However, surgically- and chemically-induced models of hip OA have not been reported in mice, likely due to the high reproducibility of the DMM procedure, and because surgical and intra-articular injection procedure of the hip joint in mice are technically challenging with significant risk of complications (505).

The expression, or effect, of genetic variants on the development of OA may be specific for certain anatomical sites (198). However, genes implicated in the development of either hip or knee OA in humans, have subsequently been demonstrated to predispose to both hip and knee OA in studies of KO mice (515, 516). This indicates that there may be some redundancy and common aetiopathological mechanisms through which genetic variants predispose to hip and knee OA, in keeping with shared risk factors associated with their development (18). A combination of examining the development of hip and knee OA in aged *Trim32* deficient mice, and the development of knee OA following DMM surgery can therefore provide initial investigation of the effect of Trim32 on the development of OA *in vivo*. Ageing of *Trim32* KO mice demonstrated a more subtle phenotype than findings from the DMM studies of *Trim32* KO mice. Aged *Trim32* KO mice showed significantly increased knee cartilage degradation, and non-significantly increased hip cartilage degradation, compared to WT littermates. These more subtle findings in aged *Trim32* KO are consistent with the results following DMM surgery, but may represent the mechanism of action and overall effect in humans more closely than results from the DMM model.

Ageing-related OA and destabilisation-mediated OA develop by different mechanisms. Destabilisation-mediated OA may represent a form of post-traumatic OA. Pro-inflammatory cytokines are elevated following joint injury. In particular, intra-articular IL1, rather than TNFα, is an important mediator of cartilage degeneration and synovitis following acute joint injury (517). MMPs, including MMP1, MMP3, and MMP13, play a key role in IL1-driven cartilage degeneration and cartilage GAG loss, and ADAMTS4 is a key mediator of aggrecanolysis in human articular cartilage (518). In contrast, in ageing-related OA, several cytokines are upregulated including IL1, IL6, and monocyte chemoattractant protein-1 (519). These cytokines are also associated with a senescence phenotype, and chondrocytes in ageing-related OA exhibit several features that are characteristic of senescent cells, including increased $p16^{INK4A}$ expression and reduced expression of the microRNA miR-24, which may predispose aged chondrocytes to undergo senescence during subsequent proliferation after injury (520-522).

Examining the development of OA after ageing of *Trim32* KO mice was performed to model spontaneous primary OA in humans. Experimental mice were aged to 10 months, as this is the youngest age at which mice of C57Bl/6 background develop spontaneous degenerative changes in the knee joint that may be detected by histology and histomorphometry. The degenerative changes that develop by 10 months in these mice is mild, and may explain the lack of significance of the increased knee joint OARSI scores in the aged *Trim32* deficient mice compared to WT mice (Figure 5.6). The non-significant increased severity of OARSI scores in *Trim32*$^{-/-}$ mice was associated with significantly increased sclerosis of the medial subchondral bone plates and femoral epiphyseal trabecular bone (Table 5.3). The number of mice included in the aged WT, *Trim32*$^{+/-}$, and *Trim32*$^{-/-}$ groups provided 70% power to detect a significant difference in the histological total knee joint cartilage degradation scores (see section 2.3.4). It is therefore possible that with increased numbers of mice in each group, the trends in cartilage degradation scores, like the subchondral bone changes, might become statistically significant. The trends of increased severity of cartilage degradation and subchondral bone sclerosis of the knee joint in aged *Trim32* KO mice are similar to the results following the DMM surgery. However, the trends of increased knee cartilage degradation scores in the aged *Trim32* KO mice compared to WT mice are not conclusive regarding the susceptibility of *Trim32* deficient mice to spontaneous OA of the knee joint, as the trends in the aged mice were not statistically significant.

The medial trabecular thickness of the subchondral bone was also significantly increased in the control knees of *Trim32* KO mice assessed in the DMM experiments (Table 5.1 and Table 5.2). The combination of altered medial subchondral bone and medial cartilage changes may indicate spontaneous abnormality of the osteochondral unit. Elevated subchondral bone remodelling is associated with progression of OA (523). These findings may, therefore, also represent a distinct subchondral bone phenotype. Subchondral bone is initially reduced in thickness in early OA due to attenuation of late phase tissue mineralisation coupled with increased bone turnover (524). In advanced OA, bone remodelling is reduced and bone deposition is increased, leading to increased density and thickness of the subchondral bone plate and the subchondral trabecular bone (525). Subchondral bone is composed of osteocytes,

osteoblasts, and osteoclasts, whose function is abnormal in OA. Osteoblasts in particular develop an abnormal phenotype in advanced OA with increased secretion of IL6, IL8, leptin, PGE_2, and Col I (526). As the medial subchondral bone was significantly increased in thickness in control knees of *Trim32* KO mice in the DMM experiments, and in knees from aged *Trim32* KO mice, these findings may imply an abnormality of osteoblast, osteoclast or osteocyte function. This could be primary in nature or in response to the associated increased weight or skeletal myopathy of *Trim32* deficient mice, or develop with cartilage changes. Although *Trim32* KO mice develop phenotypically indistinguishable from their wild type littermates, weight was not a significant confounding factor in the GLM analysis, and no gross skeletal abnormality was evident (appendix 7.3.3), it is a limitation of the experiments described in this thesis that the bone and synovium were not examined in more detail in the *Trim32* deficient mice (295). It is especially important to determine if a primary bone phenotype exists in *Trim32* KO mice as subchondral bone changes can precede the development of articular cartilage degeneration in OA (527). It is also a limitation that further time points were not examined in the DMM or ageing studies of *Trim32* KO mice, which would help determine the chronology of changes in the subchondral bone and cartilage. Further studies are required to examine the effect of *Trim32* deficiency on osteoblast, osteoclast, and osteocyte function, and also any effect in the synovium, and whether these, or effects in the cartilage or muscle, are the predominant mechanisms leading to an increased susceptibility to OA in *Trim32* KO mice.

The hip joint was also analysed in aged *Trim32* KO mice, as the 9q33.1 locus at which *TRIM32* resides was associated with hip OA in the arcOGEN study (229). The hip joint is infrequently studied in murine studies of OA, and no validated surgical model exists for hip OA, likely due to the high reproducibility of the DMM procedure and because the hip joint is more technically challenging to access surgically without complications, especially in small rodents. The hip joint was only analysed in aged WT and *Trim32* deficient mice, and was not examined following the DMM surgical procedure; analysis of the hip joint by histology and bone histomorphometry following the DMM surgical procedure has not been previously reported or validated, and analysis of the hip joint after ageing most likely represented the pathology in human hip OA

more closely. Significant alterations of subchondral bone were not identified on analysis of the femoral head of the hip joint in aged *Trim32* KO mice (Table 5.4). Altered subchondral bone parameters of the femoral head in aged *Trim32* KO mice may not have been detected due to the variable development and ossification of the femoral head in mice up to an advanced age (528). This should not preclude the hip joint in evaluation of OA in murine studies, but does indicate that more extensive ageing may be required to detect more consistent alterations of subchondral bone. A non-significant increase in hip OARSI scores was observed in the *Trim32*$^{-/-}$ mice compared to WT mice (Figure 5.7). This suggests that the effect of TRIM32 on the development of OA may not be limited to the knee joint and is consistent with the findings from DMM and ageing studies examining the knee joint in *Trim32* KO mice.

In summary, the results of surgically induced and ageing induced OA in *Trim32* KO mice indicate that TRIM32 has a protective role against the development of OA *in vivo*. An increased susceptibility to OA in mice with *Trim32* deficiency also provides support that *TRIM32* might be the candidate gene at the 9q33.1 locus conferring increased susceptibility to OA in humans.

Chapter 6

Discussion

6.1 Discussion

Primary OA is a late-onset degenerative condition of synovial joints and is the major cause of pain and disability in older persons. OA represents a significant disease burden, its management has significant economic implications, and it is therefore a focus of research. Current treatments are inadequate; no disease-modifying therapies exist to manage the condition, which is therefore treated by analgesic medications until severe OA necessitates total joint replacement. OA has an established hereditary component, though the exact genetic variation and molecular mechanisms predisposing to the disease are incompletely understood. The arcOGEN study, the most powerful genome-wide association study yet to investigate OA, identified the 9q33.1 locus to be significantly associated with hip OA in females (229). *TRIM32* lies within the 9q33.1 susceptibility locus and may have biological relevance to OA; it encodes a protein with E3 ubiquitin ligase activity. This thesis therefore had several aims: to investigate the genetic variation of *TRIM32* to identify novel or rare variants in *TRIM32* that are associated with OA of the hip in females; to examine the expression of *TRIM32* in articular tissue and to determine whether *TRIM32* expression is altered in female patients with OA of the hip; to investigate whether *Trim32* affects the response of chondrocytes to anabolic and catabolic stimuli, and whether or not *Trim32* affects the integrity of articular cartilage *in vitro;* and to examine the effect of *Trim32* knockout on the development of OA *in vivo* in response to surgically induced joint instability and upon ageing.

In chapter 3, Sanger sequencing of the proximal promoter, 5'UTR, both exons, and 3'UTR of *TRIM32* in the youngest 500 female patients with hip OA from the arcOGEN cohort detected nine variants (Figure 3.1). Two of these variants, rs811457 and rs3019, were detected in female patients with hip OA at disproportionate frequency compared to the control population, and may affect the expression of *Trim32* (Table 3.1). Indeed, it is now established that most variants that affect complex polygenic traits, such as OA, do so by regulating nearby gene expression (529, 530). The rs811457 and rs3019 variants were not in direct significant LD with the top hit SNP rs4836732 at this locus that was associated with female hip OA in the arcOGEN study (229). However,

further analysis of these two variants in larger cohorts of patients with OA, by imputation with population genome databases, by comparison with confirmed disease-free matched controls, and by conditional analysis with the rs4836732 and its immediately adjacent polymorphisms could further validate these findings. Investigating further forms of genetic variation at this locus could also be informative; DNA methylation analysis of *TRIM32* and the 9q33.1 locus in DNA isolated from peripheral blood cells and articular cartilage of the hip in both female patients with primary hip OA and controls matched for both age and gender could further inform the understanding of the genetic variation predisposing to hip OA at this locus. The cohort examined in these experiments (n = 500) was relatively low compared to the arcOGEN study that identified the 9q33.1 locus as associated with hip OA in female patients (229). The cohort examined in these experiments also only represented patients from European Caucasian populations. However, the youngest 500 female patients with primary hip OA from the arcOGEN study were selected for sequencing of *TRIM32* as disease-associated variants are most likely enriched in the youngest individuals affected by primary hip OA.

The rs811457 variant was under-represented in female patients with hip OA, while the rs3019 variant was over-represented in patients with hip OA, conferring increased risk for hip OA (Table 3.1). Correlation of the rs811457 and rs3019 variants with relevant endophenotypes including radiographic parameters of hip morphology could also indicate whether these variants confer altered risk for hip OA through altered development or geometry of the hip joint (254). Furthermore, analysis of the effect of these variants on chondrocyte function may inform understanding of associated pathological molecular mechanisms. The rs811457 variant may affect *TRIM32* expression and lies adjacent to the TFAP2A/TFAP2C transcription factor binding site (Figure 3.2); *TRIM32* expression in chondrocytes expressing this variant could be measured as could the ability of TFAP2A1/TFAP2C to bind the altered sequence in the proximal promoter of *TRIM32* be analysed by ChIP. The rs3019 variant in the 3'UTR may affect *TRIM32* expression by disrupting a binding site of miR-511, which targets *TRIM32* and is associated with joint inflammation (420, 423). It could be insightful to measure the expression of *TRIM32* and miR-511 in chondrocytes expressing the rs3019

variant. Examining the effect of these two variants on the expression of *TRIM32* and associated regulatory factors in chondrocytes may implicate a direct role in abnormal chondrocyte function and the OA disease process.

The 9q33.1 locus examined in the experiments described in this thesis was identified as an OA susceptibility locus in the arcOGEN study (229). GWAS have enabled the investigation of variability across the whole human genome in association with specific diseases and without prior hypothesis. The power of GWAS depends upon the sample size, significance threshold, the effect size of the causal SNPs, and the frequency of their alleles. GWAS and GWAS meta-analyses have identified several OA susceptibility genes, though the number of susceptibility loci identified for OA is relatively low compared to other complex trait diseases (Table 1.1 and Table 1.2). Heterogeneity of OA phenotypes and insufficient sample sizes have contributed to these limited results in GWAS in OA. The number of disease-associated susceptibility loci identified by a GWAS is a function of sample size. In GWAS investigating OA susceptibility, the sample sizes have been insufficient to identify as many susceptibility loci as generated from larger studies in disease such as myocardial infarction, Crohn's disease, breast cancer, and type 2 diabetes (531). The detection power of new variants by GWAS investigating OA could be enhanced by focusing on endophenotypes most relevant to particular types of OA (254). The detection power of causal variants is also enhanced by using control populations selected on the same criteria used to select disease cases (262). The identification of disease-associated variants by GWAS is also enhanced by reducing heterogeneity in the population of cases and controls. Another limitation of previous GWAS has been incomplete coverage provided by genotyping arrays, with limited coverage most relevant for rare genetic variants, some complex CNVs, and microsatellites (532).

The number of identified OA susceptibility loci is relatively low compared with other complex trait diseases. Strategies to improve the investigation of the genetic predisposition to OA include increasing the sample size of GWAS studies of OA, standardising the patient phenotypes, completing the genetic variation coverage using information from studies such as the 1000 genomes project, and examining genetic

variation more comprehensively through exome sequencing, epigenome-wide association studies, studying microsatellites and complex CNVs not previously examined by GWAS, and by gene-base analysis (255).

In chapter 4, altered expression of TRIM32 was identified in femoral head articular chondrocytes from female patients with primary OA of the hip, compared to age and gender-matched control patients without hip OA (Figure 4.4). These results are consistent with those from experiments, examining GAG release, as a marker of aggrecanolysis, in femoral head explants from *Trim32* KO mice; increased GAG release occurred in cartilage explants from *Trim32* KO mice compared to explants from WT mice (Figure 4.7). These results also support an association in which reduced *Trim32* expression may correlate with an OA phenotype. Although TRIM32 staining was identified in human hip and knee cartilage (Figure 4.1 and Figure 4.3) and significantly reduced expression of TRIM32 was identified by articular chondrocytes from patients with hip OA compared to control patients, these results should be reviewed with caution due to the low sample sizes (Figure 4.4A). In experiments assessing proteoglycan depletion in WT and *Trim32* deficient mice, GAG loss was measured using the DMMB dye-binding assay as a surrogate marker of aggrecanolysis. More detailed investigation of aggrecanolysis in cartilage explant cultures from WT and *Trim32* deficient mice could be achieved by Western blotting to identify ACAN fragments following ADAMTS-mediated aggrecanolysis using neoepitopes antibodies (402).

It was also demonstrated that chondrocytes deficient in *Trim32* expressed increased *Col10a1* following IL1α, increased *Col2a1* following OSM, and IGF1 stimulation, and reduced *Sox9* following IGF1 stimulation (Figures 4.10 to 4.13). Changes in expression of these genes have previously been associated with the associated with the development of OA (533, 534). Caution is required in the interpretation of the gene expression results as each experiment was performed in replicates of only three. The gene expression studies were performed in cells harvested from femoral head epiphyseal cartilage, which may comprise a heterogeneous population of cells including predominantly chondrocytes, but also osteoclasts and osteoblasts. It would also be interesting to further evaluate the effect of *Trim32*

deficiency on chondrocyte phenotype by examining the expression of chondrocyte phenotypic markers in *Trim32* deficient chondrocytes and cartilage explants in response to both physiological and pathological mechanical stimulation *in vitro*, particularly as *TRIM32* has been reported to concentrate in the retracting basal process that acts as a template for the formation of microtubules and primary cilia, which are important mechanosensors in articular chondrocytes (281, 302, 535). Although these results indicate altered chondrocyte phenotype and increased degradation of articular cartilage with deficiency of *Trim32*, the exact molecular pathways in which *TRIM32* is involved in chondrocyte and cartilage homeostasis are not known. *TRIM32*, similar to other E3 ubiquitin ligases, is implicated in a variety of molecular pathways and pathological processes due to its broad substrate specificity. Affinity purification mass spectrometry to identify interactors with TRIM32 in chondrocytes and articular cartilage could provide insights into the relevant molecular pathways in which *TRIM32* is involved in articular cartilage (440). Nevertheless, the results of these *in vitro* experiments of *TRIM32* expression in human and murine articular tissues may indicate a role for *TRIM32* in chondrocyte and cartilage homeostasis, warranting correlation of these findings with studies of the role of *TRIM32* on the development of OA *in vivo*.

The role of *Trim32* on the development of OA in mice following surgically induced knee joint instability (DMM procedure) or ageing was investigated in chapter 5. Following DMM, increased tibial epiphyseal trabecular volume and number developed in *Trim32* KO mice compared to WT mice (Figure 5.1). This was associated with more severe cartilage degeneration scores in the knee joints of *Trim32* deficient mice, compared to WT mice, after DMM (Figure 5.3 and Figure 5.4). This also correlated with more severe mechanical allodynia developing in *Trim32* KO mice compared to WT mice after the DMM procedure, though the *Trim32* deficient mice did also develop reduced muscle strength (Figure 5.9 and Figure 5.10). Upon ageing, *Trim32* deficient mice also developed increased subchondral bone changes, especially in the medial aspect of the knee joint, and not significantly changed degeneration of the cartilage of the knee joint (Table 5.3, Figure 5.5, and Figure 5.6). Meta-analysis of hip and knee joint cartilage degradation scores demonstrated increased cartilage degradation in *Trim32* KO mice compared to WT mice (Figure 5.8). The results of these *in vivo* studies

of the effect of *Trim32* on the development of OA support the findings from sequencing studies in chapter 3 and *in vitro* studies in chapter 4 that reduced *Trim32* expression may be associated with the development of OA.

There are limitations to the experiments investigating the development of OA in *Trim32* deficient mice. Following the DMM procedure only a single time point, rather than multiple time points, was used for the analysis of subchondral bone, cartilage, nociception, and grip strength following the DMM procedure. Analysis of several time points may permit more detailed analysis of whether changes occur first in the cartilage, subchondral bone, or synovium of the knee joint following the DMM procedure, and the subsequent sequence of progression of degenerative or inflammatory changes in other joint tissues (374, 493). Nociception following the DMM procedure was assessed by the development of mechanical allodynia, but other pain-relevant parameters could also be assessed such as thermal allodynia, locomotor activity, gait analysis, and response to analgesia (489, 496, 497). Grip strength testing to assess skeletal muscle strength was also only evaluated in WT and *Trim32* deficient mice following the DMM procedure, and not following ageing. Furthermore, examining the development of degenerative changes in the knee joints of aged WT and *Trim32* deficient mice may have produced more significant findings if increased numbers of mice were included in each group, as the number of mice in the ageing studies described in chapter 5 provided only 70% power to detect significant degenerative changes in the knee joint of experimental mice.

The mice examined in the surgically induced and ageing induced OA experiments had global deficiency of *Trim32*. After 5-9 months of age, *Trim32* KO mice have been shown in previous published studies, to develop a 17% reduction in skeletal muscle strength and increased weight compared to WT littermates (295). However, mice with *Trim32* haploinsufficiency have been reported in a previous study to have preserved skeletal muscle strength and similar weight, compared to WT littermates (295). In the experiments in this thesis, *Trim32* KO mice develop a mild proximal skeletal myopathy (12% reduction in grip strength; $p = 0.03$ WT *vs* KO; Figure 5.10) and non-significantly increased weight at 16 weeks of age, compared to WT littermates (WT 22.4 g, KO 23.7 g; $p = 0.09$ WT *vs* KO). The mild skeletal myopathy and increased

weight could potentially have confounded the results of the development of OA in *Trim32* deficient mice compared to WT mice. Although *Trim32* KO mice developed a non-significant increase in weight over the duration of the experiments investigating development of OA after DMM surgery in the experiments described in chapter 5, the increase in weight was shown by GLM analysis not to significantly contribute to the development of OA ($p = 0.56$). Furthermore, *Trim32*$^{+/-}$ mice, which have preserved skeletal muscle strength, also demonstrated significantly increased total knee joint OA scores in response to DMM surgery, suggesting that increased cartilage degradation may occur in *Trim32* deficient mice following the DMM procedure, independent of any alteration in skeletal muscle strength (Figure 5.4).

To validate these findings and overcome any confounding extra-articular effects of global *Trim32* deficiency, the surgically induced and ageing induced models of OA could be performed in mice with cartilage-specific knockout of *Trim32*, which could be generated using the LoxP Cre system specific for *Col2a1* (536, 537). In the experiments assessing histological and histomorphometric changes in the knee joint following DMM surgery in WT and *Trim32* deficient mice, the medial trabecular subchondral bone thickness was significantly increased in the control knee joints of *Trim32* KO mice compared to those from WT mice (Table 5.1 and Table 5.2). This may indicate a distinct subchondral bone phenotype in addition to effects on cartilage integrity, in the joints of *Trim32* deficient mice. Subchondral bone comprises osteocytes, osteoblasts, and osteoclasts, whose function is abnormal in advanced OA. In particular, osteoblasts develop an abnormal phenotype in advanced OA, with increased secretion of IL6, IL8, leptin, PGE_2, and Col I (526). The effect of *Trim32* on joint development and epiphyseal cell types could also be evaluated by examining the immunohistochemical localisation of Col II, Col X, VEGF, and tartrate-resistant acid phosphatase (TRAP) in growth plate and epiphyseal cartilage from immature WT mice and mice with cartilage-specific deletion of *Trim32* (477). Assessing the development of OA by histology and histomorphometry at several time points in surgically induced and ageing induced OA models in mice with cartilage-specific KO of *Trim32* generated using the LoxP Cre system specific for *Col2a1* may help to determine if a primary cartilage or subchondral bone phenotype exists in *Trim32* deficient mice. This could also then permit additional

studies to investigate whether the protective effects of *Trim32* for the integrity of articular cartilage can be rescued with administration of exogenous TRIM32; following induction of OA through DMM surgery, injection of *Trim32*-expressing adenovirus into operated knee joints of mice with cartilage-specific deletion of *Trim32* could be performed to investigate if the OA phenotype can be prevented (465, 538). In addition to assessing mechanical allodynia as a surrogate marker of chronic pain following surgically induced OA in mice with cartilage-specific knockout of *Trim32*, it could also be useful to examine the development of chronic pain more directly by measuring levels of the nociceptor TRPV1 (transient receptor potential cation channel subfamily V member 1) in the dorsal root ganglia (539). Such studies could further validate the potential of investigating and targeting pathways involving TRIM32 for the development of novel therapeutics to treat OA.

The mechanism of action of TRIM32 in the development of OA could be investigated further, expanding on the results described in this thesis and previous studies. Sequencing of TRIM32 in female patients with hip OA identified two variants associated with risk of developing hip OA (Table 3.1). The rs811457 variant lies adjacent to the TFAP2A/TFAP2C transcription factor binding site, and the rs3019 variant may disrupt a binding site for miR-511. The binding of TFAP2A/TFAP2C transcription factors to the variant sequence in the proximal promoter of *TRIM32* could be assessed by ChIP analysis, and the expression of TRIM32 and miR-511 in chondrocytes and synoviocytes expressing the rs3019 variant could be evaluated. Immunostaining and Western blot analysis demonstrated that TRIM32 is expressed in human articular cartilage, and that TRIM32 expression may be reduced in articular chondrocytes from patients with hip OA compared to patients without hip OA (Figure 4.1, Figure 4.3, and Figure 4.4). In experiments evaluating GAG turnover, GAG release was increased by femoral head explants from *Trim32* KO mice compared to WT mice, and most marked following RA stimulation. TRIM32 interacts with RARα and enhances RA-dependent RARα-mediated transcriptional activity, and dysregulation of RA signalling can lead to accelerated cartilage degradation (450, 459). A more accurate evaluation of aggrecanolysis in cartilage explants cultures from *Trim32* deficient mice could be achieved by Western blotting to identify ACAN fragments following

ADAMTS-mediated aggrecanolysis using neoepitopes antibodies (402). Through interactions with RARs and Pias family members, TRIM32 may mediate Wnt/β-Catenin signalling, which regulates chondrocyte phenotype and cartilage matrix homeostasis (457). *Trim32* deficiency was associated with increased expression of genes associated with chondrocyte hypertrophy following catabolic cytokine stimulation, and dysregulation of *Col2a1* and *Sox9* expression upon anabolic cytokine stimulation (Figure 4.10, Figure 4.11, Figure 4.12, and Figure 4.13). Affinity purification mass spectrometry could be performed to identify interactors with TRIM32 in chondrocytes and articular tissue to help determine the most relevant of the potential mechanisms through which TRIM32 may be involved in protection against OA (Figure 6.1).

The potential protective role for TRIM32 in the maintenance of cartilage integrity is supported by the findings of increased cartilage degradation and tibial epiphyseal bone changes, and a trend towards increased cartilage degradation and medial knee subchondral bone changes upon ageing in *Trim32* deficient mice (Figure 5.1, Figure 5.4, Table 5.3, and Figure 5.6). The results of this thesis indicate that *Trim32* may have a protective role in maintaining the integrity of articular cartilage, though the mechanisms underlying reduced TRIM32 expression in OA cartilage, or through which TRIM32 contributes to maintenance of healthy articular cartilage remain incompletely understood. In addition to examining the development of OA in joint tissues of mice with cartilage-specific deletion of *Trim32*, further studies are required to determine the most important molecular pathways through which TRIM32 may provide protection against the development of OA (Figure 6.1).

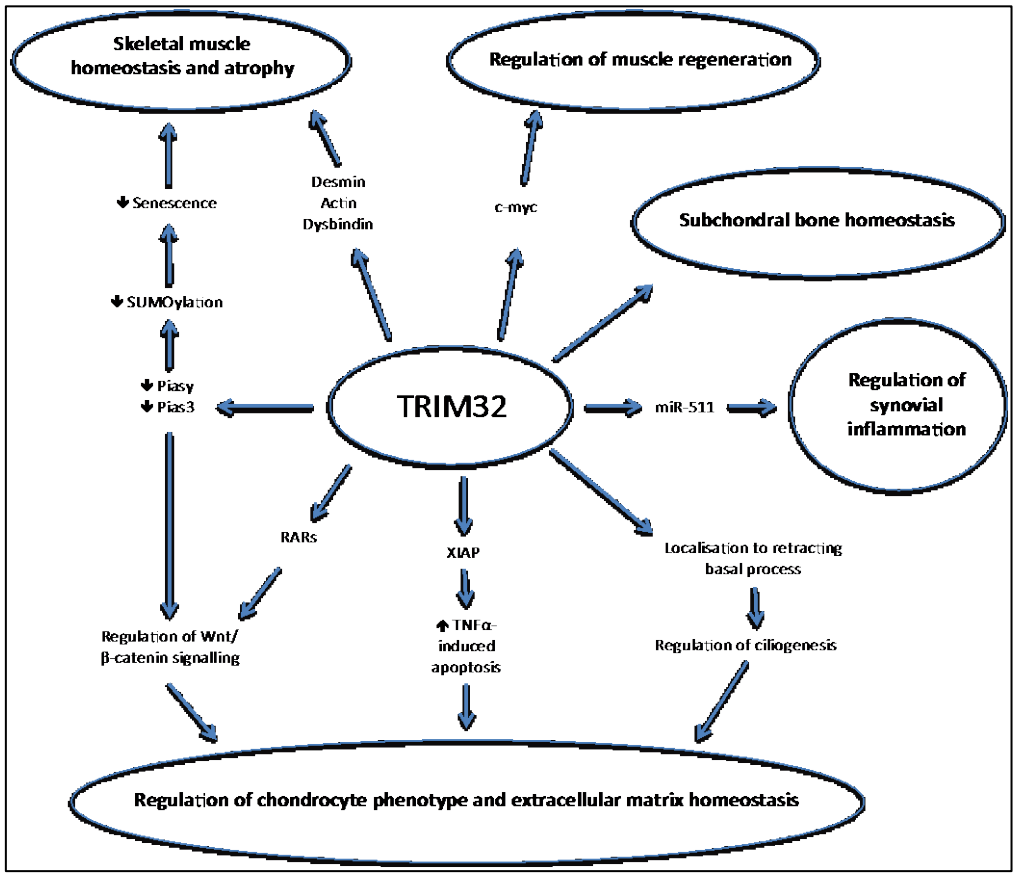

Figure 6.1 – Potential mechanisms for protective role of TRIM32 in osteoarthritis; a schematic is shown demonstrating mechanisms in which TRIM32 may be involved in joint tissues to confer protection from OA; i) TRIM32 is targeted by miR-511, which mediates TLR4-dependent cytokine production in synovial joints, and genetic variants in the TRIM32 binding site of miR-511 may predispose to hip OA in females (421, 422)(Table 3.1); ii) deficiency of *Trim32* is associated with subchondral bone changes in murine models of OA (Figure 5.1, Table 5.3); iii) TRIM32 regulates proliferation of skeletal muscle stem cells after muscle injury by ubiquitination of c-myc (298, 301); iv) TRIM32 ubiquitinates muscular substrates, such as desmin, actin, and dysbindin, to regulate muscle homeostasis and atrophy (442); v) loss of TRIM32 leads to increased levels of Piasy and accumulation of SUMOylated proteins in myoblasts (299). Disruption of these mechanisms by reduced TRIM32 activity may contribute to skeletal muscle weakness, pathological joint loading, and development of OA. TRIM32 may regulate Pias3 degradation; Pias3 protects against cartilage degradation by reducing expression of MMPs by synoviocytes (461, 462). vi) TRIM32 enhances RA-dependent RARα-mediated transcriptional activity, and both RA and Piasy mediate Wnt/β-catenin signalling in chondrocytes (459); vii) TRIM32 sensitises cells to TNFα-induced apoptosis by ubiquitinating XIAP, and viii) TRIM32 concentrates in the basal process required for microtubule and cilia formation (281, 300, 302). These mechanisms may contribute to regulation of chondrocyte phenotype and cartilage ECM homeostasis by TRIM32 and its role in protection against the development of OA.

By investigating the 9q33.1 locus associated with hip OA in females, the experiments and results described in this thesis have demonstrated variants in the proximal promoter and 3'UTR of *TRIM32* within this locus that are disproportionately represented in females with hip OA, reduced expression of *TRIM32* in femoral head chondrocytes from patients with hip OA, increased GAG release from *Trim32* deficient murine femoral head explants, increased expression of markers of hypertrophic chondrocytes upon catabolic cytokine stimulation of *Trim32* deficient murine chondrocytes, increased subchondral bone changes upon ageing of *Trim32* KO mice, and both increased subchondral bone changes and cartilage degradation after surgically induced knee joint instability in *Trim32* KO mice. These results demonstrate that genetic variation in *TRIM32* may be associated with hip OA in females, and that TRIM32 might be protective both in the maintenance of cartilage integrity and against the joint degeneration evident in OA. The results of this thesis support the further focused study of *TRIM32* in the pathophysiology of OA and the development of novel therapeutic strategies to manage OA.

Chapter 7

Appendices

7.1 Variant screening of *TRIM32*

7.1.1 Primers

TRIM32 region	Primer	Primer sequence (5'-3')	PCR product size (bp)	Annealing temperature (°C)
Proximal promoter & 5'UTR / Exon 1	Forward	tcagaagttgtaaaattcaccaaa	595	50.5
	Reverse	tgatctttagcactgtcagattg		
Exon 2 (pair 1)	Forward	tcagaagttgtaaaattcaccaaa	793	48.2
	Reverse	tgatctttagcactgtcagattg		
Exon 2 (pair 2)	Forward	ctccgggaagtgctagaatg	712	48.2
	Reverse	ggccaggaagtagtcacagc		
Exon 2 (pair 3)	Forward	ccaaggaccttcaggcaag	657	48.2
	Reverse	agttaccacggtcagcgact		
Exon 2 (pair 4)	Forward	tctgctgcctctacctctgtt	648	48.2
	Reverse	gaagtagacggtgccctcag		
Exon 2 (pair 5)	Forward	tatcacagccttgccatctg	657	56.7
	Reverse	tacccagctggaatcaggac		
Exon 2 (pair 6)	Forward	tgttagtggcacatgcagaa	569	46.7
	Reverse	atccaagatggcacagatcc		
Exon 2 (pair 7)	Forward	aagacatcatattcccgtaacatt	704	48.2
	Reverse	tgcttttggctgaattttga		
Exon 2 & 3'UTR (pair 8)	Forward	cggaattttggagatgataaga	678	48.2
	Reverse	gtgcccccacagataaagtg		

Table 7.1 – Oligonucleotide primer sequences for DNA sequencing of *TRIM32*

7.1.2 PCR reagents

Reagent	Volume (µl)
Taq Reaction Buffer	2.5
dNTPs	2
Forward Primer	1.25
Reverse Primer	1.25
Distilled H_2O	10.875
Q solution	5
DNA	2
Q-*Taq* Polymerase	0.125
Total	**25**

Table 7.2 – PCR reagents for DNA sequencing of *TRIM32*

7.1.3 PCR thermocycling conditions

Step	Temperature (ºC)	Time
1. Denature template	94	3 minutes
2. Denature template	94	45 seconds (30 cycles of steps 2-4)
3. Anneal primers	Variable	30 seconds
4. Extend primers	72	90 seconds
5. Extend primers	72	10 minutes
6. Completion	4	Incubate

Table 7.3 – PCR cycling conditions for DNA sequencing of *TRIM32*

7.2 The role of *TRIM32* in human and murine articular tissue *ex vivo*

7.2.1 Primers for qPCR reactions

Gene	Primer	Primer sequence (5'-3')	Universal probe library probe (number)
TRIM32	Forward	gtaggacacgttggtcctctg	64
	Reverse	gttaactgtccggggcttct	
COL2A1	Forward	acccccaggtgctaatgg	18
	Reverse	gaacacctttgggaccatctt	
COL10A1	Forward	gcatctcccagcaccaga	84
	Reverse	ccatgaaccagggtcaagaa	
ACAN	Forward	ccagcctacaccccagtg	76
	Reverse	gagggtgggaagccatgt	
SOX9	Forward	gtacccgcatctgcacaac	66
	Reverse	ctcctccacgaagggtctct	
GAPDH	Forward	gggttcctataaatacggactgc	52
	Reverse	ccattttgtctacgggacga	

Table 7.4 – Oligonucleotide primer sequences for qPCR reactions

7.3 The role of *Trim32* in the development of OA *in vivo*: surgically induced and ageing induced OA in *Trim32* knockout mice

7.3.1 Regions of interest at the hip and knee joint for analysis of subchondral bone by microCT

A **B**

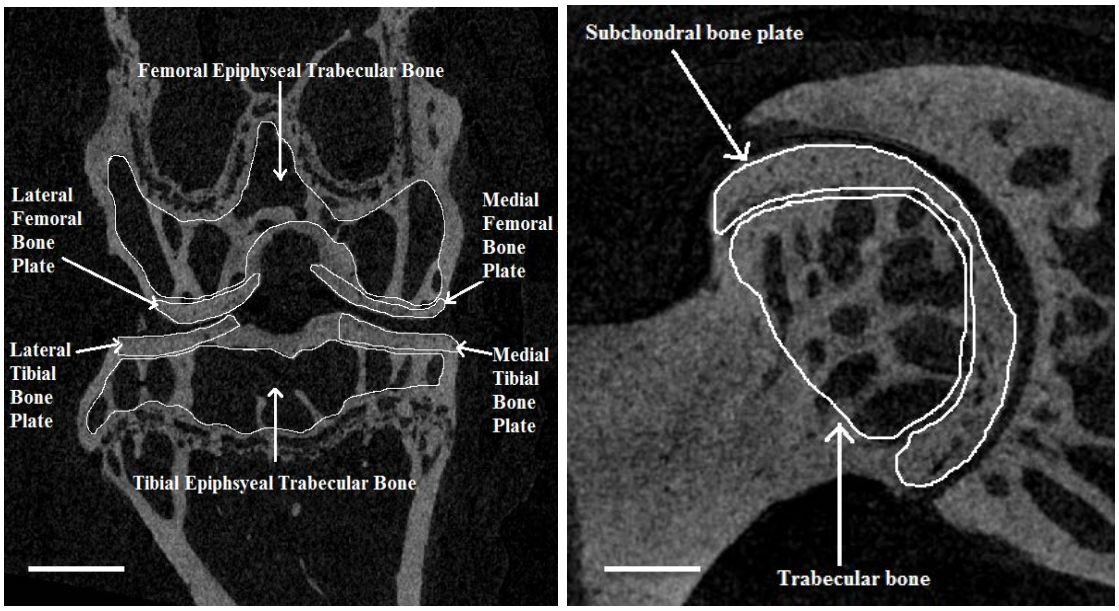

Figure 7.1 – Representative regions of interest (ROI) at the hip and knee joint for analysis of tibial and femoral subchondral bone by microCT in control, DMM-operated and aged wild-type (WT), *Trim32*$^{+/-}$ mice (HET), and *Trim32*$^{-/-}$ mice (KO); panel A shows a mid-coronal 2D-reconstruction of murine knee joint with representative regions of interest (ROI) selected for analysis of bone parameters of the epiphyseal trabecular bone, medial bone plate, and lateral bone plate of the femur and tibia following destabilisation of the medial meniscus surgery or ageing for 10 months. Panel B: mid-coronal 2D-reconstruction of murine hip joint with representative regions of interest (ROI) selected for analysis of bone parameters of the femoral head subchondral bone plate and trabecular bone following ageing for 10 months. Scale bar in panel A represents 1000 μm, and scale bar in panel B represents 200 μm.

7.3.2 3D reconstruction of microCT images of subchondral bone

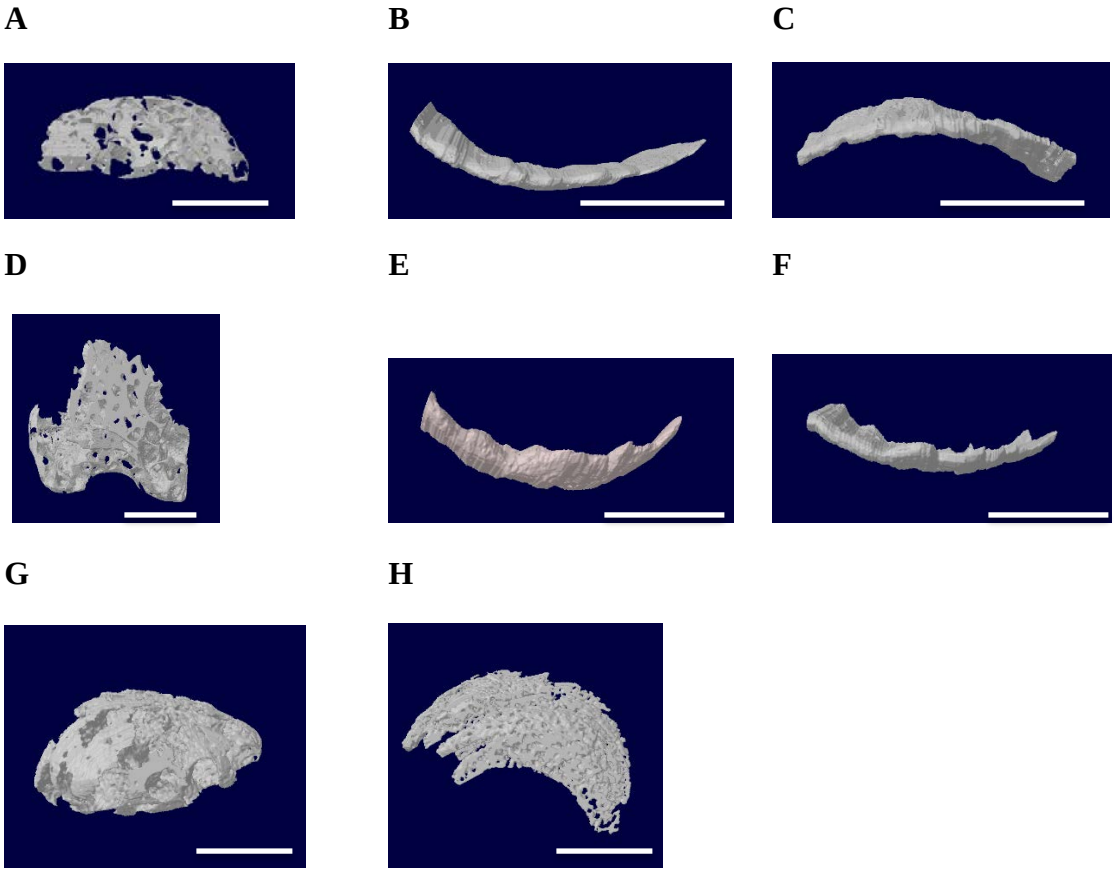

Figure 7.2 – Representative 3D reconstructions of microCT images of subchondral bone for analysis of hip and knee joint parameters in control, DMM-operated and aged wild-type (WT), *Trim32*$^{+/-}$ mice (HET), and *Trim32*$^{-/-}$ mice (KO); representative 3D-reconstructions used for analysis of subchondral bone parameters are shown for regions of interest selected for tibial trabecular bone (panel A; anterior view), tibial medial bone plate (panel B; sagittal view), tibial lateral bone plate (panel C; sagittal view), femoral trabecular bone (panel D; anterior view), femoral medial bone plate (panel E; sagittal view), and femoral lateral bone plate (panel F; sagittal view) from murine knee joints. Representative regions of interest for similar analyses are shown for femoral head trabecular bone (panel G; anterior view), and femoral head subchondral bone plate (panel H; sagittal view) from murine hip joints. Scale bars in panels A-F represents 1000 μm, and scale bars in panels G and H represent 400 μm.

7.3.3 MicroCT images of whole skeleton of *Trim32* knockout mice

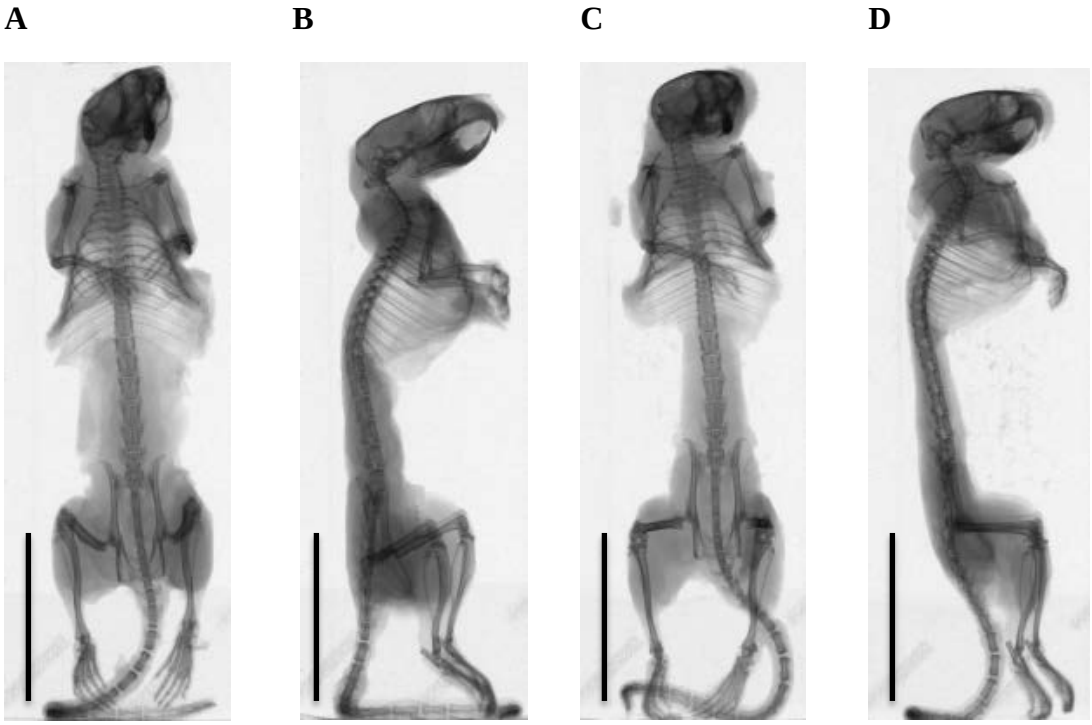

Figure 7.3 – MicroCT images of whole skeleton of adult wild-type (WT), and *Trim32*$^{-/-}$ mice (KO); representative microCT images of whole skeletons of adult wild-type (WT) mice (coronal view in Panel A; sagittal view in Panel B) and Trim32$^{-/-}$ (KO) mice (coronal view in Panel C; sagittal view in Panel D) at age 10 months. Scale bars in panels A-D represent 3 cm.

7.4 Reagents and solutions

7.4.1 Orange-G loading Dye

7.4.1.1 10X Orange-G (stock)

0.2 g Orange-G (Sigma®) + 7 ml distilled water + 3 ml 100% glycerol (BDH)

7.4.1.2 1X Orange-G

2 ml 10X Orange-G stock in 30% glycerol (BDH).

7.4.2 5X loading buffer

5.2 ml of 1 M tris-hydrogen chloride (HCl; pH 6.8, Sigma®) + 1 g DL-DDT (Sigma®) + 1.3 g sodium dodecyl sulphate (SDS; Sigma®) + 6.5 ml glycerol (BDH) and 130 µl of 10% (w/v) bromophenol blue (Sigma®).

7.4.3 1X transfer buffer

25 mM tris-base (Sigma®) + 192 mM glycine (Sigma®) + 20% (v/v) methanol (Sigma®) + 0.037% (w/v) SDS (Sigma®) in distilled H_2O.

7.4.4 TBS

7.4.4.1 20X TBS (stock)

1 M of tris-base (Sigma®) + 1M tris-HCl (pH 7.9; Sigma®) + 3 M sodium chloride (NaCl; Sigma®).

7.4.4.2 1X TBS

50 ml of 20X TBS (stock) + 950 ml distilled H_2O.

7.4.5 TBS-T

0.1% (v/v) Tween 20 (Sigma®) in 1X TBS.

7.4.6 DMMB stock

16 mg of 1,9-Dimethylmethylene blue chloride (Sigma®) + 5 ml ETOH + 2 g sodium formate + 2 ml formic acid + 993 ml distilled H_2O.

7.4.7 Papain buffer

0.1 M sodium acetate (pH 5.5) + 5 mM EDTA + 5mM L-cysteine-HCl + papain (Sigma® P3125; 0.05 M sodium acetate suspension;) for final papain buffer concentration of 125 μg/ml papain.

7.4.8 Formic acid (10%)

18 ml formic acid + 3.5 g sodium formate + 82 ml distilled H_2O.

Chapter 8

Bibliography

8.1 References

1. Online Mendelian Inheritance in Man, OMIM®. https://omim.org/ [Internet]. 2016.
2. Lane NE, Brandt K, Hawker G, Peeva E, Schreyer E, Tsuji W, et al. OARSI-FDA initiative: defining the disease state of osteoarthritis. Osteoarthritis Cartilage. 2011;19(5):478-82.
3. Arden N, Nevitt MC. Osteoarthritis: epidemiology. Best Pract Res Clin Rheumatol. 2006;20(1):3-25.
4. ARUK. Osteoarthritis in general practice. Data and perspectives. 2013.
5. Brooks PM. Impact of osteoarthritis on individuals and society: how much disability? Social consequences and health economic implications. Curr Opin Rheumatol. 2002;14(5):573-7.
6. Pulsatelli L, Addimanda O, Brusi V, Pavloska B, Meliconi R. New findings in osteoarthritis pathogenesis: therapeutic implications. Ther Adv Chronic Dis. 2013;4(1):23-43.
7. Ge Z, Hu Y, Heng BC, Yang Z, Ouyang H, Lee EH, et al. Osteoarthritis and therapy. Arthritis Rheum. 2006;55(3):493-500.
8. Hoaglund FT. Primary osteoarthritis of the hip: a genetic disease caused by European genetic variants. The Journal of bone and joint surgery American volume. 2013;95(5):463-8.
9. Buckwalter JA, Mankin HJ, Grodzinsky AJ. Articular cartilage and osteoarthritis. Instructional course lectures. 2005;54:465-80.
10. Altman RD. Criteria for classification of clinical osteoarthritis. J Rheumatol Suppl. 1991;27:10-2.
11. Goldring MB, Goldring SR. Osteoarthritis. J Cell Physiol. 2007;213(3):626-34.
12. Felson DT. Clinical practice. Osteoarthritis of the knee. N Engl J Med. 2006;354(8):841-8.
13. Ettinger WH, Jr., Burns R, Messier SP, Applegate W, Rejeski WJ, Morgan T, et al. A randomized trial comparing aerobic exercise and resistance exercise with a health education program in older adults with knee osteoarthritis. The Fitness Arthritis and Seniors Trial (FAST). JAMA. 1997;277(1):25-31.
14. Messier SP, Loeser RF, Miller GD, Morgan TM, Rejeski WJ, Sevick MA, et al. Exercise and dietary weight loss in overweight and obese older adults with knee osteoarthritis: the Arthritis, Diet, and Activity Promotion Trial. Arthritis Rheum. 2004;50(5):1501-10.
15. Berman BM, Lao L, Langenberg P, Lee WL, Gilpin AM, Hochberg MC. Effectiveness of acupuncture as adjunctive therapy in osteoarthritis of the knee: a randomized, controlled trial. Annals of internal medicine. 2004;141(12):901-10.
16. Bottegoni C, Muzzarelli RA, Giovannini F, Busilacchi A, Gigante A. Oral chondroprotection with nutraceuticals made of chondroitin sulphate plus glucosamine sulphate in osteoarthritis. Carbohydr Polym. 2014;109:126-38.
17. Leopold SS. Minimally invasive total knee arthroplasty for osteoarthritis. N Engl J Med. 2009;360(17):1749-58.
18. Culliford DJ, Maskell J, Kiran A, Judge A, Javaid MK, Cooper C, et al. The lifetime risk of total hip and knee arthroplasty: results from the UK general practice research database. Osteoarthritis Cartilage. 2012;20(6):519-24.

19. Poole AR. The Normal Synovial Joint. . 2011. In: OARSI Primer [Internet].
20. Jones EA, Crawford A, English A, Henshaw K, Mundy J, Corscadden D, et al. Synovial fluid mesenchymal stem cells in health and early osteoarthritis: detection and functional evaluation at the single-cell level. Arthritis Rheum. 2008;58(6):1731-40.
21. Castor CW. The microscopic structure of normal human synovial tissue. Arthritis Rheum. 1960;3:140-51.
22. Iwanaga T, Shikichi M, Kitamura H, Yanase H, Nozawa-Inoue K. Morphology and functional roles of synoviocytes in the joint. Arch Histol Cytol. 2000;63(1):17-31.
23. Athanasou NA. Synovial macrophages. Ann Rheum Dis. 1995;54(5):392-4.
24. Matsubara T, Spycher MA, Ruttner JR, Fehr K. The ultrastructural localization of fibronectin in the lining layer of rheumatoid arthritis synovium: the synthesis of fibronectin by type B lining cells. Rheumatol Int. 1983;3(2):75-9.
25. Yielding KL, Tomkins GM, Bunim JJ. Synthesis of hyaluronic acid by human synovial tissue slices. Science. 1957;125(3261):1300.
26. Coleman P, Kavanagh E, Mason RM, Levick JR, Ashhurst DE. The proteoglycans and glycosaminoglycan chains of rabbit synovium. Histochem J. 1998;30(7):519-24.
27. Tamer TM. Hyaluronan and synovial joint: function, distribution and healing. Interdiscip Toxicol. 2013;6(3):111-25.
28. Swann DA, Silver FH, Slayter HS, Stafford W, Shore E. The molecular structure and lubricating activity of lubricin isolated from bovine and human synovial fluids. Biochem J. 1985;225(1):195-201.
29. Mazzucco D, Scott R, Spector M. Composition of joint fluid in patients undergoing total knee replacement and revision arthroplasty: correlation with flow properties. Biomaterials. 2004;25(18):4433-45.
30. Schwarz IM, Hills BA. Surface-active phospholipid as the lubricating component of lubricin. Br J Rheumatol. 1998;37(1):21-6.
31. Xia B, Di C, Zhang J, Hu S, Jin H, Tong P. Osteoarthritis pathogenesis: a review of molecular mechanisms. Calcif Tissue Int. 2014;95(6):495-505.
32. Woods A, Wang G, Beier F. Regulation of chondrocyte differentiation by the actin cytoskeleton and adhesive interactions. J Cell Physiol. 2007;213(1):1-8.
33. Goldring MB, Marcu KB. Cartilage homeostasis in health and rheumatic diseases. Arthritis Res Ther. 2009;11(3):224.
34. Huber M, Trattnig S, Lintner F. Anatomy, biochemistry, and physiology of articular cartilage. Investigative radiology. 2000;35(10):573-80.
35. Martel-Pelletier J, Boileau C, Pelletier JP, Roughley PJ. Cartilage in normal and osteoarthritis conditions. Best Pract Res Clin Rheumatol. 2008;22(2):351-84.
36. Kronenberg HM. Developmental regulation of the growth plate. Nature. 2003;423(6937):332-6.
37. Michigami T. Regulatory mechanisms for the development of growth plate cartilage. Cell Mol Life Sci. 2013;70(22):4213-21.
38. Akiyama H, Lefebvre V. Unraveling the transcriptional regulatory machinery in chondrogenesis. J Bone Miner Metab. 2011;29(4):390-5.
39. Lefebvre V, Huang W, Harley VR, Goodfellow PN, de Crombrugghe B. SOX9 is a potent activator of the chondrocyte-specific enhancer of the pro alpha1(II) collagen gene. Mol Cell Biol. 1997;17(4):2336-46.

40. Yoshida CA, Yamamoto H, Fujita T, Furuichi T, Ito K, Inoue K, et al. Runx2 and Runx3 are essential for chondrocyte maturation, and Runx2 regulates limb growth through induction of Indian hedgehog. Genes Dev. 2004;18(8):952-63.
41. Selvamurugan N, Kwok S, Partridge NC. Smad3 interacts with JunB and Cbfa1/Runx2 for transforming growth factor-beta1-stimulated collagenase-3 expression in human breast cancer cells. J Biol Chem. 2004;279(26):27764-73.
42. Zheng Q, Zhou G, Morello R, Chen Y, Garcia-Rojas X, Lee B. Type X collagen gene regulation by Runx2 contributes directly to its hypertrophic chondrocyte-specific expression in vivo. J Cell Biol. 2003;162(5):833-42.
43. Ornitz DM. FGF signaling in the developing endochondral skeleton. Cytokine Growth Factor Rev. 2005;16(2):205-13.
44. Peters KG, Werner S, Chen G, Williams LT. Two FGF receptor genes are differentially expressed in epithelial and mesenchymal tissues during limb formation and organogenesis in the mouse. Development. 1992;114(1):233-43.
45. Kronenberg HM. PTHrP and skeletal development. Ann N Y Acad Sci. 2006;1068:1-13.
46. Mak KK, Kronenberg HM, Chuang PT, Mackem S, Yang Y. Indian hedgehog signals independently of PTHrP to promote chondrocyte hypertrophy. Development. 2008;135(11):1947-56.
47. Michigami T. Current understanding on the molecular basis of chondrogenesis. Clin Pediatr Endocrinol. 2014;23(1):1-8.
48. Aszodi A, Hunziker EB, Brakebusch C, Fassler R. Beta1 integrins regulate chondrocyte rotation, G1 progression, and cytokinesis. Genes Dev. 2003;17(19):2465-79.
49. Settembre C, Arteaga-Solis E, McKee MD, de Pablo R, Al Awqati Q, Ballabio A, et al. Proteoglycan desulfation determines the efficiency of chondrocyte autophagy and the extent of FGF signaling during endochondral ossification. Genes Dev. 2008;22(19):2645-50.
50. Koshimizu T, Kawai M, Kondou H, Tachikawa K, Sakai N, Ozono K, et al. Vinculin functions as regulator of chondrogenesis. J Biol Chem. 2012;287(19):15760-75.
51. Bruckner P, van der Rest M. Structure and function of cartilage collagens. Microsc Res Tech. 1994;28(5):378-84.
52. Kielty CM, Whittaker SP, Grant ME, Shuttleworth CA. Type VI collagen microfibrils: evidence for a structural association with hyaluronan. J Cell Biol. 1992;118(4):979-90.
53. Bruckner P, Mendler M, Steinmann B, Huber S, Winterhalter KH. The structure of human collagen type IX and its organization in fetal and infant cartilage fibrils. J Biol Chem. 1988;263(32):16911-7.
54. Chow G, Nietfeld JJ, Knudson CB, Knudson W. Antisense inhibition of chondrocyte CD44 expression leading to cartilage chondrolysis. Arthritis Rheum. 1998;41(8):1411-9.
55. Bayliss MT, Ridgway GD, Ali SY. Differences in the rates of aggregation of proteoglycans from human articular cartilage and chondrosarcoma. Biochem J. 1983;215(3):705-8.

56. Thur J, Rosenberg K, Nitsche DP, Pihlajamaa T, Ala-Kokko L, Heinegard D, et al. Mutations in cartilage oligomeric matrix protein causing pseudoachondroplasia and multiple epiphyseal dysplasia affect binding of calcium and collagen I, II, and IX. J Biol Chem. 2001;276(9):6083-92.
57. Costell M, Gustafsson E, Aszodi A, Morgelin M, Bloch W, Hunziker E, et al. Perlecan maintains the integrity of cartilage and some basement membranes. J Cell Biol. 1999;147(5):1109-22.
58. Loeser R, Carlson CS, Tulli H, Jerome WG, Miller L, Wallin R. Articular-cartilage matrix gamma-carboxyglutamic acid-containing protein. Characterization and immunolocalization. Biochem J. 1992;282 (Pt 1):1-6.
59. Poole AR, Kojima T, Yasuda T, Mwale F, Kobayashi M, Laverty S. Composition and structure of articular cartilage: a template for tissue repair. Clinical orthopaedics and related research. 2001(391 Suppl):S26-33.
60. Venn MF. Variation of chemical composition with age in human femoral head cartilage. Ann Rheum Dis. 1979;37:168-74.
61. Poole AR, Rosenberg LC, Reiner A, Ionescu M, Bogoch E, Roughley PJ. Contents and distributions of the proteoglycans decorin and biglycan in normal and osteoarthritic human articular cartilage. J Orthop Res. 1996;14(5):681-9.
62. Poole AR, Webber C, Pidoux I, Choi H, Rosenberg LC. Localization of a dermatan sulfate proteoglycan (DS-PGII) in cartilage and the presence of an immunologically related species in other tissues. J Histochem Cytochem. 1986;34(5):619-25.
63. Keene DR, Engvall E, Glanville RW. Ultrastructure of type VI collagen in human skin and cartilage suggests an anchoring function for this filamentous network. J Cell Biol. 1988;107(5):1995-2006.
64. Poole AR, Pidoux I, Reiner A, Rosenberg L. An immunoelectron microscope study of the organization of proteoglycan monomer, link protein, and collagen in the matrix of articular cartilage. J Cell Biol. 1982;93(3):921-37.
65. Sandell LJ, Aigner T. Articular cartilage and changes in arthritis. An introduction: cell biology of osteoarthritis. Arthritis Res. 2001;3(2):107-13.
66. Chubinskaya S, Merrihew C, Cs-Szabo G, Mollenhauer J, McCartney J, Rueger DC, et al. Human articular chondrocytes express osteogenic protein-1. J Histochem Cytochem. 2000;48(2):239-50.
67. Eyre DR, Weis MA, Wu JJ. Articular cartilage collagen: an irreplaceable framework? Eur Cell Mater. 2006;12:57-63.
68. Masuda K, Sah RL, Hejna MJ, Thonar EJ. A novel two-step method for the formation of tissue-engineered cartilage by mature bovine chondrocytes: the alginate-recovered-chondrocyte (ARC) method. J Orthop Res. 2003;21(1):139-48.
69. Cremer MA, Rosloniec EF, Kang AH. The cartilage collagens: a review of their structure, organization, and role in the pathogenesis of experimental arthritis in animals and in human rheumatic disease. J Mol Med (Berl). 1998;76(3-4):275-88.
70. Billinghurst RC, Dahlberg L, Ionescu M, Reiner A, Bourne R, Rorabeck C, et al. Enhanced cleavage of type II collagen by collagenases in osteoarthritic articular cartilage. J Clin Invest. 1997;99(7):1534-45.

71. Saito S, Katoh M, Masumoto M, Matsumoto S, Masuho Y. Collagen degradation induced by the combination of IL-1alpha and plasminogen in rabbit articular cartilage explant culture. J Biochem. 1997;122(1):49-54.
72. Klatt AR, Paul-Klausch B, Klinger G, Kuhn G, Renno JH, Banerjee M, et al. A critical role for collagen II in cartilage matrix degradation: collagen II induces pro-inflammatory cytokines and MMPs in primary human chondrocytes. J Orthop Res. 2009;27(1):65-70.
73. Vynios DH. Metabolism of cartilage proteoglycans in health and disease. Biomed Res Int. 2014;2014:452315.
74. Struglics A, Hansson M. Calpain is involved in C-terminal truncation of human aggrecan. Biochem J. 2010;430(3):531-8.
75. Fonovic M, Turk B. Cysteine cathepsins and extracellular matrix degradation. Biochim Biophys Acta. 2014;1840(8):2560-70.
76. O'Hara BP, Urban JP, Maroudas A. Influence of cyclic loading on the nutrition of articular cartilage. Ann Rheum Dis. 1990;49(7):536-9.
77. Leong DJ, Hardin JA, Cobelli NJ, Sun HB. Mechanotransduction and cartilage integrity. Ann N Y Acad Sci. 2011;1240:32-7.
78. Millward-Sadler SJ, Wright MO, Davies LW, Nuki G, Salter DM. Mechanotransduction via integrins and interleukin-4 results in altered aggrecan and matrix metalloproteinase 3 gene expression in normal, but not osteoarthritic, human articular chondrocytes. Arthritis Rheum. 2000;43(9):2091-9.
79. Praetorius HA, Praetorius J, Nielsen S, Frokiaer J, Spring KR. Beta1-integrins in the primary cilium of MDCK cells potentiate fibronectin-induced Ca2+ signaling. Am J Physiol Renal Physiol. 2004;287(5):F969-78.
80. Ruhlen R, Marberry K. The chondrocyte primary cilium. Osteoarthritis Cartilage. 2014;22(8):1071-6.
81. McGlashan SR, Jensen CG, Poole CA. Localization of extracellular matrix receptors on the chondrocyte primary cilium. J Histochem Cytochem. 2006;54(9):1005-14.
82. Chang CF, Ramaswamy G, Serra R. Depletion of primary cilia in articular chondrocytes results in reduced Gli3 repressor to activator ratio, increased Hedgehog signaling, and symptoms of early osteoarthritis. Osteoarthritis Cartilage. 2012;20(2):152-61.
83. McGlashan SR, Haycraft CJ, Jensen CG, Yoder BK, Poole CA. Articular cartilage and growth plate defects are associated with chondrocyte cytoskeletal abnormalities in Tg737orpk mice lacking the primary cilia protein polaris. Matrix Biol. 2007;26(4):234-46.
84. Wann AK, Knight MM. Primary cilia elongation in response to interleukin-1 mediates the inflammatory response. Cell Mol Life Sci. 2012;69(17):2967-77.
85. Strobel S, Loparic M, Wendt D, Schenk AD, Candrian C, Lindberg RL, et al. Anabolic and catabolic responses of human articular chondrocytes to varying oxygen percentages. Arthritis Res Ther. 2010;12(2):R34.
86. Cernanec J, Guilak F, Weinberg JB, Pisetsky DS, Fermor B. Influence of hypoxia and reoxygenation on cytokine-induced production of proinflammatory mediators in articular cartilage. Arthritis Rheum. 2002;46(4):968-75.

87. Duval E, Leclercq S, Elissalde JM, Demoor M, Galera P, Boumediene K. Hypoxia-inducible factor 1alpha inhibits the fibroblast-like markers type I and type III collagen during hypoxia-induced chondrocyte redifferentiation: hypoxia not only induces type II collagen and aggrecan, but it also inhibits type I and type III collagen in the hypoxia-inducible factor 1alpha-dependent redifferentiation of chondrocytes. Arthritis Rheum. 2009;60(10):3038-48.
88. Ramage L, Nuki G, Salter DM. Signalling cascades in mechanotransduction: cell-matrix interactions and mechanical loading. Scandinavian journal of medicine & science in sports. 2009;19(4):457-69.
89. Ikenoue T, Trindade MC, Lee MS, Lin EY, Schurman DJ, Goodman SB, et al. Mechanoregulation of human articular chondrocyte aggrecan and type II collagen expression by intermittent hydrostatic pressure in vitro. J Orthop Res. 2003;21(1):110-6.
90. Shelton JC, Bader DL, Lee DA. Mechanical conditioning influences the metabolic response of cell-seeded constructs. Cells Tissues Organs. 2003;175(3):140-50.
91. Mauck RL, Soltz MA, Wang CC, Wong DD, Chao PH, Valhmu WB, et al. Functional tissue engineering of articular cartilage through dynamic loading of chondrocyte-seeded agarose gels. J Biomech Eng. 2000;122(3):252-60.
92. Wong M, Siegrist M, Cao X. Cyclic compression of articular cartilage explants is associated with progressive consolidation and altered expression pattern of extracellular matrix proteins. Matrix Biol. 1999;18(4):391-9.
93. Ragan PM, Badger AM, Cook M, Chin VI, Gowen M, Grodzinsky AJ, et al. Down-regulation of chondrocyte aggrecan and type-II collagen gene expression correlates with increases in static compression magnitude and duration. J Orthop Res. 1999;17(6):836-42.
94. Honda K, Ohno S, Tanimoto K, Ijuin C, Tanaka N, Doi T, et al. The effects of high magnitude cyclic tensile load on cartilage matrix metabolism in cultured chondrocytes. Eur J Cell Biol. 2000;79(9):601-9.
95. Sanchez-Adams J, Leddy HA, McNulty AL, O'Conor CJ, Guilak F. The mechanobiology of articular cartilage: bearing the burden of osteoarthritis. Curr Rheumatol Rep. 2014;16(10):451.
96. Martinac B. Mechanosensitive ion channels: molecules of mechanotransduction. Journal of cell science. 2004;117(Pt 12):2449-60.
97. Vincent TL. Targeting mechanotransduction pathways in osteoarthritis: a focus on the pericellular matrix. Curr Opin Pharmacol. 2013;13(3):449-54.
98. Guilak F, Alexopoulos LG, Upton ML, Youn I, Choi JB, Cao L, et al. The pericellular matrix as a transducer of biomechanical and biochemical signals in articular cartilage. Ann N Y Acad Sci. 2006;1068:498-512.
99. Leitinger B, Hohenester E. Mammalian collagen receptors. Matrix Biol. 2007;26(3):146-55.
100. Wiberg C, Klatt AR, Wagener R, Paulsson M, Bateman JF, Heinegard D, et al. Complexes of matrilin-1 and biglycan or decorin connect collagen VI microfibrils to both collagen II and aggrecan. J Biol Chem. 2003;278(39):37698-704.
101. Wright M, Jobanputra P, Bavington C, Salter DM, Nuki G. Effects of intermittent pressure-induced strain on the electrophysiology of cultured human

chondrocytes: evidence for the presence of stretch-activated membrane ion channels. Clin Sci (Lond). 1996;90(1):61-71.
102. Mouw JK, Imler SM, Levenston ME. Ion-channel regulation of chondrocyte matrix synthesis in 3D culture under static and dynamic compression. Biomech Model Mechanobiol. 2007;6(1-2):33-41.
103. Ostergaard K, Salter DM, Petersen J, Bendtzen K, Hvolris J, Andersen CB. Expression of alpha and beta subunits of the integrin superfamily in articular cartilage from macroscopically normal and osteoarthritic human femoral heads. Ann Rheum Dis. 1998;57(5):303-8.
104. Wright MO, Nishida K, Bavington C, Godolphin JL, Dunne E, Walmsley S, et al. Hyperpolarisation of cultured human chondrocytes following cyclical pressure-induced strain: evidence of a role for alpha 5 beta 1 integrin as a chondrocyte mechanoreceptor. J Orthop Res. 1997;15(5):742-7.
105. Chowdhury TT, Salter DM, Bader DL, Lee DA. Integrin-mediated mechanotransduction processes in TGFbeta-stimulated monolayer-expanded chondrocytes. Biochem Biophys Res Commun. 2004;318(4):873-81.
106. Loeser RF. Growth factor regulation of chondrocyte integrins. Differential effects of insulin-like growth factor 1 and transforming growth factor beta on alpha 1 beta 1 integrin expression and chondrocyte adhesion to type VI collagen. Arthritis Rheum. 1997;40(2):270-6.
107. Vincent TL, McLean CJ, Full LE, Peston D, Saklatvala J. FGF-2 is bound to perlecan in the pericellular matrix of articular cartilage, where it acts as a chondrocyte mechanotransducer. Osteoarthritis Cartilage. 2007;15(7):752-63.
108. Millward-Sadler SJ, Khan NS, Bracher MG, Wright MO, Salter DM. Roles for the interleukin-4 receptor and associated JAK/STAT proteins in human articular chondrocyte mechanotransduction. Osteoarthritis Cartilage. 2006;14(10):991-1001.
109. Zhang M, Chen YJ, Ono T, Wang JJ. Crosstalk between integrin and G protein pathways involved in mechanotransduction in mandibular condylar chondrocytes under pressure. Arch Biochem Biophys. 2008;474(1):102-8.
110. Fitzgerald JB, Jin M, Dean D, Wood DJ, Zheng MH, Grodzinsky AJ. Mechanical compression of cartilage explants induces multiple time-dependent gene expression patterns and involves intracellular calcium and cyclic AMP. J Biol Chem. 2004;279(19):19502-11.
111. Urban JP, Hall AC, Gehl KA. Regulation of matrix synthesis rates by the ionic and osmotic environment of articular chondrocytes. J Cell Physiol. 1993;154(2):262-70.
112. de Crombrugghe B, Lefebvre V, Behringer RR, Bi W, Murakami S, Huang W. Transcriptional mechanisms of chondrocyte differentiation. Matrix Biol. 2000;19(5):389-94.
113. Bush PG, Hodkinson PD, Hamilton GL, Hall AC. Viability and volume of in situ bovine articular chondrocytes-changes following a single impact and effects of medium osmolarity. Osteoarthritis Cartilage. 2005;13(1):54-65.
114. Amin AK, Huntley JS, Bush PG, Simpson AH, Hall AC. Osmolarity influences chondrocyte death in wounded articular cartilage. The Journal of bone and joint surgery American volume. 2008;90(7):1531-42.

115. Farhan-Alanie MM, Hall AC. Temperature changes and chondrocyte death during drilling in a bovine cartilage model and chondroprotection by modified irrigation solutions. International orthopaedics. 2014;38(11):2407-12.
116. Erickson GR, Alexopoulos LG, Guilak F. Hyper-osmotic stress induces volume change and calcium transients in chondrocytes by transmembrane, phospholipid, and G-protein pathways. Journal of biomechanics. 2001;34(12):1527-35.
117. Chao PH, West AC, Hung CT. Chondrocyte intracellular calcium, cytoskeletal organization, and gene expression responses to dynamic osmotic loading. Am J Physiol Cell Physiol. 2006;291(4):C718-25.
118. Orrenius S, Zhivotovsky B, Nicotera P. Regulation of cell death: the calcium-apoptosis link. Nat Rev Mol Cell Biol. 2003;4(7):552-65.
119. Urban JP. The chondrocyte: a cell under pressure. Br J Rheumatol. 1994;33(10):901-8.
120. Thomas L, Mc CR, Potter JL, Weissmann G. Comparison of the effects of papain n vitamin A on cartilage. I. The effects in rabbits. J Exp Med. 1960;111:705-18.
121. Lucy JA, Dingle JT, Fell HB. Studies on the mode of action of excess of vitamin A. 2. A possible role of intracellular proteases in the degradation of cartilage matrix. Biochem J. 1961;79:500-8.
122. Sapolsky AI, Howell DS. Further characterization of a neutral metalloprotease isolated from human articular cartilage. Arthritis Rheum. 1982;25(8):981-8.
123. Galloway WA, Murphy G, Sandy JD, Gavrilovic J, Cawston TE, Reynolds JJ. Purification and characterization of a rabbit bone metalloproteinase that degrades proteoglycan and other connective-tissue components. Biochem J. 1983;209(3):741-52.
124. Stanton H, Rogerson FM, East CJ, Golub SB, Lawlor KE, Meeker CT, et al. ADAMTS5 is the major aggrecanase in mouse cartilage in vivo and in vitro. Nature. 2005;434(7033):648-52.
125. Fosang AJ, Neame PJ, Last K, Hardingham TE, Murphy G, Hamilton JA. The interglobular domain of cartilage aggrecan is cleaved by PUMP, gelatinases, and cathepsin B. J Biol Chem. 1992;267(27):19470-4.
126. Fosang AJ, Last K, Knauper V, Neame PJ, Murphy G, Hardingham TE, et al. Fibroblast and neutrophil collagenases cleave at two sites in the cartilage aggrecan interglobular domain. Biochem J. 1993;295 (Pt 1):273-6.
127. Fosang AJ, Last K, Knauper V, Murphy G, Neame PJ. Degradation of cartilage aggrecan by collagenase-3 (MMP-13). FEBS Lett. 1996;380(1-2):17-20.
128. Sandy JD, Neame PJ, Boynton RE, Flannery CR. Catabolism of aggrecan in cartilage explants. Identification of a major cleavage site within the interglobular domain. J Biol Chem. 1991;266(14):8683-5.
129. Zeng W, Corcoran C, Collins-Racie LA, Lavallie ER, Morris EA, Flannery CR. Glycosaminoglycan-binding properties and aggrecanase activities of truncated ADAMTSs: comparative analyses with ADAMTS-5, -9, -16 and -18. Biochim Biophys Acta. 2006;1760(3):517-24.
130. Gendron C, Kashiwagi M, Lim NH, Enghild JJ, Thogersen IB, Hughes C, et al. Proteolytic activities of human ADAMTS-5: comparative studies with ADAMTS-4. J Biol Chem. 2007;282(25):18294-306.
131. Koshy PJ, Lundy CJ, Rowan AD, Porter S, Edwards DR, Hogan A, et al. The modulation of matrix metalloproteinase and ADAM gene expression in human

chondrocytes by interleukin-1 and oncostatin M: a time-course study using real-time quantitative reverse transcription-polymerase chain reaction. Arthritis Rheum. 2002;46(4):961-7.
132. Song RH, Tortorella MD, Malfait AM, Alston JT, Yang Z, Arner EC, et al. Aggrecan degradation in human articular cartilage explants is mediated by both ADAMTS-4 and ADAMTS-5. Arthritis Rheum. 2007;56(2):575-85.
133. Sandy JD. A contentious issue finds some clarity: on the independent and complementary roles of aggrecanase activity and MMP activity in human joint aggrecanolysis. Osteoarthritis Cartilage. 2006;14(2):95-100.
134. Pratta MA, Yao W, Decicco C, Tortorella MD, Liu RQ, Copeland RA, et al. Aggrecan protects cartilage collagen from proteolytic cleavage. J Biol Chem. 2003;278(46):45539-45.
135. Karsdal MA, Madsen SH, Christiansen C, Henriksen K, Fosang AJ, Sondergaard BC. Cartilage degradation is fully reversible in the presence of aggrecanase but not matrix metalloproteinase activity. Arthritis Res Ther. 2008;10(3):R63.
136. Johnson AR, Pavlovsky AG, Ortwine DF, Prior F, Man CF, Bornemeier DA, et al. Discovery and characterization of a novel inhibitor of matrix metalloprotease-13 that reduces cartilage damage in vivo without joint fibroplasia side effects. J Biol Chem. 2007;282(38):27781-91.
137. Swingler TE, Waters JG, Davidson RK, Pennington CJ, Puente XS, Darrah C, et al. Degradome expression profiling in human articular cartilage. Arthritis Res Ther. 2009;11(3):R96.
138. Ra HJ, Parks WC. Control of matrix metalloproteinase catalytic activity. Matrix Biol. 2007;26(8):587-96.
139. Saxne T, Heinegard D. Cartilage oligomeric matrix protein: a novel marker of cartilage turnover detectable in synovial fluid and blood. Br J Rheumatol. 1992;31(9):583-91.
140. Dickinson SC, Vankemmelbeke MN, Buttle DJ, Rosenberg K, Heinegard D, Hollander AP. Cleavage of cartilage oligomeric matrix protein (thrombospondin-5) by matrix metalloproteinases and a disintegrin and metalloproteinase with thrombospondin motifs. Matrix Biol. 2003;22(3):267-78.
141. Luan Y, Kong L, Howell DR, Ilalov K, Fajardo M, Bai XH, et al. Inhibition of ADAMTS-7 and ADAMTS-12 degradation of cartilage oligomeric matrix protein by alpha-2-macroglobulin. Osteoarthritis Cartilage. 2008;16(11):1413-20.
142. Yasumoto T, Bird JL, Sugimoto K, Mason RM, Bayliss MT. The G1 domain of aggrecan released from porcine articular cartilage forms stable complexes with hyaluronan/link protein. Rheumatology (Oxford). 2003;42(2):336-42.
143. Rockel JS, Kudirka JC, Guzi AJ, Bernier SM. Regulation of Sox9 activity by crosstalk with nuclear factor-kappaB and retinoic acid receptors. Arthritis Res Ther. 2008;10(1):R3.
144. DiGiovanna JJ. Isotretinoin effects on bone. J Am Acad Dermatol. 2001;45(5):S176-82.
145. Williams JA, Kondo N, Okabe T, Takeshita N, Pilchak DM, Koyama E, et al. Retinoic acid receptors are required for skeletal growth, matrix homeostasis and growth plate function in postnatal mouse. Developmental biology. 2009;328(2):315-27.

146. Zhang Y, Ross AC. Retinoic acid and the transcription factor MafB act together and differentially to regulate aggrecan and matrix metalloproteinase gene expression in neonatal chondrocytes. J Cell Biochem. 2013;114(2):471-9.
147. Goldring MB, Goldring SR. Articular cartilage and subchondral bone in the pathogenesis of osteoarthritis. Ann N Y Acad Sci. 2010;1192:230-7.
148. Hadjidakis DJ, Androulakis, II. Bone remodeling. Ann N Y Acad Sci. 2006;1092:385-96.
149. Nakashima T. [Regulation of bone homeostasis by bone cells]. Clin Calcium. 2013;23(2):218-28.
150. Phimphilai M, Zhao Z, Boules H, Roca H, Franceschi RT. BMP signaling is required for RUNX2-dependent induction of the osteoblast phenotype. J Bone Miner Res. 2006;21(4):637-46.
151. Vaananen HK, Zhao H, Mulari M, Halleen JM. The cell biology of osteoclast function. Journal of cell science. 2000;113 (Pt 3):377-81.
152. Hofbauer LC, Lacey DL, Dunstan CR, Spelsberg TC, Riggs BL, Khosla S. Interleukin-1beta and tumor necrosis factor-alpha, but not interleukin-6, stimulate osteoprotegerin ligand gene expression in human osteoblastic cells. Bone. 1999;25(3):255-9.
153. Martin TJ, Sims NA. Osteoclast-derived activity in the coupling of bone formation to resorption. Trends Mol Med. 2005;11(2):76-81.
154. Aurich M, Squires GR, Reiner A, Mollenhauer JA, Kuettner KE, Poole AR, et al. Differential matrix degradation and turnover in early cartilage lesions of human knee and ankle joints. Arthritis Rheum. 2005;52(1):112-9.
155. Burrage PS, Mix KS, Brinckerhoff CE. Matrix metalloproteinases: role in arthritis. Front Biosci. 2006;11:529-43.
156. Sellam J, Berenbaum F. The role of synovitis in pathophysiology and clinical symptoms of osteoarthritis. Nat Rev Rheumatol. 2010;6(11):625-35.
157. Bondeson J, Wainwright SD, Lauder S, Amos N, Hughes CE. The role of synovial macrophages and macrophage-produced cytokines in driving aggrecanases, matrix metalloproteinases, and other destructive and inflammatory responses in osteoarthritis. Arthritis Res Ther. 2006;8(6):R187.
158. Roemer FW, Kwoh CK, Hannon MJ, Hunter DJ, Eckstein F, Fujii T, et al. What comes first? Multitissue involvement leading to radiographic osteoarthritis: magnetic resonance imaging-based trajectory analysis over four years in the osteoarthritis initiative. Arthritis Rheumatol. 2015;67(8):2085-96.
159. Goldring MB, Otero M, Plumb DA, Dragomir C, Favero M, El Hachem K, et al. Roles of inflammatory and anabolic cytokines in cartilage metabolism: signals and multiple effectors converge upon MMP-13 regulation in osteoarthritis. Eur Cell Mater. 2011;21:202-20.
160. Ko FC, Dragomir C, Plumb DA, Goldring SR, Wright TM, Goldring MB, et al. In vivo cyclic compression causes cartilage degeneration and subchondral bone changes in mouse tibiae. Arthritis Rheum. 2013;65(6):1569-78.
161. McGlashan SR, Cluett EC, Jensen CG, Poole CA. Primary cilia in osteoarthritic chondrocytes: from chondrons to clusters. Dev Dyn. 2008;237(8):2013-20.

162. Zhen G, Wen C, Jia X, Li Y, Crane JL, Mears SC, et al. Inhibition of TGF-beta signaling in mesenchymal stem cells of subchondral bone attenuates osteoarthritis. Nat Med. 2013;19(6):704-12.
163. Priam S, Bougault C, Houard X, Gosset M, Salvat C, Berenbaum F, et al. Identification of soluble 14-3-3 as a novel subchondral bone mediator involved in cartilage degradation in osteoarthritis. Arthritis Rheum. 2013;65(7):1831-42.
164. Suri S, Gill SE, Massena de Camin S, Wilson D, McWilliams DF, Walsh DA. Neurovascular invasion at the osteochondral junction and in osteophytes in osteoarthritis. Ann Rheum Dis. 2007;66(11):1423-8.
165. Malfait AM, Liu RQ, Ijiri K, Komiya S, Tortorella MD. Inhibition of ADAM-TS4 and ADAM-TS5 prevents aggrecan degradation in osteoarthritic cartilage. J Biol Chem. 2002;277(25):22201-8.
166. Yamanishi Y, Boyle DL, Clark M, Maki RA, Tortorella MD, Arner EC, et al. Expression and regulation of aggrecanase in arthritis: the role of TGF-beta. J Immunol. 2002;168(3):1405-12.
167. Troeberg L, Nagase H. Proteases involved in cartilage matrix degradation in osteoarthritis. Biochim Biophys Acta. 2012;1824(1):133-45.
168. Glasson SS, Askew R, Sheppard B, Carito B, Blanchet T, Ma HL, et al. Deletion of active ADAMTS5 prevents cartilage degradation in a murine model of osteoarthritis. Nature. 2005;434(7033):644-8.
169. Little CB, Barai A, Burkhardt D, Smith SM, Fosang AJ, Werb Z, et al. Matrix metalloproteinase 13-deficient mice are resistant to osteoarthritic cartilage erosion but not chondrocyte hypertrophy or osteophyte development. Arthritis Rheum. 2009;60(12):3723-33.
170. Polur I, Lee PL, Servais JM, Xu L, Li Y. Role of HTRA1, a serine protease, in the progression of articular cartilage degeneration. Histol Histopathol. 2010;25(5):599-608.
171. Xu H, Raynal N, Stathopoulos S, Myllyharju J, Farndale RW, Leitinger B. Collagen binding specificity of the discoidin domain receptors: binding sites on collagens II and III and molecular determinants for collagen IV recognition by DDR1. Matrix Biol. 2011;30(1):16-26.
172. Homandberg GA, Wen C, Hui F. Cartilage damaging activities of fibronectin fragments derived from cartilage and synovial fluid. Osteoarthritis Cartilage. 1998;6(4):231-44.
173. Bank RA, Krikken M, Beekman B, Stoop R, Maroudas A, Lafeber FP, et al. A simplified measurement of degraded collagen in tissues: application in healthy, fibrillated and osteoarthritic cartilage. Matrix Biol. 1997;16(5):233-43.
174. Happonen KE, Saxne T, Aspberg A, Morgelin M, Heinegard D, Blom AM. Regulation of complement by cartilage oligomeric matrix protein allows for a novel molecular diagnostic principle in rheumatoid arthritis. Arthritis Rheum. 2010;62(12):3574-83.
175. Berenbaum F. Signaling transduction: target in osteoarthritis. Curr Opin Rheumatol. 2004;16(5):616-22.
176. Bougault C, Gosset M, Houard X, Salvat C, Godmann L, Pap T, et al. Stress-induced cartilage degradation does not depend on the NLRP3 inflammasome in human osteoarthritis and mouse models. Arthritis Rheum. 2012;64(12):3972-81.

177. Dossumbekova A, Anghelina M, Madhavan S, He L, Quan N, Knobloch T, et al. Biomechanical signals inhibit IKK activity to attenuate NF-kappaB transcription activity in inflamed chondrocytes. Arthritis Rheum. 2007;56(10):3284-96.
178. Fanning PJ, Emkey G, Smith RJ, Grodzinsky AJ, Szasz N, Trippel SB. Mechanical regulation of mitogen-activated protein kinase signaling in articular cartilage. J Biol Chem. 2003;278(51):50940-8.
179. Del Carlo M, Jr., Loeser RF. Cell death in osteoarthritis. Curr Rheumatol Rep. 2008;10(1):37-42.
180. Carames B, Taniguchi N, Otsuki S, Blanco FJ, Lotz M. Autophagy is a protective mechanism in normal cartilage, and its aging-related loss is linked with cell death and osteoarthritis. Arthritis Rheum. 2010;62(3):791-801.
181. Scanzello CR, McKeon B, Swaim BH, DiCarlo E, Asomugha EU, Kanda V, et al. Synovial inflammation in patients undergoing arthroscopic meniscectomy: molecular characterization and relationship to symptoms. Arthritis Rheum. 2011;63(2):391-400.
182. Midwood K, Sacre S, Piccinini AM, Inglis J, Trebaul A, Chan E, et al. Tenascin-C is an endogenous activator of Toll-like receptor 4 that is essential for maintaining inflammation in arthritic joint disease. Nat Med. 2009;15(7):774-80.
183. Sofat N. Analysing the role of endogenous matrix molecules in the development of osteoarthritis. Int J Exp Pathol. 2009;90(5):463-79.
184. Heinola T, Kouri VP, Clarijs P, Ciferska H, Sukura A, Salo J, et al. High mobility group box-1 (HMGB-1) in osteoarthritic cartilage. Clin Exp Rheumatol. 2010;28(4):511-8.
185. Lees S, Golub SB, Last K, Zeng W, Jackson DC, Sutton P, et al. Bioactivity in an Aggrecan 32-mer Fragment Is Mediated via Toll-like Receptor 2. Arthritis Rheumatol. 2015;67(5):1240-9.
186. Liu-Bryan R, Terkeltaub R. Chondrocyte innate immune myeloid differentiation factor 88-dependent signaling drives procatabolic effects of the endogenous Toll-like receptor 2/Toll-like receptor 4 ligands low molecular weight hyaluronan and high mobility group box chromosomal protein 1 in mice. Arthritis Rheum. 2010;62(7):2004-12.
187. Koskinen A, Juslin S, Nieminen R, Moilanen T, Vuolteenaho K, Moilanen E. Adiponectin associates with markers of cartilage degradation in osteoarthritis and induces production of proinflammatory and catabolic factors through mitogen-activated protein kinase pathways. Arthritis Res Ther. 2011;13(6):R184.
188. Koskinen A, Vuolteenaho K, Nieminen R, Moilanen T, Moilanen E. Leptin enhances MMP-1, MMP-3 and MMP-13 production in human osteoarthritic cartilage and correlates with MMP-1 and MMP-3 in synovial fluid from OA patients. Clin Exp Rheumatol. 2011;29(1):57-64.
189. Jacques C, Holzenberger M, Mladenovic Z, Salvat C, Pecchi E, Berenbaum F, et al. Proinflammatory actions of visfatin/nicotinamide phosphoribosyltransferase (Nampt) involve regulation of insulin signaling pathway and Nampt enzymatic activity. J Biol Chem. 2012;287(18):15100-8.
190. Bekkers JE, Creemers LB, Dhert WJ, Saris DB. Diagnostic Modalities for Diseased Articular Cartilage-From Defect to Degeneration: A Review. Cartilage. 2010;1(3):157-64.

191. Kellgren JH, Lawrence JS. Radiological assessment of osteo-arthrosis. Ann Rheum Dis. 1957;16(4):494-502.
192. Altman RD, Gold GE. Atlas of individual radiographic features in osteoarthritis, revised. Osteoarthritis Cartilage. 2007;15 Suppl A:A1-56.
193. Wakefield RJ, Gibbon WW, Emery P. The current status of ultrasonography in rheumatology. Rheumatology (Oxford). 1999;38(3):195-8.
194. Bijlsma JW, Berenbaum F, Lafeber FP. Osteoarthritis: an update with relevance for clinical practice. Lancet. 2011;377(9783):2115-26.
195. Abadie E, Ethgen D, Avouac B, Bouvenot G, Branco J, Bruyere O, et al. Recommendations for the use of new methods to assess the efficacy of disease-modifying drugs in the treatment of osteoarthritis. Osteoarthritis Cartilage. 2004;12(4):263-8.
196. Collins DH, Mc ET. Sulphate (35SO4) uptake by chondrocytes in relation to histological changes in osteoarthritic human articular cartilage. Ann Rheum Dis. 1960;19:318-30.
197. Pritzker KP, Gay S, Jimenez SA, Ostergaard K, Pelletier JP, Revell PA, et al. Osteoarthritis cartilage histopathology: grading and staging. Osteoarthritis Cartilage. 2006;14(1):13-29.
198. Panoutsopoulou K, Zeggini E. Advances in osteoarthritis genetics. Journal of medical genetics. 2013;50(11):715-24.
199. van Meurs JB, Uitterlinden AG. Osteoarthritis year 2012 in review: genetics and genomics. Osteoarthritis Cartilage. 2012;20(12):1470-6.
200. Loughlin J. Genetic indicators and susceptibility to osteoarthritis. Br J Sports Med. 2011;45(4):278-82.
201. Stecher RM. Heberden's nodes; a clinical description of osteo-arthritis of the finger joints. Ann Rheum Dis. 1955;14(1):1-10.
202. Kellgren JH, Lawrence JS, Bier F. Genetic Factors in Generalized Osteo-Arthrosis. Ann Rheum Dis. 1963;22:237-55.
203. Felson DT, Couropmitree NN, Chaisson CE, Hannan MT, Zhang Y, McAlindon TE, et al. Evidence for a Mendelian gene in a segregation analysis of generalized radiographic osteoarthritis: the Framingham Study. Arthritis Rheum. 1998;41(6):1064-71.
204. Hirsch R, Lethbridge-Cejku M, Hanson R, Scott WW, Jr., Reichle R, Plato CC, et al. Familial aggregation of osteoarthritis: data from the Baltimore Longitudinal Study on Aging. Arthritis Rheum. 1998;41(7):1227-32.
205. Chitnavis J, Sinsheimer JS, Clipsham K, Loughlin J, Sykes B, Burge PD, et al. Genetic influences in end-stage osteoarthritis. Sibling risks of hip and knee replacement for idiopathic osteoarthritis. J Bone Joint Surg Br. 1997;79(4):660-4.
206. Lanyon P, Muir K, Doherty S, Doherty M. Assessment of a genetic contribution to osteoarthritis of the hip: sibling study. Bmj. 2000;321(7270):1179-83.
207. Neame RL, Muir K, Doherty S, Doherty M. Genetic risk of knee osteoarthritis: a sibling study. Ann Rheum Dis. 2004;63(9):1022-7.
208. Lindberg H. Prevalence of primary coxarthrosis in siblings of patients with primary coxarthrosis. Clinical orthopaedics and related research. 1986(203):273-5.

209. Ingvarsson T, Stefansson SE, Hallgrimsdottir IB, Frigge ML, Jonsson H, Jr., Gulcher J, et al. The inheritance of hip osteoarthritis in Iceland. Arthritis Rheum. 2000;43(12):2785-92.
210. Spector TD, Cicuttini F, Baker J, Loughlin J, Hart D. Genetic influences on osteoarthritis in women: a twin study. Bmj. 1996;312(7036):940-3.
211. MacGregor AJ, Antoniades L, Matson M, Andrew T, Spector TD. The genetic contribution to radiographic hip osteoarthritis in women: results of a classic twin study. Arthritis Rheum. 2000;43(11):2410-6.
212. Reynard LN, Loughlin J. The genetics and functional analysis of primary osteoarthritis susceptibility. Expert Rev Mol Med. 2013;15:e2.
213. Miyamoto Y, Mabuchi A, Shi D, Kubo T, Takatori Y, Saito S, et al. A functional polymorphism in the 5' UTR of GDF5 is associated with susceptibility to osteoarthritis. Nat Genet. 2007;39(4):529-33.
214. Gene. http://www.ncbi.nlm.nih.gov/gene/ [Internet]. 2016.
215. Chapman K, Takahashi A, Meulenbelt I, Watson C, Rodriguez-Lopez J, Egli R, et al. A meta-analysis of European and Asian cohorts reveals a global role of a functional SNP in the 5' UTR of GDF5 with osteoarthritis susceptibility. Hum Mol Genet. 2008;17(10):1497-504.
216. Valdes AM, Evangelou E, Kerkhof HJ, Tamm A, Doherty SA, Kisand K, et al. The GDF5 rs143383 polymorphism is associated with osteoarthritis of the knee with genome-wide statistical significance. Ann Rheum Dis. 2011;70(5):873-5.
217. Evangelou E, Chapman K, Meulenbelt I, Karassa FB, Loughlin J, Carr A, et al. Large-scale analysis of association between GDF5 and FRZB variants and osteoarthritis of the hip, knee, and hand. Arthritis Rheum. 2009;60(6):1710-21.
218. Valdes AM, Evangelou E, Kerkhof HJ, Tamm A, Doherty SA, Kisand K, et al. The GDF5 rs143383 polymorphism is associated with osteoarthritis of the knee with genome-wide statistical significance. Ann Rheum Dis. 2011;70(5):873-5.
219. Syddall CM, Reynard LN, Young DA, Loughlin J. The identification of trans-acting factors that regulate the expression of GDF5 via the osteoarthritis susceptibility SNP rs143383. PLoS Genet. 2013;9(6):e1003557.
220. Meulenbelt I, Min JL, Bos S, Riyazi N, Houwing-Duistermaat JJ, van der Wijk HJ, et al. Identification of DIO2 as a new susceptibility locus for symptomatic osteoarthritis. Hum Mol Genet. 2008;17(12):1867-75.
221. Bos SD, Bovee JV, Duijnisveld BJ, Raine EV, van Dalen WJ, Ramos YF, et al. Increased type II deiodinase protein in OA-affected cartilage and allelic imbalance of OA risk polymorphism rs225014 at DIO2 in human OA joint tissues. Ann Rheum Dis. 2012;71(7):1254-8.
222. Bomer N, den Hollander W, Ramos YF, Bos SD, van der Breggen R, Lakenberg N, et al. Underlying molecular mechanisms of DIO2 susceptibility in symptomatic osteoarthritis. Ann Rheum Dis. 2015;74(8):1571-9.
223. van de Laar IM, Oldenburg RA, Pals G, Roos-Hesselink JW, de Graaf BM, Verhagen JM, et al. Mutations in SMAD3 cause a syndromic form of aortic aneurysms and dissections with early-onset osteoarthritis. Nat Genet. 2011;43(2):121-6.
224. McCarthy MI, Abecasis GR, Cardon LR, Goldstein DB, Little J, Ioannidis JP, et al. Genome-wide association studies for complex traits: consensus, uncertainty and challenges. Nat Rev Genet. 2008;9(5):356-69.

225. Genomes Project C, Abecasis GR, Altshuler D, Auton A, Brooks LD, Durbin RM, et al. A map of human genome variation from population-scale sequencing. Nature. 2010;467(7319):1061-73.
226. Ioannidis JP, Thomas G, Daly MJ. Validating, augmenting and refining genome-wide association signals. Nat Rev Genet. 2009;10(5):318-29.
227. Gonzalez A. Osteoarthritis year 2013 in review: genetics and genomics. Osteoarthritis Cartilage. 2013;21(10):1443-51.
228. Panoutsopoulou K, Southam L, Elliott KS, Wrayner N, Zhai G, Beazley C, et al. Insights into the genetic architecture of osteoarthritis from stage 1 of the arcOGEN study. Ann Rheum Dis. 2011;70(5):864-7.
229. Zeggini E, Panoutsopoulou K, Southam L, Rayner N, Day-Williams A, Lopes M, et al. Identification of new susceptibility loci for osteoarthritis (arcOGEN): a genome-wide association study. Lancet. 2012;380(9844):815-23.
230. Karlsson MK, Karlsson C, Magnusson H, Coster M, von Schewelov T, Nilsson JA, et al. Individuals with primary osteoarthritis have different phenotypes depending on the affected joint - a case control study from southern sweden including 514 participants. Open Orthop J. 2014;8:450-6.
231. Wilson PM, Fryer RH, Fang Y, Hatten ME. Astn2, a novel member of the astrotactin gene family, regulates the trafficking of ASTN1 during glial-guided neuronal migration. J Neurosci. 2010;30(25):8529-40.
232. GLT8D1 glycostyltransferase 8 domain containing 1 [Homo sapiens (human)]. http://http://www.ncbi.nlm.nih.gov/gene/55830 [Internet]. 2016.
233. Homo sapiens guanine nucleotide binding protein-like 3 (nucleolar) (GNL3) transcript variant 1, mRNA. http://www.ncbi.nlm.nih.gov/nuccore/NM_014366.4 [Internet]. 2016.
234. Tsai RY, McKay RD. A multistep, GTP-driven mechanism controlling the dynamic cycling of nucleostemin. J Cell Biol. 2005;168(2):179-84.
235. Izu Y, Sun M, Zwolanek D, Veit G, Williams V, Cha B, et al. Type XII collagen regulates osteoblast polarity and communication during bone formation. J Cell Biol. 2011;193(6):1115-30.
236. Pelosi M, Lazzarano S, Thoms BL, Murphy CL. Parathyroid hormone-related protein is induced by hypoxia and promotes expression of the differentiated phenotype of human articular chondrocytes. Clin Sci (Lond). 2013;125(10):461-70.
237. Karlsson C, Dehne T, Lindahl A, Brittberg M, Pruss A, Sittinger M, et al. Genome-wide expression profiling reveals new candidate genes associated with osteoarthritis. Osteoarthritis Cartilage. 2010;18(4):581-92.
238. Kluppel M, Wight TN, Chan C, Hinek A, Wrana JL. Maintenance of chondroitin sulfation balance by chondroitin-4-sulfotransferase 1 is required for chondrocyte development and growth factor signaling during cartilage morphogenesis. Development. 2005;132(17):3989-4003.
239. Mills AA, Zheng B, Wang XJ, Vogel H, Roop DR, Bradley A. p63 is a p53 homologue required for limb and epidermal morphogenesis. Nature. 1999;398(6729):708-13.
240. Yang A, Schweitzer R, Sun D, Kaghad M, Walker N, Bronson RT, et al. p63 is essential for regenerative proliferation in limb, craniofacial and epithelial development. Nature. 1999;398(6729):714-8.

241. Lohmander LS, Gerhardsson de Verdier M, Rollof J, Nilsson PM, Engstrom G. Incidence of severe knee and hip osteoarthritis in relation to different measures of body mass: a population-based prospective cohort study. Ann Rheum Dis. 2009;68(4):490-6.
242. Stein GS, Lian JB, van Wijnen AJ, Stein JL, Montecino M, Javed A, et al. Runx2 control of organization, assembly and activity of the regulatory machinery for skeletal gene expression. Oncogene. 2004;23(24):4315-29.
243. Miyamoto Y, Shi D, Nakajima M, Ozaki K, Sudo A, Kotani A, et al. Common variants in DVWA on chromosome 3p24.3 are associated with susceptibility to knee osteoarthritis. Nat Genet. 2008;40(8):994-8.
244. Meulenbelt I, Chapman K, Dieguez-Gonzalez R, Shi D, Tsezou A, Dai J, et al. Large replication study and meta-analyses of DVWA as an osteoarthritis susceptibility locus in European and Asian populations. Hum Mol Genet. 2009;18(8):1518-23.
245. Nakajima M, Takahashi A, Kou I, Rodriguez-Fontenla C, Gomez-Reino JJ, Furuichi T, et al. New sequence variants in HLA class II/III region associated with susceptibility to knee osteoarthritis identified by genome-wide association study. PLoS One. 2010;5(3):e9723.
246. Kerkhof HJ, Lories RJ, Meulenbelt I, Jonsdottir I, Valdes AM, Arp P, et al. A genome-wide association study identifies an osteoarthritis susceptibility locus on chromosome 7q22. Arthritis Rheum. 2010;62(2):499-510.
247. Day-Williams AG, Southam L, Panoutsopoulou K, Rayner NW, Esko T, Estrada K, et al. A variant in MCF2L is associated with osteoarthritis. Am J Hum Genet. 2011;89(3):446-50.
248. Lane NE, Schnitzer TJ, Birbara CA, Mokhtarani M, Shelton DL, Smith MD, et al. Tanezumab for the treatment of pain from osteoarthritis of the knee. N Engl J Med. 2010;363(16):1521-31.
249. Evangelou E, Kerkhof HJ, Styrkarsdottir U, Ntzani EE, Bos SD, Esko T, et al. A meta-analysis of genome-wide association studies identifies novel variants associated with osteoarthritis of the hip. Ann Rheum Dis. 2014;73(12):2130-6.
250. Otsuki S, Taniguchi N, Grogan SP, D'Lima D, Kinoshita M, Lotz M. Expression of novel extracellular sulfatases Sulf-1 and Sulf-2 in normal and osteoarthritic articular cartilage. Arthritis Res Ther. 2008;10(3):R61.
251. Styrkarsdottir U, Thorleifsson G, Helgadottir HT, Bomer N, Metrustry S, Bierma-Zeinstra S, et al. Severe osteoarthritis of the hand associates with common variants within the ALDH1A2 gene and with rare variants at 1p31. Nat Genet. 2014;46(5):498-502.
252. Evans DS, Cailotto F, Parimi N, Valdes AM, Castano-Betancourt MC, Liu Y, et al. Genome-wide association and functional studies identify a role for IGFBP3 in hip osteoarthritis. Ann Rheum Dis. 2015;74(10):1861-7.
253. Evangelou E, Valdes AM, Castano-Betancourt MC, Doherty M, Doherty S, Esko T, et al. The DOT1L rs12982744 polymorphism is associated with osteoarthritis of the hip with genome-wide statistical significance in males. Ann Rheum Dis. 2013;72(7):1264-5.
254. Castano Betancourt MC, Cailotto F, Kerkhof HJ, Cornelis FM, Doherty SA, Hart DJ, et al. Genome-wide association and functional studies identify the DOT1L gene to be involved in cartilage thickness and hip osteoarthritis. Proc Natl Acad Sci U S A. 2012;109(21):8218-23.

255. Rodriguez-Fontenla C, Calaza M, Evangelou E, Valdes AM, Arden N, Blanco FJ, et al. Assessment of osteoarthritis candidate genes in a meta-analysis of nine genome-wide association studies. Arthritis Rheumatol. 2014;66(4):940-9.
256. Robin NH, Moran RT, Ala-Kokko L. Stickler Syndrome. In: Pagon RA, Adam MP, Ardinger HH, Wallace SE, Amemiya A, Bean LJH, et al., editors. GeneReviews(R). Seattle (WA)1993.
257. Janeczko L, Janeczko M, Chrzanowski R, Zielinski G. The role of polymorphisms of genes encoding collagen IX and XI in lumbar disc disease. Neurol Neurochir Pol. 2014;48(1):60-2.
258. Bekdache GN, Begam MA, Chedid F, Al-Gazali L, Mirghani H. Fibrochondrogenesis: prenatal diagnosis and outcome. J Obstet Gynaecol. 2013;33(7):663-8.
259. Stempel J, Fritsch H, Pfaller K, Blumer MJ. Development of articular cartilage and the metaphyseal growth plate: the localization of TRAP cells, VEGF, and endostatin. J Anat. 2011;218(6):608-18.
260. Ludin A, Sela JJ, Schroeder A, Samuni Y, Nitzan DW, Amir G. Injection of vascular endothelial growth factor into knee joints induces osteoarthritis in mice. Osteoarthritis Cartilage. 2013;21(3):491-7.
261. Reynard LN, Loughlin J. Insights from human genetic studies into the pathways involved in osteoarthritis. Nat Rev Rheumatol. 2013;9(10):573-83.
262. Rodriguez-Fontenla C, Gonzalez A. Genetics of osteoarthritis. Reumatol Clin. 2015;11(1):33-40.
263. Chapman K, Valdes AM. Genetic factors in OA pathogenesis. Bone. 2012;51(2):258-64.
264. McCarroll SA, Altshuler DM. Copy-number variation and association studies of human disease. Nat Genet. 2007;39(7 Suppl):S37-42.
265. Freilinger T, Anttila V, de Vries B, Malik R, Kallela M, Terwindt GM, et al. Genome-wide association analysis identifies susceptibility loci for migraine without aura. Nat Genet. 2012;44(7):777-82.
266. Bis JC, DeCarli C, Smith AV, van der Lijn F, Crivello F, Fornage M, et al. Common variants at 12q14 and 12q24 are associated with hippocampal volume. Nat Genet. 2012;44(5):545-51.
267. Wang KS, Liu XF, Aragam N. A genome-wide meta-analysis identifies novel loci associated with schizophrenia and bipolar disorder. Schizophr Res. 2010;124(1-3):192-9.
268. Lesch KP, Timmesfeld N, Renner TJ, Halperin R, Roser C, Nguyen TT, et al. Molecular genetics of adult ADHD: converging evidence from genome-wide association and extended pedigree linkage studies. Journal of neural transmission. 2008;115(11):1573-85.
269. Glessner JT, Wang K, Cai G, Korvatska O, Kim CE, Wood S, et al. Autism genome-wide copy number variation reveals ubiquitin and neuronal genes. Nature. 2009;459(7246):569-73.
270. Lionel AC, Tammimies K, Vaags AK, Rosenfeld JA, Ahn JW, Merico D, et al. Disruption of the ASTN2/TRIM32 locus at 9q33.1 is a risk factor in males for autism spectrum disorders, ADHD and other neurodevelopmental phenotypes. Hum Mol Genet. 2014;23(10):2752-68.

271. Wang KS, Tonarelli S, Luo X, Wang L, Su B, Zuo L, et al. Polymorphisms within ASTN2 gene are associated with age at onset of Alzheimer's disease. J Neural Transm (Vienna). 2015;122(5):701-8.
272. Conover CA, Bale LK, Overgaard MT, Johnstone EW, Laursen UH, Fuchtbauer EM, et al. Metalloproteinase pregnancy-associated plasma protein A is a critical growth regulatory factor during fetal development. Development. 2004;131(5):1187-94.
273. Mason EJ, Grell JA, Wan J, Cohen P, Conover CA. Insulin-like growth factor (IGF)-I and IGF-II contribute differentially to the phenotype of pregnancy associated plasma protein-A knock-out mice. Growth Horm IGF Res. 2011;21(5):243-7.
274. Phang D, Rehage M, Bonafede B, Hou D, Xing W, Mohan S, et al. Inactivation of insulin-like-growth factors diminished the anabolic effects of pregnancy-associated plasma protein-A (PAPP-A) on bone in mice. Growth Horm IGF Res. 2010;20(3):192-200.
275. Conover CA, Durham SK, Zapf J, Masiarz FR, Kiefer MC. Cleavage analysis of insulin-like growth factor (IGF)-dependent IGF-binding protein-4 proteolysis and expression of protease-resistant IGF-binding protein-4 mutants. J Biol Chem. 1995;270(9):4395-400.
276. Bayes-Genis A, Schwartz RS, Lewis DA, Overgaard MT, Christiansen M, Oxvig C, et al. Insulin-like growth factor binding protein-4 protease produced by smooth muscle cells increases in the coronary artery after angioplasty. Arterioscler Thromb Vasc Biol. 2001;21(3):335-41.
277. Conover CA, Faessen GF, Ilg KE, Chandrasekher YA, Christiansen M, Overgaard MT, et al. Pregnancy-associated plasma protein-a is the insulin-like growth factor binding protein-4 protease secreted by human ovarian granulosa cells and is a marker of dominant follicle selection and the corpus luteum. Endocrinology. 2001;142(5):2155.
278. Pennings JL, Kuc S, Rodenburg W, Koster MP, Schielen PC, de Vries A. Integrative data mining to identify novel candidate serum biomarkers for pre-eclampsia screening. Prenat Diagn. 2011;31(12):1153-9.
279. Christians JK, de Zwaan DR, Fung SH. Pregnancy associated plasma protein A2 (PAPP-A2) affects bone size and shape and contributes to natural variation in postnatal growth in mice. PLoS One. 2013;8(2):e56260.
280. Yokota T, Mishra M, Akatsu H, Tani Y, Miyauchi T, Yamamoto T, et al. Brain site-specific gene expression analysis in Alzheimer's disease patients. Eur J Clin Invest. 2006;36(11):820-30.
281. Wulczyn FG, Cuevas E, Franzoni E, Rybak A. MiRNA need a TRIM regulation of miRNA activity by Trim-NHL proteins. Advances in experimental medicine and biology. 2010;700:85-105.
282. Barlow PN, Luisi B, Milner A, Elliott M, Everett R. Structure of the C3HC4 domain by 1H-nuclear magnetic resonance spectroscopy. A new structural class of zinc-finger. Journal of molecular biology. 1994;237(2):201-11.
283. Koliopoulos MG, Esposito D, Christodoulou E, Taylor IA, Rittinger K. Functional role of TRIM E3 ligase oligomerization and regulation of catalytic activity. EMBO J. 2016;35(11):1204-18.

284. Micale L, Chaignat E, Fusco C, Reymond A, Merla G. The tripartite motif: structure and function. Advances in experimental medicine and biology. 2012;770:11-25.
285. Massiah MA, Simmons BN, Short KM, Cox TC. Solution structure of the RBCC/TRIM B-box1 domain of human MID1: B-box with a RING. Journal of molecular biology. 2006;358(2):532-45.
286. Tao H, Simmons BN, Singireddy S, Jakkidi M, Short KM, Cox TC, et al. Structure of the MID1 tandem B-boxes reveals an interaction reminiscent of intermolecular ring heterodimers. Biochemistry. 2008;47(8):2450-7.
287. Loedige I, Gaidatzis D, Sack R, Meister G, Filipowicz W. The mammalian TRIM-NHL protein TRIM71/LIN-41 is a repressor of mRNA function. Nucleic Acids Res. 2013;41(1):518-32.
288. Loedige I, Stotz M, Qamar S, Kramer K, Hennig J, Schubert T, et al. The NHL domain of BRAT is an RNA-binding domain that directly contacts the hunchback mRNA for regulation. Genes Dev. 2014;28(7):749-64.
289. Kudryashova E, Kudryashov D, Kramerova I, Spencer MJ. Trim32 is a ubiquitin ligase mutated in limb girdle muscular dystrophy type 2H that binds to skeletal muscle myosin and ubiquitinates actin. Journal of molecular biology. 2005;354(2):413-24.
290. Chiang AP, Beck JS, Yen HJ, Tayeh MK, Scheetz TE, Swiderski RE, et al. Homozygosity mapping with SNP arrays identifies TRIM32, an E3 ubiquitin ligase, as a Bardet-Biedl syndrome gene (BBS11). Proc Natl Acad Sci U S A. 2006;103(16):6287-92.
291. Gascue C, Tan PL, Cardenas-Rodriguez M, Libisch G, Fernandez-Calero T, Liu YP, et al. Direct role of Bardet-Biedl syndrome proteins in transcriptional regulation. Journal of cell science. 2012;125(Pt 2):362-75.
292. Forsythe E, Beales PL. Bardet-Biedl syndrome. European journal of human genetics : EJHG. 2013;21(1):8-13.
293. Kaushik AP, Martin JA, Zhang Q, Sheffield VC, Morcuende JA. Cartilage abnormalities associated with defects of chondrocytic primary cilia in Bardet-Biedl syndrome mutant mice. J Orthop Res. 2009;27(8):1093-9.
294. Song B, Haycraft CJ, Seo HS, Yoder BK, Serra R. Development of the post-natal growth plate requires intraflagellar transport proteins. Developmental biology. 2007;305(1):202-16.
295. Kudryashova E, Wu J, Havton LA, Spencer MJ. Deficiency of the E3 ubiquitin ligase TRIM32 in mice leads to a myopathy with a neurogenic component. Hum Mol Genet. 2009;18(7):1353-67.
296. Saccone V, Palmieri M, Passamano L, Piluso G, Meroni G, Politano L, et al. Mutations that impair interaction properties of TRIM32 associated with limb-girdle muscular dystrophy 2H. Hum Mutat. 2008;29(2):240-7.
297. Kudryashova E, Struyk A, Mokhonova E, Cannon SC, Spencer MJ. The common missense mutation D489N in TRIM32 causing limb girdle muscular dystrophy 2H leads to loss of the mutated protein in knock-in mice resulting in a Trim32-null phenotype. Hum Mol Genet. 2011;20(20):3925-32.
298. Nicklas S, Otto A, Wu X, Miller P, Stelzer S, Wen Y, et al. TRIM32 regulates skeletal muscle stem cell differentiation and is necessary for normal adult muscle regeneration. PLoS One. 2012;7(1):e30445.

299. Albor A, El-Hizawi S, Horn EJ, Laederich M, Frosk P, Wrogemann K, et al. The interaction of Piasy with Trim32, an E3-ubiquitin ligase mutated in limb-girdle muscular dystrophy type 2H, promotes Piasy degradation and regulates UVB-induced keratinocyte apoptosis through NFkappaB. J Biol Chem. 2006;281(35):25850-66.
300. Ryu YS, Lee Y, Lee KW, Hwang CY, Maeng JS, Kim JH, et al. TRIM32 protein sensitizes cells to tumor necrosis factor (TNFalpha)-induced apoptosis via its RING domain-dependent E3 ligase activity against X-linked inhibitor of apoptosis (XIAP). J Biol Chem. 2011;286(29):25729-38.
301. Schwamborn JC, Berezikov E, Knoblich JA. The TRIM-NHL protein TRIM32 activates microRNAs and prevents self-renewal in mouse neural progenitors. Cell. 2009;136(5):913-25.
302. Kosodo Y, Huttner WB. Basal process and cell divisions of neural progenitors in the developing brain. Development, growth & differentiation. 2009;51(3):251-61.
303. Kuehn EW, Walz G, Benzing T. Von hippel-lindau: a tumor suppressor links microtubules to ciliogenesis and cancer development. Cancer research. 2007;67(10):4537-40.
304. Le LT, Swingler TE, Clark IM. Review: the role of microRNAs in osteoarthritis and chondrogenesis. Arthritis Rheum. 2013;65(8):1963-74.
305. Feil R, Fraga MF. Epigenetics and the environment: emerging patterns and implications. Nat Rev Genet. 2011;13(2):97-109.
306. Dominguez-Salas P, Moore SE, Baker MS, Bergen AW, Cox SE, Dyer RA, et al. Maternal nutrition at conception modulates DNA methylation of human metastable epialleles. Nat Commun. 2014;5:3746.
307. Rakyan VK, Down TA, Maslau S, Andrew T, Yang TP, Beyan H, et al. Human aging-associated DNA hypermethylation occurs preferentially at bivalent chromatin domains. Genome Res. 2010;20(4):434-9.
308. Houseman EA, Accomando WP, Koestler DC, Christensen BC, Marsit CJ, Nelson HH, et al. DNA methylation arrays as surrogate measures of cell mixture distribution. BMC Bioinformatics. 2012;13:86.
309. Sesselmann S, Soder S, Voigt R, Haag J, Grogan SP, Aigner T. DNA methylation is not responsible for p21WAF1/CIP1 down-regulation in osteoarthritic chondrocytes. Osteoarthritis Cartilage. 2009;17(4):507-12.
310. Delgado-Calle J, Fernandez AF, Sainz J, Zarrabeitia MT, Sanudo C, Garcia-Renedo R, et al. Genome-wide profiling of bone reveals differentially methylated regions in osteoporosis and osteoarthritis. Arthritis Rheum. 2013;65(1):197-205.
311. Fernandez-Tajes J, Soto-Hermida A, Vazquez-Mosquera ME, Cortes-Pereira E, Mosquera A, Fernandez-Moreno M, et al. Genome-wide DNA methylation analysis of articular chondrocytes reveals a cluster of osteoarthritic patients. Ann Rheum Dis. 2014;73(4):668-77.
312. Rushton MD, Reynard LN, Barter MJ, Refaie R, Rankin KS, Young DA, et al. Characterization of the cartilage DNA methylome in knee and hip osteoarthritis. Arthritis Rheumatol. 2014;66(9):2450-60.
313. den Hollander W, Ramos YF, Bos SD, Bomer N, van der Breggen R, Lakenberg N, et al. Knee and hip articular cartilage have distinct epigenomic landscapes: implications for future cartilage regeneration approaches. Ann Rheum Dis. 2014;73(12):2208-12.

314. Fernandez MP, Young MF, Sobel ME. Methylation of type II and type I collagen genes in differentiated and dedifferentiated chondrocytes. J Biol Chem. 1985;260(4):2374-8.
315. Hashimoto K, Otero M, Imagawa K, de Andres MC, Coico JM, Roach HI, et al. Regulated transcription of human matrix metalloproteinase 13 (MMP13) and interleukin-1beta (IL1B) genes in chondrocytes depends on methylation of specific proximal promoter CpG sites. J Biol Chem. 2013;288(14):10061-72.
316. de Andres MC, Imagawa K, Hashimoto K, Gonzalez A, Roach HI, Goldring MB, et al. Loss of methylation in CpG sites in the NF-kappaB enhancer elements of inducible nitric oxide synthase is responsible for gene induction in human articular chondrocytes. Arthritis Rheum. 2013;65(3):732-42.
317. Kim KI, Park YS, Im GI. Changes in the epigenetic status of the SOX-9 promoter in human osteoarthritic cartilage. J Bone Miner Res. 2013;28(5):1050-60.
318. Iliopoulos D, Malizos KN, Tsezou A. Epigenetic regulation of leptin affects MMP-13 expression in osteoarthritic chondrocytes: possible molecular target for osteoarthritis therapeutic intervention. Ann Rheum Dis. 2007;66(12):1616-21.
319. Reynard LN, Bui C, Canty-Laird EG, Young DA, Loughlin J. Expression of the osteoarthritis-associated gene GDF5 is modulated epigenetically by DNA methylation. Hum Mol Genet. 2011;20(17):3450-60.
320. Reynard LN, Bui C, Syddall CM, Loughlin J. CpG methylation regulates allelic expression of GDF5 by modulating binding of SP1 and SP3 repressor proteins to the osteoarthritis susceptibility SNP rs143383. Hum Genet. 2014;133(8):1059-73.
321. Taylor SE, Smeriglio P, Dhulipala L, Rath M, Bhutani N. A global increase in 5-hydroxymethylcytosine levels marks osteoarthritic chondrocytes. Arthritis Rheumatol. 2014;66(1):90-100.
322. Zimmermann P, Boeuf S, Dickhut A, Boehmer S, Olek S, Richter W. Correlation of COL10A1 induction during chondrogenesis of mesenchymal stem cells with demethylation of two CpG sites in the COL10A1 promoter. Arthritis Rheum. 2008;58(9):2743-53.
323. Poschl E, Fidler A, Schmidt B, Kallipolitou A, Schmid E, Aigner T. DNA methylation is not likely to be responsible for aggrecan down regulation in aged or osteoarthritic cartilage. Ann Rheum Dis. 2005;64(3):477-80.
324. Roach HI, Yamada N, Cheung KS, Tilley S, Clarke NM, Oreffo RO, et al. Association between the abnormal expression of matrix-degrading enzymes by human osteoarthritic chondrocytes and demethylation of specific CpG sites in the promoter regions. Arthritis Rheum. 2005;52(10):3110-24.
325. Hashimoto K, Oreffo RO, Gibson MB, Goldring MB, Roach HI. DNA demethylation at specific CpG sites in the IL1B promoter in response to inflammatory cytokines in human articular chondrocytes. Arthritis Rheum. 2009;60(11):3303-13.
326. de Andres MC, Imagawa K, Hashimoto K, Gonzalez A, Goldring MB, Roach HI, et al. Suppressors of cytokine signalling (SOCS) are reduced in osteoarthritis. Biochem Biophys Res Commun. 2011;407(1):54-9.
327. Scott JL, Gabrielides C, Davidson RK, Swingler TE, Clark IM, Wallis GA, et al. Superoxide dismutase downregulation in osteoarthritis progression and end-stage disease. Ann Rheum Dis. 2010;69(8):1502-10.

328. Fabbri M, Garzon R, Cimmino A, Liu Z, Zanesi N, Callegari E, et al. MicroRNA-29 family reverts aberrant methylation in lung cancer by targeting DNA methyltransferases 3A and 3B. Proc Natl Acad Sci U S A. 2007;104(40):15805-10.
329. Kobayashi T, Lu J, Cobb BS, Rodda SJ, McMahon AP, Schipani E, et al. Dicer-dependent pathways regulate chondrocyte proliferation and differentiation. Proc Natl Acad Sci U S A. 2008;105(6):1949-54.
330. Iliopoulos D, Malizos KN, Oikonomou P, Tsezou A. Integrative microRNA and proteomic approaches identify novel osteoarthritis genes and their collaborative metabolic and inflammatory networks. PLoS One. 2008;3(11):e3740.
331. Jones SW, Watkins G, Le Good N, Roberts S, Murphy CL, Brockbank SM, et al. The identification of differentially expressed microRNA in osteoarthritic tissue that modulate the production of TNF-alpha and MMP13. Osteoarthritis Cartilage. 2009;17(4):464-72.
332. Diaz-Prado S, Cicione C, Muinos-Lopez E, Hermida-Gomez T, Oreiro N, Fernandez-Lopez C, et al. Characterization of microRNA expression profiles in normal and osteoarthritic human chondrocytes. BMC musculoskeletal disorders. 2012;13:144.
333. Miyaki S, Nakasa T, Otsuki S, Grogan SP, Higashiyama R, Inoue A, et al. MicroRNA-140 is expressed in differentiated human articular chondrocytes and modulates interleukin-1 responses. Arthritis Rheum. 2009;60(9):2723-30.
334. Swingler TE, Wheeler G, Carmont V, Elliott HR, Barter MJ, Abu-Elmagd M, et al. The expression and function of microRNAs in chondrogenesis and osteoarthritis. Arthritis Rheum. 2012;64(6):1909-19.
335. Tsezou A. Osteoarthritis year in review 2014: genetics and genomics. Osteoarthritis Cartilage. 2014;22(12):2017-24.
336. Higashiyama R, Miyaki S, Yamashita S, Yoshitaka T, Lindman G, Ito Y, et al. Correlation between MMP-13 and HDAC7 expression in human knee osteoarthritis. Mod Rheumatol. 2010;20(1):11-7.
337. Saito T, Nishida K, Furumatsu T, Yoshida A, Ozawa M, Ozaki T. Histone deacetylase inhibitors suppress mechanical stress-induced expression of RUNX-2 and ADAMTS-5 through the inhibition of the MAPK signaling pathway in cultured human chondrocytes. Osteoarthritis Cartilage. 2013;21(1):165-74.
338. Culley KL, Hui W, Barter MJ, Davidson RK, Swingler TE, Destrument AP, et al. Class I histone deacetylase inhibition modulates metalloproteinase expression and blocks cytokine-induced cartilage degradation. Arthritis Rheum. 2013;65(7):1822-30.
339. Gagarina V, Gabay O, Dvir-Ginzberg M, Lee EJ, Brady JK, Quon MJ, et al. SirT1 enhances survival of human osteoarthritic chondrocytes by repressing protein tyrosine phosphatase 1B and activating the insulin-like growth factor receptor pathway. Arthritis Rheum. 2010;62(5):1383-92.
340. Fujita N, Matsushita T, Ishida K, Kubo S, Matsumoto T, Takayama K, et al. Potential involvement of SIRT1 in the pathogenesis of osteoarthritis through the modulation of chondrocyte gene expressions. J Orthop Res. 2011;29(4):511-5.
341. Matsushita T, Sasaki H, Takayama K, Ishida K, Matsumoto T, Kubo S, et al. The overexpression of SIRT1 inhibited osteoarthritic gene expression changes induced by interleukin-1beta in human chondrocytes. J Orthop Res. 2013;31(4):531-7.

342. Moon MH, Jeong JK, Lee YJ, Seol JW, Jackson CJ, Park SY. SIRT1, a class III histone deacetylase, regulates TNF-alpha-induced inflammation in human chondrocytes. Osteoarthritis Cartilage. 2013;21(3):470-80.
343. El Mansouri FE, Chabane N, Zayed N, Kapoor M, Benderdour M, Martel-Pelletier J, et al. Contribution of H3K4 methylation by SET-1A to interleukin-1-induced cyclooxygenase 2 and inducible nitric oxide synthase expression in human osteoarthritis chondrocytes. Arthritis Rheum. 2011;63(1):168-79.
344. Rodova M, Lu Q, Li Y, Woodbury BG, Crist JD, Gardner BM, et al. Nfat1 regulates adult articular chondrocyte function through its age-dependent expression mediated by epigenetic histone methylation. J Bone Miner Res. 2011;26(8):1974-86.
345. Kevorkian L, Young DA, Darrah C, Donell ST, Shepstone L, Porter S, et al. Expression profiling of metalloproteinases and their inhibitors in cartilage. Arthritis Rheum. 2004;50(1):131-41.
346. Murata K, Yoshitomi H, Tanida S, Ishikawa M, Nishitani K, Ito H, et al. Plasma and synovial fluid microRNAs as potential biomarkers of rheumatoid arthritis and osteoarthritis. Arthritis Res Ther. 2010;12(3):R86.
347. Lokk K, Modhukur V, Rajashekar B, Martens K, Magi R, Kolde R, et al. DNA methylome profiling of human tissues identifies global and tissue-specific methylation patterns. Genome Biol. 2014;15(4):r54.
348. Loughlin J. Genetic contribution to osteoarthritis development: current state of evidence. Curr Opin Rheumatol. 2015;27(3):284-8.
349. Glasson SS. In vivo osteoarthritis target validation utilizing genetically-modified mice. Curr Drug Targets. 2007;8(2):367-76.
350. Austin CP, Battey JF, Bradley A, Bucan M, Capecchi M, Collins FS, et al. The knockout mouse project. Nat Genet. 2004;36(9):921-4.
351. Puente XS, Sanchez LM, Overall CM, Lopez-Otin C. Human and mouse proteases: a comparative genomic approach. Nat Rev Genet. 2003;4(7):544-58.
352. Zambrowicz BP, Sands AT. Knockouts model the 100 best-selling drugs--will they model the next 100? Nat Rev Drug Discov. 2003;2(1):38-51.
353. Zambrowicz BP, Turner CA, Sands AT. Predicting drug efficacy: knockouts model pipeline drugs of the pharmaceutical industry. Curr Opin Pharmacol. 2003;3(5):563-70.
354. Thysen S, Luyten FP, Lories RJ. Targets, models and challenges in osteoarthritis research. Dis Model Mech. 2015;8(1):17-30.
355. Fang H, Beier F. Mouse models of osteoarthritis: modelling risk factors and assessing outcomes. Nat Rev Rheumatol. 2014;10(7):413-21.
356. Wilhelmi G, Faust R. Suitability of the C57 black mouse as an experimental animal for the study of skeletal changes due to ageing, with special reference to osteo-arthrosis and its response to tribenoside. Pharmacology. 1976;14(4):289-96.
357. Sokoloff L, Crittenden LB, Yamamoto RS, Jay GE, Jr. The genetics of degenerative joint disease in mice. Arthritis Rheum. 1962;5:531-46.
358. Walton M. Degenerative joint disease in the mouse knee; histological observations. J Pathol. 1977;123(2):109-22.
359. Saamanen AK, Salminen HJ, Dean PB, De Crombrugghe B, Vuorio EI, Metsaranta MP. Osteoarthritis-like lesions in transgenic mice harboring a small deletion mutation in type II collagen gene. Osteoarthritis Cartilage. 2000;8(4):248-57.

360. Hu K, Xu L, Cao L, Flahiff CM, Brussiau J, Ho K, et al. Pathogenesis of osteoarthritis-like changes in the joints of mice deficient in type IX collagen. Arthritis Rheum. 2006;54(9):2891-900.
361. Neuhold LA, Killar L, Zhao W, Sung ML, Warner L, Kulik J, et al. Postnatal expression in hyaline cartilage of constitutively active human collagenase-3 (MMP-13) induces osteoarthritis in mice. J Clin Invest. 2001;107(1):35-44.
362. Blagojevic M, Jinks C, Jeffery A, Jordan KP. Risk factors for onset of osteoarthritis of the knee in older adults: a systematic review and meta-analysis. Osteoarthritis Cartilage. 2010;18(1):24-33.
363. Griffin TM, Huebner JL, Kraus VB, Yan Z, Guilak F. Induction of osteoarthritis and metabolic inflammation by a very high-fat diet in mice: effects of short-term exercise. Arthritis Rheum. 2012;64(2):443-53.
364. Griffin TM, Huebner JL, Kraus VB, Guilak F. Extreme obesity due to impaired leptin signaling in mice does not cause knee osteoarthritis. Arthritis Rheum. 2009;60(10):2935-44.
365. Christiansen BA, Anderson MJ, Lee CA, Williams JC, Yik JH, Haudenschild DR. Musculoskeletal changes following non-invasive knee injury using a novel mouse model of post-traumatic osteoarthritis. Osteoarthritis Cartilage. 2012;20(7):773-82.
366. De Souza RL, Matsuura M, Eckstein F, Rawlinson SC, Lanyon LE, Pitsillides AA. Non-invasive axial loading of mouse tibiae increases cortical bone formation and modifies trabecular organization: a new model to study cortical and cancellous compartments in a single loaded element. Bone. 2005;37(6):810-8.
367. Furman BD, Strand J, Hembree WC, Ward BD, Guilak F, Olson SA. Joint degeneration following closed intraarticular fracture in the mouse knee: a model of posttraumatic arthritis. J Orthop Res. 2007;25(5):578-92.
368. Guzman RE, Evans MG, Bove S, Morenko B, Kilgore K. Mono-iodoacetate-induced histologic changes in subchondral bone and articular cartilage of rat femorotibial joints: an animal model of osteoarthritis. Toxicol Pathol. 2003;31(6):619-24.
369. van der Kraan PM, Vitters EL, van de Putte LB, van den Berg WB. Development of osteoarthritic lesions in mice by "metabolic" and "mechanical" alterations in the knee joints. Am J Pathol. 1989;135(6):1001-14.
370. Kamekura S, Hoshi K, Shimoaka T, Chung U, Chikuda H, Yamada T, et al. Osteoarthritis development in novel experimental mouse models induced by knee joint instability. Osteoarthritis Cartilage. 2005;13(7):632-41.
371. Knights CB, Gentry C, Bevan S. Partial medial meniscectomy produces osteoarthritis pain-related behaviour in female C57BL/6 mice. Pain. 2012;153(2):281-92.
372. Glasson SS, Askew R, Sheppard B, Carito BA, Blanchet T, Ma HL, et al. Characterization of and osteoarthritis susceptibility in ADAMTS-4-knockout mice. Arthritis Rheum. 2004;50(8):2547-58.
373. Miller RE, Tran PB, Das R, Ghoreishi-Haack N, Ren D, Miller RJ, et al. CCR2 chemokine receptor signaling mediates pain in experimental osteoarthritis. Proc Natl Acad Sci U S A. 2012;109(50):20602-7.

374. Huesa C, Ortiz AC, Dunning L, McGavin L, Bennett L, McIntosh K, et al. Proteinase-activated receptor 2 modulates OA-related pain, cartilage and bone pathology. Ann Rheum Dis. 2016;75(11):1989-97.
375. Loeser RF, Olex AL, McNulty MA, Carlson CS, Callahan M, Ferguson C, et al. Disease progression and phasic changes in gene expression in a mouse model of osteoarthritis. PLoS One. 2013;8(1):e54633.
376. Ma HL, Blanchet TJ, Peluso D, Hopkins B, Morris EA, Glasson SS. Osteoarthritis severity is sex dependent in a surgical mouse model. Osteoarthritis Cartilage. 2007;15(6):695-700.
377. Loeser RF, Olex AL, McNulty MA, Carlson CS, Callahan MF, Ferguson CM, et al. Microarray analysis reveals age-related differences in gene expression during the development of osteoarthritis in mice. Arthritis Rheum. 2012;64(3):705-17.
378. Sniekers YH, Weinans H, Bierma-Zeinstra SM, van Leeuwen JP, van Osch GJ. Animal models for osteoarthritis: the effect of ovariectomy and estrogen treatment - a systematic approach. Osteoarthritis Cartilage. 2008;16(5):533-41.
379. Ahern BJ, Parvizi J, Boston R, Schaer TP. Preclinical animal models in single site cartilage defect testing: a systematic review. Osteoarthritis Cartilage. 2009;17(6):705-13.
380. Collins DH. Observations on the Pathology of Acute Rheumatism and Rheumatoid Arthritis. Ann Rheum Dis. 1939;1(1):38-45.
381. Jevsevar DS, Brown GA, Jones DL, Matzkin EG, Manner PA, Mooar P, et al. The American Academy of Orthopaedic Surgeons evidence-based guideline on: treatment of osteoarthritis of the knee, 2nd edition. The Journal of bone and joint surgery American volume. 2013;95(20):1885-6.
382. Watters JW, Cheng C, Pickarski M, Wesolowski GA, Zhuo Y, Hayami T, et al. Inverse relationship between matrix remodeling and lipid metabolism during osteoarthritis progression in the STR/Ort mouse. Arthritis Rheum. 2007;56(9):2999-3009.
383. Glasson SS, Chambers MG, Van Den Berg WB, Little CB. The OARSI histopathology initiative - recommendations for histological assessments of osteoarthritis in the mouse. Osteoarthritis Cartilage. 2010;18 Suppl 3:S17-23.
384. Botter SM, van Osch GJ, Waarsing JH, Day JS, Verhaar JA, Pols HA, et al. Quantification of subchondral bone changes in a murine osteoarthritis model using micro-CT. Biorheology. 2006;43(3-4):379-88.
385. Goebel JC, Bolbos R, Pham M, Galois L, Rengle A, Loeuille D, et al. In vivo high-resolution MRI (7T) of femoro-tibial cartilage changes in the rat anterior cruciate ligament transection model of osteoarthritis: a cross-sectional study. Rheumatology (Oxford). 2010;49(9):1654-64.
386. Kraus VB, Burnett B, Coindreau J, Cottrell S, Eyre D, Gendreau M, et al. Application of biomarkers in the development of drugs intended for the treatment of osteoarthritis. Osteoarthritis Cartilage. 2011;19(5):515-42.
387. Inglis JJ, McNamee KE, Chia SL, Essex D, Feldmann M, Williams RO, et al. Regulation of pain sensitivity in experimental osteoarthritis by the endogenous peripheral opioid system. Arthritis Rheum. 2008;58(10):3110-9.
388. Piel MJ, Kroin JS, van Wijnen AJ, Kc R, Im HJ. Pain assessment in animal models of osteoarthritis. Gene. 2014;537(2):184-8.

389. Untergasser A, Cutcutache I, Koressaar T, Ye J, Faircloth BC, Remm M, et al. Primer3--new capabilities and interfaces. Nucleic Acids Res. 2012;40(15):e115.
390. UCSC In-silico PCR. http://genome.ucsc.edu/cgi-bin/hgPcr?command=start [Internet]. 2011.
391. 1000 Genomes Project. http://www.1000genomes.org [Internet]. 2016.
392. Barrett JC, Fry B, Maller J, Daly MJ. Haploview: analysis and visualization of LD and haplotype maps. Bioinformatics. 2005;21(2):263-5.
393. SNP Annotation and Proxy Search. https://www.broadinstitute.org/mpg/snap/ [Internet]. 2016.
394. Kumar P, Henikoff S, Ng PC. Predicting the effects of coding non-synonymous variants on protein function using the SIFT algorithm. Nat Protoc. 2009;4(7):1073-81.
395. SIFT v.4.0.3 (Sorting Intolerant From Tolerant). http://sift.jcvi.org [Internet]. 2016.
396. Adzhubei IA, Schmidt S, Peshkin L, Ramensky VE, Gerasimova A, Bork P, et al. A method and server for predicting damaging missense mutations. Nat Methods. 2010;7(4):248-9.
397. PolyPhen-2. PolyPhen-2 preciction of functional effects of human nsSNPs. http://genetics.bwh.harvard.edu/pph2/. 2016.
398. eQTL browser. http://eqtl.uchicago.edu/cgi-bin/gbrowse/eqtl/ [Internet]. 2016.
399. GTEx Portal. http://www.gtexportal.org [Internet]. 2016.
400. SwissRegulon Portal. http://www.swissregulon.unibas.ch [Internet]. 2016.
401. Thirion S, Berenbaum F. Culture and phenotyping of chondrocytes in primary culture. Methods in molecular medicine. 2004;100:1-14.
402. Stanton H, Golub SB, Rogerson FM, Last K, Little CB, Fosang AJ. Investigating ADAMTS-mediated aggrecanolysis in mouse cartilage. Nat Protoc. 2011;6(3):388-404.
403. Salvat C, Pigenet A, Humbert L, Berenbaum F, Thirion S. Immature murine articular chondrocytes in primary culture: a new tool for investigating cartilage. Osteoarthritis Cartilage. 2005;13(3):243-9.
404. Pfaffl MW. Relative quantification. In: Dorak T, editor. Real-time PCR. 1. 1st ed. Abingdon, U.K.: Taylor & Francis Group; 2006. p. 63-82.
405. Glasson SS, Blanchet TJ, Morris EA. The surgical destabilization of the medial meniscus (DMM) model of osteoarthritis in the 129/SvEv mouse. Osteoarthritis Cartilage. 2007;15(9):1061-9.
406. Hashimoto K, Oda Y, Nakamura F, Kakinoki R, Akagi M. Lectin-like, oxidized low-density lipoprotein receptor-1-deficient mice show resistance to age-related knee osteoarthritis. Eur J Histochem. 2017;61(1):2762.
407. Hubbard T, Barker D, Birney E, Cameron G, Chen Y, Clark L, et al. The Ensembl genome database project. Nucleic Acids Res. 2002;30(1):38-41.
408. Kent WJ, Sugnet CW, Furey TS, Roskin KM, Pringle TH, Zahler AM, et al. The human genome browser at UCSC. Genome Res. 2002;12(6):996-1006.
409. Barski A, Cuddapah S, Cui K, Roh TY, Schones DE, Wang Z, et al. High-resolution profiling of histone methylations in the human genome. Cell. 2007;129(4):823-37.
410. Flanagan JF, Mi LZ, Chruszcz M, Cymborowski M, Clines KL, Kim Y, et al. Double chromodomains cooperate to recognize the methylated histone H3 tail. Nature. 2005;438(7071):1181-5.

411. Schneider R, Bannister AJ, Weise C, Kouzarides T. Direct binding of INHAT to H3 tails disrupted by modifications. J Biol Chem. 2004;279(23):23859-62.
412. Wenke AK, Bosserhoff AK. Roles of AP-2 transcription factors in the regulation of cartilage and skeletal development. FEBS J. 2010;277(4):894-902.
413. Huang Z, Xu H, Sandell L. Negative regulation of chondrocyte differentiation by transcription factor AP-2alpha. J Bone Miner Res. 2004;19(2):245-55.
414. Tuli R, Seghatoleslami MR, Tuli S, Howard MS, Danielson KG, Tuan RS. p38 MAP kinase regulation of AP-2 binding in TGF-beta1-stimulated chondrogenesis of human trabecular bone-derived cells. Ann N Y Acad Sci. 2002;961:172-7.
415. Sinnett D, Beaulieu P, Belanger H, Lefebvre JF, Langlois S, Theberge MC, et al. Detection and characterization of DNA variants in the promoter regions of hundreds of human disease candidate genes. Genomics. 2006;87(6):704-10.
416. Arnold M, Ellwanger DC, Hartsperger ML, Pfeufer A, Stumpflen V. Cis-acting polymorphisms affect complex traits through modifications of microRNA regulation pathways. PLoS One. 2012;7(5):e36694.
417. Landi D, Gemignani F, Landi S. Role of variations within microRNA-binding sites in cancer. Mutagenesis. 2012;27(2):205-10.
418. Delay C, Calon F, Mathews P, Hebert SS. Alzheimer-specific variants in the 3'UTR of Amyloid precursor protein affect microRNA function. Mol Neurodegener. 2011;6:70.
419. Clop A, Marcq F, Takeda H, Pirottin D, Tordoir X, Bibe B, et al. A mutation creating a potential illegitimate microRNA target site in the myostatin gene affects muscularity in sheep. Nat Genet. 2006;38(7):813-8.
420. Thomas LF, Saito T, Saetrom P. Inferring causative variants in microRNA target sites. Nucleic Acids Res. 2011;39(16):e109.
421. Tserel L, Runnel T, Kisand K, Pihlap M, Bakhoff L, Kolde R, et al. MicroRNA expression profiles of human blood monocyte-derived dendritic cells and macrophages reveal miR-511 as putative positive regulator of Toll-like receptor 4. J Biol Chem. 2011;286(30):26487-95.
422. Yang K, He YS, Wang XQ, Lu L, Chen QJ, Liu J, et al. MiR-146a inhibits oxidized low-density lipoprotein-induced lipid accumulation and inflammatory response via targeting toll-like receptor 4. FEBS Lett. 2011;585(6):854-60.
423. Ji JD, Kim, T-H., Lee, B., Na K-S., Choi S-J., Lee Y-H., Song, G.G. Integrated analysis of microRNA and mRNA expression profiles in rheumatoid arthritis synovial monocytes. Journal of Rheumatic Diseases. 2011;18(4):253-63.
424. Unguryte A, Bernotiene E, Bagdonas E, Garberyte S, Porvaneckas N, Jorgensen C. Human articular chondrocytes with higher aldehyde dehydrogenase activity have stronger expression of COL2A1 and SOX9. Osteoarthritis Cartilage. 2016;24(5):873-82.
425. Niederreither K, Subbarayan V, Dolle P, Chambon P. Embryonic retinoic acid synthesis is essential for early mouse post-implantation development. Nat Genet. 1999;21(4):444-8.
426. Dupe V, Matt N, Garnier JM, Chambon P, Mark M, Ghyselinck NB. A newborn lethal defect due to inactivation of retinaldehyde dehydrogenase type 3 is prevented by maternal retinoic acid treatment. Proc Natl Acad Sci U S A. 2003;100(24):14036-41.
427. Lassen N, Bateman JB, Estey T, Kuszak JR, Nees DW, Piatigorsky J, et al. Multiple and additive functions of ALDH3A1 and ALDH1A1: cataract phenotype and

ocular oxidative damage in Aldh3a1(-/-)/Aldh1a1(-/-) knock-out mice. J Biol Chem. 2007;282(35):25668-76.
428. Black WJ, Stagos D, Marchitti SA, Nebert DW, Tipton KF, Bairoch A, et al. Human aldehyde dehydrogenase genes: alternatively spliced transcriptional variants and their suggested nomenclature. Pharmacogenet Genomics. 2009;19(11):893-902.
429. Gonzalez-Cano L, Hillje AL, Fuertes-Alvarez S, Marques MM, Blanch A, Ian RW, et al. Regulatory feedback loop between TP73 and TRIM32. Cell Death Dis. 2013;4:e704.
430. Durigova M, Roughley PJ, Mort JS. Mechanism of proteoglycan aggregate degradation in cartilage stimulated with oncostatin M. Osteoarthritis Cartilage. 2008;16(1):98-104.
431. Jenniskens YM, Koevoet W, de Bart AC, Weinans H, Jahr H, Verhaar JA, et al. Biochemical and functional modulation of the cartilage collagen network by IGF1, TGFbeta2 and FGF2. Osteoarthritis Cartilage. 2006;14(11):1136-46.
432. Sophia Fox AJ, Bedi A, Rodeo SA. The basic science of articular cartilage: structure, composition, and function. Sports Health. 2009;1(6):461-8.
433. Studer D, Millan C, Ozturk E, Maniura-Weber K, Zenobi-Wong M. Molecular and biophysical mechanisms regulating hypertrophic differentiation in chondrocytes and mesenchymal stem cells. Eur Cell Mater. 2012;24:118-35; discussion 35.
434. Hardingham TE, Oldershaw RA, Tew SR. Cartilage, SOX9 and Notch signals in chondrogenesis. J Anat. 2006;209(4):469-80.
435. Toegel S, Huang W, Piana C, Unger FM, Wirth M, Goldring MB, et al. Selection of reliable reference genes for qPCR studies on chondroprotective action. BMC Mol Biol. 2007;8:13.
436. Fowler CB, Evers DL, O'Leary TJ, Mason JT. Antigen retrieval causes protein unfolding: evidence for a linear epitope model of recovered immunoreactivity. J Histochem Cytochem. 2011;59(4):366-81.
437. Tsolis KC, Bei ES, Papathanasiou I, Kostopoulou F, Gkretsi V, Kalantzaki K, et al. Comparative proteomic analysis of hypertrophic chondrocytes in osteoarthritis. Clin Proteomics. 2015;12(1):12.
438. Foldager CB, Munir S, Ulrik-Vinther M, Soballe K, Bunger C, Lind M. Validation of suitable house keeping genes for hypoxia-cultured human chondrocytes. BMC Mol Biol. 2009;10:94.
439. Heywood HK, Nalesso G, Lee DA, Dell'accio F. Culture expansion in low-glucose conditions preserves chondrocyte differentiation and enhances their subsequent capacity to form cartilage tissue in three-dimensional culture. Biores Open Access. 2014;3(1):9-18.
440. Fu B, Wang L, Ding H, Schwamborn JC, Li S, Dorf ME. TRIM32 Senses and Restricts Influenza A Virus by Ubiquitination of PB1 Polymerase. PLoS Pathog. 2015;11(6):e1004960.
441. Neri M, Selvatici R, Scotton C, Trabanelli C, Armaroli A, De Grandis D, et al. A patient with limb girdle muscular dystrophy carries a TRIM32 deletion, detected by a novel CGH array, in compound heterozygosis with a nonsense mutation. Neuromuscular disorders : NMD. 2013;23(6):478-82.

442. Cohen S, Zhai B, Gygi SP, Goldberg AL. Ubiquitylation by Trim32 causes coupled loss of desmin, Z-bands, and thin filaments in muscle atrophy. J Cell Biol. 2012;198(4):575-89.
443. Hong BS, Cho JH, Kim H, Choi EJ, Rho S, Kim J, et al. Colorectal cancer cell-derived microvesicles are enriched in cell cycle-related mRNAs that promote proliferation of endothelial cells. BMC Genomics. 2009;10:556.
444. Ichimura T, Taoka M, Shoji I, Kato H, Sato T, Hatakeyama S, et al. 14-3-3 proteins sequester a pool of soluble TRIM32 ubiquitin ligase to repress autoubiquitylation and cytoplasmic body formation. Journal of cell science. 2013;126(Pt 9):2014-26.
445. Ramachandran H, Schafer T, Kim Y, Herfurth K, Hoff S, Lienkamp SS, et al. Interaction with the Bardet-Biedl gene product TRIM32/BBS11 modifies the half-life and localization of Glis2/NPHP7. J Biol Chem. 2014;289(12):8390-401.
446. Locke M, Tinsley CL, Benson MA, Blake DJ. TRIM32 is an E3 ubiquitin ligase for dysbindin. Hum Mol Genet. 2009;18(13):2344-58.
447. Kano S, Miyajima N, Fukuda S, Hatakeyama S. Tripartite motif protein 32 facilitates cell growth and migration via degradation of Abl-interactor 2. Cancer research. 2008;68(14):5572-80.
448. Kiani C, Chen L, Wu YJ, Yee AJ, Yang BB. Structure and function of aggrecan. Cell Res. 2002;12(1):19-32.
449. Aspberg A. The different roles of aggrecan interaction domains. J Histochem Cytochem. 2012;60(12):987-96.
450. Sato T, Okumura F, Kano S, Kondo T, Ariga T, Hatakeyama S. TRIM32 promotes neural differentiation through retinoic acid receptor-mediated transcription. Journal of cell science. 2011;124(Pt 20):3492-502.
451. Koyama E, Golden EB, Kirsch T, Adams SL, Chandraratna RA, Michaille JJ, et al. Retinoid signaling is required for chondrocyte maturation and endochondral bone formation during limb skeletogenesis. Developmental biology. 1999;208(2):375-91.
452. Iwamoto M, Shapiro IM, Yagami K, Boskey AL, Leboy PS, Adams SL, et al. Retinoic acid induces rapid mineralization and expression of mineralization-related genes in chondrocytes. Exp Cell Res. 1993;207(2):413-20.
453. Shum AS, Poon LL, Tang WW, Koide T, Chan BW, Leung YC, et al. Retinoic acid induces down-regulation of Wnt-3a, apoptosis and diversion of tail bud cells to a neural fate in the mouse embryo. Mech Dev. 1999;84(1-2):17-30.
454. Weston AD, Blumberg B, Underhill TM. Active repression by unliganded retinoid receptors in development: less is sometimes more. J Cell Biol. 2003;161(2):223-8.
455. Fukuo K, Takigawa M, Tajima K, Enomoto M, Kumahara Y, Suzuki F. Comparison of inhibition by a tumor promoter (12-O-tetradecanoylphorbol-13-acetate) of expression of the differentiated phenotype of chondrocytes in rabbit costal chondrocytes in culture with inhibition by retinoic acid. J Biochem. 1986;99(2):385-96.
456. Ballock RT, Heydemann A, Wakefield LM, Flanders KC, Roberts AB, Sporn MB. Inhibition of the chondrocyte phenotype by retinoic acid involves upregulation of metalloprotease genes independent of TGF-beta. J Cell Physiol. 1994;159(2):340-6.

457. Yuasa T, Otani T, Koike T, Iwamoto M, Enomoto-Iwamoto M. Wnt/beta-catenin signaling stimulates matrix catabolic genes and activity in articular chondrocytes: its possible role in joint degeneration. Lab Invest. 2008;88(3):264-74.
458. Chun JS, Oh H, Yang S, Park M. Wnt signaling in cartilage development and degeneration. BMB Rep. 2008;41(7):485-94.
459. Yasuhara R, Yuasa T, Williams JA, Byers SW, Shah S, Pacifici M, et al. Wnt/beta-catenin and retinoic acid receptor signaling pathways interact to regulate chondrocyte function and matrix turnover. J Biol Chem. 2010;285(1):317-27.
460. Mendelsohn C, Ruberte E, Chambon P. Retinoid receptors in vertebrate limb development. Developmental biology. 1992;152(1):50-61.
461. Qu J, Liu GH, Wu K, Han P, Wang P, Li J, et al. Nitric oxide destabilizes Pias3 and regulates sumoylation. PLoS One. 2007;2(10):e1085.
462. Hess DT, Matsumoto A, Kim SO, Marshall HE, Stamler JS. Protein S-nitrosylation: purview and parameters. Nat Rev Mol Cell Biol. 2005;6(2):150-66.
463. Bitter T, Muir HM. A modified uronic acid carbazole reaction. Anal Biochem. 1962;4:330-4.
464. Gosset M, Berenbaum F, Thirion S, Jacques C. Primary culture and phenotyping of murine chondrocytes. Nat Protoc. 2008;3(8):1253-60.
465. Oh H, Chun CH, Chun JS. Dkk-1 expression in chondrocytes inhibits experimental osteoarthritic cartilage destruction in mice. Arthritis Rheum. 2012;64(8):2568-78.
466. Akasaki Y, Hasegawa A, Saito M, Asahara H, Iwamoto Y, Lotz MK. Dysregulated FOXO transcription factors in articular cartilage in aging and osteoarthritis. Osteoarthritis Cartilage. 2014;22(1):162-70.
467. Kirsch T, von der Mark K. Isolation of bovine type X collagen and immunolocalization in growth-plate cartilage. Biochem J. 1990;265(2):453-9.
468. Schmid TM, Linsenmayer TF. Immunoelectron microscopy of type X collagen: supramolecular forms within embryonic chick cartilage. Developmental biology. 1990;138(1):53-62.
469. Phornphutkul C, Wu KY, Yang X, Chen Q, Gruppuso PA. Insulin-like growth factor-I signaling is modified during chondrocyte differentiation. J Endocrinol. 2004;183(3):477-86.
470. Wang Y, Cheng Z, Elalieh HZ, Nakamura E, Nguyen MT, Mackem S, et al. IGF-1R signaling in chondrocytes modulates growth plate development by interacting with the PTHrP/Ihh pathway. J Bone Miner Res. 2011;26(7):1437-46.
471. El Mabrouk M, Sylvester J, Zafarullah M. Signaling pathways implicated in oncostatin M-induced aggrecanase-1 and matrix metalloproteinase-13 expression in human articular chondrocytes. Biochim Biophys Acta. 2007;1773(3):309-20.
472. Wahl AF, Wallace PM. Oncostatin M in the anti-inflammatory response. Ann Rheum Dis. 2001;60 Suppl 3:iii75-80.
473. Sanchez C, Deberg MA, Burton S, Devel P, Reginster JY, Henrotin YE. Differential regulation of chondrocyte metabolism by oncostatin M and interleukin-6. Osteoarthritis Cartilage. 2004;12(10):801-10.
474. Grimmer C, Balbus N, Lang U, Aigner T, Cramer T, Muller L, et al. Regulation of type II collagen synthesis during osteoarthritis by prolyl-4-hydroxylases: possible influence of low oxygen levels. Am J Pathol. 2006;169(2):491-502.

475. Nelson F, Dahlberg L, Laverty S, Reiner A, Pidoux I, Ionescu M, et al. Evidence for altered synthesis of type II collagen in patients with osteoarthritis. J Clin Invest. 1998;102(12):2115-25.
476. Aigner T, Bertling W, Stoss H, Weseloh G, von der Mark K. Independent expression of fibril-forming collagens I, II, and III in chondrocytes of human osteoarthritic cartilage. J Clin Invest. 1993;91(3):829-37.
477. Valverde-Franco G, Lussier B, Hum D, Wu J, Hamadjida A, Dancause N, et al. Cartilage-specific deletion of ephrin-B2 in mice results in early developmental defects and an osteoarthritis-like phenotype during aging in vivo. Arthritis Res Ther. 2016;18:65.
478. Blumer MJ, Longato S, Schwarzer C, Fritsch H. Bone development in the femoral epiphysis of mice: the role of cartilage canals and the fate of resting chondrocytes. Dev Dyn. 2007;236(8):2077-88.
479. Ashraf S, Cha BH, Kim JS, Ahn J, Han I, Park H, et al. Regulation of senescence associated signaling mechanisms in chondrocytes for cartilage tissue regeneration. Osteoarthritis Cartilage. 2016;24(2):196-205.
480. Rogerson FM, Chung YM, Deutscher ME, Last K, Fosang AJ. Cytokine-induced increases in ADAMTS-4 messenger RNA expression do not lead to increased aggrecanase activity in ADAMTS-5-deficient mice. Arthritis Rheum. 2010;62(11):3365-73.
481. Sheu SY, Ho SR, Sun JS, Chen CY, Ke CJ. Arthropod steroid hormone (20-Hydroxyecdysone) suppresses IL-1beta-induced catabolic gene expression in cartilage. BMC Complement Altern Med. 2015;15:1.
482. Liu X, Liu R, Croker BA, Lawlor KE, Smyth GK, Wicks IP. Distinctive pro-inflammatory gene signatures induced in articular chondrocytes by oncostatin M and IL-6 are regulated by Suppressor of Cytokine Signaling-3. Osteoarthritis Cartilage. 2015;23(10):1743-54.
483. Jacques C, Recklies AD, Levy A, Berenbaum F. HC-gp39 contributes to chondrocyte differentiation by inducing SOX9 and type II collagen expressions. Osteoarthritis Cartilage. 2007;15(2):138-46.
484. Moodie JP, Stok KS, Muller R, Vincent TL, Shefelbine SJ. Multimodal imaging demonstrates concomitant changes in bone and cartilage after destabilisation of the medial meniscus and increased joint laxity. Osteoarthritis Cartilage. 2011;19(2):163-70.
485. Yang S, Kim J, Ryu JH, Oh H, Chun CH, Kim BJ, et al. Hypoxia-inducible factor-2alpha is a catabolic regulator of osteoarthritic cartilage destruction. Nat Med. 2010;16(6):687-93.
486. Waung JA, Maynard SA, Gopal S, Gogakos A, Logan JG, Williams GR, et al. Quantitative X-ray microradiography for high-throughput phenotyping of osteoarthritis in mice. Osteoarthritis Cartilage. 2014;22(10):1396-400.
487. Bateman JF, Rowley L, Belluoccio D, Chan B, Bell K, Fosang AJ, et al. Transcriptomics of wild-type mice and mice lacking ADAMTS-5 activity identifies genes involved in osteoarthritis initiation and cartilage destruction. Arthritis Rheum. 2013;65(6):1547-60.
488. Vasheghani F, Zhang Y, Li YH, Blati M, Fahmi H, Lussier B, et al. PPARgamma deficiency results in severe, accelerated osteoarthritis associated with

aberrant mTOR signalling in the articular cartilage. Ann Rheum Dis. 2015;74(3):569-78.
489. Malfait AM, Ritchie J, Gil AS, Austin JS, Hartke J, Qin W, et al. ADAMTS-5 deficient mice do not develop mechanical allodynia associated with osteoarthritis following medial meniscal destabilization. Osteoarthritis Cartilage. 2010;18(4):572-80.
490. Pan J, Wang B, Li W, Zhou X, Scherr T, Yang Y, et al. Elevated cross-talk between subchondral bone and cartilage in osteoarthritic joints. Bone. 2012;51(2):212-7.
491. Sondergaard BC, Catala-Lehnen P, Huebner AK, Bay-Jensen AC, Schinke T, Henriksen K, et al. Mice over-expressing salmon calcitonin have strongly attenuated osteoarthritic histopathological changes after destabilization of the medial meniscus. Osteoarthritis Cartilage. 2012;20(2):136-43.
492. Muramatsu Y, Sasho T, Saito M, Yamaguchi S, Akagi R, Mukoyama S, et al. Preventive effects of hyaluronan from deterioration of gait parameters in surgically induced mice osteoarthritic knee model. Osteoarthritis Cartilage. 2014;22(6):831-5.
493. Valverde-Franco G, Pelletier JP, Fahmi H, Hum D, Matsuo K, Lussier B, et al. In vivo bone-specific EphB4 overexpression in mice protects both subchondral bone and cartilage during osteoarthritis. Arthritis Rheum. 2012;64(11):3614-25.
494. Mogil JS, Chesler EJ, Wilson SG, Juraska JM, Sternberg WF. Sex differences in thermal nociception and morphine antinociception in rodents depend on genotype. Neurosci Biobehav Rev. 2000;24(3):375-89.
495. Chan CC, Roberts CR, Steeves JD, Tetzlaff W. Aggrecan components differentially modulate nerve growth factor-responsive and neurotrophin-3-responsive dorsal root ganglion neurite growth. J Neurosci Res. 2008;86(3):581-92.
496. Ferreira-Gomes J, Adaes S, Castro-Lopes JM. Assessment of movement-evoked pain in osteoarthritis by the knee-bend and CatWalk tests: a clinically relevant study. J Pain. 2008;9(10):945-54.
497. Liu P, Okun A, Ren J, Guo RC, Ossipov MH, Xie J, et al. Ongoing pain in the MIA model of osteoarthritis. Neurosci Lett. 2011;493(3):72-5.
498. Sandell LJ. Obesity and osteoarthritis: is leptin the link? Arthritis Rheum. 2009;60(10):2858-60.
499. Ahima RS. Adipose tissue as an endocrine organ. Obesity (Silver Spring). 2006;14 Suppl 5:242S-9S.
500. Presle N, Pottie P, Dumond H, Guillaume C, Lapicque F, Pallu S, et al. Differential distribution of adipokines between serum and synovial fluid in patients with osteoarthritis. Contribution of joint tissues to their articular production. Osteoarthritis Cartilage. 2006;14(7):690-5.
501. Schaffler A, Ehling A, Neumann E, Herfarth H, Tarner I, Scholmerich J, et al. Adipocytokines in synovial fluid. JAMA. 2003;290(13):1709-10.
502. Mooney RA, Sampson ER, Lerea J, Rosier RN, Zuscik MJ. High-fat diet accelerates progression of osteoarthritis after meniscal/ligamentous injury. Arthritis Res Ther. 2011;13(6):R198.
503. Sophocleous A, Landao-Bassonga E, Van't Hof RJ, Idris AI, Ralston SH. The type 2 cannabinoid receptor regulates bone mass and ovariectomy-induced bone loss by affecting osteoblast differentiation and bone formation. Endocrinology. 2011;152(6):2141-9.

504. Kadri A, Ea HK, Bazille C, Hannouche D, Liote F, Cohen-Solal ME. Osteoprotegerin inhibits cartilage degradation through an effect on trabecular bone in murine experimental osteoarthritis. Arthritis Rheum. 2008;58(8):2379-86.
505. Miyamoto S, Nakamura J, Ohtori S, Orita S, Omae T, Nakajima T, et al. Intra-articular injection of mono-iodoacetate induces osteoarthritis of the hip in rats. BMC musculoskeletal disorders. 2016;17:132.
506. Omae T, Nakamura J, Ohtori S, Orita S, Yamauchi K, Miyamoto S, et al. A novel rat model of hip pain by intra-articular injection of nerve growth factor-characteristics of sensory innervation and inflammatory arthritis. Mod Rheumatol. 2015;25(6):931-6.
507. Bentley G. Articular cartilage studies and osteoarthrosis. Annals of the Royal College of Surgeons of England. 1975;57(2):86-100.
508. Hassan EA, Lambrechts NE, Moore GE, Weng HY, Heng HG, Breur GJ. Development of a model to induce transient synovitis and lameness in the hip joint of dogs. Am J Vet Res. 2015;76(10):869-76.
509. Little D, Johnson S, Hash J, Olson SA, Estes BT, Moutos FT, et al. Functional outcome measures in a surgical model of hip osteoarthritis in dogs. J Exp Orthop. 2016;3(1):17.
510. Song W, Pei F, Xiang M, Liu B. [Effects on biomechanical properties of hip articular cartilage degeneration following the femoral neck fracture in rabbits]. Sheng Wu Yi Xue Gong Cheng Xue Za Zhi. 2006;23(5):1024-7.
511. Maniwa S, Nishikori T, Furukawa S, Kajitani K, Ochi M. Alteration of collagen network and negative charge of articular cartilage surface in the early stage of experimental osteoarthritis. Archives of orthopaedic and trauma surgery. 2001;121(4):181-5.
512. Fu M, Liu J, Huang G, Huang Z, Zhang Z, Wu P, et al. Impaired ossification coupled with accelerated cartilage degeneration in developmental dysplasia of the hip: evidences from muCT arthrography in a rat model. BMC musculoskeletal disorders. 2014;15:339.
513. Ning B, Sun J, Yuan Y, Yao J, Wang P, Ma R. Early articular cartilage degeneration in a developmental dislocation of the hip model results from activation of beta-catenin. Int J Clin Exp Pathol. 2014;7(4):1369-78.
514. Siebenrock KA, Kienle KP, Steppacher SD, Tannast M, Mamisch TC, von Rechenberg B. Biochemical MRI predicts hip osteoarthritis in an experimental ovine femoroacetabular impingement model. Clinical orthopaedics and related research. 2015;473(4):1318-24.
515. Kwan Tat S, Pelletier JP, Amiable N, Boileau C, Lavigne M, Martel-Pelletier J. Treatment with ephrin B2 positively impacts the abnormal metabolism of human osteoarthritic chondrocytes. Arthritis Res Ther. 2009;11(4):R119.
516. Regan E, Flannelly J, Bowler R, Tran K, Nicks M, Carbone BD, et al. Extracellular superoxide dismutase and oxidant damage in osteoarthritis. Arthritis Rheum. 2005;52(11):3479-91.
517. Furman BD, Mangiapani DS, Zeitler E, Bailey KN, Horne PH, Huebner JL, et al. Targeting pro-inflammatory cytokines following joint injury: acute intra-articular inhibition of interleukin-1 following knee injury prevents post-traumatic arthritis. Arthritis Res Ther. 2014;16(3):R134.

518. Clements KM, Flannelly JK, Tart J, Brockbank SM, Wardale J, Freeth J, et al. Matrix metalloproteinase 17 is necessary for cartilage aggrecan degradation in an inflammatory environment. Ann Rheum Dis. 2011;70(4):683-9.
519. Tsuchida AI, Beekhuizen M, t Hart MC, Radstake TR, Dhert WJ, Saris DB, et al. Cytokine profiles in the joint depend on pathology, but are different between synovial fluid, cartilage tissue and cultured chondrocytes. Arthritis Res Ther. 2014;16(5):441.
520. Lotz M, Loeser RF. Effects of aging on articular cartilage homeostasis. Bone. 2012;51(2):241-8.
521. Sousa-Victor P, Gutarra S, Garcia-Prat L, Rodriguez-Ubreva J, Ortet L, Ruiz-Bonilla V, et al. Geriatric muscle stem cells switch reversible quiescence into senescence. Nature. 2014;506(7488):316-21.
522. Philipot D, Guerit D, Platano D, Chuchana P, Olivotto E, Espinoza F, et al. p16INK4a and its regulator miR-24 link senescence and chondrocyte terminal differentiation-associated matrix remodeling in osteoarthritis. Arthritis Res Ther. 2014;16(1):R58.
523. Burr DB. Anatomy and physiology of the mineralized tissues: role in the pathogenesis of osteoarthrosis. Osteoarthritis Cartilage. 2004;12 Suppl A:S20-30.
524. Intema F, Sniekers YH, Weinans H, Vianen ME, Yocum SA, Zuurmond AM, et al. Similarities and discrepancies in subchondral bone structure in two differently induced canine models of osteoarthritis. J Bone Miner Res. 2010;25(7):1650-7.
525. Burr DB, Gallant MA. Bone remodelling in osteoarthritis. Nat Rev Rheumatol. 2012;8(11):665-73.
526. Cucchiarini M, de Girolamo L, Filardo G, Oliveira JM, Orth P, Pape D, et al. Basic science of osteoarthritis. J Exp Orthop. 2016;3(1):22.
527. Buckland-Wright JC, Lynch JA, Dave B. Early radiographic features in patients with anterior cruciate ligament rupture. Ann Rheum Dis. 2000;59(8):641-6.
528. Cole HA, Yuasa M, Hawley G, Cates JM, Nyman JS, Schoenecker JG. Differential development of the distal and proximal femoral epiphysis and physis in mice. Bone. 2013;52(1):337-46.
529. Smemo S, Tena JJ, Kim KH, Gamazon ER, Sakabe NJ, Gomez-Marin C, et al. Obesity-associated variants within FTO form long-range functional connections with IRX3. Nature. 2014;507(7492):371-5.
530. Cookson W, Liang L, Abecasis G, Moffatt M, Lathrop M. Mapping complex disease traits with global gene expression. Nat Rev Genet. 2009;10(3):184-94.
531. Visscher PM, Brown MA, McCarthy MI, Yang J. Five years of GWAS discovery. Am J Hum Genet. 2012;90(1):7-24.
532. Gibson G. Rare and common variants: twenty arguments. Nat Rev Genet. 2012;13(2):135-45.
533. van der Kraan PM, van den Berg WB. Chondrocyte hypertrophy and osteoarthritis: role in initiation and progression of cartilage degeneration? Osteoarthritis Cartilage. 2012;20(3):223-32.
534. Uusitalo H, Salminen H, Vuorio E. Activation of chondrogenesis in response to injury in normal and transgenic mice with cartilage collagen mutations. Osteoarthritis Cartilage. 2001;9 Suppl A:S174-9.

535. Jeon JE, Schrobback K, Meinert C, Sramek V, Hutmacher DW, Klein TJ. Effect of preculture and loading on expression of matrix molecules, matrix metalloproteinases, and cytokines by expanded osteoarthritic chondrocytes. Arthritis Rheum. 2013;65(9):2356-67.
536. Zhang Y, Vasheghani F, Li YH, Blati M, Simeone K, Fahmi H, et al. Cartilage-specific deletion of mTOR upregulates autophagy and protects mice from osteoarthritis. Ann Rheum Dis. 2015;74(7):1432-40.
537. Vasheghani F, Monemdjou R, Fahmi H, Zhang Y, Perez G, Blati M, et al. Adult cartilage-specific peroxisome proliferator-activated receptor gamma knockout mice exhibit the spontaneous osteoarthritis phenotype. Am J Pathol. 2013;182(4):1099-106.
538. Liu J, Zhang C, Wang XL, Ly P, Belyi V, Xu-Monette ZY, et al. E3 ubiquitin ligase TRIM32 negatively regulates tumor suppressor p53 to promote tumorigenesis. Cell Death Differ. 2014;21(11):1792-804.
539. Gunthorpe MJ, Szallasi A. Peripheral TRPV1 receptors as targets for drug development: new molecules and mechanisms. Curr Pharm Des. 2008;14(1):32-41.